# DEVELOPMENT OF ELECTROCHEMICAL SENSORS FOR ANALYSIS OF MEDICAL AND ENVIRONMENTAL ANALYTES

**TANIN TANGKUARAM**

**A THESIS SUBMITTED IN PARTIAL FULFILLMENT**
**OF THE REQUIREMENTS FOR**
**THE DEGREE OF DOCTOR OF PHILOSOPHY**
**(ANALYTICAL CHEMISTRY)**
**FACULTY OF GRADUATE STUDIES**
**MAHIDOL UNIVERSITY**
**2007**

Thesis
Entitled

# DEVELOPMENT OF ELECTROCHEMICAL SENSORS FOR ANALYSIS OF MEDICAL AND ENVIRONMENTAL ANALYTES

Mr. Tanin Tangkuaram
Candidate

Lect. Waret Veerasai,
Dr. rer. nat. (Physical Inorganic Chemistry)
Major-Advisor

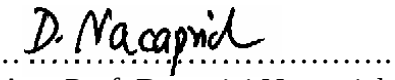

Asst.Prof. Duangjai Nacapricha,
Ph.D. (Analytical Chemistry)
Co-Advisor

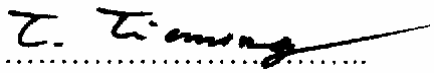

Lect. Tinnakorn Tiensing,
Ph.D. (Environmental Science)
Co-Advisor

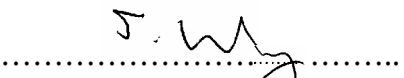

Prof. Joseph Wang,
D.Sc. (Chemistry)
Co-Advisor

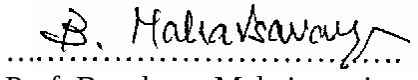

Prof. Banchong Mahaisavariya,
M.D.
Dean
Faculty of Graduate Studies

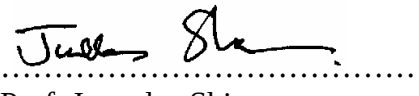

Prof. Juwadee Shiowatana,
Ph.D. (Analytical Chemistry)
Chair
Doctor of Philosophy Programme
in Analytical Chemistry
Faculty of Science

Thesis
Entitled

# DEVELOPMENT OF ELECTROCHEMICAL SENSORS FOR ANALYSIS OF MEDICAL AND ENVIRONMENTAL ANALYTES

was submitted to the Faculty of Graduate Studies, Mahidol University
for the Degree of Doctor of Philosophy (Analytical Chemistry)
on
December 26, 2007

Tanin Tangkuaram.
.....
Mr. Tanin Tangkuaram
Candidate

.....
Assoc.Prof. Werasak Suraruengchai,
Ph.D. (Electroanalysis)
Chair

Waret Veerasai
.....
Lect. Waret Veerasai,
Dr. rer. nat. (Physical Inorganic Chemistry)
Member

D. Nacapricha
.....
Asst.Prof. Duangjai Nacapricha,
Ph.D. (Analytical Chemistry)
Member

T. Tiensing
.....
Lect. Tinnakorn Tiensing,
Ph.D. (Environmental Science)
Member

B. Mahaisavariya
.....
Prof. Banchong Mahaisavariya,
M.D.
Dean
Faculty of Graduate Studies
Mahidol University

.....
Prof. Skorn Mongkolsuk,
Ph.D. (Biological Science)
Dean
Faculty of Science
Mahidol University

# ACKNOWLEDGEMENTS

I would like to express my gratitude to thank my advisor, Dr. W. Veerasai, for continuously providing important guidance and challenging ideas in my Ph.D. research. I truly appreciate and thank him for his unwavering encouragements during the writing of this thesis. I also would like to thank my co-adisors, Asst.Prof. D. Nacapricha and Dr. T. Tiensing, for their helpful comments, advice and their valuable time spent as member of the thesis examination committee. My sincere appreciation is also extended to the chair and the external committee member, Assoc.Prof. W. Suraruengchai, for his suggestions.

I truly thank my co-advisors, Prof. J. Wang, for his support, advice, discussions and suggestions over a year of conducting research at the Center for Bioelectronics and Biosensors, The Biodesign Institute, Arizona State University, USA. I also would like to thank Prof. L. Joshi for his suggestions and discussions on the glycosidases project. I would like to thank all my great friends when I was there: A. Preechaworapun, S. Loyprasert, T. Vazquez-Alvarez, Dr. S. Thongngamdee, and all those others whom I can not write here. They helped me in many ways and I will never forget.

I especially want to thank the staff of the Department of Chemistry, Mahidol University, who taught me throughout my degree. This attribution can be extended to the Interfacial Electrochemistry (IFEC-MU) friends for their help throughout this research. I would like to thank Dr. P. Sritongkum, King Mongkut's University of Technology Thonburi, for giving me some of electrodes. Also, I would like to thank the Maejo University for grant and the Center for Innovation in Chemistry: Postgraduate Education and Research Program in Chemistry (PERCH-CIC) for partial financial support.

Finally, my heartfelt thanks go to my family for their love, belief, support and encouragement until I graduated.

*Tanin Tangkuaram*

DEVELOPMENT OF ELECTROCHEMICAL SENSORS FOR ANALYSIS OF MEDICAL AND ENVIRONMENTAL ANALYTES

TANIN TANGKUARAM 4636250 SCAC/D

Ph.D. (ANALYTICAL CHEMISTRY)

THESIS ADVISORS: WARET VEERASAI, Dr. rer. nat. (PHYSICAL INORGANIC CHEMISTRY), DUANGJAI NACAPRICHA, Ph.D. (ANALYTICAL CHEMISTRY), TINNAKORN TIENSING, Ph.D. (ENVIRONMENTAL SCIENCE), JOSEPH WANG, D.Sc. (CHEMISTRY)

## ABSTRACT

Four different electrochemical sensors were developed for analysis of some selected analytes, namely: (i) insulin, (ii) glycosidases, (iii) hydrogen peroxide ($H_2O_2$), and (iv) phosphate ($PO_4^{3-}$). These are very important in health care and environmental monitoring. The improvement of sensitivity, selectivity, detection limit and stability of these sensors were investigated.

(i) Insulin is a pancreatic endocrine hormone for controlling body cells adsorbing and using glucose. The insulin sensor was developed by using a bilayer surface coating of ruthenium oxide ($RuO_x$) onto a carbon nanotube (CNT) layer. $RuO_x$/CNT offers dramatic improvement in the stability and sensitivity of voltammetric and amperometric measurements of insulin. A wide linear dynamic range (10 - 800 nM) was achieved with a detection limit of 1 nM insulin.

(ii) Glycosidases are index enzymes for cancer screening. The mechanism of the glycosidases sensor involved the enzymes converting a probe substrate, 4-nitrophenol-β-D-galactopyranoside, to an electrochemical active form as *p*-nitrophenol. The detection signal of *p*-nitrophenol oxidation is a proportion of the glycosidases content. The electrochemical assay for glycosidases enzymes is better than the conventional spectrophotometric techniques.

(iii) Hydrogen peroxide is an intermediate species in many enzymatic reactions. The $H_2O_2$ biosensor was designed on a screen printed carbon electrode (SPCE). A bare SPCE was modified by horseradish peroxidase (HRP)/gold nanoparticles (AuNP) in the matrix of chitosan (HRP/AuNP/CHIT). The HRP/AuNP incorporated with CHIT yielded the higher performance. It retained amperometric response over 95% of the initial current of the first day up to 30 days of storage at 4 °C. The biosensor showed a linear range of 0.01 – 11.3 mM $H_2O_2$, with a detection limit of 0.65 µM $H_2O_2$.

(iv) Phosphate is an important nutrient form of phosphorus related to the algae bloom phenomenon. A phosphate biosensor was designed by immobilizing pyruvate oxidase on $H_2O_2$ biosensor. Pyruvate associated phosphate via a phosphorylation reaction to generate $H_2O_2$ is an important step of phosphate biosensor. The detectable $H_2O_2$ is proportional to the phosphate content in the samples. The practical use of this biosensor for phosphate determination in real samples was demonstrated and validated with UV-Vis spectrophotometry.

KEY WORDS: INSULIN SENSOR / GLYCOSIDASES SENSOR / HYDROGEN PEROXIDE BIOSENSOR / AMPEROMETRIC PHOSPHATE BIOSENSOR / NANOTECHNOLOGY

174 pp.

การพัฒนาเซนเซอร์ทางเคมีไฟฟ้าเพื่อการวิเคราะห์สารทางแพทย์และสิ่งแวดล้อม
(DEVELOPMENT OF ELECTROCHEMICAL SENSORS FOR ANALYSIS OF MEDICAL AND ENVIRONMENTAL ANALYTES)

ธานินทร์ แตงกวารัมย์ 4636250 SCAC/D

ปร.ด. (เคมีวิเคราะห์)

คณะกรรมการควบคุมวิทยานิพนธ์: วเรศ วีระสัย, Dr. rer. nat. (Physical Inorganic Chemistry), ดวงใจ นาคะปรีชา, Ph.D. (Analytical Chemistry), ทินกร เตียนสิงห์, Ph.D. (Environmental Science), Joseph Wang, D.Sc. (Chemistry)

บทคัดย่อ

การพัฒนาเซนเซอร์ทางเคมีไฟฟ้า 4 ชนิดซึ่งมีความสำคัญทางด้านการแพทย์และการเฝ้าระวังสิ่งแวดล้อมได้แก่ (i) อินซูลิน, (ii) ไกลโคซิเดส, (iii) ไฮโดรเจนเปอร์ออกไซด์ และ (iv) ฟอสเฟต เพื่อทำให้ความไว, ความเลือกเฉพาะ, ขีดจำกัดการตรวจวัดและความเสถียรดีขึ้นดังนี้

(i) อินซูลิน เป็นฮอร์โมนจากตับอ่อนเพื่อควบคุมการดูดซึมและการใช้น้ำตาลกลูโคส อินซูลินเซนเซอร์ถูกพัฒนาโดยใช้ไบเลเยอร์ของรูธีเนียมออกไซด์บนชั้นของคาร์บอนนาโนทิวป์ การวิจัยพบว่าอินซูลินเซนเซอร์ที่ใช้ไบเลเยอร์ให้เสถียรภาพดีกว่าและว่องไวกว่าโมโนเลเยอร์ของรูธีเนียมออกไซด์หรือคาร์บอนนาโนทิวป์ ช่วงความสัมพันธ์ที่เป็นเส้นตรงมีค่าระหว่าง 10 ถึง 800 นาโนโมลาร์และมีขีดจำกัดการตรวจวัด 1 นาโนโมลาร์

(ii) ไกลโคซิเดสเป็นเอนไซม์ดัชนีสำหรับการตรวจคัดกรองโรคมะเร็งในเบื้องต้น กลไกของไกลโคซิเดสเซนเซอร์เริ่มจากเอนไซม์ดังกล่าวเปลี่ยนสับสเตรท 4-ไนโทรฟีนอล-เบตา-กาแลคโทไพราโนไซด์ไปเป็นพาราไนโทรฟีนอลที่ไวต่อการตรวจวัดทางเคมีไฟฟ้า สัญญาณการวัดเป็นปฏิภาคโดยตรงกับปริมาณของไกลโคซิเดส การวิเคราะห์ด้วยเซนเซอร์ทางเคมีไฟฟ้าให้การวัดที่ดีกว่าเทคนิคสเปกโทรโฟโทเมทริคแบบดั้งเดิม

(iii) ไฮโดรเจนเปอร์ออกไซด์เป็นสารมัธยันตร์จากปฏิกิริยาของเอนไซม์ ไบโอเซนเซอร์สำหรับสารนี้ถูกพัฒนาบนขั้วไฟฟ้าคาร์บอนพิมพ์สกรีน โดยนำขั้วไฟฟ้าเปลือยมาตรึงผิวหน้าด้วยเอนไซม์ฮอสแรดิชเปอร์ออกซิเดสในเมทริกของไคโทซาน-ทองนาโน การตรึงร่วมกันดังกล่าวทำให้เซนเซอร์มีประสิทธิภาพสูงขึ้น เซนเซอร์นี้ให้ความเสถียรมากกว่า 95 เปอร์เซนต์ ในช่วงเวลา 30 วันของการวิเคราะห์โดยเก็บเซนเซอร์ไว้ที่อุณหภูมิ 4 องศาเซลเซียส ไบโอเซนเซอร์มีช่วงการใช้งานตั้งแต่ 0.01 ถึง 11.3 มิลลิโมลาร์และมีขีดจำกัดการตรวจวัดที่ 0.65 ไมโครโมลาร์

(iv) ฟอสเฟตเป็นธาตุอาหารอีกรูปหนึ่งของธาตุฟอสฟอรัสซึ่งมีผลต่อการเจริญจนผิดปกติของสาหร่าย ฟอสเฟตไบโอเซนเซอร์ถูกพัฒนาโดยใช้เอนไซม์ไพรูเวตออกซิเดสตรึงบนผิวหน้าของ (iii) สารไพรูเวตและฟอสเฟตทำปฏิกิริยาฟอสโฟไรเลชันแล้วให้ไฮโดรเจนเปอร์ออกไซด์ออกมา ไฮโดรเจนเปอร์ออกไซด์ดังกล่าวเป็นปฏิภาคโดยตรงกับฟอสเฟต การใช้งานฟอสเฟตเซนเซอร์เพื่อวิเคราะห์ฟอสเฟตในน้ำตัวอย่างจริงแสดงให้เห็นว่ามีความถูกต้องเมื่อเทียบกับวิธียูวีวิสิเบิลสเปกโทรโฟโทเมทรี

174 หน้า.

# CONTENTS

# CONTENTS (CONTS.)

**Page**

# CONTENTS (CONTS.)

**Page**

# CONTENTS (CONTS.)

**Page**

# CONTENTS (CONTS.)

**Page**

# LIST OF TABLES

# LIST OF TABLES (CONTS.)

**Table** **Page**

# LIST OF FIGURES

# LIST OF FIGURES (CONTS.)

# LIST OF FIGURES (CONTS.)

# LIST OF FIGURES (CONTS.)

# LIST OF FIGURES (CONTS.)

# LIST OF FIGURES (CONTS.)

# LIST OF ABBREVIATIONS

| | |
|---|---|
| A | Amperes |
| $A$ | Geometrical electrode area ($cm^2$) |
| A/D | Analog to digital converter |
| AuNP | Gold nanoparticles |
| $a$ | Ion activity, diameter of the input nozzle in flow cell (cm) |
| $C$ | Concentration (mol $cm^{-3}$) |
| $C_0$ | Concentration at the electrode surface (mol $cm^{-3}$) |
| $C_b$ | Bulk concentration (mol $cm^{-3}$) |
| CE | Counter electrode |
| CHIT | Chitosan |
| CNT | Carbon nanotubes |
| CPE | Carbon paste electrode |
| CV | Cyclic voltammetry |
| $D$ | Diffusion coefficient ($cm^2$ $s^{-1}$) |
| D/A | Digital to analog converter |
| $E$ | Potential (V) |
| $e^-$ | Electron |
| $E^0$ | Standard potential (V) |
| $E^{0'}$ | Formal potential (V) |
| $E_{1/2}$ | Half-wave potential (V) |
| $E_P$ | Peak potential (V) |
| erf | Error function |
| E•S | Enzyme-substrate complex |
| $F$ | Faraday ( 96485 C $mol^{-1}$) |
| F | Farad |
| $f$ | Frequency (Hertz ($s^{-1}$)) |
| FAD | Flavin adenine dinucleotide |

# LIST OF ABBREVIATIONS (CONTS.)

| | |
|---|---|
| FIA | Flow injection analysis |
| $G$ | Gibbs free energy |
| GCE | Glassy carbon electrode |
| GPE | Graphite electrode |
| $H$ | Enthalpy |
| $h$ | Planck constant ($6.6208 \times 10^{-34}$ J s) |
| HEPES | 4-(2-Hydroxyethyl)-1-piperazineethanesulfonic acid |
| HRP | Horseradish peroxidase |
| $i$ | Current (A) |
| $I$ | Ionic strength, current (A) |
| $i_d$ | Diffusion current (A) |
| $i_p$ | Peak current (A) |
| $I_{lim}$ | Limiting current (A) |
| $I_{max}$ | Maximum current when the substrate is saturated |
| $I_{ss}$ | Current at steady-state |
| $J$ | Current density (A $cm^{-2}$) |
| $K$ | Equilibrium constant |
| $k$ | Boltzmann constant ($1.38066 \times 10^{-23}$ J $K^{-1}$), Reaction rate |
| $k_a$ | Heterogeneous electrochemical rate constant for the anodic process |
| $k_b$ | Backward homogenous rate constant |
| $k_c$ | Heterogeneous electrochemical rate constant for the cathodic process |
| $k_f$ | Forward homogeneous rate constant |
| $K_m$ | Michaelis–Menten constant |
| $K_m^{app}$ | Apparent Michaelis-Menten constant |
| $k_s$ | Heterogeneous electrochemical rate constant at $E^{0'}$ |
| min | Minute |
| $n$ | Number of electrons |

# LIST OF ABBREVIATIONS (CONTS.)

| | |
|---|---|
| 4-NP-β-Gal | 4-Nitrophenyl-β-galactopyranoside |
| 4-NP-α-GalNAc-Gal | *p*-Nitrophenyl-2-acetamido-2-deoxy-*o*-(β -D-galactopyranosyl)- α -D-galactopyranoside |
| OA | Operational amplifier |
| *ox* | Oxidizing species |
| pH | Negative logarithm of hydronium ion ($H_3O^+$) activity |
| PNP | *p*-Nitrophenol |
| PtNP | Platinum nanoparticles |
| PyOD | Pyruvate oxidase |
| *Q* | Number of coulombs |
| *R* | Resistance (Ω), Gas constant (8.317 J $mol^{-1}$ $K^{-1}$) |
| RE | Reference electrode |
| *red* | Reducing species |
| $RuO_x$ | Ruthenium oxide ($RuO_x$, x = 1, 2) |
| sec | Second |
| SEM | Scanning electron microscope |
| SPCE | Screen printed carbon electrode |
| SWV | Square wave voltammetry |
| *T* | Temperature (K) |
| TEM | Transmission electron microscope |
| TPP | Thiamine pyrophosphate |
| *U* | The volume flow rate ($cm^3$ $s^{-1}$) |

# LIST OF ABBREVIATIONS (CONTS.)

| | |
|---|---|
| Unit | Endo-α-N-acetylgalactosaminidase;<br>One unit is defined as the amount of enzyme that will catalyze the release of 1.0 μmol *p*-nitrophenol from *p*-nitrophenyl-2-acetamido-2-deoxy-3-*o*-(β-D-galactopyranosyl)-α-D-galactopyranoside per min at 37 °C, pH 5.0.<br><br>β-1,3-Galactosidase;<br>One unit is defined as the amount of enzyme that will cleave >95% of the β-D-galactose from 1 nmol Galβ1,3GlcNAcβ1,3Galβ1,4Glc-7-amino-4-ethylcoumarin in 1 h at 37 °C, pH 4.5 in a total volume of 10 μL. |
| UV-Vis | UV-Visible |
| V | Voltage (V) |
| vs. | Versus |
| WE | Working electrode |
| $z$ | Ion charge |
| $\gamma_{\pm}$ | Mean activity coefficient |
| $\Delta E$ | Potential difference across the electrode-solution interface |
| $\Delta E_e$ | Equilibrium potential different |
| $\Delta G_c^{\neq}$ | Activation energy for reduction |
| $\delta$ | Thickness of the diffusion layer |
| $v$ | Scan rate ($V\ s^{-1}$) |
| $v_{max}$ | The maximum enzyme velocity. |
| $\Delta\psi_p$ | Dimensionless current |
| $\gamma$ | The kinetic viscosity ($cm^2\ s^{-1}$) |

# THE RELEVANCE OF THE RESEARCH WORK TO THAILAND

Diabetes, cancer, and algae bloom or eutrophic phenomenon, are major diseases and problems of the rapid growth of the modern society. The release of phosphate ($PO_4^{3-}$) into the aquatic environment, low quality of foods and lack of necessary nutrients may lead to abnormal phenomena harmful to living organisms and human health. The parallel program with the Thai development plan is improving citizens' quality of life and monitoring the natural resources. The fast, robust electrochemical sensors of insulin, glycosidases, hydrogen peroxide ($H_2O_2$), and $PO_4^{3-}$ were considered as representative diagnostic or monitored tools to demonstrate the effectiveness and contribution of electrochemical research. They are relevant to Thailand for the following reasons.

(i) Insulin is an excreted pancreatic endocrine hormone for controlling body cells adsorbing and using glucose. Monitoring a patient’s diabetes with a cheap operation cost is necessary not only for Thailand but also worldwide.

(ii) Glycosidases are involved enzymes in the catabolism of glycoconjugates and its activities are of tremendous importance for cancer screening. Screening and alerting people with cancer cells early should be able to be carried out without complicated equipment.

(iii) $H_2O_2$ is an intermediate substance of enzymatic reactions. Wide applications of $H_2O_2$ based sensors for health care, industrial processes control, and environmental monitoring as well as bioreactors are known.

(iv) $PO_4^{3-}$ is a necessary nutrient for plants and animals. The excess of $PO_4^{3-}$ content in natural water resources can lead to eutrophic phenomenon. With simple and inexpensive sensor, monitoring $PO_4^{3-}$ content in natural water can be performed by local communities with minimum training.

Finally, knowledge about the design concepts and the operating mechanisms of these sensors is the first important key for developing new sensors, which will be applicable and suitable for Thai society.

PUBLICATIONS
Available online at www.sciencedirect.com
ScienceDirect
Analytica Chimica Acta 581 (2007) 1–6
ANALYTICA CHIMICA ACTA
www.elsevier.com/locate/aca

# Electrocatalytic detection of insulin at RuOx/carbon nanotube-modified carbon electrodes

Joseph Wang [a,*], Tanin Tangkuaram [a,b], Suchera Loyprasert [a,c], Terannie Vazquez-Alvarez [a], Waret Veerasai [b], Proespichaya Kanatharana [c], Panote Thavarungkul [c]

[a] *Departments of Chemical and Material Engineering, Chemistry and Biochemistry, The Biodesign Institute, Arizona State University, Tempe, AZ 85287-5801, USA*
[b] *Department of Chemistry, Mahidol University, Bangkok 10400, Thailand*
[c] *Department of Chemistry, Prince of Songkla University, Songkhla 90000, Thailand*

Received 29 May 2006; received in revised form 20 July 2006; accepted 31 July 2006
Available online 7 August 2006

**Abstract**

A bilayer surface coating, prepared by electrodepositing ruthenium oxide (RuOx) onto a carbon nanotube (CNT) layer, offers dramatic improvements in the stability and sensitivity of voltammetric and amperometric measurements of insulin compared to the individual (CNT or RuOx) coated electrodes. The enhanced electrocatalytic activity towards insulin is indicated from lowering the potential of the oxidation process (starting around 0.35 versus Ag/AgCl) and the substantially higher sensitivity over the entire potential range. A wide linear dynamic range (10–800 nM) was achieved with a detection limit of 1 nM. The marked electrocatalytic activity of the RuOx/CNT coating towards insulin is coupled with a greatly enhanced stability. For example, the insulin amperometric response of the RuOx/CNT-coated electrodes is highly stable, with 97% of the initial activity remaining after 60 min stirring of $2 \times 10^{-6}$ M solution (compared to significantly faster current diminutions at the RuOx- or CNT-coated surfaces). The results suggest great promise for miniaturized sensors and detectors for monitoring insulin.


*Keywords:* Insulin; Electrocatalysis; Carbon nanotubes; Ruthenium

## 1. Introduction

Insulin is a very important peptide hormone that is used to control glucose levels in blood within a narrow concentration range. Insulin-dependent type I diabetes is caused by the destruction of insulin-secreting beta cells of the pancreatic islets of Langerhans. Direct electrochemical measurements of insulin are of considerable interest in connection to the development of time-resolved in vivo sensors and chromatographic detectors for monitoring insulin secretion and therapeutic insulin formulations, respectively. However, such measurements are limited because of the slow kinetics of insulin oxidation at common electrode materials. Various chemically modified electrodes have thus been developed for promoting the oxidation and detection of insulin [1–9]. These include electrodes coated with inorganic films – based primarily on ruthenium [1–6] or iridium [7] electrocatalytic systems – or more recently surfaces coated with carbon nanotube (CNT) layers [8,9]. However, these electrocatalytic-modified electrodes still lack the specificity, sensitivity and stability essential for meeting the demands of practical monitoring and detection of insulin secretion [4].

Here we describe the development of a RuOx/CNT-modified carbon electrode that offers substantial improvements in the stability and sensitivity of voltammetric and amperometric measurements of insulin. Recent studies have illustrated that the electrocatalytic response of CNT-modified electrodes towards carbohydrate, peroxide or alcohol compounds can be greatly enhanced by coupling with catalytic metal centers (such as Cu or Pt) [10–12]. Similarly, the RuOx/CNT coating described in the present work offers marked acceleration of the insulin oxidation compared to the individual (RuOx and CNT) coated electrodes. The enhanced electrocatalytic activity leads to a substantial improvement in the sensitivity, and is coupled with a greatly enhanced stability. The results suggest great promise

* Corresponding author. Tel.: +1 480 727 0399.
*E-mail address:* joseph.wang@asu.edu (J. Wang).

0003-2670/$ – see front matter © 2006 Elsevier B.V. All rights reserved.
doi:10.1016/j.aca.2006.07.084

for miniaturized sensors for monitoring insulin secretion. Such advantages, along with detailed characterization and optimization of the RuOx/CNT-modified electrode, are reported in the following sections.

## 2. Experimental

### 2.1. Apparatus

Amperometric experiments were performed with a CHI 1030 Electrochemical Analyzer (CH Instruments, Austin, TX) in batch analysis and a μAutolab III analysis system with GPES software (Eco Chemie) in flow-injection analysis. The flow-injection system consisted of a carrier solution reservoir, an injection valve with a 200 μL sample loop, interconnecting PVC tubing, a peristaltic pump (Minipuls 3, Gilson, Inc., Middleton, WI), and a large-volume wall-jet amperometric flow detector. The glassy-carbon working electrode (3 mm diameter; CH Instruments), the Ag/AgCl reference electrode (CHI 111; CH Instruments), and the platinum wire counter-electrode were inserted into the detector through holes in its Teflon cover. A conventional electrochemical cell (2 mL), with the same three-electrode system, was used for voltammetric and amperometric batch experiments. Magnetic stirring was employed during the batch amperometric (stability) experiment.

Scanning electron microscopy (SEM) images of the modified electrodes were obtained with a FEI XL 60 EFSEM electron microscope. A gold film, sputtered on the electrode surface, provided an enhanced conductivity.

### 2.2. Reagents

All solutions were prepared from deionized water (PURELAB system, $R \geq 18.2\,M\Omega\,cm$). Insulin [from Bovine Pancreas; 28 USP units $mg^{-1}$, anhydrous (HPLC)], disodium hydrogen phosphate, sodium dihydrogen phosphate, sodium hydroxide, sodium chloride and 70% perchloric acid were purchased from Sigma. Hydrochloric acid and nitric acid were received from EMD Chemical Inc. (Gibbstown, NJ). *N*,*N*-Dimethylformamide was obtained from Aldrich. Ruthenium(III) chloride (99% $RuCl_3$) was purchased from Acros Organics N.V. (Fair Lawn, NJ). Multi-wall carbon nanotubes (CNT), with 95% purity, were obtained from NanoLab Inc. (Brighton, MA); further purification was accomplished by sonicating the CNT in concentrated nitric acid at 60 °C for 12 h. Stock solutions of insulin (0.40 mM) were prepared daily by dissolving powdered insulin in 0.02 M HCl. Further dilution was carried out using a 0.10 M NaCl/0.05 M phosphate buffer (pH 7.40) solution. The pH of the supporting electrolyte solution (7.40) was adjusted using NaOH and HCl. The total soluble insulin concentration was determined by measuring the absorption at 275 nm using a UV–vis recording spectrophotometer (UV-2501 PC, Shimadzu).

### 2.3. Electrode preparation

The glassy-carbon electrode (GCE) was polished to a mirror-like surface with 3 and 0.05 μm alumina slurries and was then sonicated for 5 min in water. The RuOx-modified GCE was prepared by electrodeposition of the RuOx film from a 0.30 mM $RuCl_3$/10 mM $HClO_4$ solution by cycling the potential between −0.80 and +0.65 V at 10 V $s^{-1}$ for 12.5 min. The electrode modification was initiated immediately after sonicating the $RuCl_3$ solution for 5 min.

CNT-modified GCE were prepared by dissolving the desired amount of CNT in 1 mL DMF, and sonicating the resulting CNT 'slurry' for 1 h. Then, 30 μL of the sonicated CNT 'slurry' (usually containing 2 mg $mL^{-1}$ CNT) was cast on the surface of the glassy-carbon disk. The electrode was allowed to dry at room temperature for 2 h.

The RuOx/CNT-modified GCE was prepared by a similar drop casting of CNT 'slurry' on the surface of the glassy-carbon disk, followed by electrochemical deposition of $RuCl_3$ using a 12.5 min potential cycling (in a manner described above). All modified electrodes were rinsed with deionized water before used.

### 2.4. Electroanalysis of insulin

Measurements were carried out in a 0.05 M phosphate buffer (pH 7.40) supporting electrolyte carrier solution containing 0.10 M NaCl. Amperometric detection was performed under flow-injection conditions using a flow rate of 1.0 mL $min^{-1}$. The desired working potential was applied, and transient currents were allowed to decay to a steady-state value. All measurements were performed at room temperature.

Batch amperometric experiments involved spiking 10 μL aliquot solutions of 0.40 mM insulin into a stirred solution of 0.05 M phosphate buffer (pH 7.40) containing 0.10 M NaCl at a fixed potential of +0.70 V. Cyclic voltammetric experiments were conducted after immersing the modified electrode in the supporting electrolyte solution for 30 min before scanning the potential. All raw experimental data were smoothed by using the adjacent averaging method ($n = 7$).

## 3. Results and discussion

Fig. 1 displays cyclic voltammograms (CV) at the RuOx-modified (a), CNT-modified (b) and RuOx/CNT-modified (c) glassy-carbon electrodes in the absence and presence of 72 μM insulin (dotted and solid lines, respectively). The three modified electrodes display a defined insulin oxidation peak. However, the onset of the insulin oxidation at the RuOx/CNT-coated GC electrode occurs at a substantially lower potentials (0.29 V), compared to its RuOx (0.67 V) and CNT (0.48 V) counterparts. The RuOx/CNT-modified electrode yields also a substantially higher sensitivity over the entire potential range (notice the different current scales; a versus b, c). Oxidation peak potentials of 0.83, 0.67 and 0.65 V are observed at the RuOx-, CNT- and RuOx/CNT-modified electrodes, respectively. A negligible reduction peak is observed in the reversed scan (around 0.35 V), indicating that the electrochemically generated product cannot be readily reduced in the potential range studied. While the anodic signal of the RuOx-modified surface reflects the mediated disulfide oxidation by the ruthenium in the film [4], the insulin

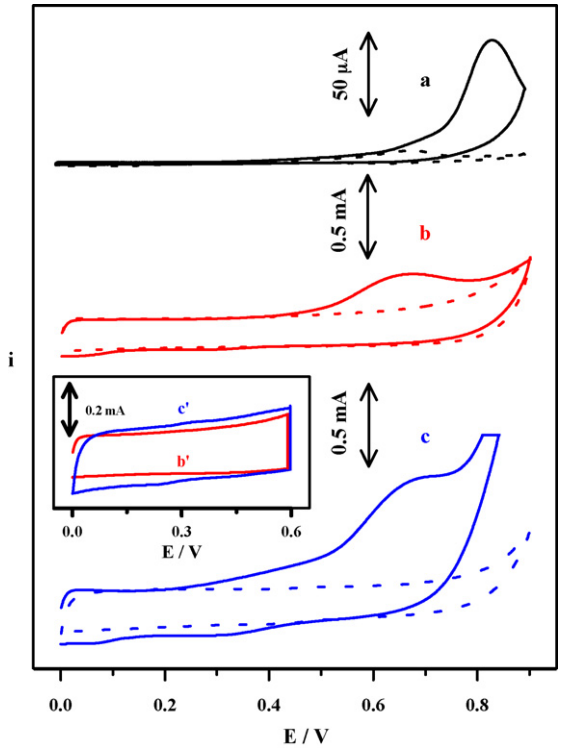


Fig. 1. Cyclic voltammograms recorded in blank (dotted line) and 72 μM insulin (solid line) solutions at the (a) RuOx, (b) CNT and (c) RuOx/CNT-modified GCE. Inset shows background current signals at the (b′) CNT and (c′) RuOx/CNT-modified GCE. Conditions: supporting electrolyte, 0.05 M phosphate buffer (pH 7.40) containing 0.10 M NaCl; scan rate 0.05 V $s^{-1}$.

response at CNT electrodes has been attributed to the accelerated oxidation of the tyrosine residues [11]. The exact nature of the insulin catalytic process at the RuOx/CNT-modified electrode is not fully understood at this stage. Such accelerated response is attributed to a synergistic enhancement, rather than a combination of the individual coatings or surface area effects. This is supported by the background cyclic voltammetric runs in the blank solution (shown in the inset of Fig. 1) that indicate a negligible change in the background current envelop, i.e., in the active surface area, upon depositing the RuOx layer onto the CNT film (b′ versus c′). The SEM data (reported below) also indicate minimal change in the surface area. It was shown earlier that the electrocatalytic properties of CNT towards other slow redox systems can be improved by coupling the CNT with catalytic metal centers [10–12]. We also conducted a control experiment, at the CNT-modified electrode, involving a potential scanning (similar to that employed for plating the RuOx) but without the $RuCl_3$. No apparent change in the insulin oxidation peak was observed, indicating that such potential cyclization has no effect upon the electrocatalytic behavior.

The synergy in the RuOx/CNT system is demonstrated also in Fig. 2 that depicts typical hydrodynamic voltammograms (HDV) for the oxidation of 0.8 μM insulin at the RuOx-modified (a), CNT-modified (b) and RuOx/CNT-modified (c) electrodes. The curves, developed pointwise (in steps of 0.1 V) over the 0.3–0.9 V range during a flow-injection operation, display the same trend as the cyclic voltammetric profiles. The three modified electrodes thus exhibit defined anodic signals with oxidation starting at 0.60 V (c), 0.50 V (b) and 0.40 V (c). These HDV indicate that the RuOx/CNT-coated electrode offers a greatly improved performance, with a substantially higher sensitivity over the entire potential range. Its current rises rapidly up to +0.70 V and decreases slightly above +0.80 V. The marked electrocatalytic activity towards insulin permits effective low-potential amperometric detection. The greatly improved low-potential detection of insulin offered by the RuOx/CNT surface is illustrated in the inset of Fig. 2 that depicts amperometric flow-injection response (at +0.50 V) of the RuOx-modified (a), CNT-modified (b), and RuOx/CNT-modified (c) electrodes to the 0.8 μM insulin solution. As expected from the HDV profile, the RuOx-coated electrode displays a negligible response to insulin at this potential. A defined response is observed at the CNT-modified electrode. An even (five-fold) larger peak is observed at the RuOx/CNT detector. As will be illustrated below, similar improvements can be obtained at significantly lower insulin concentrations, facilitating ultratrace measurements of this hormone.

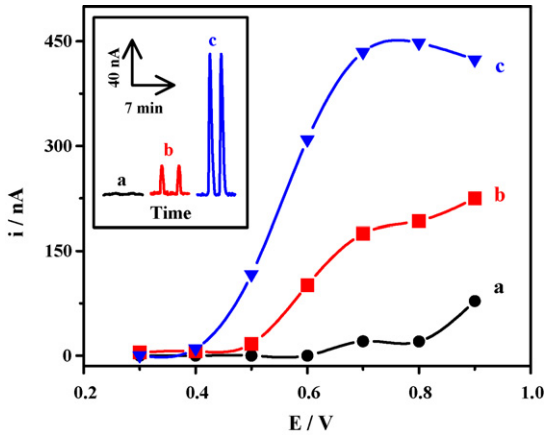


Fig. 2. Hydrodynamic voltammograms of 800 nM insulin using the (a) RuOx-modified, (b) CNT-modified and (c) RuOx/CNT-modified GCE. Also shown (inset) are the corresponding flow-injection peaks recorded at +0.50 V. Conditions: carrier/supporting electrolyte, 0.05 M phosphate buffer (pH 7.40) containing 0.10 M NaCl; sample loop, 200 μL; flow rate, 1.0 mL $min^{-1}$.

We examined different routes for preparing RuOx/CNT-modified electrodes. These include the entrapment of CNT during the electrodeposition of the RuOx film, and bilayers involving casting of CNT onto the RuOx film or growing the RuOx film on a CNT layer. The latter approach offered the most favorable results and was used in all subsequent work. The preparation of such RuOx/CNT bilayer film was optimized by systematically varying the volume of the cast CNT between 10 and 30 μL, and the electrodeposition time between 10 and 40 min in connection to a flow-injection operation. The most favorable insulin response was obtained using 30 μL CNT in connection to a 12.5 min electrodeposition.

The different modified electrodes were characterized by SEM. Fig. 3 compares SEM images of the bare (A) and the RuOx-modified (B), CNT-modified (C) and RuOx/CNT-modified (D) glassy-carbon electrodes. The micrograph of the RuOx-modified surface (B) shows spherical RuOx particles of

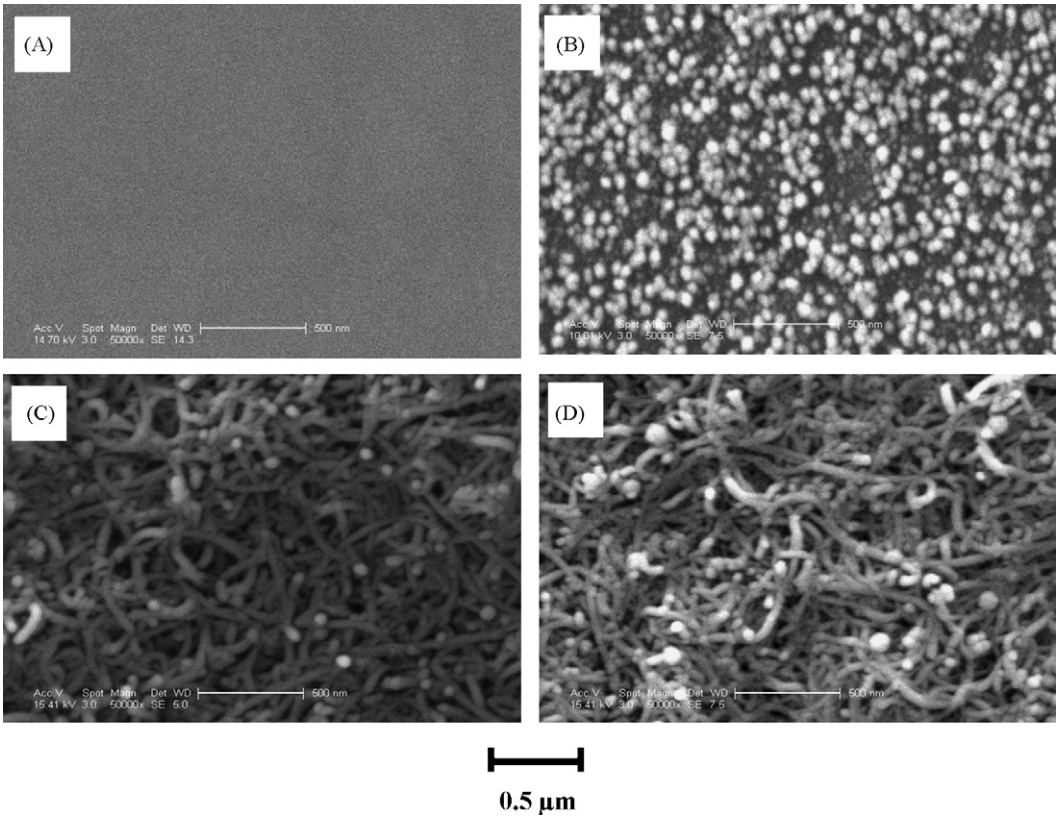


Fig. 3. SEM images of the surface of the bare (A), RuOx-modified (B), CNT-modified (C), and RuOx/CNT-modified (D) GCE. Scale, 0.5 μm; magnification, 50,000×; accelerating voltage, 14.7 kV (A), 10.01 kV (B) and 15.41 kV (C and D).

ca. 50 nm diameter, covering quite uniformly the glassy-carbon surface. As expected [13], casting the CNT on the carbon surface results in a highly porous layer comprising of interwoven tubes of ca. 40 nm diameter (C). The morphology of the RuOx/CNT-modified electrode is similar to that of the CNT electrode (D versus C), except of the presence of few non-uniformly dispersed ∼80 nm RuOx particles.

Owing to the limited lifetime of existing electroacatalytic insulin sensors (particularly those based on inorganic films), such devices cannot be used for routine in vivo monitoring of insulin secretion [9]. Such limited stability reflects the progressive fouling associated with the adsorption of the thiyl radicals products of the disulfide oxidation process associated with the anodic detection of insulin [14], and a reduced stability of inorganic mediators [9]. Recent studies have illustrated that CNT surface coatings impart higher stability onto amperometric insulin sensors [8,9]. A detailed investigation of the oxidation process at CNT-modified electrodes indicated a different reaction mechanism, proceeding through the tyrosine moieties [9]. As indicated in Fig. 4, the new RuOx/CNT-modified carbon electrode further enhances the operational stability compared to the CNT-coated surface. This figure compares the amperometric response for 2 μM insulin recorded over different time periods at the (a) RuOx-modified, (b) CNT-modified and (c) RuOx/CNT-modified GCE (notice the different time scales). The RuOx-modified electrode displays a sharp and rapid loss of the signal (of 55 and 100% current depressions after 50 and 100 s, respectively), indicating a complete passivation of the oxidation process. The CNT-coated electrodes retained more than 90% of the initial activity over the first 18 min of operation, but displayed a fast decay of the signal thereafter (to 55% of the initial response at 24 min). In contrast, the response of the RuOx/CNT-modified electrode remains highly stable

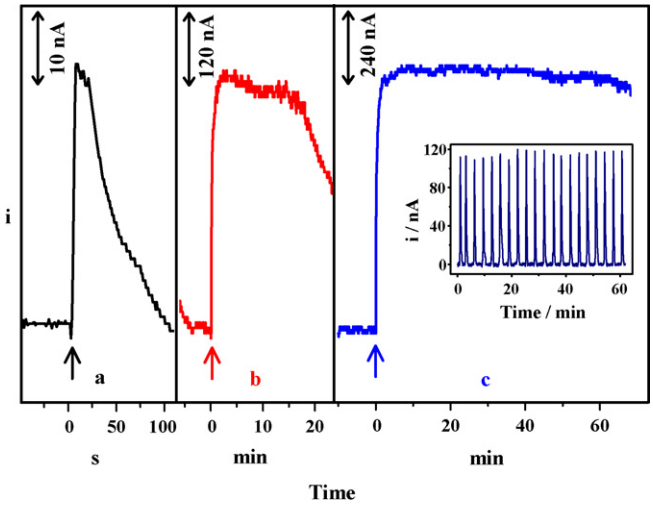


Fig. 4. Stability of amperometric response to 2 μM insulin at an applied potential of +0.70 V at (a) RuOx, (b) CNT and (c) RuOx/CNT-modified GCE in a stirred solution of 0.05 M phosphate buffer (pH 7.40) containing 0.10 M NaCl. Inset displays the flow-injection amperometric response of the RuOx/CNT-modified GCE to 20 successive injections of a 200 nM insulin solution (using the conditions of Fig. 2.).

throughout a significantly longer (1 h) operation, with only 1 and 3% current diminutions at 30 and 60 min, respectively. The high stability is illustrated also in the inset of Fig. 4C which depicts the reproducibility of the flow-injection amperometric response to 20 successive injections of a 200 nM insulin solution over a similar (60 min) period. This series yielded a stable response with a mean peak current of 115.5 nA, along with a relative standard deviation of 2.9%. CNT coatings have recently been shown useful for alleviating surface fouling associated with the electrogeneration of phenoxy radicals [15], such as those generated during the oxidation of the insulin tyrosine residues. We have yet to understand the higher resistance to fouling accrued from the coupling of RuOx with the CNT layer.

The attractive analytical performance of the RuOx/CNT electrode is demonstrated from the amperometric calibration data of Fig. 5. This figure displays flow-injection response peaks for increasing levels of insulin (10–800 nM, a–g). Well-defined current signals are observed for these nanomolar changes in the concentration of insulin. The response increases linearly with the concentration, as indicated from the corresponding calibration plot (also shown as inset; sensitivity, 541 nA $\mu M^{-1}$; correlation coefficient, 0.999). Peaks of Fig. 5 indicate convenient measurements of extremely low insulin concentrations. An additional experiment, described in Fig. 6, provided a closer examination of the response to the 10 nM insulin solution at the three modified electrodes. While the RuOx-modified electrode is not responding to this insulin concentration (a), a defined anodic peak is observed at the CNT-coated electrode (b). An even larger and sharper peak is observed at the RuOx/CNT-modified electrode (c). Note also the corresponding data (and absence of background peak) for a blank injection (dotted line). A low detection limit of around 1 nM can be estimated from the signal-to-noise characteristics (S/N = 3). Detection limits of 30 and 14 nM insulin were reported for CNT-modified electrodes [8,9]. Close examination of Fig. 6 indicates that the response time is not compromised by the bilayer coating. The RuOx/CNT

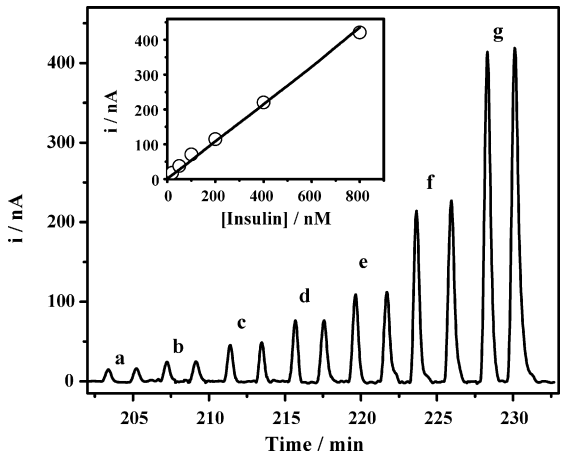


Fig. 5. Flow-injection amperometric response obtained at the RuOx/CNT-modified GCE held at +0.70 V, for increasing levels of insulin: (a) 10, (b) 20, (c) 50, (d) 100, (e) 200, (f) 400 and (g) 800 nM. Inset shows the corresponding calibration plot. Conditions, as in Fig. 2.

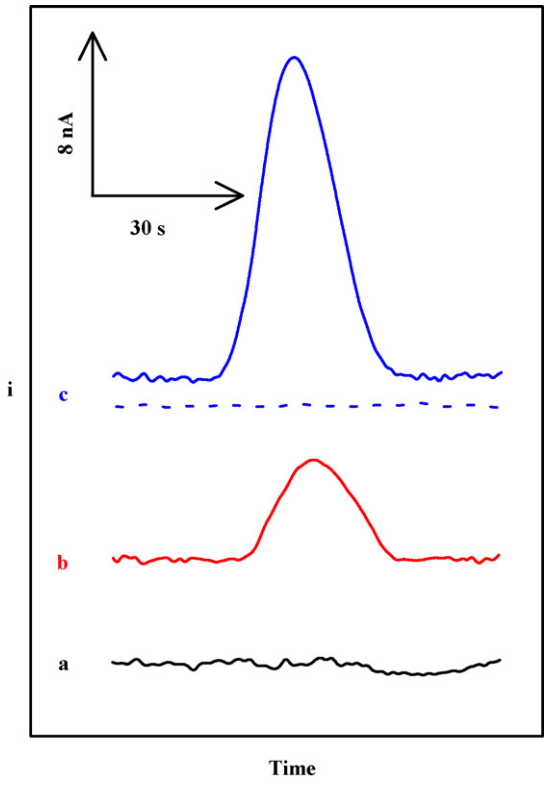


Fig. 6. Flow-injection amperometric response to 10 nM insulin at an applied potential of +0.70 V using the (a) RuOx-modified, (b) CNT-modified and (c) RuOx/CNT-modified GCE. The dotted line shows the flow-injection response for a blank injection at the RuOx/CNT-modified GCE. Other conditions, as in Fig. 2.

electrode displays similar peak widths and peak half widths as the CNT-modified electrode.

## 4. Conclusions

In summary, we have demonstrated that RuOx/CNT-modified electrodes exhibit greater electrochemical activity towards the oxidation of insulin compared to its RuOx and CNT counterparts. The observed improvements are attributed to synergistic enhancement rather the combination of the two individual layers. Current efforts in our laboratory, aimed at extending this approach to microscale-electrodes, involve the modification of carbon-fiber ultramicroelectrodes with the RuOx/CNT layer. Additional studies are required for understanding the unique behavior of RuOx/CNT-modified electrodes towards insulin. The greatly improved insulin detection indicates great promise for diabetes-related in vivo microsensors for monitoring insulin and chromatographic detectors for insulin.

## Acknowledgements

Financial support from the National Science Foundation (Grant no. CHE 0506529) and the National Institutes of Health (Award no. R01 EP 0002189) is gratefully acknowledged. TT, SL and TV wish to thank to fellowships of Thailand government

through the Maejo University, Thailand Research Fund through the Royal Golden Jubilee Ph.D. Program and Western Alliance to Expand Student Opportunities (WAESO), respectively. Jared Burdick is also acknowledged for assisting in the SEM imaging.

## References

[1] J.A. Cox, T. Gray, Anal. Chem. 61 (1989) 2462.
[2] W. Gorski, C.A. Aspinwall, J.R.T. Lakey, R.T. Kennedy, J. Electroanal. Chem. 425 (1997) 191.
[3] L. Cheng, G.E. Pacey, J.A. Cox, Anal. Chem. 73 (2001) 5607.
[4] R.T. Kennedy, L. Huang, M.A. Atkinson, P. Dush, Anal. Chem. 65 (1993) 1882.
[5] R.T. Kennedy, L. Huang, A.C. Aspinwall, J. Am. Chem. Soc. 118 (1996) 1795.
[6] A. Salimi, S. Pourbeyram, H. Haddadzadeh, J. Electroanal. Chem. 18 (2003) 39.
[7] M. Pikulski, W. Gorski, Anal. Chem. 72 (2000) 2696.
[8] J. Wang, M. Musameh, Anal. Chim. Acta 539 (2005) 209.
[9] M. Zhang, C. Mullens, W. Gorski, Anal. Chem. 77 (2005) 6396.
[10] J. Wang, G. Chen, M. Wang, M.P. Chatrathi, Analyst 129 (2004) 512.
[11] S. Hrapovic, Y.L. Liu, K.B. Male, J.H.T. Luong, Anal. Chem. 76 (2004) 1083.
[12] Z. He, J. Chen, D. Liu, H. Tang, W. Deng, Y. Kuang, Mater. Chem. Phys. 85 (2004) 396.
[13] N.S. Lawrence, R.P. Deo, J. Wang, Electroanalysis 17 (2005) 65.
[14] J. Pradac, J. Koryta, J. Electroanal. Chem. 17 (1968) 167.
[15] J. Wang, R.P. Deo, M. Musameh, Electroanalysis 15 (2003) 1830.

# Sensitive and rapid electrochemical bioassay of glycosidase activity

**Tanin Tangkuaram,[ab] Jared Q. Gerlach,[a] Yun Xiang,[a] Abdel-Nasser Kawde,[a] Zong Dai,[a] Veer P. Bhavanandan,[a] Jeffrey T. La Belle,[a] Waret Veerasai,[b] Lokesh Joshi*[a] and Joseph Wang*[a]**

***Received 26th April 2006, Accepted 27th June 2006***
***First published as an Advance Article on the web 6th July 2006***
**DOI: 10.1039/b605943k**

**Here we present a highly sensitive, rapid and simple electrochemical assay for glycosidases based on treatment of the glycosidase with the appropriate *p*-nitrophenyl glycoside and anodic detection of released *p*-nitrophenol. The attractive characteristics of the new bioassay should facilitate advanced glycomic research and routine clinical diagnostics since glycosidases are associated with various diseases.**

Advances in glycomics are discovering new and important glycan biomarkers. Glycosidases are an important class of enzymes that are involved in the catabolism of glycoconjugates and are indispensable for structural analysis of these complex molecules. These enzymes catalyze the hydrolysis of glycosidic bonds in simple glycosides, oligosaccharides, polysaccharides, glycoproteins and glycolipids. They are broadly classified as *exo*-glycosidases, which act on glycosidic linkages at the non-reducing end of the saccharide chains, and *endo*-glycosidases, which act on glycosidic linkages within saccharide chains.

The lack of a specific glycosidase can cause inherited metabolic disorders such as glycogen, glycosaminoglycan and glycolipid storage diseases.[1] Enzyme replacement therapy holds great promise for treating these diseases. Various glycosidases, including sialidase and α-*N*-acetylgalactosaminidase, are associated with tumor progression and can be used as reliable cancer markers.[2,3] Correlating the levels of glycosidases with the type and degree of cancer should lead to a better understanding of their clinical role. Accordingly, bioassays of glycosidase activities are of tremendous importance for diagnosing metabolic disorders, for cancer screening, and for glycomic research, in general.

Most current methods to determine the activity of glyco-active enzymes rely on colorimetric and/or radiological measurements.[4,5] Synthetic chromogenic substrates, such as 4-nitrophenyl (4-NP) and 4-methyl umbelliferyl (4-MU) glycosidases, are commonly used for optical assays of the activity of glycosidases.[4,5] Optical and radiological assays of glyco-active enzymes are time consuming, not amenable for kinetic activity assays, expensive and require extensive experimental set ups. Highly sensitive, rapid, simple and low-cost methods of glycosidase activity measurements are urgently needed to facilitate the detection of these important enzymes.

Here we describe a sensitive and rapid electrochemical bioassay for monitoring an exo- and an *endo*-glycosidase activity. Electrochemical devices are uniquely qualified for meeting the size, cost, low-volume, and power requirements of point-of-care diagnostics.[6] One common glycosidase, galactosidase, has been widely used as an enzyme label for electrochemical sandwich immunoassays.[7] Amperometric bioassays have been used earlier for measuring the activity of clinically important enzymes such as alkaline phosphatase[8] or alanine aminotransferase.[9] The new bioassay for glycosidase activity is based on the anodic detection of the enzymatically-generated *p*-nitrophenol from a fixed concentration of the corresponding glycoside substrate (Scheme 1).

Amperometric measurements were conducted using a CHI 1030 Electrochemical Analyzer (CH Instruments, Austin, TX) in a conventional three-electrode electrochemical cell (1.5 mL). The glassy carbon working electrode (3 mm diameter; CH Instruments), the Ag/AgCl(saturated KCl) reference electrode (CHI 111; CH Instruments), and the platinum wire counter-electrode were inserted into the cell through holes in a Teflon cover. Magnetic stirring was employed for all experiments. Optical absorbance measurements of the endo-α-*N*-acetylgalactosaminidase activity were performed using a SpectraMax M5 instrument (Molecular Devices, Sunnyvale, CA).

β-1,3-Galactosidase (*Escherichia coli*, recombinant), and *endo*-α-*N*-acetylgalactosaminidase (*Streptococcus pneumoniae*, recombinant, *E. coli*) were obtained from EMD Bioscience Inc. (La Jolla, CA, USA). 4-Nitrophenol-β-D-galactopyranoside (4-NP-β-Gal), citric acid monohydrate and sodium hydroxide were purchased from Sigma. Hydrochloric acid was received from EMD Chemical Inc. (Gibbstown, NJ, USA). *p*-Nitrophenyl-2-acetamido-2-deoxy-*O*-(β-D-galactopyranosyl)-α-D-galactopyranoside (4-NP-α-GalNAc-Gal) was obtained from Toronto Chemical Research Inc. (North York, ON, Canada). The 4-NP-β-Gal and 4-NP-α-GalNAc-Gal solutions (10 mM) were prepared by dissolving the

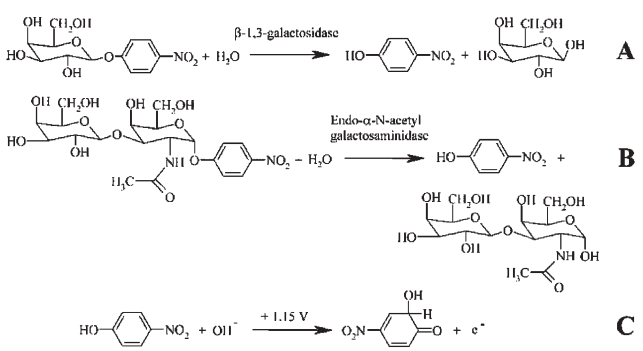


**Scheme 1** Enzymatic reactions of β-1,3-galactosidase (A) and *endo*-α-*N*-acetylgalactosaminidase (B), followed by the electrooxidation of the liberated *p*-nitrophenol on GCE at +1.15 V (C).

[a]*The Biodesign Institute and Fulton School of Engineering, Arizona State University, Tempe, AZ 85287-5801 E-mail: lokesh.joshi@asu.edu; joseph.wang@asu.edu*
[b]*Department of Chemistry, Faculty of Science, Mahidol University, Bangkok 10400, Thailand*

desired amount of each substrate in citrate buffer solution (pH 4.4). All other solutions were prepared using deionized water.

Amperometric experiments were performed at room temperature using 1.5 mL of a 0.05 M citrate buffer solution (pH 4.4) by monitoring the current continuously at an applied potential of +1.15 V. A given volume of the β-1,3-galactosidase or *endo*-α-*N*-acetylgalactosaminidase solutions was added to a stirred solution containing 133 μM of 4-NP-β-Gal or 200 μM of 4-NP-α-GalNAc-Gal, respectively, while recording the corresponding current *vs*. time curves.

Optical absorbance assays of *endo*-α-*N*-acetylgalactosaminidase were performed over the 0.2–1.0 mU $(1.5\ mL)^{-1}$ range. The 4-NP-α-GalNAc-Gal substrate solution (200 μM, 1.5 mL) was prepared in 0.05 M citrate buffer (pH 4.4). Negative controls were used as references for each set of reactions. Prior to incubation with enzymes, a 100 μL aliquot of the substrate solution was removed for use in the blank mixture. To the remaining 1.4 mL of substrate, an appropriate dilution of *endo*-α-*N*-acetylgalactosaminidase in 10 μL of 0.05 M citrate buffer (pH 4.4) was added and the mixture incubated at 37 °C with gentle mixing. At 10 minute intervals, a 100 μL aliquot of the reaction mixture was immediately transferred to a well in a 96-well polystyrene plate preloaded with 50 μL of 0.5 M $Na_2CO_3$ per well. After mixing, the absorbance was measured at 405 nm.

The new assay for glycosidases relies on the anodic detection of the enzymatically-generated *p*-nitrophenol in the presence of a fixed concentration of the corresponding glycoside substrate. Generally, 10 μL of the enzyme solution was added to 1.5 mL of the stirred 200 μM substrate solution. The anodic signal arising from the oxidation of the *p*-nitrophenol product is proportional to the activity of the enzyme (Scheme 1). Nitrophenol-sugar conjugates are widely available commercially and are one of the most common substrates for glycosidase assays; phenol products are commonly detected amperometrically in connection to alkaline-phosphatase or organophosphorus-hydrolase bioassays.

Variables of the new electrochemical assay, including the detection potential and substrate concentration, were examined and optimized. Fig. 1 displays the influence of the applied potential at the glassy carbon electrode upon the amperometric response of *p*-nitrophenol. While no response is observed at potentials lower than 0.95 V, the current rises rapidly between 0.95 and 1.15 V, and decreases slightly at higher potentials. Subsequent bioassays were thus carried out using a potential of 1.15 V. Additional electrode materials, including screen-printed carbon strips and carbon-nanotube-modified glassy carbon electrodes were examined, but displayed inferior *p*-nitrophenol responses (not shown).

Fig. 2 shows the influence of the 4-NP-β-Gal substrate concentration upon the response for 10 U β-1,3-galactosidase over the 5–200 μM 4-NP-β-Gal range (a–e). For all substrate concentrations the response increases linearly with the time at first and then more slowly. The current response at 60 s was found to be proportional to the substrate concentration (see inset for the corresponding linear plot).

The optimized bioassay offers sensitive and rapid detection of glyco-active enzymes. Fig. 3 displays amperometric current–time tracings recorded upon adding different levels of β-1,3-galactosidase (A) and *endo*-α-*N*-acetylgalactosaminidase (B). The amperometric current starts to increase upon adding the enzyme (see arrow), reflecting *p*-nitrophenol production and oxidation. As expected,[10] the shape of these amperograms depends on the enzyme activity. As the concentration of the enzyme increases the observed curvature is shifted in the direction of shorter time periods. A sharp initial current rise (within the first 10 s) is also observed in the case of the *endo*-α-*N*-acetylgalactosaminidase. Such profiles allow convenient quantitation of the enzymatic activity. For example, measuring the response 60 s after adding the enzymes results in highly linear current–activity dependence over the entire range [see insets for the corresponding calibration plots; correlation coefficients, 0.978 (A) and 0.981 (B)]. Note also the substantially higher sensitivity towards *endo*-α-*N*-acetylgalactosaminidase that facilitates convenient measurements of mU levels (*vs*. U ones for the β-1,3-galactosidase). A detection limit of 200 μU can thus be estimated in connection to

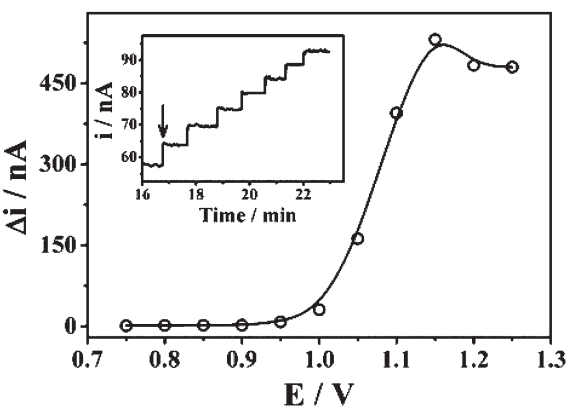


**Fig. 1** Hydrodynamic voltammogram for the oxidation of 10 μM *p*-nitrophenol (PNP) at a glassy carbon electrode (GCE); $n = 1$. Inset shows the amperometric response ($E = +1.15$ V) to successive additions of 0.1 μM PNP in a stirred 1.5 mL 0.05 M citrate buffer solution (pH 4.4).

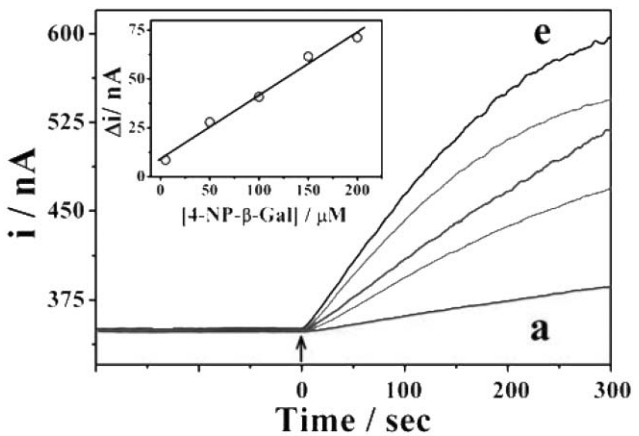


**Fig. 2** Amperometric responses of successive additions of (a) 5, (b) 50, (c) 100, (d) 150 and (e) 200 μM of 4-NP-β-Gal at GCE into a 1.5 mL stirred 0.05 M citrate buffer solution (pH 4.4) containing 10 U of β-1,3-galactosidase. Inset shows the corresponding calibration plot based on measuring the current 60 s after adding the 4-NP-β-Gal. Other conditions, as in the inset of Fig. 1.

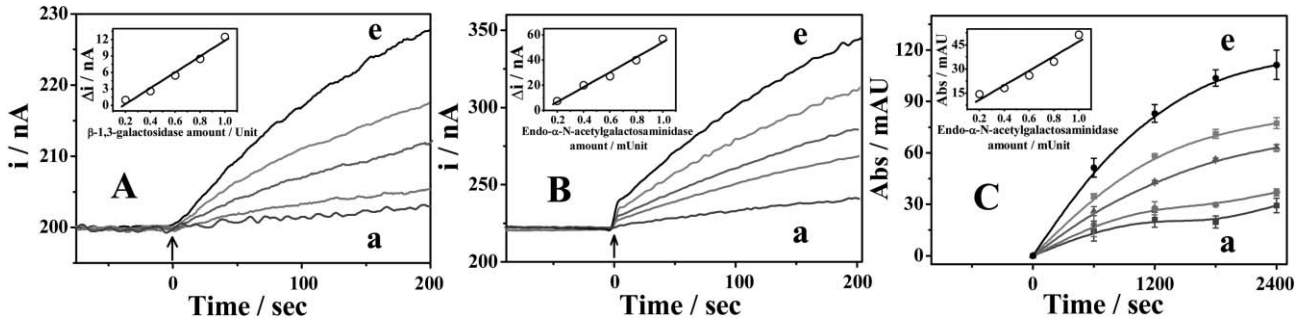


**Fig. 3** (A) Amperometric responses of 0.2 U successive additions from 0.2 (a) to 1.0 U (e) of β-1,3-galactosidase at GCE in a 1.5 mL of stirred solution of 133 μM of 4-NP-β-Gal. (B) Amperometric responses of 0.2 mU successive additions of *endo*-α-*N*-acetylgalactosaminidase from 0.2 (a) to 1 mU (e) at GCE in a 1.5 mL of stirred 0.05 M citrate buffer solution containing 200 μM of 4-NP-α-GalNAc-Gal. (C) Absorbance of released PNP by action of 0.2 (a) to 1.0 mU (e) of *endo*-α-*N*-acetylgalactosaminidase on 1.5 mL citrate buffer solution containing 200 μM of 4-NP-α-GalNAc-Gal substrate. End-point data were collected by measuring absorbance at 405 nm. Reaction samples were collected at 0, 600, 1200, 1800, and 2400 s. Insets (A and B) show the corresponding calibration plots after a 60 s enzymatic reaction. Other conditions, as in Fig. 2. Inset C shows the optical calibration plot using a 600 s reaction time.

short reaction times of 20–40 s (Fig. 3B, a). Such a detection limit corresponds to 49 fmol in the 1.5 mL solution. In contrast, in the standard optical assay[4] the detection of 400 μU *endo*-α-*N*-acetylgalactosaminidase required significantly longer (600 s) incubation time (Fig. 3C). Further, the assay measures only end-point results and does not provide real-time measurements.

We describe a simple and low-cost electrochemical assay for monitoring glycosidase activity, which couples high sensitivity with a fast response. Current efforts aim at developing reagentless microsensors (based on a surface confined substrate and different disposable electrode materials) for routine point-of-care clinical applications.

This research was supported by grants from the National Science Foundation (Grant number CHE 0506529), from the National Institutes of Health (Award Numbers R01A 1056047-02 and R01 EP 0002189), The Wallace Research Foundation and The Biodesign Institute at Arizona State University.

## Notes and references

1 K. Kodama, H. Kobayashi, R. Abe, A. Ohkawara, N. Yoshii, S. Yotsumoto, T. Fukushige, Y. Nagatsuka, Y. Hirabayashi and T. Kanzaki, *Br. J. Dermatol.*, 2001, **144**, 363.
2 T. Miyagi, T. Wada, K. Yamaguchi and K. Hata, *Glycoconjugate J.*, 2004, **20**, 189.
3 S. B. Mohamad, H. Nagasawa, Y. Uto and H. Hori, *Comp. Biochem. Physiol. A: Mol. Integr. Physiol.*, 2002, **132**, 1.
4 J. Umemoto, K. L. Matta, J. J. Barlow and V. P. Bhavanandan, *Anal. Biochem.*, 1978, **91**, 186.
5 J. Lo, K. Mukerji, Y. C. Awashthi, E. Hanada, K. Suzuki and K. Srivastava, *J. Biol. Chem.*, 1979, **254**, 6710.
6 J. Wang, *Trends Anal. Chem.*, 2002, **21**, 226.
7 J. Thomas, S. Kim, P. Hesketh, H. B. Halsall and W. R. Heineman, *Anal. Biochem.*, 2004, **328**, 113.
8 R. E. Gyurcsanyi, A. Bereczki, G. Nagy, M. R. Neuman and E. Lindner, *Analyst*, 2002, **127**, 235.
9 J. M. Cooper, C. J. McNeil and J. A. Spoors, *Anal. Chim. Acta*, 1991, **245**, 57.
10 G. Nagy, X. Xu, R. P. Buck, E. Lindner and M. R. Neuman, *Anal. Chem.*, 1998, **70**, 2156.

Available online at www.sciencedirect.com
ScienceDirect
Biosensors and Bioelectronics 22 (2007) 2071–2078
BIOSENSORS & BIOELECTRONICS
www.elsevier.com/locate/bios

# Design and development of a highly stable hydrogen peroxide biosensor on screen printed carbon electrode based on horseradish peroxidase bound with gold nanoparticles in the matrix of chitosan

Tanin Tangkuaram *, Chatchai Ponchio, Thippayawadee Kangkasomboon, Panadda Katikawong, Waret Veerasai *

*Department of Chemistry, Faculty of Science, Mahidol University, Bangkok 10400, Thailand*

Received 2 May 2006; received in revised form 17 August 2006; accepted 6 September 2006
Available online 13 October 2006

**Abstract**

The design and development of a screen printed carbon electrode (SPCE) on a polyvinyl chloride substrate as a disposable sensor is described. Six configurations were designed on silk screen frames. The SPCEs were printed with four inks: silver ink as the conducting track, carbon ink as the working and counter electrodes, silver/silver chloride ink as the reference electrode and insulating ink as the insulator layer. Selection of the best configuration was done by comparing slopes from the calibration plots generated by the cyclic voltammograms at 10, 20 and 30 mM $K_3Fe(CN)_6$ for each configuration. The electrodes with similar configurations gave similar slopes. The 5th configuration was the best electrode that gave the highest slope.

Modifying the best SPCE configuration for use as a biosensor, horseradish peroxidase (HRP) was selected as a biomaterial bound with gold nanoparticles (AuNP) in the matrix of chitosan (HRP/AuNP/CHIT). Biosensors of HRP/SPCE, HRP/CHIT/SPCE and HRP/AuNP/CHIT/SPCE were used in the amperometric detection of $H_2O_2$ in a solution of 0.1 M citrate buffer, pH 6.5, by applying a potential of −0.4 V at the working electrode. All the biosensors showed an immediate response to $H_2O_2$. The effect of HRP/AuNP incorporated with CHIT (HRP/AuNP/CHIT/SPCE) yielded the highest performance. The amperometric response of HRP/AuNP/CHIT/SPCE retained over 95% of the initial current of the 1st day up to 30 days of storage at 4 °C. The biosensor showed a linear range of 0.01–11.3 mM $H_2O_2$, with a detection limit of 0.65 μM $H_2O_2$ (S/N = 3). The low detection limit, long storage life and wide linear range of this biosensor make it advantageous in many applications, including bioreactors and biosensors.


*Keywords:* Screen printed carbon electrode; Chitosan; Gold nanoparticles; Electrodeposition; $H_2O_2$ biosensors

## 1. Introduction

Screen-printing technology is a technique often used in the fabrication of electrodes for the development of disposable electrochemical biosensors. A screen printed electrode is a planar device based on multiple layers of printed inks on a polyimide (Nagata et al., 1995), plastic (Miserere et al., 2006), epoxy (Zhang et al., 2001) or alumina ceramic (Ledru et al., 2006) substrates. The advantages of designable techniques, adapted from microelectronics, have made screen-printing technology one of the most important for fabrication of single-use biosensors in the market of handheld instruments. The main advantages of the screen printed electrode include simplicity, versatility, modest cost, portability, ease of operation, reliability, small size and mass production capabilities, leading to its development in various applications in the electroanalytical chemistry field.

Hydrogen peroxide ($H_2O_2$) is an enzymatic intermediate substance of many enzyme-substrate reactions. Determination of hydrogen peroxide has been reported by many methodologies, e.g. UV–vis spectroscopic, fluorescence, chemiluminescence, acoustic emission and electrochemical techniques. The most common electrochemical technique investigated is via the anodic oxidation of $H_2O_2$ at a platinum metal electrode (Clark, 1979), metal-dispersed carbon paste electrodes (Wang et al.,

* Corresponding authors. Tel.: +66 2 2015168; fax: +66 2 3547151.
*E-mail addresses:* pengtangkua@yahoo.com (T. Tangkuaram), scwvr@mahidol.ac.th (W. Veerasai).

0956-5663/$ – see front matter © 2006 Elsevier B.V. All rights reserved.
doi:10.1016/j.bios.2006.09.011

1992) and a platinized sputtered glassy carbon electrode (Zhang et al., 1996); however, a main problem occurs from the high overpotential and subsequent interference from matrix species. This problem has been minimized by using the cathodic reduction of $H_2O_2$ by use of enzyme-linked osmium bipyridine redox wired polymers (Vreeke et al., 1995), Nafion-methylene blue composite (Liu et al., 1996), prussian blue and derivatives (O'Halloran et al., 2001; Ricci et al., 2003; Tseng et al., 2005), carbon nanotube-cobalt hexacyanoferrate/chitosan composite (Yang et al., 2006a), mediated electron transfer of horseradish peroxidase (HRP) by hydroquinone (Delvaux et al., 2004) and via direct electron transfer (DET) of the third generation of biosensors by HRP (Lindgren et al., 2000; Kong et al., 2003; Jia et al., 2005). The DET method is used often in the fabrication of $H_2O_2$ biosensor. It easily facilitates the electron transfer between the enzyme and electrode surface and makes a more sensitive and convenient environment for the electrochemical biosensor.

In recent years, nanotechnology, including nanoparticles, nanotubes, nano-quantum dots and nanowires, has been used in various applications. This is owed to the essential properties of high chemical and thermal stability, surface to volume ratio, elasticity, and tensile strength. These properties along with the metallic conductivity exhibited by some nanotechnology, allow for their use as functional components in the fabrication of medical sensing devices (Vo-Dinh et al., 2001). In the field of electroanalytical chemistry, gold nanoparticles (AuNP) have attracted enormous interest in the application of hydrogen peroxide determination (Gu et al., 2001; Liu and Ju, 2002; Zhang and Oyama, 2004), lactate determination (Gu et al., 2004), glucose determination (Zhang et al., 2005; Yang et al., 2006b), protein functionalization (Abad et al., 2005), DNA determination (Cai et al., 2001) and antigen determination (Wang et al., 2004). The AuNP assist in constructing an interface for direct electron transfer of redox-active proteins while retaining their bioactivity. The AuNP provide a natural environment for bimolecular immobilization allowing for longer life stability. Colloidal Au has gained much more attention in electroanalytical studies because of its unique properties such as easy preparation, good biocompatibility and relatively large surface area.

CHIT is a polysaccharide consisting of the functional groups –OH and $–NH_2$, and possessing many properties such as good film-forming ability, chemical inertness, high mechanical strength, high hydrophilicity and biocompatibility (Kumar, 2000). There have been several reports of CHIT used as an immobilization matrix by cross-linking with enzymes through glutaraldehyde or other substances. This form of enzyme-CHIT is often manually coated on electrode surfaces to fabricate biosensors. As is known, covalent cross-linking of enzymes may lead to partial loss of enzyme activity and manual coating of electrodes may result in uncontrollable thickness of films. Thus the selective depositing method for creating films with controllable thickness and a comfortable microenvironment for enzyme activity is very important. It has been reported that CHIT hydrogel can be electrochemically deposited onto electrodes and other substances, such as gold nanoparticles (Luo et al., 2005; Zhang et al., 2005). Enzymes can also be effectively incorporated into the sol–gels to form biocomposites during the electrodeposition while retaining their natural properties. In the literature there is no report of screen printed electrode design. The electrode configuration is a very important role that affects the reaction potential of substances on electrode surfaces. In this report we wish to: (1) design and develop a screen printed carbon electrode that gives the highest performance and (2) use the electrodeposition of CHIT to avoid the uncontrolled thickness of CHIT on the surface of the designated SPCE assembled with HRP/AuNP for determination of enzymatic intermediate substances.

## 2. Experimental

### 2.1. Reagents

Horseradish peroxidase (HRP, EC 1.11.1.7, type XII), chitosan (CHIT, from crab shells, medium molecular, 85% deacetylated), $KH_2PO_4$, $NaH_2PO_4$, citric acid monohydrate, gold chloride ($HAuCl_4$), HCl, and NaOH were purchased from Sigma. All solutions were prepared using deionized water purified with a Millipore system ($R \geq 18.2\,M\Omega\,cm$).

### 2.2. Screen printed equipment

Homemade screen printed frames were designed in six configurations (Fig. 1A) by a silk screen pattern with CAD/CAM software. Carbon, silver and silver/silver chloride inks were obtained from Acheson Inc. (Netherlands), while the insulator ink was obtained from Chaiyaboon Co. (Thailand). The electrodes were screened in four layers by hand on the polyvinyl chloride (PVC) sheet, 48 cm long, 18 cm wide and 0.4 mm thick. Using the designated template for each ink, the first layer was applied with an Ag ink as the conductive wire. The carbon ink was then screened as the working and counter electrodes. Then the Ag/AgCl ink was screened as the reference electrode. Finally the layer of insulator was printed using the pattern to define the electrode area. Each layer was subsequently cured for 1 h at 60 °C and allowed to cool in desiccators to avoid any reaction with oxygen. The six configuration electrodes were cut into a single electrode before use.

### 2.3. Apparatus

An AUTOLAB-30 electrochemical analyzer was used to carry out the cyclic voltammetric and amperometric measurements. In all cases, a screen printed carbon electrode with three electrodes was employed, consisting of a carbon electrode serving as working and counter electrodes and pseudo Ag/AgCl serving as the reference electrode. The reaction cell volume of $4\,cm^3$ was used for electrochemical experiments at room temperature (25 °C).

UV–visible spectrophotometry (UV–vis, Shimadzu UV-2501PC) was selected for preliminary size analysis of AuNP. The transmission electron microscope (TEM, Hitachi H-300) was used to capture the morphology of AuNP. The size charac-

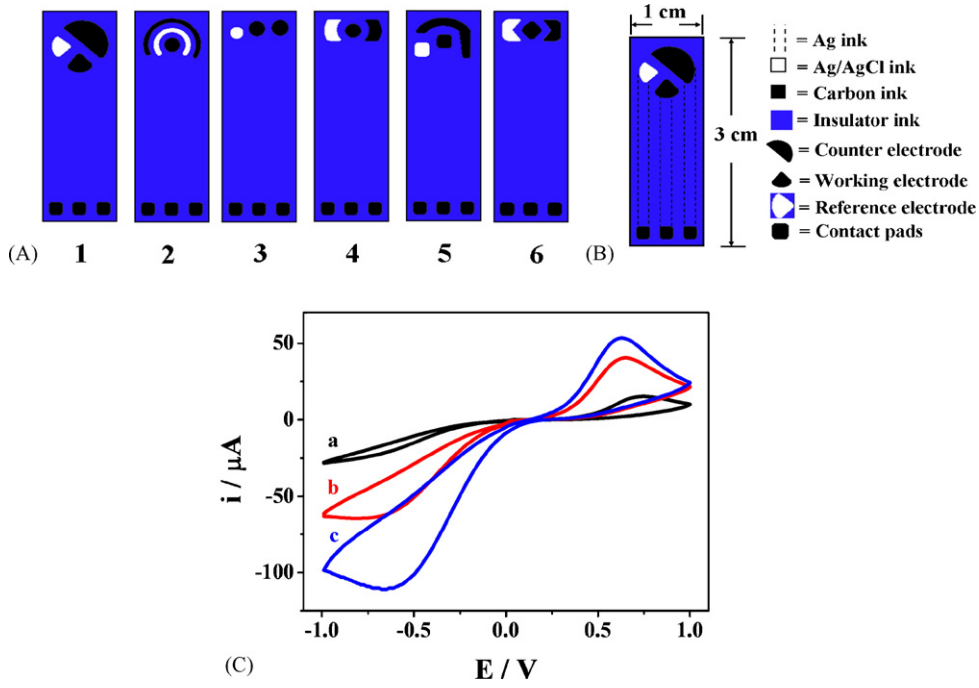


Fig. 1. (A) Six configurations of screen printed carbon electrodes and (B) the electrode construction of the 1st configuration. The other configurations are arranged in a similar manner, with the working electrode in the center. (C) Cyclic voltammograms of the 1st configuration SPCE in 10 mM (a), 20 mM (b) and 30 mM $K_3Fe(CN)_6$ (c). Condition: scan rate 100 mV $s^{-1}$.

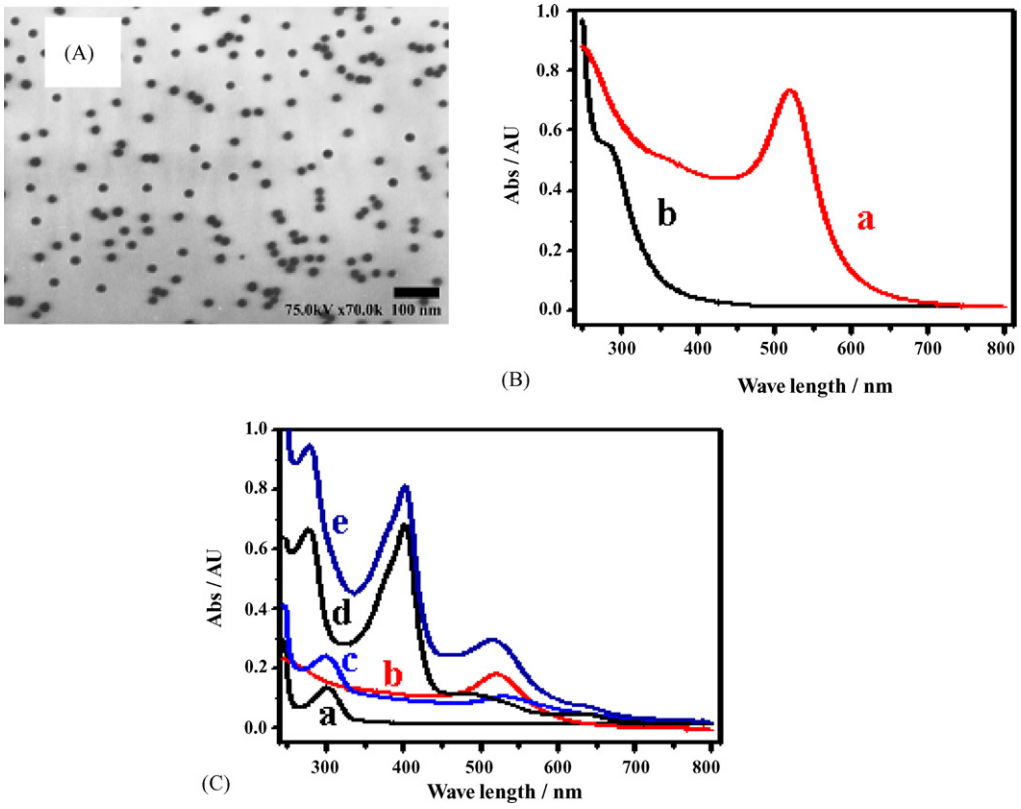


Fig. 2. (A) TEM photograph of AuNP; (B) UV–vis spectra of solutions of 1.7 nM AuNP (a) and $HAuCl_4$ (b); (C) UV–vis spectra of solutions of CHIT (a), 0.8 nM AuNP (b), mixed of AuNP–CHIT (c), HRP (d) and mixed of HRP/AuNP/CHIT (e).

terization of AuNP was determined using Carl Zeiss software (KS300).

### 2.4. CHIT–AuNP preparation

CHIT solutions were prepared by adding 1 g CHIT flakes, as received, to 60 mL water with stirring and gradually adding concentrated HCl to the solution to maintain the pH near 3 until complete dissolution. The undissolved material was filtered then the pH was gradually adjusted to 5.0 using 1.0 M NaOH. This clear and colorless filtrate's volume was adjusted to make 100 mL of a 1% CHIT stock solution. The CHIT stock solution was kept at 4 °C when not in use.

The AuNP were synthesized according to Neiman et al. (2001) with slight modification. Briefly, 10 mL of a 0.01% Au solution was heated to 125 °C and 340 μL of a 0.01% sodium citrate was added with continuous heating for 30 min while the color of solution changed to brownish red. The solution was left to cool at room temperature. The AuNP particles had a size of 16.8 nm as shown in Fig. 2(A) with a UV–vis spectrum peak at 521 nm as shown in Fig. 2(B, a).

### 2.5. Modification of electrodes

The high quality SPCE was rinsed with DI water before use. The mixed solution of HRP (3 mg/mL), AuNP (0.8 nM) and CHIT (0.1%) in DI water was scanned with the UV–vis spectroscopy. The SPCE was dipped into the mixed solution while a fixed potential of −2.0 V was applied to the working electrode for the desired time. The CHIT was deposited with HRP and AuNP embedded on the electrode surface simultaneously as Scheme 1 with continuous $H_2$ gas bubbling. The electrode was then removed from the mixed solution and cleaned with DI water and kept at 4 °C when not in use.

### 2.6. Electroanalysis of biosensor

The amperometry was employed at the HRP/AuNP/CHIT/SPCE biosensor at $E_{applied} = -0.4$ V, the desired amount of $H_2O_2$ was spiked into a stirred solution of citrate buffer solution pH 6.5.

## 3. Results and discussion

### 3.1. The design of screen printed carbon electrode

SPCEs were designed in many configurations based on theoretical concept. The working electrode should be small for complete polarization of the electroactive species. The reference electrode should be as close as possible to the working electrode to maintain the stability of the potential by minimizing the effect of resistance between the WE and RE. Finally, the counter electrode should be of larger size than the others to allow unlimited current transfer in the circuit, the designed SPCEs were shown in Fig. 1A and B. To investigate whether the configuration of the SPCE affects the reaction of the electroactive material, cyclic voltammetric techniques were performed on the six different SPCE configurations in 10, 20 and 30 mM $K_3Fe(CN)_6$.

All six electrodes show poor reversibility with a large $\Delta E_p$ (from 1.1 to 1.4 V) and did not have a current ratio of unity. They also show small charge transfer with low sensitivity, 0.23 to 0.35 μA/mM for oxidation and −0.69 to −0.85 μA/mM for reduction reaction (data not show). These results agree with Morrin et al. (2003) and are due to the material resistance affecting electron transfer from the electrode surface to the conductive pads. It is hypothesized that the use of silver as conducting tracks might enhance the charge transfer. However, while in our study the use of silver tracks does improve the charge transfer, the slow electron transfer phenomena still exists. We have examined the affect of 0.1 M KCl as a supporting electrolyte on the peak potential and current. It influenced the $\Delta E_p$ closer to 0.6 V by increasing the current by 1.8 and 1.5 times for the oxidation and reduction currents, respectively.

Fig. 1C shows the cyclic voltammograms for the 1st configuration of SPCE. A pair of well-defined peaks for 20 mM $K_3Fe(CN)_6$ is seen at 0.63 and −0.77 V ($\Delta E_p = 1.40$ V). The peak potential is shifted slightly towards zero as the concentration of $K_3Fe(CN)_6$ is increased. The second SPCE configuration exhibits very high errors for the current measurements for electrode-to-electrode repetition. In this configuration the electron movement between the WE and CE is impeded by the RE due to its placement completely between the WE and CE. The remaining electrode configurations do not have this

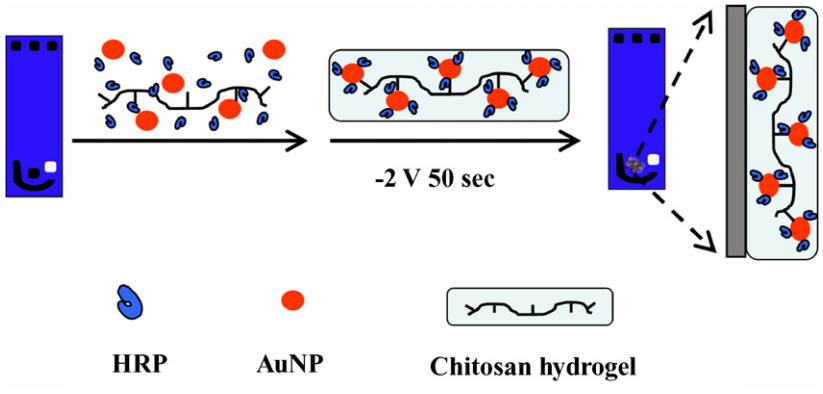


Scheme 1. Preparation of HRP/AuNP/CHIT/SPCE.

problem, and they show a significantly small value of deviation. The SPCEs having similar configurations 3, 4 and 6, show very similar responses and high reproducibility. The slopes of the corresponding calibration curves of current versus concentration of $K_3Fe(CN)_6$ were compared to select the best SPCE configuration. The most sensitive and reproducible SPCE was the 5th configuration. The sensitivity of the 5th configuration is ascribed to the larger size of the counter electrode, which does not hinder the large amount of ions passing through the electrodes. The 5th configuration was used in all of the following experiments. The response of this electrode showed linearity to the square root of the scan rate versus current in the range of 10–200 mV $s^{-1}$ in 20 mM $K_3Fe(CN)_6$ implying that it is a diffusion controlled process.

### 3.2. Preparation of HRP/AuNP/CHIT

The AuNP were synthesized by reducing $HAuCl_4$ in trisodium citrate. The size and photometric adsorption properties of AuNP were examine by TEM and UV–vis shown in Fig. 2A and B, respectively. The AuNP were very homogeneous with the size of 16.8 nm (Fig. 2A). The concentration of AuNP was calculated at 1.7 nM in agreement with the literature (Luo et al., 2005). The UV–vis spectra of the synthesized AuNP shows a peak at 521 nm (Fig. 2B, a) with agreement with Na-citrate reduction methods (Neiman et al., 2001) while the $HAuCl_4$ solution shows a peak at 282 nm (Fig. 2B, b). These results demonstrate that the AuNP have good homogeneous particles in the nano size range (Khanna et al., 2005). The size of AuNP is very sensitive to the synthesis temperature. The Au particles, when synthesized without heat, have a reddish purple color, but they became a brownish red color after heating. The TEM image was not homogeneous and the UV–vis spectrum has a weak absorbance around 530 nm (data not show).

The UV–vis spectrum of the CHIT (Fig. 2C, a) solution exhibits a peak at 305 nm while the AuNP peak is at 521 nm (Fig. 2C, b). When mixed with AuNP solution there is a slightly broad peak at 620 nm (Fig. 2C, c), which may be due to less aggregation of the AuNP with the biomolecule, a suppressed peak for AuNP at 521 nm, while the CHIT still exhibits a distinct peak at 305 nm. The UV–vis spectrum of HRP (Fig. 2C, d) has very high absorption peaks at 278 and 403 nm (Lu et al., 2006). The spectrum of the mixed solution of HRP/AuNP/CHIT (Fig. 2C, e) is distinct with the peaks of HRP and AuNP, while the peak of CHIT is covered by the HRP peak. One point should be highlighted that there is an increased absorption peak at about 643 nm (higher than Fig. 2C, b), which may be due to more aggregation of the AuNP with the CHIT and HRP molecules (Luo et al., 2004).

### 3.3. Optimization of $H_2O_2$ biosensor

#### 3.3.1. Effect of HRP/AuNP/CHIT/SPCE to electrocatalytic reduction of $H_2O_2$

The $H_2O_2$ biosensor was studied with four modifications of CHIT/SPCE, HRP/SPCE, HRP/CHIT/SPCE and HRP/AuNP/CHIT/SPCE shown in Fig. 3. To avoid the blocking

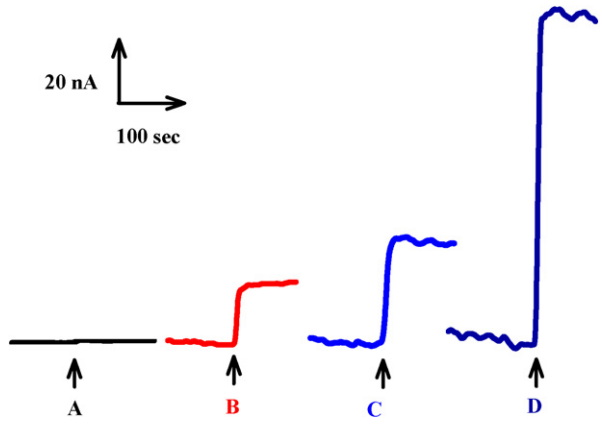


Fig. 3. Amperometric response of one 500 μM $H_2O_2$ addition at CHIT/SPCE (A), HRP/SPCE (B), HRP/CHIT/SPCE (C) and HRP/AuNP/CHIT/SPCE (D) ($E_{applied} = -0.4$ V) into a stirred solution of 0.1 M citrate buffer, pH 6.5.

of $O_2$ from electrocatalytic oxidation, the electrocatalytic reduction of $H_2O_2$ to $H_2O$ was selected. The CHIT was immobilized on the SPCE by electrodeposition where the CHIT hydrogel film was visible on the electrode surface after immobilization. The amperometric response at −0.4 V of the CHIT/SPCE (Fig. 3A) shows a very low sensitivity. Many reports show that HRP is easily modified on the electrode surface, so we immobilized HRP by immersing the SPCE in a solution of 3 mg/mL HRP for 1 h. The amperometric response of the HRP/SPCE (Fig. 3B) increased immediately with $H_2O_2$ spiking. It has also been reported that CHIT can be immobilized with HRP, so we modified CHIT with HRP to fabricate a very stable film, and improve the amperometric response of $H_2O_2$. The response of HRP/CHIT/SPCE to spiking with $H_2O_2$ was achieved and, as shown in Fig. 3C, is 1.8 times higher than the HRP/SPCE. One advantageous property of CHIT is that when the pH is slightly basic, the CHIT becomes a solid phase, allowing for simple electrodeposition through application of a potential (Wu et al., 2002). This technique is easily adaptable to include the deposition of AuNP and HRP. The amperometric response of HRP/AuNP/CHIT/SPCE when spiked with $H_2O_2$ is immediate (within 1–5 s) and shows the highest current, 3.3 and 5.7 times higher than the HRP/CHIT/SPCE and HRP/SPCE, respectively. This phenomenon is due to the AuNP which allow the enzyme to adsorb more effectively than without AuNP. This increases the sensitivity of biosensors because a larger amount of enzyme is adsorbed which then provides more substrate ($H_2O_2$) to be reduced at the electrode surface leading to a larger signal. Moreover, the AuNP provide a larger conductive area, resulting in improvement electron transfer kinetics and enhancement in the reduction current for $H_2O_2$.

#### 3.3.2. Hydrodynamic voltammogram, electrodeposition time and pH

The electrocatalytic reduction of $H_2O_2$ by HRP to water at a fixed potential is used as the amperometric sensing principle. It has been shown that HRP can catalyze $H_2O_2$ by direct electron transfer (without a mediator). Within the low potential range, $H_2O_2$ has less interference from biological species, e.g.

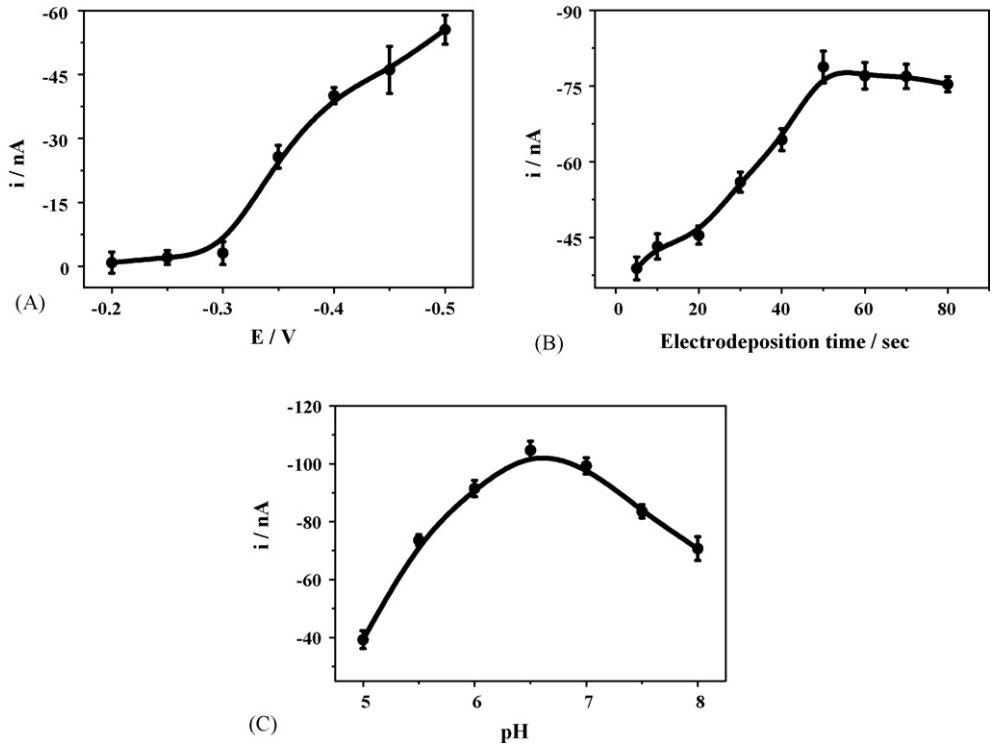


Fig. 4. Optimization of the potential (A), electrodeposition time (B) and pH (C) on the HRP/AuNP/CHIT/SPCE while addition of 500 μM $H_2O_2$. Other conditions as in Fig. 3, $n = 3$.

ascorbic acid and uric acid. Our hydrodynamic voltammogram has been examined for the HRP/AuNP/CHIT/SPCE in the range of −0.20 to −0.50 V with injection of 500 μM $H_2O_2$ (Fig. 4A). The HRP/AuNP/CHIT/SPCE was prepared by applying a potential of −2.0 V to the working electrode while immersed in a HRP/AuNP/CHIT solution. The advantages of SPCEs due to their single-use nature mean no cleaning is necessary and the signal is very reproducible. Very little current was seen below −0.30 V, but is highly increased at −0.40 V. The current was keeping continuously increased until −0.5 V, as we known at the high operating potential resulting in interference from matrix species. Therefore the operating potential of −0.40 V was determined to give a good sensitivity and a short setting time and was selected for further study.

The effect of electrodeposition on the enzyme electrode was scrutinized to optimize the electroanalytical performance. The possibility of the electrodeposition of HRP/AuNP/CHIT/SPCE at the electrode surface is examined for different deposition times as shown in Fig. 4B. About 500 μM $H_2O_2$ was added to the stirred solution of 0.1 M citrate buffer solution, pH 6.5, with an applied potential of −0.4 V to the working electrode. The current was starting observed at 5 s of electrodeposition time and increased rapidly at 40 s. At 50 s of deposition, the electroreduction of $H_2O_2$ reached the maximum. When the electrodeposition time was increased in the range of 60–80 s, the electroreduction of $H_2O_2$ was as stable as at 50 s. The above effect was ascribed to the transferring of electrons in the conducting network of HRP/AuNP/CHIT affected by the amount of their molecules and distance on the SPCE surface. The lower currents are caused by the lower amount of HRP/AuNP/CHIT (10–30 s), while the higher amount of HRP/AuNP/CHIT (60–80 s) had reached the maximum kinetics for the enzyme-substrate reaction. On the other hand, a greater film thickness gave a large background current rendering the measurement difficult for low currents. The electrodeposition time of 50 s was selected for the following experiments.

The effect of pH on the $H_2O_2$ electrocatalytic biosensor is mainly due to the effect on the activity of the enzyme. The effect of pH was investigated from pH 5.0 to 8.0. Fig. 4C shows the current response increased from pH 6.0 and reached the maximum at pH 6.5, and then decreased form pH 7.0 to 8.0. The maximum response is obtained at pH 6.5, in agreement with Qian et al. (1995). The acidic solution enhances the reaction because $H^+$ is needed for HRP to reduce the $H_2O_2$ and produce water. This pH is close to the results in Lei et al. (2003) which demonstrates that the biocatalytic properties of HRP towards $H_2O_2$ are maintained in the AuNP/CHIT microenvironment. To obtain the maximum sensitivity and bioactivity, a citrate buffer of pH 6.5 is used throughout the research.

### *3.4. Amperometric measurements of HRP/AuNP/CHIT/SPCE toward $H_2O_2$ performance*

To demonstrate the success of $H_2O_2$ determination at HRP/AuNP/CHIT/SPCE, amperometry was selected for tracking the response of the successive additions of $H_2O_2$ shown in Fig. 5. With each additional aliquot of $H_2O_2$, the reduction current rises sharply and hits a stable plateau. The calibration

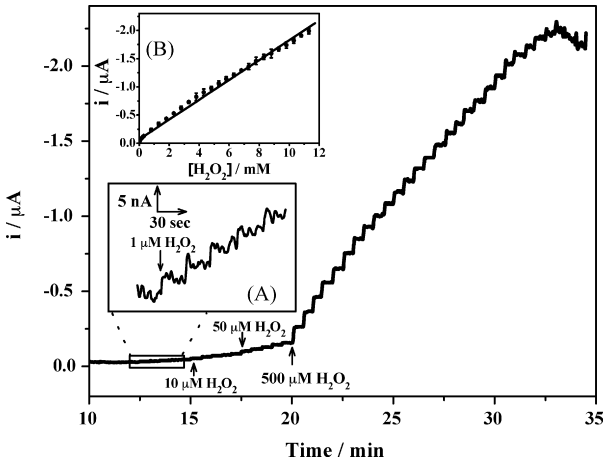


Fig. 5. Amperometric of successive additions of various concentrations of $H_2O_2$ at HRP/AuNP/CHIT/SPCE. Inset (A) shows successive addition of 1 μM $H_2O_2$ and (B) shows a linear calibration plot of $H_2O_2$ concentration vs. the corresponding current. Other condition as in Fig. 3, $n = 3$.

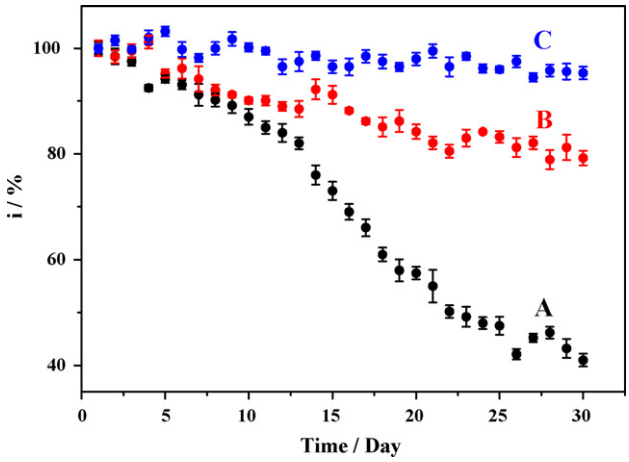


Fig. 6. Shelf life stability usage of HRP/SPCE (A), HRP/CHIT/SPCE (B) and HRP/AuNP/CHIT/SPCE (C) that was kept in 0.1 M citrate buffer, pH 6.5 (at 4 °C) when not in use. The data was normalized with respect to the data on the day 1. Other condition as in Fig. 3, $n = 3$.

plot of steady state current versus $H_2O_2$ concentration is linear ($R^2 = 0.995$) in the wide range of 10 μM to 11.3 mM with a sensitivity of −0.176 nA/μM (Fig. 5B). The smallest spiked concentration of $H_2O_2$ is observed at 1 μM (Fig. 5A). The limit of detection is obtained at 0.65 μM with a signal-to-noise ratio of 3. When the concentration of $H_2O_2$ is added over 11.3 mM, the current response will be unreliable and not usable. The linearity of this sensor has a range with a magnitude order of 3. The high linear range can be attributed to first-order chemical kinetics, and is preferred for the development of sensors. The linear range of this sensor was higher in scale when compared to HRP/Au/SPCE (Xu et al., 2003) and PB modified GC particles/SPCE (Ricci et al., 2003) with ranges of 0.8 μM to 2.2 mM and 0.3 μM to 1 mM $H_2O_2$, respectively, but all of them have the same magnitude of linearity.

The kinetic parameter, the apparent Michaelis–Menten constant ($K_M^{app}$), is an indication of the enzyme-substrate kinetics. According to Lineweaver–Burk equation (Kamin and Wilson, 1980):

$$\frac{1}{I_{ss}} = \frac{I}{I_{max}} + \frac{K_M^{app}}{I_{max} C}$$

After successive additions of a certain concentration of the substrate ($H_2O_2$) ($C$) into the stirred solution the current will reach a steady-state ($I_{ss}$). The maximum current when the substrate is saturated ($I_{max}$), is used to determine the $K_M^{app}$ value by analysis of the slope and the intercept for the relation of the increased current versus $H_2O_2$ concentrations. The $K_M^{app}$ was found to be 4.51 mM and close to the $K_M^{app}$ of 1.3 mM from the system of HRP/AuNP/SPCE (Xu et al., 2003). This value is smaller than $K_M^{app}$ value of 41 mM for hemoglobin, which has been immobilized in carbon nanotubes for direct electron transfer of $H_2O_2$ to the electrode surface (Cai and Chen, 2004). Thus, these results indicate that the new environment of the AuNP/CHIT creates a good affinity of the immobilized enzyme for $H_2O_2$ electrocatalytic reduction.

### 3.5. Reproducibility and stability of the HRP/AuNP/CHIT/SPCE

The reproducibility of this sensor was evaluated with successive additions of 500 μM $H_2O_2$ in a stirred solution. The mean steady-state current of HRP/Au/CHIT/SPCE is 107.3 nA with the relative standard deviation (R.S.D.) of 4.9% for 30 replications, hence, these electrodes are very reproducible. In stability studies, three types of $H_2O_2$ sensors were examined (Fig. 6). The current response was normalized with respect to the response on day 1. The HRP/SPCE electrode (Fig. 6A) shows the lowest stability: on the 3rd day the response was decreased to 90% of the initial signal with continued attenuation until day 8 when the signal decreased more than 50%. This degradation is due to the inactivation of the enzyme during storage. For the HRP/CHIT/SPCE (Fig. 6B), the electrode stability is higher, maintaining over 90% of its initial signal on day 10 of use and over 80% on day 30. Overall the HRP/AuNP/CHIT/SPCE (Fig. 6C) exhibited the best storage life stability. It maintained its response over 95% up to day 30, this result shows an improvement in the long-term stability when compared to the report of HRP/Silica sol–gel/CHIT for $H_2O_2$ biosensors (Miao and Tan, 2001) which showed stability of 85% for 1 month storage. This phenomenon indicates that the strong binding of AuNP and HRP prevents the loss of enzyme from the surface. The CHIT hydrogel serves as a biocompatible environment for stabilizing the enzyme activity.

## 4. Conclusions

A novel and superior SPCE, composed of a high counter electrode area, a much closed distance between RE and WE and good conductivity, has been successfully developed. The advantage of determining the best SPCE configuration makes it advanced in analytical performance. The incorporation of the HRP with AuNP in the matrix of CHIT on the SPCE surface for direct electron transfer of $H_2O_2$ produces very satisfying results

with enhanced sensitivity, high reproducibility, wide linearity and a low detection limit. The ease of the one-step immobilization creates a very reproducible and stable sensor for long-term storage, which has proven difficult for other $H_2O_2$-based biosensors. It is inferred that this AuNP/CHIT material can provide a suitable microenvironment for HRP immobilization.

## Acknowledgements

This project was mainly supported from Maejo University (Thailand) through the staff development program and partially supported by the Postgraduate Education and Research Program in Chemistry (PERCH). Andrea Lynn Kagie is also acknowledged for her kind proof of the English manuscript and discussion.

## References

Abad, J.M., Mertens, S.F.L., Pita, M., Fernandez, V.M., Schiffrin, D.J., 2005. J. Am. Chem. Soc. 127 (15), 5689–5694.
Cai, C., Chen, J., 2004. Anal. Biochem. 325 (2), 285–292.
Cai, H., Xu, C., He, P., Fang, Y., 2001. J. Electroanal. Chem. 510 (1/2), 78–85.
Clark, L.C., 1979. Method. Enzymol. 56, 448–479.
Delvaux, M., Walcarius, A., Demoustier-Champagne, S., 2004. Anal. Chim. Acta 525 (2), 221–230.
Gu, H.-Y., Chen, Z., Sa, R.-X., Yuan, S.-S., Chen, H.-Y., Ding, Y.-T., Yu, A.-M., 2004. Biomaterials 25 (17), 3445–3451.
Gu, H.-Y., Yu, A.-M., Chen, H.-Y., 2001. J. Electroanal. Chem. 516 (1/2), 119–126.
Jia, N., Zhou, Q., Liu, L., Yan, M., Jiang, Z., 2005. J. Electroanal. Chem. 580 (2), 213–221.
Kamin, R.A., Wilson, G.S., 1980. Anal. Chem. 52 (8), 1198–1205.
Khanna, P.K., Gokhale, R., Subbarao, V.V.V.S., Vishwanath, A.K., Das, B.K., Satyanarayana, C.V.V., 2005. Mater. Chem. Phys. 92 (1), 229–233.
Kong, Y.-T., Boopathi, M., Shim, Y.-B., 2003. Biosens. Bioelectron. 19 (3), 227–232.
Kumar, M.N.V.R., 2000. React. Funct. Polym. 46 (1), 1–27.
Ledru, S., Ruille, N., Boujtita, M., 2006. Biosens. Bioelectron. 21 (8), 1591–1598.
Lei, C.-X., Hu, S.-Q., Shen, G.-L., Yu, R.-Q., 2003. Talanta 59 (5), 981–988.
Lindgren, A., Ruzgas, T., Gorton, L., Csöregi, E., Ardila, G.B., Sakharov, I.Y., Gazaryan, I.G., 2000. Biosens. Bioelectron. 15 (9/10), 491–497.
Liu, H., Ying, T., Sun, K., Qi, D., 1996. J. Electroanal. Chem. 417 (1/2), 59–64.
Liu, S.-Q., Ju, H.-X., 2002. Anal. Biochem. 307 (1), 110–116.
Lu, X., Zhang, Q., Zhang, L., Li, J., 2006. Electrochem. Commun. 8 (5), 874–878.
Luo, X.-L., Xu, J.-J., Du, Y., Chen, H.-Y., 2004. Anal. Biochem. 334 (2), 284–289.
Luo, X.-L., Xu, J.-J., Zhang, Q., Yang, G.-J., Chen, H.-Y., 2005. Biosens. Bioelectron. 21 (1), 190–196.
Miao, Y., Tan, S.N., 2001. Anal. Chim. Acta 437 (1), 87–93.
Miserere, S., Ledru, S., Ruille, N., Griveau, S., Boujtita, M., Bedioui, F., 2006. Electrochem. Commun. 8 (2), 238–244.
Morrin, A., Killard, A.J., Smyth, M.R., 2003. Anal. Lett. 36 (9), 2021–2039.
Nagata, R., Clark, S.A., Yokoyama, K., Tamiya, E., Karube, I., 1995. Anal. Chim. Acta 304 (2), 157–164.
Neiman, B., Grushka, E., Lev, O., 2001. Anal. Chem. 73 (21), 5220–5227.
O'Halloran, M.P., Pravda, M., Guilbault, G.G., 2001. Talanta 55 (3), 605–611.
Qian, J., Liu, Y., Liu, H., Yu, T., Deng, J., 1995. J. Electroanal. Chem 397 (1/2), 157–162.
Ricci, F., Amine, A., Tuta, C.S., Ciucu, A.A., Lucarelli, F., Palleschi, G., Moscone, D., 2003. Anal. Chim. Acta 485 (1), 111–120.
Tseng, K.-S., Chen, L.-C., Ho, K.-C., 2005. Sens. Actuat. B 108 (1/2), 738–745.
Vo-Dinh, T., Cullum, B.M., Stokes, D.L., 2001. Sens. Actuat. B 74 (1/3), 2–11.
Vreeke, M., Rocca, P., Heller, A., 1995. Anal. Chem. 67 (2), 303–306.
Wang, J., Naser, N., Angnes, L., Wu, H., Chen, L., 1992. Anal. Chem. 64 (11), 1285–1288.
Wang, M., Wang, L., Wang, G., Ji, X., Bai, Y., Li, T., Gong, S., Li, J., 2004. Biosens. Bioelectron. 19 (6), 575–582.
Wu, L.-Q., Gadre, A.P., Yi, H., Kastantin, M.J., Rubloff, G.W., Bentley, W.E., Payne, G.F., Ghodssi, R., 2002. Langmuir 18 (22), 8620–8625.
Xu, X., Liu, S., Ju, H., 2003. Sensors 3 (9), 350–360.
Yang, M., Jiang, J., Yang, Y., Chen, X., Shen, G., Yu, R., 2006a. Biosens. Bioelectron. 21 (9), 1791–1797.
Yang, W., Wang, J., Zhao, S., Sun, Y., Sun, C., 2006b. Electrochem. Commun. 8 (4), 665–672.
Zhang, C., Gao, Q., Aizawa, M., 2001. Anal. Chim. Acta 426 (1), 33–41.
Zhang, J., Oyama, M., 2004. Electrochim. Acta 50 (1), 85–90.
Zhang, S., Wang, N., Niu, Y., Sun, C., 2005. Sens. Actuat. B 109 (2), 367–374.
Zhang, Z., Liu, H., Deng, J., 1996. Anal. Chem. 68 (9), 1632–1638.

# CHAPTER I
# INTRODUCTION

## 1.1 The world of electrochemical sensors

After the born of electrochemical sensors was dated in 1962 by J. Clark who successfully used electrochemical technique for gas monitoring in cardiovascular surgery [1, 2]. Nowadays the electrochemical sensors have been widely used and rapidly developed in many laboratories. Three main types of electrochemical sensors are classified as (i) potentiometric, (ii) amperometric and (iii) conductometric sensor [3]. The potentiometric sensors, a local equilibrium is established at the sensor interface, where either the electrode or membrane potential is measured. Information about the composition of a sample is obtained from the potential difference between two electrodes. Amperometric sensors exploit the use of a potential applied between a reference and a working electrode, to cause the oxidation or reduction of an electroactive species; the resultant current is measured. While the conductometric sensors are involved with the measurement of conductivity of the solution between two electrodes. The adapted conceptual diagram of generic sensors is illustrated in figure 1.1, consisting of recognition and signal elaboration parts.

The electrochemical sensors are becoming increasingly important in three main areas, (i) health care (ii) industrial control processes and (iii) environmental monitoring. In health care, samples might be blood, urine, gases, ions, oxidizable and reducible substances and metabolites [4, 5]. Selected sensors were applied for indicating a patient's metabolite state. Many substances such as sodium, potassium, calcium, insulin and glucose have been considered in routinely diagnostic work within patients.

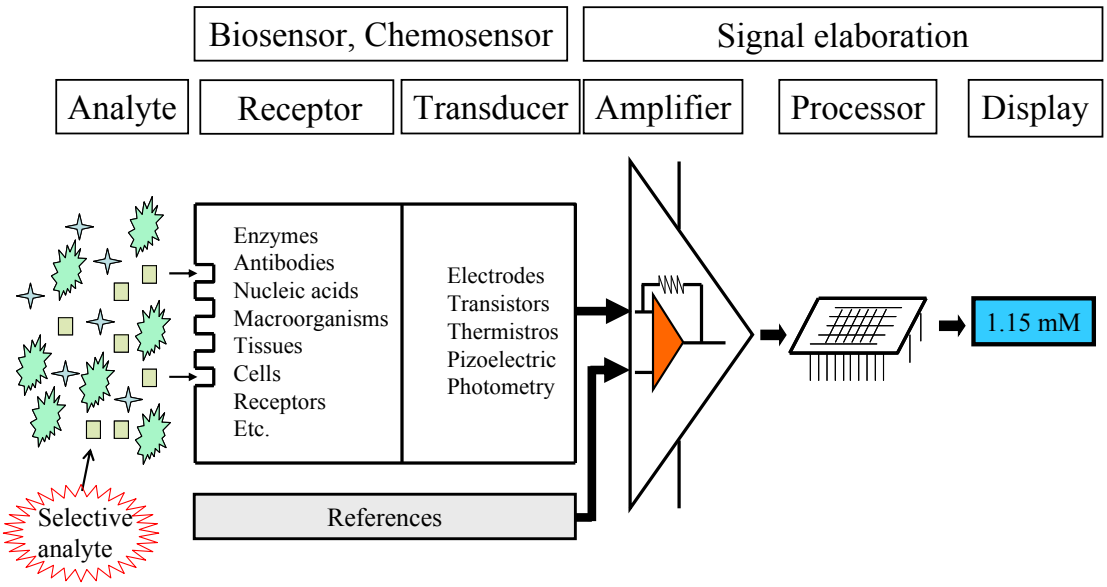


**Figure 1.1** The conceptual diagram of either chemosensors or biosensors that combining with amplifier, signal processing and readout device. Adapted from ref. [6].

Industrial applications of electrochemical sensors are classified in three different aspects of control processes i.e. (i) off-line in a laboratory, (ii) off-line, but close to the operation site, and (iii) on-line in real time [7]. The monitoring could results in improved product quality, increased product yields, checks on tolerance of variations in quality of raw material and optimized energy efficiency. Enormous ranges of analytes in environmental situations have been monitored such as biochemical oxygen demand (BOD), acidity, salinity, nitrate, phosphate, calcium and fluoride, while pesticides, fertilizers and both industrial and domestic wastes require extensive analysis.

## 1.2 Selected analytes and their importances

The electrochemical sensors for insulin hormone, glycosidases enzyme, hydrogen peroxide ($H_2O_2$), and phosphate ($PO_4^{3-}$) ion are intensively developed based on four different design concepts. These substances are important in health care and environmental monitoring by the following topics.

### 1.2.1 Insulin

Insulin is an excreted important pancreatic endocrine hormone [8]. It is the first hormone discovered in the late 1920s. Insulin is secreted by groups of cells within the pancreas called islet cells. The pancreas is an organ that sits behind the stomach and has many functions in addition to insulin production. Insulin is composed of 51 amino acid residues and has a molecular weight of 5808 Da [9]. The element of insulin is composed of carbon, hydrogen, oxygen, nitrogen, sulfur and zinc. The speculated model of the insulin hexamer believed to be the stored form is shown as figure 1.2. The insulin hexamers are highlighting the three fold symmetry, the zinc ion holding them together, and the tyrosine residues [10] bounded onto a zinc ion.

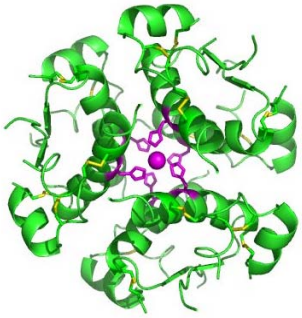

**Figure 1.2** The speculated model of the insulin hexamer composed of three fold symmetry of protein (green color), the zinc ion as circle purple shape, and tyrosine residues (ring-purple shape) [10].

Lack of insulin, which involving in many essential functions, the body cells can not work properly for adsorbing glucose from blood stream, and the cells are unable to gain calories obtained from food. A person may develop insulin deficiency, known as Type 1 deficiency [11]. Insulin is replaced via shots or pumps in daily to lead a normal and healthy life. Another of insulin deficiency is Type 2 which occurs when a person develops insulin resistance [12]. The term "insulin resistance" refers to a condition in which the levels of insulin in the blood are slightly higher than, or within, the normal range, but the body cells respond slowly and inefficiently

to this insulin. As a result, the cells do not absorb the sugar molecules as required, and blood sugar levels rise.

### 1.2.2 Glycosidases

Glycosidases are an important class of enzymes that are involved in the catabolism of glycoconjugates and are indispensable for structural analysis of these complex molecules. These enzymes catalyze the hydrolysis of glycosidic bonds in simple glycosides, oligosaccharides, polysaccharides, glycoproteins and glycolipids. They are broadly classified as exo-glycosidases, which act on glycosidic linkages at the non-reducing end of the saccharide chains, and endo-glycosidases, which act on glycosidic linkages within saccharide chains [13]. The lack of a specific glycosidases can cause inherited metabolic disorders such as glycogen, glycosaminoglycan and glycolipid storage diseases. Enzyme replacement therapy holds great promise for treating these diseases. Various glycosidases, including sialidase and a-N-acetylgalactosaminidase, are associated with tumor progression and can be used as reliable cancer markers. Correlating the levels of glycosidases with the type and degree of cancer should lead to a better understanding of their clinical role. Accordingly, bioassays of glycosidases activities are of tremendous importance for diagnosing metabolic disorders, for cancer screening, and for glycomic research, in general.

### 1.2.3 Hydrogen peroxide

Hydrogen peroxide ($H_2O_2$), as well as being an incredibly simple inorganic compound, is a beautifully versatile one. It is also a chemical material in historical context with particular useful in turbine propellants, etching industrial, foods productive, and environmental applications [14]. Over the last decade it has had somewhat of a rebirth in both industrial and academic circles. The rather glib explanation for such a renaissance is due to regulatory forces causing the chemical industry to reduce, and in some instances eliminate, environmental pollution. It is a very pale blue liquid which appears colorless in a dilute solution, and possesses the

strong oxidizing properties. Its solution is slightly more viscous than water, quite weak acid. The $H_2O_2$ for a mass production is produced form the acidification of barium peroxide. Hydrogen peroxide is available in commercial as a stock solution as 30% solution from commercial agency or at 2.5-3% store at drugstore.

Besides traditional applications as mention above, $H_2O_2$ is also used as a key substance in medical applications. The enzymatic reaction involves the $H_2O_2$ as an intermediate, tracking and observing of its leading in disease diagnostics or for substances determination.

### 1.2.4 Phosphate

In aquatic systems, phosphorus occurs as organic $PO_4^{3-}$ and inorganic $PO_4^{3-}$. Organic $PO_4^{3-}$ consists of $PO_4^{3-}$ associated with carbon-based molecules, as in plants or animal tissues. Phosphate that is not associated with organic material is inorganic.

Phosphate is required for many different functions in body tissues, serving as a buffering component in cellular fluids and as an important factor in cellular energy metabolism [15, 16]. The metabolism of inorganic $PO_4^{3-}$ is closely linked to that of calcium. Under typical dietary conditions of excessive $PO_4^{3-}$ intake relative to calcium, i.e., a low Ca:P ratio, osteopenia (the presence of a less than normal amount of bone) is likely to result. Phosphate is also a major constituent of all plant and animal cells and in modern agriculture this element has to be supplied as fertilizer to crops. Phosphate is predominantly found in the form of orthophosphate. Because of its widespread presence in detergents and fertilizers, increased environmental $PO_4^{3-}$ concentrations can lead to eutrophic phenomena contaminating water resources.

The determination of $PO_4^{3-}$ in natural water provides essential data for assessing the health of ecosystems, investigating biogeochemical processes and monitoring compliance with legislation. The Environmental protection agency (EPA)

makes the following recommendations [17]. Total $PO_4^{3-}$ should not exceed 0.05 mg $L^{-1}$ (as phosphorus) in a stream at a point where it enters a lake or reservoir, and should not exceed 0.1 mg $L^{-1}$ in streams that do not discharge directly into lakes or reservoirs. The implications for $PO_4^{3-}$ monitoring imply the need of an analytical method that can determine $PO_4^{3-}$ at designed levels as low as 0.01 mg $L^{-1}$.

## 1.3 Fundamental of electrochemistry

Electrochemistry generally deals with the phenomena associated with charge heterogeneously transfer across electrolyte/electrode interfaces [18, 19], and also with ionic mobility in bulk electrolyte. At the cathode, molecules or ions are transformed within the interface via reaction with electron to produce reduced molecules or ions**.** At the anode, molecules or ions (from the solution) are transformed to oxidized ions and molecules within the interface to produce electrons (at the electrode surface). The resultant electrons move from the anode through the wires of the external circuit to the cathode as electronic current (amperes; coulombs per second). Within the solution phase the current is carried by the electroactive species and the ions of the supporting electrolyte (positive ions toward the cathode and negative ions toward the anode). The limitation of ionic current in the solution phase is defined by the difference of an incompatibility for electrochemistry and electronics.

### 1.3.1 Electron-transfer dynamics

The rate of electron transfer at an electrode/solution interface for the direct reduction of an oxidizing (*ox*) to its reducing (*red*) species is written as (R1.1).

$$ox + ne^- \underset{k_a}{\overset{k_c}{\rightleftharpoons}} red \qquad \text{(R1.1)}$$

The electron transfer rate constant ($k_a$, $k_c$; anodic and cathodic processes, respectively) is a function of the potential difference across the

electrode/solution interfaces ($\Delta E$), which is directly proportional to the activation energy for reduction ($\Delta G_c^{\neq}$). Only a fraction of $\Delta E$ is effective for accelerating the rate of reduction, which is represented by a transfer coefficient, $\alpha$, $0.0<\alpha<1.0$ (usually about 0.5).

The flux ($\upsilon_c$), amount of *ox* passed to electrode surface at time, that is reduced at the electrode has the dimensions of moles per unit area ($cm^2$) per second, as equation (1.1),

$$\upsilon_c = d(C_{ox})_o/Adt = k_c(C_{ox})_o = j_c/nF \quad (1.1)$$

where $(C_{ox})_o$ is concentration (mol $cm^{-3}$) at the electrode surface, $A$ is area of the electrode ($cm^2$), and $j_c$ is net cathodic (reductive) current density (A $cm^{-2}$). When the cathodic current density ($j_c$) is equal to the anodic current density ($j_a$), the net current flow across the electrode/solution interface is zero and the net flux of *ox* and *red* is zero. For this unique condition (at zero net current) the current densities represent the equilibrium exchange current density ($j_o$), which is associated with the equilibrium potential difference, $\Delta E_e$. Thus,

$$j_o = j_c = (C_{ox})_o\, nF(k_c)_{\Delta E=0} \exp(-\alpha \Delta E_e F/RT) \quad (1.2)$$

$$j_o = j_a = (C_{red})_o\, nF(k_a)_{\Delta E=0} \exp[(1-\alpha)\Delta E_e F/RT] \quad (1.3)$$

The difference between $\Delta E$ and $\Delta E_e$ is the activation overpotential ($\eta$), $\eta = \Delta E - \Delta E_e$. These relationships can be combined to give an expression for the net current density ($j$), which by definition is equal to $j_a - j_c$ in terms of the activation overpotential substitute ($\eta + \Delta E_e = \Delta E$), which is referred to as the Butler-Volmer equation,

$$j = j_a - j_c = j_o \exp([(1-\alpha)n_a F\eta/RT] - \exp[-\alpha n_a F\eta/RT]) \quad (1.4)$$

At the equilibrium potential,

$$\Delta E = \Delta E_{\mathrm{e}}, j = 0,\ C_{ox}^{\mathrm{o}} = C_{ox}^{\mathrm{b}}, \text{ and } C_{red}^{\mathrm{o}} = C_{red}^{\mathrm{b}} \tag{1.5}$$

where $C^{\mathrm{o}}$ denotes the concentration of a species at the electrode surface, whereas $C^{b}$ its bulk concentration. Then,

$$\frac{C_{ox}^{\mathrm{b}}}{C_{red}^{\mathrm{b}}} = \exp[\frac{(-nF(\Delta E - \Delta E^{0'})}{RT}] \tag{1.6}$$

and relates with the Nernst equation for a half reaction at equilibrium.

$$\Delta E_{\mathrm{e}} = \Delta E^{\circ\prime} + \frac{RT}{nF} \ln \frac{C_{ox}^{\mathrm{b}}}{C_{red}^{\mathrm{b}}} \tag{1.7}$$

### 1.3.2 Electrode and cell potentials

For a half reaction (R1.1), the free energy is given by,

$$\Delta G = \Delta G^{\circ} + \frac{RT}{nF} \ln \frac{a_{red}}{a_{ox}} \tag{1.8}$$

where $-\Delta G$ indicates the tendency for the reaction to go to the right; R is the gas constant and in the units appropriate for electrochemistry has a value of 8.317 J $\mathrm{mol}^{-1}$ $\mathrm{K}^{-1}$; T is the temperature of the system in K; and the logarithmic terms in the bracketed expression represent the activities (effective concentrations) of the electroactive pair at the electrode surface. The free energy of this half reaction is related to the electrode potential, $E$, by the expression,

$$-\Delta G = nFE; \qquad -\Delta G^{\circ} = nFE^{\circ}; \qquad -\Delta G^{\circ} = RT \ln K \tag{1.9}$$

The quantity $\Delta G°$ is the free energy of the half reaction when the activities of the reactant and product have values of unity and is directly proportional to the standard half cell potential for the reaction as written. It also is a measure of the equilibrium constant for the half reaction, assuming the activity of electrons is unity.

Standard potentials are thermodynamic quantities that usually are evaluated via caloriometry for a cell reaction. The half-cell potential to the effective concentrations (activities) of the redox couple expresses,

$$E = E° - \frac{RT}{nF}\ln\frac{\{red\}}{\{ox\}} = E° + \frac{RT}{nF}\ln\frac{\{ox\}}{\{red\}} \tag{1.10}$$

The activity of a species is indicated as the symbol of the species enclosed in a bracket. This quantity is equal to the concentration of the species times a mean activity coefficient,

$$\{M^{n+}\} = a_{M^{n+}} = \gamma_{\pm} C_{M^{n+}} \tag{1.11}$$

Although there is no straightforward and convenient method for evaluating activity coefficients for individual ions, the Debye-Huckel relationship permits an evaluation of the mean activity coefficient ($\gamma_{\pm}$) at low concentrations (usually below 0.01 M),

$$\log\gamma_{\pm} = -0.509z^2\frac{\sqrt{I}}{1+\sqrt{I}} \tag{1.12}$$

where $z$ is the charge on the ion and $I$ is the ionic strength,

$$I = \left(\frac{1}{2}\right)\sum c_i z_i^2 \tag{1.13}$$

The reaction of an electrochemical cell always involves a combination of two redox half reactions such that one species oxidizes a second species to give the respective redox products. Thus, the overall cell reaction can be expressed by a balanced chemical equation,

$$a\ ox_1 + b\ red_2 \rightarrow c\ red_1 + d\ ox_2 \qquad \text{(R1.2)}$$

The potential can be calculated from each half-cell electrode system by the algebraic difference between the potential of the more positive half-cell and the potential of the less positive half-cell,

$$E_{\text{cell}} = E_{(\text{more positive})} - E_{(less\ positive)} = E_1 - E_2 \qquad (1.14)$$

An overall expression for the cell potential,

$$E_{\text{cell}} = E_1^{\text{o}} - E_2^{\text{o}} + \frac{RT}{nF} \ln \frac{\{ox_1\}^a \{red_2\}^b}{\{ox_2\}^d \{red_1\}^c} \qquad (1.15)$$

To apply potentiometric measurements to the determination of the concentration of electroactive species, a number of conditions have to be met. The basic measurement system must include an indicator electrode, which is capable of monitoring the activity of the species of interest, and a reference electrode, which gives a constant, known half cell potential to which the indicator electrode potential can be referred.

### 1.3.3 Diffusion current

The current in electrochemistry is occurred and measured at the working electrode while control potential is sufficient for electrolyzation the electroactive species. The reaction recalled (R1.1) is at $k_a << k_c$,

$$ox + ne^- \underset{k_a}{\overset{k_c}{\rightleftharpoons}} red \qquad \text{(R1.1)}$$

The current transportation in and out from the electrode surface required material to transport. The relationships involve the flux and diffusion of materials is accomplished by starting with Fick's second law of diffusion,

$$\frac{\partial C_{(x,t)}}{\partial t} = \frac{D\partial C_{(x,t)}}{\partial x^2} \qquad (1.16)$$

where $D$ represents the diffusion coefficient, $C$ represents the concentration of the electroactive species at a distance $x$ from the electrode surface, and time $t$ that the concentration gradient has existed.

Equation (1.16) can be solved to give a relationship for concentration in terms of parameters $x$ and $t$,

$$C_{(x,t)} = C^b \text{erf} \frac{x}{2D^{1/2}t^{1/2}} \qquad (1.17)$$

where $C^b$ is the bulk concentration of the electroactive species, and erf is an error function.

The derivative of Eq. (1.17) for the proper boundary condition, namely at the electrode surface ($x$ =0), the diffusion gradient at the electrode surface is expressed by the relation,

$$\left(\frac{\partial C}{\partial x}\right)_{(o,t)} = \frac{C^b}{\pi^{1/2}D^{1/2}t^{1/2}} \qquad (1.18)$$

This flux of material crossing the electrode boundary can be converted to current by the expression,

$$i = nFAD\frac{\partial C_{(o,t)}}{\partial x} \tag{1.19}$$

where $n$ is the number of electrons involved in the electrode reaction, $F$ is the faraday, and $A$ is the area of the electrode. The current that results from semi infinite linear diffusion is obtained as the Cottrell equation for a planar electrode,

$$i = \frac{nFAC^{1/2}D^{1/2}}{\pi^{1/2}t^{1/2}} \tag{1.20}$$

This equation is applied for any solid electrode voltammetry with a preset initial potential on a plateau region of the current-voltage curve such as the voltammetry, the polarography and the controlled potential electrolysis.

## 1.4 Electrochemical methods

The electrochemical techniques are classified and defined their names on the basis of their working principles by the International Union for Pure and Applied Chemistry (IUPAC) [20, 21]. The different classes of electrochemical techniques are electrolytic, potentiometric, conductometric, polarographic or voltammetric amperometric, impedimetric and coulometric methods. In potentiometry, measurements are based on the equilibrium potential existing between a selective electrode and a reference electrode. The detection limit of this technique is in the range of micro molar. On the contrary, the detection limit of voltammetry is better in comparison to that of potentiometry, so the latter technique can be used precisely for trace analysis. Although, many electrochemical methods are available, only cyclic voltammetry (CV), square wave voltammetry (SWV), and amperometry techniques are used thoroughly in this thesis.

### 1.4.1 Cyclic voltammetry

Cyclic voltammetry (CV) is a completed voltage scan (y axis) versus time (x axis) in forward and backward direction as figures 1.3. The voltage scan reversed after the current maximum (peak) of the reduction process has been passed. The backward scanned is an opposite direction signal versus the forward scan. This technique provides even more information about the properties and characteristics of the electrochemical process and also gives insight into any complicating side processes such as pre- and post-electron-transfer reactions as well as kinetic considerations [22].

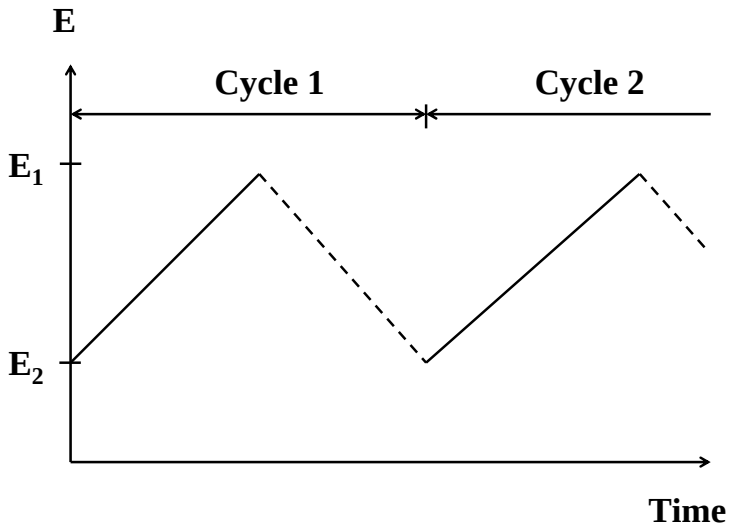


**Figure 1.3** A potential-time profile that is used for cyclic voltammetry. Solid line is for forward and dashed line is for backward scans.

Figure 1.4 illustrates the shape of a reversible cyclic voltammogram with an electrode of fixed area. The voltammogram is characterized by a peak potential, $E_p$, at which the current reaches a maximum value, and by value of the peak current, $i_p$. The peak current is given by the Randles-Sevcik equation,

$$i_p = 2.69\times10^5 n^{3/2} A D^{1/2} C^b v^{1/2} \qquad \text{at 25 °C} \qquad (1.21)$$

where $i_p$ is in A, $A$ is in $cm^2$, $D$ is in $cm^2\ s^{-1}$, $C^b$ is in mol $cm^{-3}$, and $v$ is in $V\ s^{-1}$.

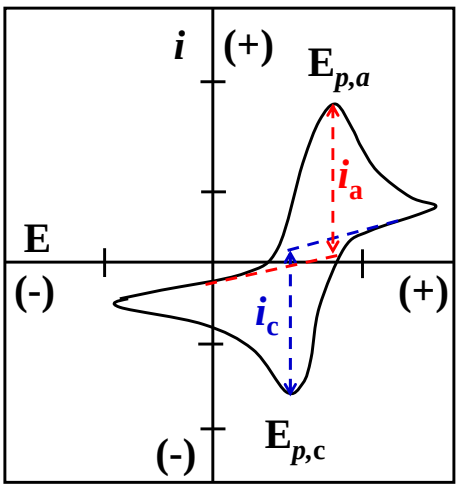


**Figure 1.4** Typical reversible cyclic voltammogram with the initial sweep direction is to more positive potential. $i_{p,a}$ and $E_{p,a}$ are peak current and peak potential of anodic current, respectively, the $i_{p,c}$ and $E_{p,c}$ are peak current and peak potential of cathodic current, respectively.

The useful parameter of the voltammetric curves is the half-peak potential, $E_{p/2}$, which is the potential at which the registered current reaches half its maximum value and is used to characterize a voltammogram. For a reversible process, $E_{1/2}$ is located halfway in between $E_p$ and $E_{p/2}$. The ratio of the peak current for the cathodic process relative to the peak current for the anodic process is equal to unity ($i_{p,c}/i_{p,a}$ =1). To measure the peak current for the anodic process the extrapolated baseline going from the foot of the cathodic wave to the extension of this cathodic current beyond the peak must be used as a reference, as illustrated in figure 1.4. The difference in the peak potentials between the anodic and cathodic processes of the reversible reaction is given by the relationship,

$$\left|\Delta E_p\right| = \left|\Delta E_{p,a} - \Delta E_{p,c}\right| = \frac{0.059}{n} \tag{1.22}$$

which provides a rapid and convenient means to determine the number of electrons involved in the electrochemical reaction. For a reversible system, $i_p$ is a linear function of $v^{1/2}$, and $E_p$ is independent of $v$.

### 1.4.2 Square wave voltammetry

The second voltammetric technique used in this thesis is square-wave voltammetry that have been developed by Osteryoungs and theirs coworks [23-26]. Its applied waveform composed of a symmetric square wave, superimposed on a base staircase potential, is applied to the working electrode as figure 1.5. The current is sampled twice during each square-wave cycle, once at the end of the forward pulse (at $t_1$) and once at the end of the reverse pulse (at $t_2$). Since the square-wave modulation amplitude is large (~ 50 mV), the reverse pulses cause the reverse reaction of the product.

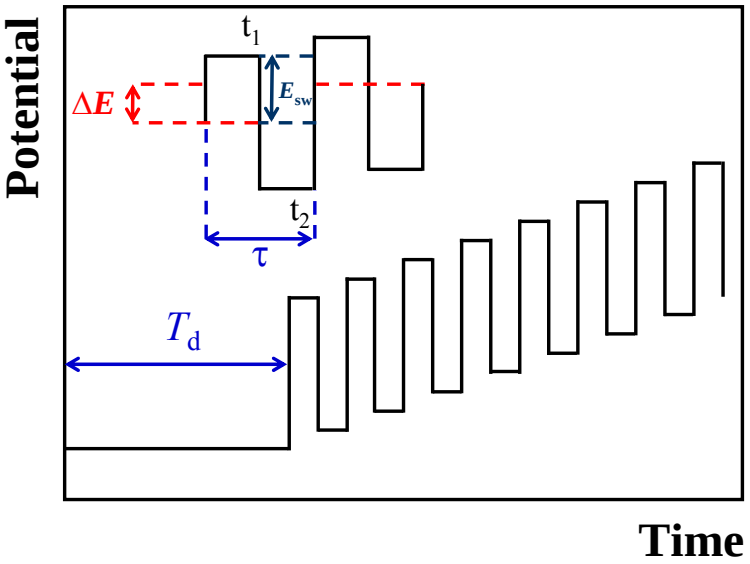


**Figure 1.5** Square-wave waveform showing the amplitude $E_{sw}$, step height $\Delta E$, squarewave period $\tau$, delay time $T_d$, and current measurement $t_1$ and $t_2$.

Dimensionless plotting of different currents of forward and backward is given in figure 1.6 for a reversible redox system [27]. The half peak potential, $E_{1/2}$, of voltammetric was expressed by the equation,

$$E_{1/2} = E^{0'} + \frac{RT}{nF}\ln\left(\frac{D_{red}}{D_{ox}}\right)^{1/2} \qquad (1.23)$$

and the actual peak current, $\Delta i_p$, is proportional to the concentration,

$$\Delta i_p = \frac{nAFD_{Ox}^{1/2}C_{Ox}}{\pi^{1/2}t_p^{1/2}}\Delta\psi_p \tag{1.24}$$

where $\Delta\psi_p$ is a dimensionless current, $A$ is in $cm^2$, $D_{ox}$ is in $cm^2\ s^{-1}$ and $C_{ox}$ is in mol $cm^{-3}$.

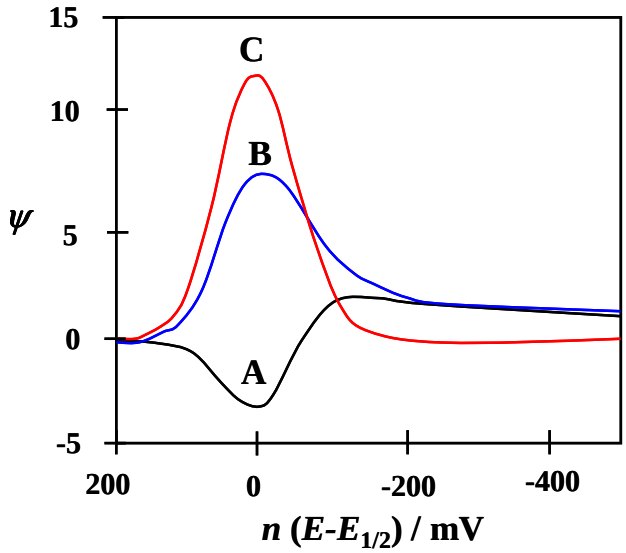


**Figure 1.6** Typical square wave voltammograms for reversible electron transfer: (curve A) forward current; (curve B) reverse current; (curve C) net current.

The sensitivity of square wave voltammetry increases from the fact that the net current is larger than either the forward or backward components. The first of advantages is its speed. The scan rate is given by $f\Delta E_s$., $f$ is the square-wave frequency and $\Delta E_s$ is the step height. Each of experiment of square wave voltammetry can be done with a minute by the profit of high scan rate [28]. The second of advantages is the way that the capacitive contributions of the overall are minimized. Thirdly of advantages, the oxygen need not be excluded from the analyte solution because of it is more provided cathodic curve than for the reduction of oxygen, then the magnitude of $i_{forward}$ or $i_{reverse}$ will incorporate an equal current due to the reduction of $O_2$ [29].

### 1.4.3 Amperometry

Amperometry is an electrochemical technique for measurement of the current that a fixed potential is applied on a working electrode [30, 31]. A heterogeneous electron transfer reaction, i.e., the oxidation and reduction of electroactive substance, take place on the working electrode as figure 1.7. The reaction considered as a set of equilibrium involved in the diffusion of the reactant to the electrode, the reaction at the electrode, and the diffusion of the product away from the electrode surface into the bulk of the solution.

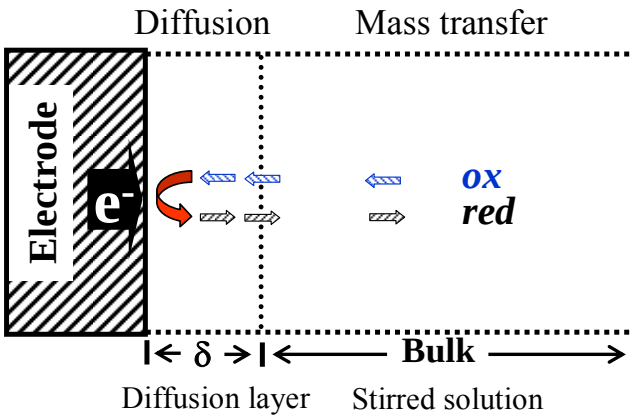


**Figure 1.7** Schematic diagram of electrode reaction processes involved in stirred solution. Arrows indicated the direction of oxidizing species (*ox*) move into the electrode and reduced to reducing species (*red*) which move out to the bulk solution. The δ is thickness of the diffusion layer**.**

All amperometric determination ultimately depend on Faraday's law [30],

$$Q = nFN \tag{1.25}$$

where $Q$ is the number of coulombs used in converting $N$ moles of material, $n$ is the number of electron equivalent lost or gained in the transfer process per mole of the material, and $F$ is Faraday's constant. It is respect to current, $i$, by,

$$\frac{dQ}{dt} = i = nFA\frac{dN}{dt} \tag{1.26}$$

and mass transfer is given by,

$$\frac{dN}{dt} = -D\left(\frac{dc_{x,t}}{dx}\right)_{x=0} \tag{1.27}$$

Under controlled hydrodynamics condition, the rate of the whole process is controlled by diffusion mass transfer. The diffusion current, $i_d$ is proportional to the concentration of the substance to be determined, $C$,

$$i_d = \mathrm{nFA}D\frac{C}{\delta} \tag{1.28}$$

where δ is thickness of the diffusion layer (being constant at given convection). The low detection limits and wide linear measuring range are the main advantages of amperometry techniques.

## 1.5 Electrochemical instruments

The potentiostat, three electrode system, and the cell design are described in this section.

### 1.5.1 Potentiostat

A potentiostat is an electronic device, which used for investigating dynamic phenomena in several electrochemical systems, it is necessary to control the potential between the working and the reference electrode, while measures the current passed to the counter electrode [32-34]. The most widely used potentiostats today are

assembled from discrete integrated-circuit operational amplifiers and other digital modules. In many cases, especially in the larger instruments, the potentiostat package also includes electrometer circuits, analog to digital (A/D) and digital to analog (D/A) converters, and dedicated microprocessors with memory as figure 1.8.

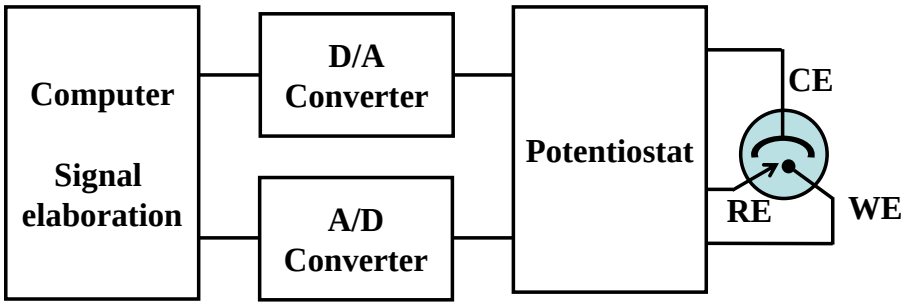


**Figure 1.8** Block diagram of a potentiostat package consisting of analog to digital (A/D) and digital to analog (D/A) converters, and dedicated processors [30]. WE = working, CE = counter, and RE = reference electrodes.

A simple potentiostat circuit for a three-electrode cell with three operational amplifiers (OA) is shown in figure 1.9 [35, 36]. The three electrode system arranges to control the potential of working electrode with respect to the reference electrode whilst measuring the current between the working electrode and the counter electrode [37]. The output of OA-1 is connected to the counter electrode with feedback to its own inverting input through the reference electrode. This feedback decreases the difference between the inverting and noninverting inputs of OA-1 and causes the reference electrode to assume the same potential as $E_{in}$ of OA-1. Because the potential difference between the working electrode and the reference electrode is zero, the working electrode is set to the same potential as applied to the OA-1 input. With the reference electrode connected to $E_{in}$ through the high impedance of OA-3, the current must flow through the counter electrode. Current flow through the reference not only is undesirable because of its higher resistance but also would eventually cause its potential to become unreliable. Another OA acting as a current-to-voltage converter (OA-2) provides the output signal for the A/D converter.

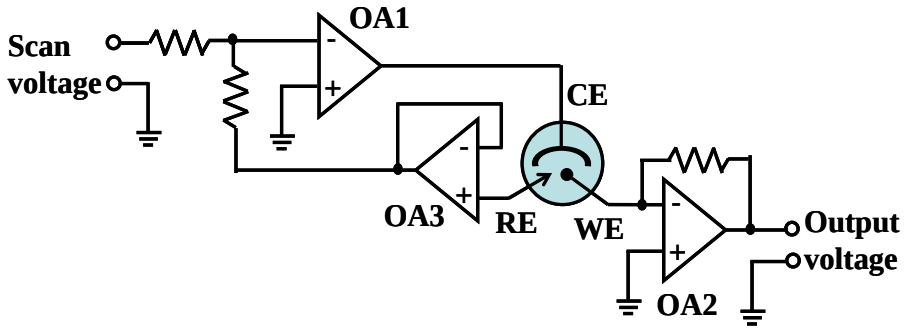


**Figure 1.9** The basic electronic diagram of potentiostat [34, 38]. OA = operational amplifier, WE = working, CE = counter, and RE = reference electrodes.

An accurate and flexible control of the applied potential is a critical function of the potentiostat. In early analog instruments, a linear scan meant just that, a continuous linear change in potential from one preset value to another. Since the advent of digital electronics almost all potentiostats operate in a digital (incremental) fashion. Thus, the application of a linear scan is actually the application of a "staircase" modulated potential with small enough steps to be equivalent to the analog case. Not surprisingly, digital fabrication of the applied potential has opened up a whole new area of pulsed voltammetry, which gives fast experiments and increases sensitivity. High-speed scanning techniques such as square-wave voltammetry require very fast response times from the electronics. In the simpler stand alone potentiostats the excitation signal used to modulate the applied potential is usually provided by an externally adjustable waveform generator. In the computer-controlled instruments, the properties of the modulation and the waveform are under software control and can be specified by the operator. The most commonly used waveforms are linear scan, differential pulse, triangular and square wave.

### 1.5.2 Electrochemical cells

#### 1.5.2.1 The three electrode system

The three electrode system consisting of working, reference and counter electrodes is commonly used for voltammetry, and amperometry techniques.

The current or charge with responding to the occurrence reaction is measured at the electrochemical cell where those three electrodes placement [39].

The placement of the electrodes is an important factor in the performance of a cell. The electrodes should be arranged in a way that: (i) provides a symmetrical electric field and uniform current distribution across the working electrode surface, and (ii) minimizes the ohmic potential (*i*Ru) drop between the working and the reference electrodes.

The first requirement can be satisfied by having a symmetrical arrangement of the working and counter electrodes. Planar electrodes place parallel to each other, or cylindrical or spherical working electrodes placed in the center of concentric counter electrode, are suitable arrangements. The requirement of minimal *i*R drop can be achieved by placing the tip of the reference electrode close to the working electrode. While the *i*R drop between the reference and counter electrodes is corrected for by the potentiostat, the ohmic potential drop ($iR_u$) between the reference and working electrodes remains uncompensated, and therefore the actual working electrode potential is in error. Although the ohmic drop is usually small, for accurate work the use of Luggin capillary, a device that effectively allows the placing of the reference electrode tip very close to the working electrode surface, is advisable. As a general rule, it is recommended that the reference electrode should be placed close to the working electrode in a line between the working and counter electrodes.

#### 1.5.2.2 Stationary cells

The design of the cell and materials used in its construction must be chosen according to both the nature of the samples and the experiments. Cells are usually constructed in glass or, occasionally, quartz. Advantage such as cost, high chemical resistance, impermeability and transparency make glass the most convenient and satisfactory material. For work with substances with attack glass, a range of polymers such as Teflon, Kel-F, Nylon or polyethylene are suitable [40].

In its simplest form, an electrochemical cell is a beaker, or similar container, with a plastic top which allows insertion of the three electrodes as figure 1.10. There is normally a fourth hole to allow the introduction of a nitrogen gas line. Purging the solution with nitrogen to eliminate oxygen is usually necessary, particularly for monitoring of possesses of negative potentials.

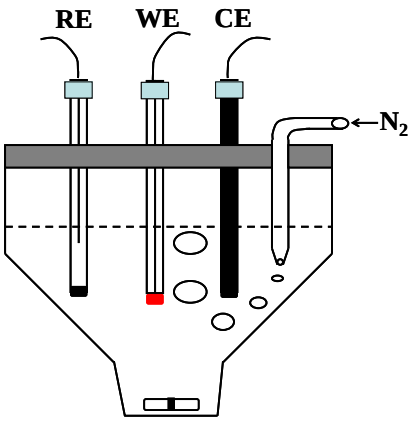


**Figure 1.10** Schematic diagram of electrochemical cell. WE, CE and RE are working, counter and reference electrodes, respectively. $N_2$ is nitrogen gas.

#### 1.5.2.3 Flow through cells

Flow through cells [41] is a one part of flow injection analysis (FIA) system as in figure 1.11A, that it placed at the detection part. FIA is an analytical technique based on the injection of a liquid sample into a moving, nonsegmented continuous carrier stream of a suitable liquid [42]. It is taken an advantage of a rapid automated analysis of liquid samples. The technique was first reported by Ruzicka and Hansen in 1975, and has been increased dramatically and widespread.

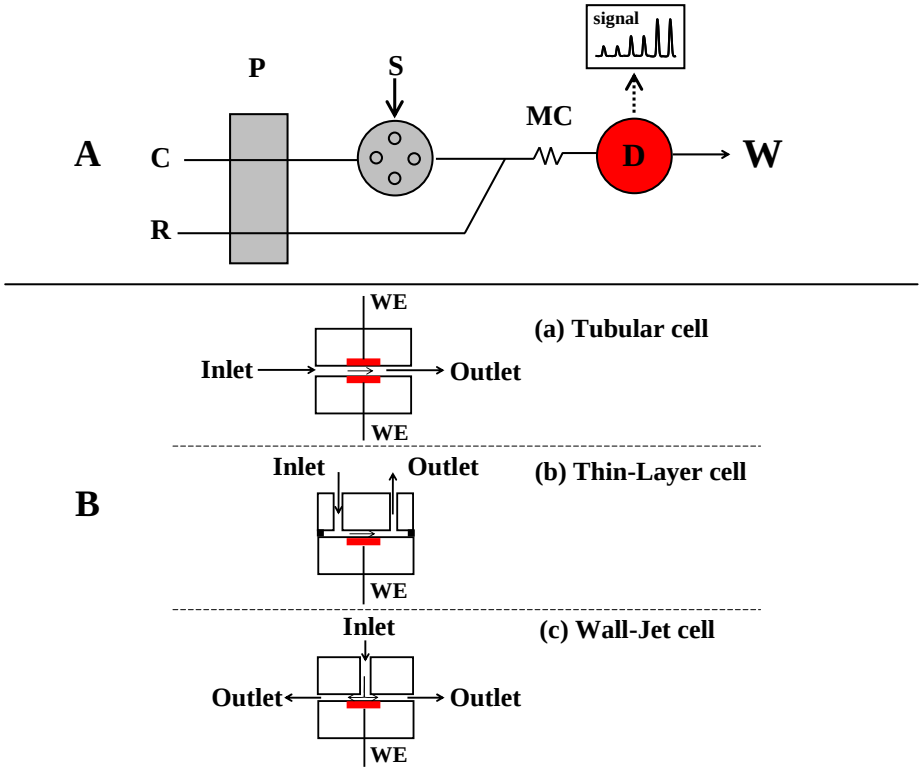


**Figure 1.11** (A) Schematic diagram of a typical flow injection analysis manifold. P is a pump, C and R are carrier and reagent lines respectively, S is sample injection, MC is mixing coil, D is a flow through cell, and W is the waste line. (B) Schematics diagrams of (a) tubular, (b) thin-layer and (c) wall-jet electrochemical cells. WE is working electrode.

In a flow injection analyser, a small, fixed volume of a liquid sample is injected as a discrete zone using an injection device into a liquid carrier which flows through a narrow bore tube. The sample zone is progressively dispersed into the carrier, initially by convection, and later by axial and radial diffusion, as it is transported along the conduit under laminar flow conditions. Reagents may be added at various confluence points and these mix with the sample zone under the influence of radial dispersion, to produce reactive or detectable species which can be sensed by any one of a variety of flow-though detection devices. The height or area of the peak is used to quantify the analyte after comparison with the peaks obtained for solutions containing known concentrations of the analyte.

The electrochemical cell configuration of flow through cell is based on the working electrode lay out with the cell. The solution from the introduction port

(injection valve) can pass through the electrode (flow-through), or flow parallel to (flow-by), or perpendicularly to (flow-on) the electrode surfaces. The common configurations of flow through cell are Tubular, Thin-Layer and Wall-Jet cells as figure 1.11B.

Flow cells configuration of stream solution emerging from a tube impinges perpendicularly on an electrode surface is called a wall-jet cell. Amperometric detection involves the measurement of the current passing through an electrode held at a potential chosen to allow a particular analyte react. The equation relating with the current (i) and concentration (C) depends on the position of the nozzle with respect to the planar electrode. If the nozzle is moved closing to the electrode, the current equation becomes,

$$i = 0.898nFCD^{2/3}\gamma^{-5/12}a^{-1/2}\mathrm{A}^{2/3}U^{3/4} \qquad (1.29)$$

where $a$ is the diameter of the input nozzle, $\gamma$ is the kinetic viscosity, $D$ is diffusion coefficient and $U$ is the volume flow rate.

The detection processes occur at the electrode surface of the detection cell while the transport of the analyte towards the electrode. The transport of the analyte towards the electrode surface is a fundamental part of the measurement process. Consequently, the hydrodynamic conditions within the cell are important. Therefore, the designing an electrochemical cell, parameters such as cell geometry, fluid flow pattern and i$R$ drop must be optimized.

The i$R$ drop (non-linearity of calibration curves and distortion responses with non-DC detection techniques) can be eliminated by the appropriate positioning in the cell of the reference, counter and working electrodes. The electrode should be close to one another to minimize the uncompensated resistance (i$R_u$). A convenient arrangement is that, with either the reference electrode, or preferably the counter electrodes, opposite the working electrode. This ensures that i$R_u$ is small and that the potential is uniform across the working electrode, particularly with very thin

cells, low flow rates and large electrode areas. For these reasons, the reference and counter electrodes are usually placed downstream of the working electrode.

## 1.6 Enzyme

Enzymes are amphoteric molecules containing a large number of acidic and basic functional groups, mainly situated on their surface [13]. The alternation of surface charges depends on their dissociation constants, ionic strength, and pH. This will affect to the reactivity of the catalytically active groups, especially important in the neighborhood of the active sites. The changes in charges with pH affect the activity, structural stability and solubility of the enzyme.

### 1.6.1 Enzyme classifications

Enzymes are classified according the report of a Nomenclature Committee appointed by the International Union of Biochemistry (1984). This enzyme commission assigned each enzyme a recommended name and a 4-part distinguishing number. It should be appreciated that some alternative names remain in such common usage that they will be used, where appropriate, in this text. The enzyme commission (EC) numbers divides enzymes into six main groups according to the type of reactions catalyzed:

#### 1.6.1.1 Oxido-reductases

Enzymes involve the redox reactions in which hydrogen or oxygen atoms or electrons are transferred between molecules. This extensive class includes the dehydrogenases (hydride transfer), oxidases (electron transfer to molecular oxygen), oxygenases (oxygen transfer from molecular oxygen) and peroxidases (electron transfer to peroxide). For example: glucose oxidase (EC 1.1.3.4, systematic name, β-D-glucose:oxygen 1-oxidoreductase) as reaction (R1.3).

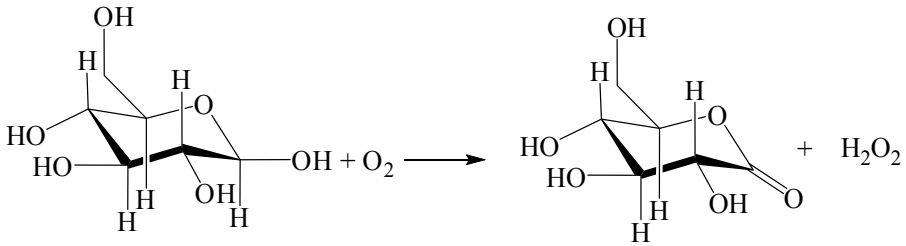


β-D-glucose D-glucono-1,5-lactone (R1.3)

### 1.6.1.2 Transferases

Enzymes catalyze the transfer of an atom or group of atoms (e.g. acyl-, alkyl- and glycosyl-), between two molecules, but excluding such transfers as are classified into other groups (e.g. oxidoreductases and hydrolases). For example: aspartate aminotransferase (EC 2.6.1.1, systematic name, L-aspartate: 2-oxoglutarate aminotransferase; also called glutamic-oxaloacetic transaminase or simply GOT) as reaction (R1.4).

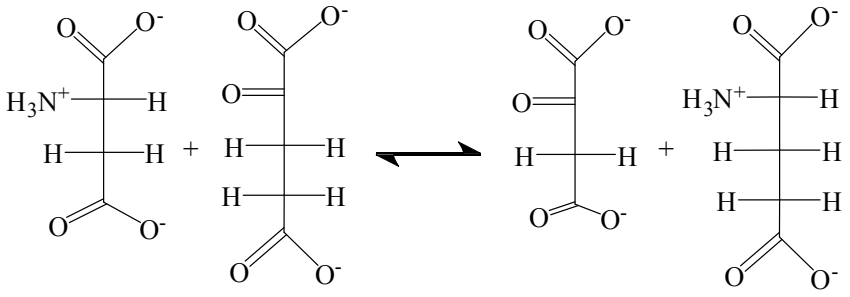


L-aspartate 2-oxoglutarate oxaloacetate L-glutamate (R1.4)

### 1.6.1.3 Hydrolases

Enzymes involve the hydrolytic reactions and their reversal. This is presently the most commonly encountered class of enzymes within the field of enzyme technology and includes the esterases, glycosidases, lipases and proteases. For example: chymosin (EC 3.4.23.4, no systematic name declared; also called rennin) as reaction (R1.5).

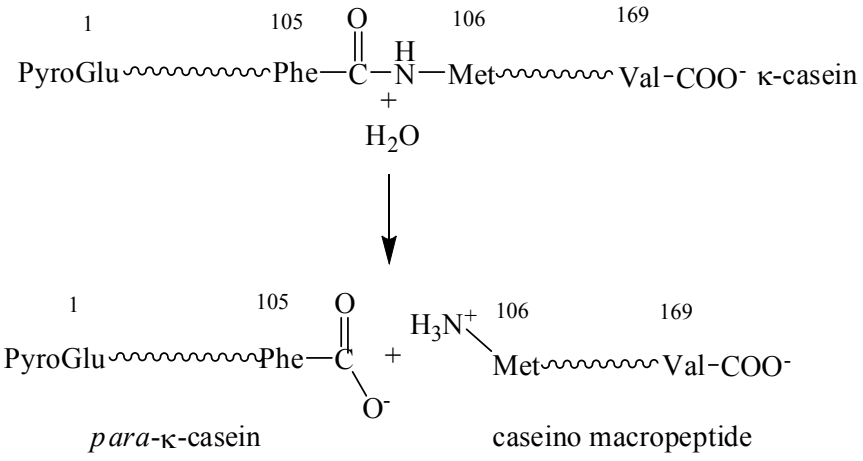


(R1.5)

### 1.6.1.4 Lyases

Enzymes involve elimination reactions in which a group of atoms is removed from the substrate. This includes the aldolases, decarboxylases, dehydratases and some pectinases but does not include hydrolases. For example: histidine ammonia-lyase (EC 4.3.1.3, systematic name, L-histidine ammonia-lyase; also called histidase) as reaction (R1.6).

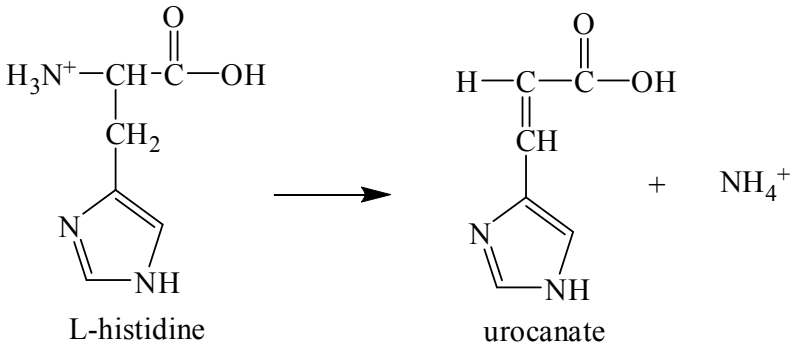


(R1.6)

### 1.6.1.5 Isomerases

Enzymes catalyze molecular isomerisations and include the epimerases, racemases and intramolecular transferases. For example: xylose isomerase (EC 5.3.1.5, systematic name, D-xylose ketol-isomerase; commonly called glucose isomerase) as reaction (R1.7).

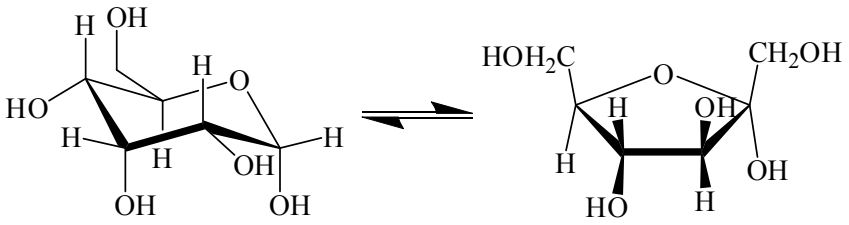

α-D-glucopyranose α–D-fructofuranose (R1.7)

### 1.6.1.6 Ligases

Enzymes which are known as synthetases, form a relatively small group of enzymes involve the formation of a covalent bond joining two molecules together, coupled with the hydrolysis of a nucleoside triphosphate. For example: glutathione synthase (EC 6.3.2.3, systematic name, γ-L-glutamyl-L-cysteine:glycine ligase (ADP-forming); also called glutathione synthetase) as reaction (R1.8).

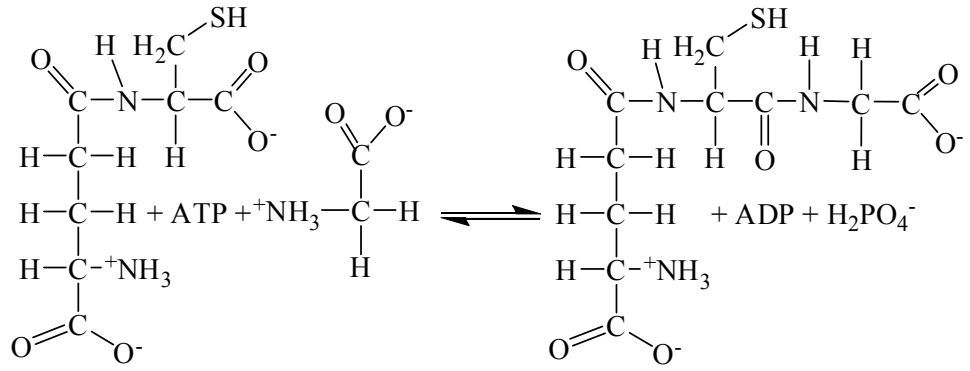

γ-L-glutamyl-L-cysteine glycine glutathione (R1.8)

### 1.6.2 Enzyme kinetics

The dramatic increases in reaction rates those occur in represent enzyme-catalyzed reactions are demonstrated in the data given in Table 1.1.

**Table 1.1** Examples of the catalytic power of enzymes [43].

| Substrate | Catalyst | T(K) | $k$* ($M^{-1}$ $s^{-1}$) | Catalytic power |
|---|---|---|---|---|
| Amide (hydrolysis) | | | | |
| -Benzamide | $H^+$ | 325 | 2.4 x $10^{-6}$ | $10^6$ |
| -Benzamide | $OH^-$ | 326 | 8.5 x $10^{-6}$ | |
| -Benzoyl-L-tyrosinamide | α-Chymotrypsin | 298 | 14.9 | |
| Urea (hydrolysis) | $H^+$ | 335 | 7.4 x $10^{-7}$ | $10^{13}$ |
| | Urease | 294 | 5.0 x $10^6$ | |
| Hydrogen peroxide | $Fe^{2+}$ | 295 | 56 | $10^6$ |
| | Catalase | 295 | 3.5 x $10^7$ | |

* $k$ = Reaction rates

The hydrolysis of the representative amide benzamide by acid or base yields second-order rate constants that are over 6 orders of magnitude (see catalytic power) lower than that measured for benzoyl-L-tyrosinamide in the presence of the enzyme a-chymotrypsin. An even more dramatic rate enhancement is observed for the hydrolysis of urea: The acid catalyzed hydrolysis is nearly 13 orders of magnitude (see catalytic power) slower than hydrolysis with the enzyme urease. The disproportional conversion of $H_2O_2$ into water and molecular oxygen is enhanced by a factor of 1 million (see catalytic power) in the presence of catalase. Enzymes derive both their selectivities and their reaction rate enhancements by the formation of enzyme–substrate complexes. This complex formation results in a transition state for the reaction, that lowers $\Delta G^{\neq}$, the activation energy, but does not affect the net free

energy for the conversion of the substrate to the product as figure 1.12 for the simple one-substrate enzyme reaction shown in reaction (R1.9),

$$E + S \rightleftharpoons E{\bullet}S \rightarrow E + P \qquad \text{(R1.9)}$$

where E is the enzyme, S is the substrate, E•S is the enzyme–substrate complex, and P is the product of the reaction.

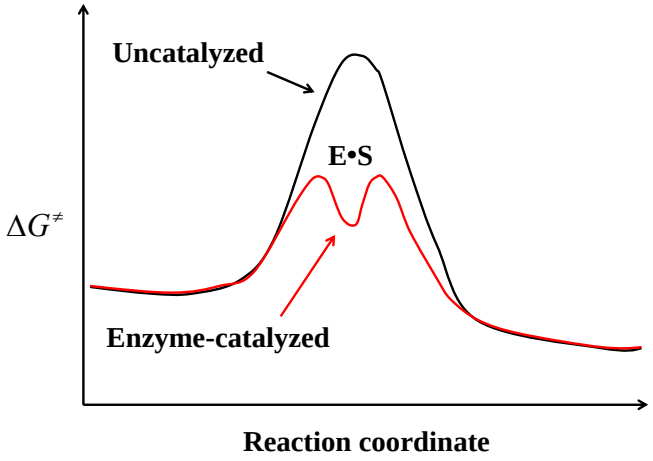


**Figure 1.12** Free energy profiles during uncatalyzed and enzyme–catalyzed reactions

The critical first step in enzyme-catalyzed reactions is the formation of E•S, activated complex, usually represented as a simple association reaction [44]. The reaction rate will reach a maximum when all available enzyme effectively exists in the form of the E•S complex. This situation occurs at high substrate concentrations, where the enzyme is said to be saturated with the substrate. If the enzyme concentration is held constant, a plot of initial reaction rate against initial substrate concentration will yield a typical curve of saturation kinetics, as shown in figure 1.13A. Two analytical regions are important. First, at low [S], the reaction rate is linearly related to [S]; under this condition of first-order kinetics, reaction rates can be used to quantify the substrate. Second, at high [S], the reaction rate is independent of [S] or zero order kinetics, all of the available enzyme exists as E•S, and the reaction rate can be used to determine the total amount of enzyme present in the sample.

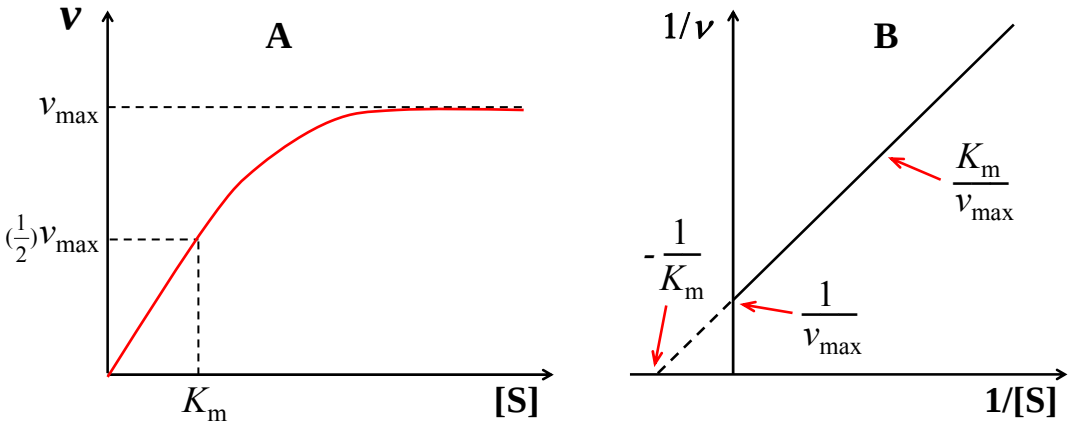


**Figure 1.13** (A) Reaction rate ($v$) versus substrate concentration ([S]) for an enzyme catalyzed reaction at constant enzyme concentration. (B) Lineweaver–Burk plot for $v$ measured as a function of [S].

One of the kinetic parameter, Michaelis–Menten constant, $K_m$, is related to the dissociation constant for the enzyme–substrate complex. It is defined as the substrate concentration at $v = (\frac{1}{2})\, v_{max}$.

The Michaelis–Menten equation may be algebraically rearranged to equation 1.30, yielding a third linear plot, called the Lineweaver–Burk or double-reciprocal plot:

$$\frac{1}{v} = \frac{1}{v_{max}} + \frac{K_m}{(v_{max})} \times \frac{1}{[S]} \qquad (1.30)$$

The invertion reaction rate $(\frac{1}{v})$ plotted against the invertion substrate concentration $(\frac{1}{[S]})$, yielding a straight line with a positive slope of $\frac{K_m}{v_{max}}$ and a y intercept of $\frac{1}{v_{max}}$. The parameter $K_m$ is then calculated from the linear regression values of the slope divided by the y intercept (figure 1.13B).

## 1.7 Nanotechnology in sensor design

Now a day, nanotechnology is playing an increasingly important role in the development of electrochemical sensors and biosensors. Sensitivity and other attributes of biosensors can be improved by using nanomaterials in their construction. Nanomaterials, or matrices with at least one of their dimensions ranging in scale from 1 to 100 nm, display unique physical and chemical features because of effects such as the quantum size effect, mini size effect, surface effect and macro-quantum tunnel effect. The nanomaterials can be classified by the shape and structure as nanoparticles, nanotubes, nanofibers, nanorods, nanowires, and thin films. The Au nanoparticles and carbon nanotubes are shortly explained in this thesis.

### 1.7.1 Gold nanoparticles

Gold nanoparticles (AuNP) is one of the most attractive nanoparticles in nanoparticle-based research due to it possess the good properties such as (i) identical size of all particles, (ii) identical shapes and morphology, (iii) identical chemical composition and crystal structure, and (iv) individually dispersed or monodispersed and no agglomeration [45]. The potential technical importance of monolayer-protected of gold nanoparticles is developing in nanoscale optoelectronic devices, corrosion-resistant materials, and new catalysts. It is used in the acoustic wave, optical, and magnetic biosensors. The AuNP have been assisted in electrochemical biosensors development via bounded the functional nanoparticles with a biological molecules (e.g. peptides, proteins, nucleic acids) for detection and amplifying response signals. The shortly review of AuNP in biosensor application is in chapter 3.3.

### 1.7.2 Carbon nanotubes

The nano-dimensions, graphitic surface with appealing geometrical, mechanical, optical, electrical, and chemical properties of carbon nanotubes (CNT) [46, 47] make it an ideal material for use in many fields of applications [48, 49].

Easily chemical modification and solubilization of the CNT represent the articles in polymeric nanocomposite, nanotube-probe interaction, and nanotube-proteins conjugates in the area of nanotechnology research [50]. Oligonucleotides, enzymes, and proteins were functionalized on multi-walled carbon nanotubes (MWCNT) to take advantage of MWCNT shape and exceptional rigidity [51].

The biocompatibility of the CNT in biosensors technology [52] is a significant issue on the sensor development. For example, both single-walled carbon nanotubes (SWCNT) and MWCNT have been used in biosensors. In one case, glucose oxidase was immobilized by coating onto the surface of the CNT without a gross loss of enzyme activity. The enhanced performance was partly due to the high enzyme loading and partly because of better electrical communication ability of the CNT. The direct electron transfer ability of carbon nanotubes has been exploited. The combination of the CNT with redox active enzymes appears to offer a convenient platform for a fundamental understanding of biological redox reactions and the future development of reagentless biosensors and nanobiosensors.

# CHAPTER II
# OBJECTIVES

To apply four important design concepts of the novel sensors for monitoring (i) electroactive species as insulin, (ii) electroinactive species as glycosidases by direct conversion to electroactive species as *p*-nitrophenol, (iii) electroactive spcecies as hydrogen peroxide ($H_2O_2$), and (iv) electroinactive species as phosphate ($PO_4^{3-}$) by assisting of enzymatic reaction to generate a common electroactive species as $H_2O_2$.

To design and fabricate (i) insulin chemical sensor, (ii) glycosidases sensor, (iii) $H_2O_2$ biosensor, and (iv) $PO_4^{3-}$ biosensor and then characterize these novel design sensors. This thesis is divided into four sub topics following:

## 2.1 Insulin chemical sensor

**Aim:** To obtain a highly stable insulin electrochemical sensor by incorporation of carbon nanotubes and ruthenium salt.

**Scope:**

2.1.1 Modify surface of glassy carbon electrode (GCE), with (i) preteatmented carbon nanotube (CNT), (ii) ruthenium oxide ($RuO_x$) and (iii) $RuO_x$/CNT bilayer.

2.1.2 Characterize the modified GCE with electrochemcial and transmission electron microscope techniques.

2.13 Apply the insulin electrochemical sensor in flow injection system.

## 2.2 Glycosidases sensor

**Aim:** To develop a novel sensitive and rapid glycosidases electrochemical sensor.

**Scope:**

2.2.1 Develop hydrodynamic voltammetric technique for detect *p*-nitrophenol as a probe molecule of enzymatic reaction product from glycosidases on screen printed carbon electrode (SPCE) and GCE.

2.2.2 Attempt to achieve the appropriated condition for high enzyme activity and the optimum substrate content by amperometric technique.

2.2.3 Compare analytical results, obtained by the glycosidases electrochemical sensor with spectroscopic assay.

## 2.3 Hydrogen peroxide biosensor

**Aim:** To develop a $H_2O_2$ biosensor with nanoelectrochemical deposition of gold nanoparticles (AuNP) and horseradish peroxidase (HRP) in chitosan (CHIT) matrix on a SPCE.

**Scope:**

2.3.1 Design and fabricate various configurations of SPCE, select the best configuration of SPCE by testing with cyclic voltammetry (CV).

2.3.2 Modify the selected SPCE with in-house synthesized AuNP and HRP by electrodeposition with CHIT. The in-house AuNP must be well characterized by UV-Vis spectroscopy and transmission electron microscope.

2.3.3 Characterize the $H_2O_2$ based biosensor by amperometric technique

## 2.4 Phosphate biosensor

**Aim:** To fabricate $PO_4^{3-}$ biosensor for real samples analysis.

**Scope:**

2.4.1 Fabricate a $PO_4^{3-}$ biosensor by deposition pyruvate oxidase (PyOD) on the $H_2O_2$ based biosensor.

2.4.2 Optimize an amount of enzyme PyOD, cosubstrate pyruvate, cofactor types, and coenzymes thiamine pyrophosphate (TPP) and flavin adenine dinucleotide (FAD).

2.4.3 Study effect of interferences such as $K_2SO_4$ and $NaNO_3$.

2.4.4 Validate this $PO_4^{3-}$ biosensor with standard UV-Vis method.

2.4.5 Use this $PO_4^{3-}$ biosensor to analyte the $PO_4^{3-}$ content in real water samples.

# CHAPTER III
# LITERATURE REVIEW

## 3.1 Insulin chemical sensor

Insulin is an endocrine protein hormone that is produced from pancreas for controlling the level of sugar in body. The pancreas is an organ that sits behind the stomach and has many functions. Carbohydrates or others sugars absorbed to the bloodstream are controlled by insulin in order to regulate them into inside of the cell. Narrow insulin concentration is very potent on blood glucose levels.

The detection of insulin is of great importance for clinical diagnostics, because it serves as a predictor of diabetes and hypoglycosimea. Bioassay [53, 54], immunoassay [55, 56], microchip-immunoassay [57], enzyme linked immunosorbent assay [58], chromatographic methods with UV-Visible (UV-Vis) [59, 60] or fluorescent detectors [61], fluorescence spectrophotometry [62, 63], mass spectrometry (MS) with isotope dilution assay (IDA) [64-67] are available procedures for the determination of insulin. Although these techniques are showed the great ability for insulin measurements, but all of them suffer from many disadvantages and are uncomfortable for general diagnostic laboratory. Bioassays have a relatively low precise and insensitive. While immunoassay of insulin that usually is deal with biological specimen, the cross reaction, non-specific binding and also biological against anti-insulin antibody in the biological samples are the major problems of immunoassay. The chromatographic method with UV-Vis as a detector is a practical of insulin determination. However, by the poor sensitivity of UV-Vis detector, this technique can not achieve precise results at nanomole-level of insulin in biological samples. The fluorescence is a very dominant detector of insulin in biological specimen but this technique is crucially needed the fluoregenic reagents for derivatization. The IDA method allows the precise determination of human insulin at

physiological concentrations in blood but requires labeled insulin with stable isotopes as an internal standard and an expensive instrument.

The development of insulin electrochemical sensors is considerable on direct electrochemical measurement, none time consuming, and capability at low level of insulin secretion. The electrochemical techniques are limited because of the slow kinetics of insulin oxidation at common electrode materials. Various chemically modified electrodes have thus been developed for promoting the oxidation and detection of insulin. These include electrodes coated with inorganic films based primarily on ruthenium [68-71] or iridium [72] electrocatalytic systems or more recently surfaces coated with carbon nanotube (CNT) layers [10].

Gorski *et. al.* [73] reported a ruthenium oxide ($RuO_x$) film was voltammetric deposition from a 0.2 mM $RuCl_3$, 10 mM $HClO_4$ mixture onto carbon fiber yielded a modified electrode that permitted the amperometric determination of insulin at pH 7.4 at the sub-micromolar level over a 3-day period. They also performed to find a stable catalyst that promoted the oxidation of insulin at physiological pH, the $RuO_x$ was working stable in physiological pH. Films that were formed with 0.1 M $KNO_3$ rather than 10 mM $HClO_3$ as the supporting electrolyte yielded a slower response to insulin. Pikulski and Gorski [72] explained the iridium oxide ($IrO_x$) film were inherent stability at physiological pH and the catalytic activity of the $IrO_x$ film toward insulin oxidation was ascribed to a combination of electron transfer mediation and oxygen transfer which was related to the acid/base chemistry of the film.

Kennedy *et. al.* [74] used 10 μm $RuO_x$ in diameter to monitor insulin from pancreatic β-cell by glucose stimulation. Their system was limited by the instability of the $RuO_x$ film at pH above about 5. Apparently the oxidized form of $RuO_x$ slowly dissolves in aqueous solution except at low pH values explored by Gorski and Cox [75]. These electrodes still lack of the specificity, sensitivity and stability. Either reducing the stability of mediators and electrocatalysis under physiological conditions or progressive fouling of electrode surface during insulin oxidation was the main

reason. In addition the modified electrodes employed for insulin determination reveal more major limitations such as; high detection limit.

Recent studies have illustrated that the electrocatalytic response of CNT modified electrodes towards carbohydrate, peroxide or alcohol compounds can be greatly enhanced by coupling with catalytic metal centers (such as Cu or Pt) [76].

In this topic of thesis, the development of $RuO_x$/CNT modified carbon electrode will offers substantial improvements in the stability and sensitivity of voltammetric and amperometric measurements of insulin. The enhanced electrocatalytic activity leads to a substantial improvement in the sensitivity, and is coupled with a greatly enhanced stability. Moreover, the $RuO_x$/CNT coating will be marked acceleration of the insulin oxidation compared to the individual ($RuO_x$ and CNT) coated electrodes.

## 3.2 Glycosidases sensor

The glycoproteins studying are new and important branch of medical science as a guide of discovering and understanding genetic diseases. The great uncover in glycomics research are glycan biomarkers [77]. One of glycomics is glycosidases enzymes that catalyze the reaction by hydrolyzed the glycosidic bonds in simple glycosides, oligosaccharides, polysaccharides, mucopolysaccharide, glycoproteins and glycolipids. Glycosidases are an important class of hydrolase enzymes as mention in chapter 1, they are involved the hydrolysis in the catabolism of glycoconjugates and are indispensable for structural analysis of these complex molecules. The lack of a specific glycosidases can cause inherited metabolic disorders such as glycogen, glycosaminoglycan and glycolipid storage diseases [78].

Accordingly, bioassays of glycosidases activities are of tremendous importance for diagnosing metabolic disorders, for cancer screening, and for glycomic research. Most current methods to determine the activity of glyco-active enzymes rely

on colorimetric [79], radiological [78], and enzyme immunoassay [80] measurements. Synthetic chromogenic substrates, such as *p*-nitrophenol (PNP) and *p*-methyl umbelliferyl (PMU), are commonly used for optical assays of the activity of glycosidases [81]. Nitrophenol-sugar conjugates are widely available commercially and are one of the most common substrates for glycosidases assays. Phenolic products are commonly detected amperometrically in connection to alkaline-phosphatase [82] or organophosphorushydrolase bioassays [82-84]. The new electrochemically assay for glycosidases activity is proposed on the anodic detection of the enzymatically-generated PNP from a fixed concentration of the corresponding glycoside substrate.

Amperometric bioassays have been used earlier for measuring the activity of clinically important enzymes such as alkaline phosphatase [85] or aspartate aminotransferase and alanine aminotransferase [86]. It is also used as well in the immunoassay for estradiol in human serum extracts [87].

In most enzyme activity measurements, the kinetics of the enzyme-catalyzed reactions is followed under optimal conditions (temperature, pH, and substrate concentration, etc.). The concentration change of a reaction partner or product is measured in the bulk of the media after the sample of unknown enzyme activity is introduced. However, optical and radiological assays of glycoactive enzymes are time consumed, not amenable for kinetic activity assays, expensive and require extensive experimental set ups. Highly sensitive, rapid, simple and low-cost methods of glycosidases activity measurements are urgently needed to facilitate the detection of these important enzymes [88].

In this topic of thesis, the electrochemical bioassay for monitoring of glycosidases activity required for encounter above requirements. Electrochemical devices are uniquely qualified for meeting the size, cost, low-volume, and power requirements of point-of-care diagnostics. The surface fouling problems associated with phenolic compounds oxidative reaction on an electrode surface is one of major problems for sensor development [89-91], it is also studied to get rid these problems.

The sensitivity of this bioassay will be kinetically compared with the results obtained by using UV-Vis spectrophotometer.

## 3.3 Hydrogen peroxide biosensor

Screen-printing technology is a technique often used in the fabrication of electrodes for the development of disposable electrochemical biosensors. A screen printed carbon electrode (SPCE) is a planar device based on multiple layers of printed inks on a polyimide [92], plastic [93], epoxy [94] or alumina ceramic [95] substrates. The advantages of designable techniques, adapted from microelectronics, have made screen-printing technology one of the most important for thefabrication of single-use biosensors in the market of handheld instruments. The main advantages of the SPCE include simplicity, versatility, modest cost, portability, ease of operation, reliability, small size and mass production capabilities, leading to its development in various applications in the electroanalytical chemistry field.

Hydrogen peroxide ($H_2O_2$) is an enzymatic intermediate substance of many enzyme-substrate reactions. Determination of hydrogen peroxide has been reported by many methodologies, e.g. UV-Visible (UV-Vis), fluorescence, chemiluminescence, acoustic emission and electrochemical techniques. The most common electrochemical technique investigated is via the anodic oxidation of $H_2O_2$ at a platinum metal electrode [96], metal-dispersed carbon paste electrodes [97] and platinized sputtered glassy carbon electrode [98]; however, a main problem occurs from the high overpotential and subsequent interference from matrix species. This problem has been minimized by using the cathodic reduction of $H_2O_2$ by use of enzyme-linked osmium bipyridine redox wired polymers [99], Nafion-methylene blue composite [100], prussian blue and derivatives [101-103], carbon nanotube-cobalt hexacyanoferrate/chitosan composite [104], mediated electron transfer of horseradish peroxidase (HRP) by hydroquinone [105] and via direct electron transfer (DET) of the third generation of biosensors by HRP [106-108].

The report on the simplest electrode for the detection of peroxide consists of a layer of peroxidase molecules adsorbed onto the electrode surface. The reduction current is observed while the electrode is placed into a sample and poised at a negative potential. This reduction behavior was discovered for HRP adsorbed on carbon black [109] and later it was demonstrated on carbon and graphite [110-116], carbon fibers [117], gold [118] and platinum [119, 120] electrodes. The DET method is used often in the fabrication of $H_2O_2$ biosensor. It easily facilitates the electron transfer between the enzyme and electrode surface and makes a more sensitive and convenient environment for the electrochemical biosensor.

In the 21$^{st}$ century, the nanoscience encompasses the phenomena in the dimension spanning of atom, molecule, supermolecule, polymers and biomolecules. Scientists from chemistry, physics, biology, colloid and polymer chemistry, materials and surface science, biochemistry, biophysics and molecular biology have begun to examine and characterize the superior properties and phenomena of materials at the nanoscale dimensions, smaller than 100 nm [121]. There is little doubt that the use of these new nanosciences will lay the ground for the new technological revolution. Nanotechnology, the technological use of properties and phenomena of nanoscience, has across practically all domains of human activity. These nanotechnologies are swanking to revolutionize a breathtaking range of fields. The intense interest in using nanotechnology promises that they boast superior electrical, optical, mechanical, chemical, or biochemical properties. Nanotechnology, including nanoparticles, nanotubes, nano-quantum dots and nanowires, has been used in various applications. This is owed to the essential properties of high chemical and thermal stability, surface to volume ratio, elasticity, and tensile strength. These properties along with the metallic conductivity exhibited by some nanotechnology, allow for their use as functional components in the fabrication of medical sensing devices [122].

In the field of electroanalytical chemistry, gold nanoparticles (AuNP) have attracted enormous interest in the application of $H_2O_2$ determination [123-125], lactate determination [126], glucose determination [127, 128], protein functionalization [129], DNA determination [130], antigen determination [131], and

antibody determination [132]. The AuNP assist in constructing an interface for direct electron transfer of redox-active proteins while retaining their bioactivity. The AuNP provide a natural environment for bimolecular immobilization allowing for longer life stability. Colloidal Au has gained much more attention in electroanalytical studies because of its unique properties such as easy preparation, good biocompatibility and relatively large surface area.

Chitosan (CHIT) is a polysaccharide consisting of the functional groups -OH and -$NH_2$, and possesses many properties such as good film-forming ability, chemical inertness, high mechanical strength, high hydrophilicity, biodegradable, bioabsorbable and biocompatibility [133] where the degradation products do not have any toxic effect (see appendix C for CHIT structure). CHIT has been reported on many applications such as in medical healing, delivery and sensors. In medical healing and delivery applications, Sashiwa and Aiba [134] investigated the role of individual functional groups in applications of CHIT. They modified CHIT by attaching sugars, dendrimers, cyclodextrins, crown ethers, and glass beads to CHIT and concluded that among these derivatives, sugar-modified CHIT were excellent candidates as drug delivery systems or for cell culture while CHIT–dendrimer hybrids were interesting multifunctional macromolecules in biomedicinal applications. It was reported that unmodified CHIT has ability to condense DNA and form small discrete particles [135]. Also they have been reported that CHIT preparations as gene delivery systems used non-N-alkylated CHIT samples containing only primary aminogroups along with N-acetyl moiety. For medical sensors applications, there have been several reports of CHIT used as an immobilization matrix by cross-linking with enzymes through glutaraldehyde or other substances. This form of enzyme-CHIT is often manually coated on electrode surfaces to fabricate biosensors. As is known, covalent cross-linking of enzymes may lead to partial loss of enzyme activity and manual coating of electrodes may result in uncontrollable thickness of films. The selective depositing method for creating films with controllable thickness and a comfortable microenvironment for enzyme activity is very important for sensor applications.

It has been reported that CHIT hydrogel can be electrochemically deposited onto electrodes and other substances, such as gold nanoparticles [127, 136]. Enzymes can also be effectively incorporated into the sol–gels to form biocomposites during the electrodeposition while retaining their natural properties. In the literature there is no report of SPCE design. The electrode configuration is a very important role that affects the reaction potential of substances on electrode surfaces.

In this topic of thesis, two main tasks are focused as, (i) design and develop a SPCE that gives the highest performance and (ii) use the electrodeposition of CHIT to avoid the uncontrolled thickness of CHIT on the surface of the designated SPCE assembled with HRP/AuNP for determination of enzymatic intermediate substances.

## 3.4 Phosphate biosensor

Phosphate ($PO_4^{3-}$) is an essential nutrient and energy carrier on many different levels of life. It is a key element in coupling biotic and a biotic of the biosphere because it allows the construction of long-term feedback mechanisms between climate, environment and ecology. The recommended maximum level of $PO_4^{3-}$ in water is generally very low; for example, the EPA recommended that it should not exceed 0.05 mg $L^{-1}$ P (1.53 μM $PO_4^{3-}$) if streams discharge into lakes or reservoirs, 0.025 mg $L^{-1}$ P (0.76 μM $PO_4^{3-}$) within a lake reservoir and 0.1 mg $L^{-1}$ P (3.06 μM $PO_4^{3-}$) in streams or flowing waters not discharging into lakes or reservoir.

Some examples of $PO_4^{3-}$ determination methods have been effective and available but they belonging disadvantage by their own analytical properties, namely chromatography with spectrophotometric detector [137, 138], ion chromatographic - inductively couple plasma spectrometric [139, 140], and X-ray spectrometric methods [141, 142].

Spectrophotometric methods, based on colorimetric detection, have been widely applied for the determination of orthophosphate. Basically, the methods involve the treatment of the sample with an acidic molybdate solution to produce a phosphomolybdate complex, which is further reduced by ascorbic acid to an intensely

colored product. These methods require a careful selection of experimental conditions.

Inductively couple plasma spectroscopy (ICP) has certainly been the answer to many needs in this respect but this method can not be used in the remote area or outside of the well equipped laboratory.

X-ray spectroscopy is the method that can easily analyze samples without any digestion. The disadvantage of X-ray were a bulky and heavy instrument, high capital cost, including it need an expertise for operation. Consequently, it is not possible for field analysis.

As mentioned above, the need for accurate methods for measuring true concentrations of inorganic $PO_4^{3-}$ is obvious. Therefore, analytical methods need to be analyzer very sensitive. Furthermore, for widespread applications, the developed method should be reliable, cost-effective and applicable for on-site monitoring. Phosphate sensor has potential to fulfill these requirements. A lot of potentiometric and amperometric $PO_4^{3-}$ sensors have been investigated. The potentiometric $PO_4^{3-}$ sensors have been developed with various types of modified such as liquid-membrane electrodes [143-145], coated-wire electrodes [146], heterogeneous membrane electrodes [147], solid-state electrodes [148, 149] and metal electrodes [150, 151]. Phosphate biosensor is known as amperometric $PO_4^{3-}$ sensors, with mono- or multi-enzymes.

The $PO_4^{3-}$ biosensors are normally classified where $PO_4^{3-}$ acts as inhibitor or substrate. Others classification taken by enzyme species as (i) alkaline phosphatase [152-155], (ii) phosphorylase A [156], (iii) nucleoside phosphorylase [157-159], (iv) pyruvate oxidase (PyOD) [160-169] and (v) maltose phosphorylase [170-173] which is immobilized on the electrode membrane. The development has taken into mono, bi, tri, and/or quad enzymes for obtaining a great sensitivity. The detection is achieved via $O_2$ reduction, $H_2O_2$ oxidation, and nicotinamide adenine dinucleotide (phosphate) reduced form (NAD(P)H) oxidation. Table 3.1 is summarized the reaction of $PO_4^{3-}$ biosensors.

**Table 3.1** Summary of the phosphate biosensor

| Authors | System | Reaction | Linearity / µM | Detection limit / µM | Refe-rences |
|---|---|---|---|---|---|
| Guilbault and Nanjo | Alkaline phosphatase | $\beta$–Glucose-6-phosphate + $H_2O_2$ $\xrightarrow{\text{Alkaline phosphatase}}$ $\beta$–Glucose + Orthophosphate<br>$\beta$–Glucose + $O_2$ + $H_2O$ $\xrightarrow{\text{Glucose oxidase}}$ Gluconic acid + $H_2O_2$<br>$O_2 + 2H_2O + 2e^- \xrightarrow{\text{-0.6 V vs SCE}} H_2O_2 + 2OH^-$ | - | 100 | [152] |
| Guilbault and Cserfalvi | Phospho-rylase A | Glycogen (n) + Orthophosphate $\xrightarrow{\text{Phosphorylase A}}$ $\alpha$–Glucose-1-phosphate + Glycogen (n-1)<br>$\alpha$–Glucose-1-phosphate $\xrightarrow{\text{Phospho glucomutase}}$ $\alpha$–Glucose-6-phosphate<br>$\alpha$–Glucose-6-phosphate + NADP $\xrightarrow{\text{Glucose-6-phosphate dehydrogenase}}$ 6-phosphogluconic acid + NADPH<br>NADPH $\longrightarrow$ $NADP^+ + H^+ + 2e^-$ | *50 - 1000 | *10 | [174, 175] |
| Watanabe *et. al.* | Nucleoside phosphorylase + Xanthine oxidase | Ionosine + Orthophosphate $\xrightarrow{\text{Nucleoside phosphorylase}}$ Ribose-1- phosphate + Hypoxanthine<br>Hypoxanthine + $2H_2O$ + $2O_2$ $\xrightarrow{\text{Xanthine oxidase}}$ Uric acid + $2H_2O_2$<br>$O_2 + 2H_2O + 2e^- \xrightarrow{\text{- 0.6 V vs SCE}} H_2O_2 + 2OH^-$ | **0.1 - 10 | **0.1 | [176, 177] |

*Reported by Wollenberger and Scheller [175] with addition of glucose oxidase/mutarotase.

** Reported by d'Urso and Coulet [177].

**Table 3.1** Summary of the phosphate biosensor (CONTS.)

| Authors | System | Reaction | Linearity / µM | Detection limit /µM | Refe-rences |
|---|---|---|---|---|---|
| Kubo *et. al.* | Pyruvate Oxidase | $\text{Pyruvate} + \text{Orthophosphate} + O_2 \xrightarrow{\text{Pyruvate oxidase}} \text{Acetyl phosphate} + H_2O_2 + CO_2$<br>$O_2 + 2H_2O + 2e^- \xrightarrow{-0.6\ \text{V vs SCE}} H_2O_2 + 2OH^-$ | 12 - 80 | - | [160] |
| Conrath *et. al.* | Maltose Phospho-rylase | $\text{Maltose} + \text{Orthophosphate} \xrightarrow{\text{Maltose phosphorylase}} \beta\text{-Glucose-1-phosphate} + \alpha\text{-Glucose}$<br>$\beta\text{-Glucose-1-phosphate} + 2H_2O \xrightarrow{\text{Acid phosphatase}} \beta\text{-Glucose} + \text{Orthophsphate}$<br>$\alpha\text{-Glucose} \xrightarrow{\text{Mutarotase}} \beta\text{-Glucose}$<br>$\beta\text{-Glucose} + H_2O + O_2 \xrightarrow{\text{Glucose oxidase}} \text{Gluconic acid} + H_2O_2$<br>$2H_2O_2 \xrightarrow{+0.6\ \text{V vs SCE}} O_2 + 2H^+ + 2e^-$ | 0.1 - 1 | 0.001 | [170] |

A rapid alternative is the use of $PO_4^{3-}$ biosensors as mention above is advantage over other old methods, including high selectivity, simple use, and possibility to miniaturization. However, some of $PO_4^{3-}$ biosensors suffer from a low reproducibility, less stable, a poor enzyme activity, slow response time, and a poor spatially controlled deposition of enzymes. For example, the response time of $PO_4^{3-}$ biosensor was reported to be 3 min [161] for one measurement, which is not efficient for rapid monitoring. In the multi-enzymes based $PO_4^{3-}$ biosensors, the optimal operating conditions of multi-enzymes might be different, which do not give the sensor long-term stability. The biosensors are prepared from the physical adsorption of a monomer and an enzyme from a mixed solution followed by electrochemical co-polymerization of the adsorbed monomer and enzyme in an aqueous solution could only give a less stable sensor due to the loss of enzyme during the measurement [178]. Moreover, the high concentration of monomer in the mixed solution can affect the enzyme activity, which can make a less sensitive $PO_4^{3-}$ biosensor.

This topic of thesis needs to develop the $PO_4^{3-}$ biosensor on a simple SPCE and apply to use with real sample water. The simple enzyme, PyOD, is required to react with $PO_4^{3-}$ by equation of Kubo *et. al.* [160] and is detected at the $H_2O_2$ biosensor. The sensing response can be obtained from the reduction current of generated $H_2O_2$ with assisting of AuNP and CHIT on the SPCE.

# CHAPTER IV
# EXPERIMENTAL

Materials, electrochemical instruments setup and electrode modification are explained thoroughly by this chapter. For topics are separately elucidated as insulin, glycosidases, hydrogen peroxide and phosphate sensors.

## 4.1. Insulin chemical sensor

### 4.1.1 Chemicals

The materials used in this work were obtained as in the list of table 4.1. All of materials were prepared by deionized (DI) water ($R \geq 18.2$ MΩ-cm) obtained from the PURELAB® ultra analytic system, Munich, Germany.

**Table 4.1** List of chemicals for fabrication of insulin electrochemical sensor

| Chemicals | Suppliers |
|---|---|
| *N*,*N*-Dimethylformamide, DMF | Aldrich, Germany |
| Disodium hydrogen phosphate hepta hydrate 99%, $Na_2HPO_4$ 7 $H_2O$ | Sigma, USA |
| Hydrochloric acid 36%, HCl | EMD Chemical Inc. Gibbtown, NJ, USA |
| Insulin from Bovine pancreas; 28 USP units $mg^{-1}$ | Sigma, USA |
| Multi-wall carbon nanotubes 95%, CNT | NanoLab Inc. Brighton, MA, USA |
| Nitric acid, 69%, $HNO_3$ | EMD Chemical Inc. Gibbtown, NJ, USA |
| Perchloric acid 70%, $H_3ClO_4$ | Sigma, USA |

**Table 4.1** List of chemicals for fabrication of insulin electrochemical sensor (CONTS.)

| Chemicals | Suppliers |
|---|---|
| Ruthenium(III)chloride 99 %, $RuCl_3$ | Acros Organics, Fair Lawn, NJ, USA |
| Sodium chloride 99.5%, NaCl | Sigma, USA |
| Sodium hydroxide 99%, NaOH | Sigma, USA. |
| Sodium dihydrogen phosphate mono hydrate 98%, $NaH_2PO_4$ $H_2O$ | Sigma, USA |

### 4.1.2 Instrumentals

The fabrication of insulin electrochemical sensor had been involved many instruments, all of them were listed in table 4.2.

**Table 4.2** List of instruments for fabrication of insulin electrochemical sensor

| Instruments | Details |
|---|---|
| Analytical balance | Denver instrument TC 254, Denver, CO, USA |
| DI water system, R ≥ 18.2 MΩ-cm | PURELAB® ultra analytic system, Munich, Germany |
| Electrochemical analyzer | (i) CHI 1030 (CH instruments, Austin, TX, USA), with a platinum wire (Sigma USA) as counter electrode (CE), an Ag/AgCl in 3 M KCl (CH111) as reference electrode (RE), a 3 mm Ø glassy carbon (GC) (CH104) as working electrode (WE).<br>(ii) μAutolab 2 (Eco Chemie B. V., The Netherlands), CE, RE, and WE as above. |

**Table 4.2** List of instruments for fabrication of insulin electrochemical sensor (CONTS.)

| Instruments | Details |
|---|---|
| Flow injection system | Consisting of a peristaltic pump (Miniplus, Gilson Inc. WI, USA), injection valve (200 μL stainless steel loop, Rheodyne model 7010, USA), and a wall-jet flow through detector provided by Prof. J. Wang, the Center for Bioelectronics and Biosensors, ASU, USA |
| pH meter | Denver 300735.1, CO, USA |
| Scanning electron microscope | Philips FEI XL60 EFSEM scanning electron microscope, Mahwah, NJ, USA |
| UV-Visible spectrophotometer | Shimadzu UV-2501 PC, Columbia, MD, USA |

### 4.1.3 Chemical preparation

**- 0.4 mM insulin/1.25 mL**

Weigh 2.9 mg of insulin and dissolve in 1.25 mL of 0.02 mM HCl. Shake with shaking machine for 1 hour for making a solution clear. Further dilution was carried out using a 0.10 M NaCl/0.05 M phosphate buffer solution. The solution was freshly prepared before used.

**- 0.1 M NaCl/250 mL**

Weigh 1.4610 g of NaCl and dissolve in 150 mL DI water. The solution was adjusted to 250 mL.

**- 0.05 M $NaH_2PO_4$/250 mL in 0.1 M NaCl solution**

Weigh 1.7600 g of $NaH_2PO_4 \bullet H_2O$ and dissolve in 150 mL 0.1 M NaCl. The clear solution was adjusted to 250 mL by 0.1 M NaCl.

**- 0.05 M $Na_2HPO_4$/250 mL in 0.1 M NaCl solution**

Weigh 3.4192 g of $Na_2HPO_4 \bullet 7H_2O$ and dissolve in 150 mL 0.1 M NaCl. The clear solution was adjusted to 250 mL by 0.1 M NaCl.

**- 1 M NaOH/250 mL**

Weigh 10.10xx g of NaOH and dissolve in 150 mL DI water. The solution was adjusted to 250 mL.

**- 3 M HCl/20 mL**

Pipette 5.149 mL (5 + 0.149 mL) of concentrated HCl and dissolve in 20 mL DI water.

**- Phosphate buffer solution; PBS (0.05 M PBS pH 7.4 in 0.1 M NaCl)**

Transfer 19.2 mL of 0.05 M $NaH_2PO_4$/0.1 M NaCl to mix with 81.8 mL of 0.05 M $Na_2HPO_4$/0.1 M NaCl for obtaining 0.05 M PBS/0.05 M NaCl. The pH value of PBS was adjusted to pH 7.40 by 0.1 M NaOH or 3 M HCl.

**- 10 mM $HClO_4$/20 mL**

Pipette 17 μL of concentrated $HClO_4$ and dissolve in 20 mL DI water.

**- 0.3 mM $RuCl_3$/2 mL 10 mM $HClO_4$**

Weigh 0.1257 mg $RuCl_3$, dissolve and sonicate (~ 5 minutes) in 2 mL of 10 mM $HClO_4$. The solution was freshly prepared before used.

### 4.1.4 Electrode modification

**- MWCNT Pretreatment**

Weigh 100 mg of MWCNT and put in 100 mL of concentrated nitric acid. Keep heating and sonicating simultaneously at 60 °C and for 12 hours. 3 L of DI water added to the MWCNT slurry and left it until setting. The upper solution was pour and added the DI water again, checked the pH with pH meter. Repeat the rinse step until obtained pH 7 (~ a week). Pour DI water and keep the CNT suspension in a small beaker. Transfer CNT suspension to glass plate and dry it in oven at 120 °C.

**- Drop casting CNT on GCE (CNT/GCE)**

Weigh 2 mg CNT-pretreated and sonicate in 1 mL DMF until obtaining CNT slurry. Take 30 μL slurry of 2 mg $mL^{-1}$ CNT/DMF and drop on the mirrored-like cleaned GCE, then let it dry to get CNT modified GCE (CNT/GCE). Rinse CNT/GCE with DI water prior to use.

**- $RuO_x$/GCE**

The $RuO_x$ modified GCE was prepared by electrodeposition of the $RuO_x$ film from a 0.30 mM $RuCl_3$ in 10 mM $HClO_4$ solution by cycling the potential between –0.80 and +0.65 V at 10 V $s^{-1}$ for 12.5 minutes.

**- $RuO_x$/CNT/GCE**

The $RuO_x$/CNT modified GCE was prepared by a similar drop casting of CNT 'slurry' on the surface of the cleaned GC disk, followed by electrochemical deposition of $RuCl_3$ using a 12.5 min potential cycling as described in 4.1.4.

### 4.1.5 Electrochemical cells setup

**- Stirred and quiescent cell**

A conventional electrochemical cell (2 mL), with three electrode system, was used for voltammetric and amperometric batch experiments. Magnetic stirring was employed during the batch amperometric (stability) experiment. The schematic diagrams of stirred and quiescent electrochemical cells were set up as figure 4.1. See appendix A.1 for photos of electrochemical cell.

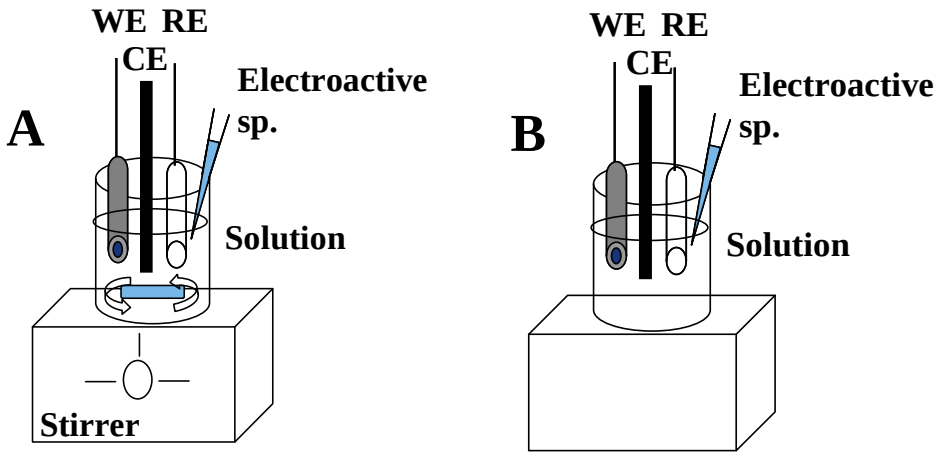


**Figure 4.1** Schematic diagrams of (A) stirred and (B) quiescent electrochemical cells for testing insulin sensor. WE, CE and RE are working, counter and reference electrodes, respectively. See appendix A.1 and A.2 for photos.

**- Flow injection system**

The flow injection system consisted of a carrier solution reservoir (C), an injection valve with a 200 µL sample loop, interconnecting PVC tubing, a peristaltic pump, and a large-volume wall-jet amperometric flow detector (D). The GCE, the Ag/AgCl reference electrode and the Pt wire counter-electrode were inserted into the detector through holes in its Teflon cover. The flow injection analysis system was set as figure 4.2. See appendix A.1 for photo of FIA setup.

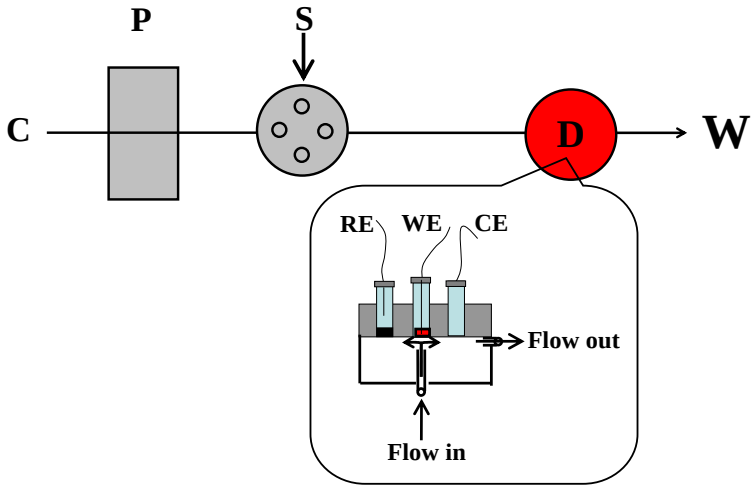


**Figure 4.2** Schematic diagram of flow injection analysis manifold for insulin sensor development. P is a pump, C is a carrier line, S is a sample injection port, D is a flow through electrochemical detector with wall jet pattern consisting of working (WE), counter (CE) and reference (RE) electrodes, and W is the waste line. See appendix A.1 for photo of FIA setup.

### 4.1.6 SEM characterization

Scanning electron microscopy (SEM) images of the modified electrodes were obtained with a FEI XL 60 EFSEM at operating voltage of 15.41 kV. A gold film, sputtered on the electrode surface, provided an enhanced conductivity. Bare GCE, CNT/GCE, Ru/GCE, and Ru/CNT/GCE were characterized and compared.

## 4.2 Glycosidases sensor

### 4.2.1 Chemicals

All chemicals of this work were obtained as in the list of table 4.3.

**Table 4.3** List of chemicals for fabrication of glycosidases sensor

| Chemicals | Suppliers |
|---|---|
| Carbon ink | Ercon, G-449(I), Wareham, MA, USA |
| Citric acid monohydrate ≥ 99.5% | Sigma, USA. |
| Endo-α-N-acetylgalactosaminidase (Streptococcus pneumoniae, recombinant, E. coli, EC 3.2.1.97) | EMD Bioscience Inc., La Jolla, CA, USA |
| β-1,3-Galactosidase (Escherichia coli, recombinant, EC 3.2.1.23) | EMD Bioscience Inc., La Jolla, CA, USA |
| Hydrochloric acid 37%, HCl | EMD Chemical Inc. Gibbstown, NJ, USA |
| *p*-Nitrophenyl-2-acetamido-2-deoxy-*o*-(β-D-galactopyranosyl)-α-D-galactopyranoside (4-NP-α-GalNAc-Gal) | Toronto Chemical Research Inc. North York, ON, Canada |
| 4-Nitrophenol-β-D-galactopyranoside (4-NP-β-Gal) | Sigma, USA. |
| *p*-Nitrophenol 98%, PNP | Aldrich, USA |
| Pt powder, 0.05 μm, 99.9% | Aldrich, USA |
| Sodium hydroxide 99%, NaOH | Sigma, USA. |

### 4.2.2 Instrumentals

Instruments for glycosidases sensors development were listed in table 4.4.

**Table 4.4** List of instruments for fabrication of glycosidases sensor

| Instruments | Details |
|---|---|
| Analytical Balance | Denver instrument TC 254, Denver, CO, USA |
| DI water system, R ≥ 18.2 MΩ-cm | PURELAB® ultra analytic system, Munich, Germany |
| Electrochemical instrument | CHI 1030 (CH instruments, Austin, TX, USA), with a platinum wire (Sigma USA) as counter electrode (CE), an silver/silver chloride (Ag/AgCl) in 3 M KCl (CH111) as reference electrode (RE), a 3 mm Ø glassy carbon (GC) (CH104) as working electrode (WE). |
| pH meter | Denver 300735.1, CO, USA |
| High precision screen printed machine | SPM/B, MPM, Franklin, MA, USA |
| UV-Visible spectrophotometer | SpectraMax M5 instrument, Sunnyvale, CA, USA |

### 4.2.3 Chemical preparation

**- 10 mM *p*-nitrophenol/5 mL**

Weigh 6.9 mg of *p*-nitrophenol and dissolve in 5 mL DI water.

**- 0.2 M NaOH/200 mL**

Weigh 1.61xx g of NaOH and dissolve in 200 mL DI water.

**- 0.1 M HCl/250 mL**

Pipette 2.109 mL (2 + 0.109 mL) of concentrated HCl and dissolve in 250 mL DI water.

**- 0.1 M Citric acid in 200 mL 0.2 M NaOH solution**

Weigh 4.2453 g of citric acid monohydrate and dissolve in 200 mL of 0.2 M NaOH.

**- 0.05 M Citrate buffer solution pH 4.4/100 mL**

Mix 66.4 mL of 0.1 M citric acid/0.2 M NaOH with 33.6 mL of 0.1 M HCl and adjust to a desired pH by 0.1 M citric acid/0.2 M NaOH or 0.1 M HCl.

**- 10 mM 4-Nitrophenyl β-D-galactopyranoside / 1 mL**

Weigh 3 mg of 4-nitrophenyl β-D-galactopyranoside and dissolve in 1 mL of DI water. The solution was keep at 4 °C until use.

**- 0.1 Unit / μL β-1,3-galactosidase**

Pipette 5 μL of stock β-1,3-galactosidase and dilute in 50 μL DI water. The solution was kept at 4 °C prior to use.

**- 1% Pt nanoparticle (PtNP)/carbon ink**

Weigh 0.05 g of PtNP and mix in 5 g carbon ink.

**- 3% Pt Nanoparticle (PtNP)/carbon ink**

Weigh 0.15 g of PtNP and mix in 5 g carbon ink.

**- 5% Pt nanoparticle (PtNP)/carbon ink**

Weigh 0.25 g of PtNP and mix in 5 g carbon ink.

### 4.2.4 Screen printed carbon electrode fabrication

The nanoparticle mixed carbon inks were printed by an automatic screen printer machine on alumina ceramic plate with working electrode area of 1.5 mm x 6 mm. The screening of insulator ink was applied on top of screened-alumina plated for figuring working area. The electrode was cured at 140 °C for 1 hour. These screen printed carbon electrodes (SPCEs**)** have been electrochemical characterized by SWV and cyclic voltammetry (CV). Results of peak height from SPCE were compared with GCE.

### 4.2.5 Electrochemical cell setup

Amperometric and SWV measurements were conducted by using a CHI 1030 Electrochemical Analyzer in a conventional three electrode electrochemical cell (1.5 mL). The GCE or SPCE, the Ag/AgCl (saturated KCl) reference, and the platinum wire counter electrodes were inserted into the cell. Magnetic stirring was employed for amperometric experiments. The setup of the electrochemical cell was the same as figure 4.1.

**- *p*-Nitrophenol (PNP) optimization**

Hydrodynamic voltammetry was conducted by adding a solution of stock PNP to obtained 10 μM PNP into a stirred solution for the PNP oxidation at a GCE. Successive additions of 0.1 μM PNP in a stirred 1.5 mL 0.05 M citrate buffer solution was carried out by amperometric technique.

**- Substrate studies**

Successive additions of 5, 50, 100, 150 and 200 μM of 4-NP-β-Gal at GCE into a 1.5 mL stirred 0.05 M citrate buffer solution (pH 4.4) containing 10 units of β-1,3-galactosidase enzyme. The calibration was plotted based on current measuring at 60 sec after adding the 4-NP-β-Gal.

**- Enzyme reaction studies**

Successive additions from 0.2 to 1.0 Unit of β-1,3-galactosidase at GCE in a 1.5 mL of stirred solution of 133 μM of 4-NP-β-Gal were conducted. The endo-α-N-acetylgalactosaminidase were also monitored by amperometric technique from 0.2 mUnit to 1 mUnit (e) at GCE in a 1.5 mL of stirred 0.05 M citrate buffer solution containing 200 μM of 4-NP-α-GalNAc-Gal.

### 4.2.6 Spectrophotometric assay

A procedure for optical assay was adapted in details form Lo *et. al.* [81]. Briefly, the endo-α-N-acetylgalactosaminidase activity were performed using a SpectraMax M5 instrument with 1 cm path length photo cell over the 0.2-1.0 mU (1.5 mL)$^{-1}$ range. The 4-NP-α-GalNAc-Gal substrate solution (200 μM, 1.5 mL) was prepared in 0.05 M citrate buffer (pH 4.4). Negative controls were used as references for each set of reactions. Prior to incubation with enzymes, a 100 μL aliquot of the substrate solution was removed for use in the blank mixture. To the remaining 1.4 mL

of substrate, an appropriate dilution of endo-α-N-acetylgalactosaminidase in 10 μL of 0.05 M citrate buffer (pH 4.4) was added and the mixture incubated at 37 °C with gentle mixing. At 10 minute intervals, a 100 μL aliquot of the reaction mixture was immediately transferred to a well in a 96-well polystyrene plate preloaded with 50 μL of 0.5 M $Na_2CO_3$ per well. After mixing, the absorbance was measured at 405 nm.

## 4.3 Hydrogen peroxide biosensor

### 4.3.1 Chemicals

All chemicals for development of hydrogen peroxide ($H_2O_2$) biosensor were obtained as in the list of table 4.5.

**Table 4.5** List of chemicals for fabrication of hydrogen peroxide biosensor

| Chemicals | Details |
|---|---|
| Ag ink, C7019 | Acheson-Electrodag, USA |
| Ag/AgCl ink, 479SS | Acheson-Electrodag, Canada |
| Carbon ink, PF407C | Acheson-Electrodag, USA |
| Chitosan deacetylation 80% | Sigma, USA |
| Citric acid monohydrate ≥ 99.5% | Sigma, USA |
| Graphite powder < 20 μm | Aldrich, USA |
| Gold chloride trihydrate 49 % gold, $HAuCl_4 \cdot 3H_2O$ | Sigma, USA |
| Horseradish peroxidase (HRP, EC 1.11.1.7, type XII) | Sigma, USA |
| Hydrochloric acid 37%, HCl | Sigma, USA |
| Hydrogen peroxide 30%, $H_2O_2$ | AnalaR®, BDH laboratory supplies, England |
| Mineral oil | Fluka, Switzerland |

**Table 4.5** List of chemicals for fabrication of hydrogen peroxide biosensor (CONTS.)

| Chemicals | Details |
|---|---|
| Potassium hexacyanoferrate(III) 99%, $K_3Fe(CN)_6$ | Fluka, Switzerland |
| Trisodium citrate dihydrate 99% | Sigma, USA |
| Sodium hydroxide 97%, NaOH | Sigma, USA |

### 4.3.2 Instrumentals

All of instruments in this section were listed in table 4.6.

**Table 4.6** List of instruments for fabrication of hydrogen peroxide biosensor

| Instruments | Details |
|---|---|
| Analytical Balance | Denver instrument TC 254, Denver, CO, USA |
| DI water system, R ≥ 18.2 MΩ-cm | Barnstead/Thermolyne NANOPure UltraPure Water system, Model D4742, Dubuque, IA, USA |
| Electrochemical instruments | Autolab-30 (Eco Chemie B. V., The Netherlands) with 2 mm Ø glassy carbon (GC) (Model 6.1204.110, Metrohm, The netherlands) as working electrode |
| Hot air oven | Gallenkamb model OV-420, England |
| pH meter | ThermoOrion pH meter model 420 with a glass electrode model 15600, USA |

**Table 4.6** List of instruments for fabrication of hydrogen peroxide biosensor (CONTS.)

| Instruments | Details |
|---|---|
| Transmission Electron Microscope, TEM | Hitachi H-300 from Japan for TEM micrographs of Au nanoparticles on Carbon-covered Cu-grid, and for particles size determination with Carl Zeiss software version KS300 from Germany |
| UV-Visible spectrophotometer | PerkinElmer Lambda800, Waltham, MA, USA |

### 4.3.3 Chemical preparation

**- 0.01 % $HAuCl_4$/10 mL**

Weigh 1 mg $HAuCl_4 \bullet 3H_2O$ and dissolve in 10 mL DI water.

**- 1 % trisodium citrate/100 mL**

Weigh 1 g of trisodium citrate dihydrate and dissolve in 100 mL DI water.

**- 1.0 M NaOH/250 mL**

Weigh 10.10xx g of NaOH and dissolve in 250 mL of DI water.

**- 250 mM $H_2O_2$/10 mL**

Pipette 259 μL of stock $H_2O_2$ and dissolve in 10 mL of DI water. The solution should be prepared freshly before use.

**- 1% Chitosan (CHIT) stock solution/100 mL**

CHIT solutions were prepared by adding 1 g CHIT flakes, as received, to 60 mL DI water with stirring and gradually adding concentrated HCl to the solution to maintain the pH near 3 until complete dissolution (~ a week). The undissolved material was filtered then the pH was gradually adjusted to 5.0 using 1.0 M NaOH. This clear and colorless filtrate's volume was adjusted to make 100 mL of a 1% CHIT stock solution. The CHIT stock solution was kept at 4 °C when not in use.

**- 10, 20 and 30 mM $K_3Fe(CN)_6$**

Weigh 0.3226, 0.6651, 0.9977 g of $K_3Fe(CN)_6$ and dissolve each of them in 100 mL of DI water to obtain 10, 20 and 30 mM $K_3Fe(CN)_6$, respectively.

### 4.3.4 Gold nanoparticles synthesis and characterization

10 mL of 0.01% $HAuCl_4$ solution was heated to 65 °C for 10 minutes and then 340 μL of 1 % sodium citrate was added with continued heating to 125 °C for 30 min while the color of solution changed to brownish red. The solution was left to cool at room temperature and Au nanoparticles were obtained.

The sizes of AuNP were characterized by TEM-H-300. The carbon-covered Cu-grid was used to retain the AuNP. A drop of AuNP solution was cast on carbon-covered Cu-grid which dries by evaporation in desiccators for 12 hours. The TEM-H300 was operated at 75 kV and the photos were taken on the phosphorescence film.

The photometric adsorption property of AuNP was tested by the PerkinElmer-Lambda 800 UV-Vis instrument. A Pyrex 1 cm photometric cell was used as a sample holder.

### 4.3.5 Carbon paste electrode preparation

A homemade carbon paste electrode was fabricated according to Ponchio [179]. Briefly, 0.60 g graphite powder was homogeneously mixed with 0.40 g of mineral oil by using a mortar and pestle. The homogenous graphite paste that contained 60 % (w/w) graphite powder was packed into an electrode body made from glass with 2.0 mm and 12 cm as inner diameter and long, respectively. The electrode surface was smoothed with a paper or an oil removing paper. The electrode connection to the carbon paste was established via a copper wire.

### 4.3.6 Screen printed carbon electrode fabrication

Homemade screen printed frames were designed in 6 configurations by a silk screen pattern with CAD/CAM software. SPCE fabrication describe as figure 4.3. The electrodes were screened with the 4 layers by hand on the polyvinyl chloride (PVC) sheet 48 cm long, 18 cm wide and 0.4 mm thick. Using the designated template, the first layer was applied with an Ag ink as the conductive wire. The carbon ink was then screened as the WE. Then the Ag/AgCl ink was screened as the RE. Finally the layer of insulator was printed using the pattern to define the electrode area. Interval of each layers were cured for 1 h at 60 °C and allowed to cool in desiccators. The set of SPCEs were cut to a single electrode for investigation.

### 4.3.7 Screen printed carbon electrode selection

The CV was performed for selection the performance of all six configuration SPCEs in 10, 20 and 30 mM $K_3Fe(CN)_6$. The selecting criteria of the best SPCE are high sensitivity, low relative standard deviation, and narrow peak potential.

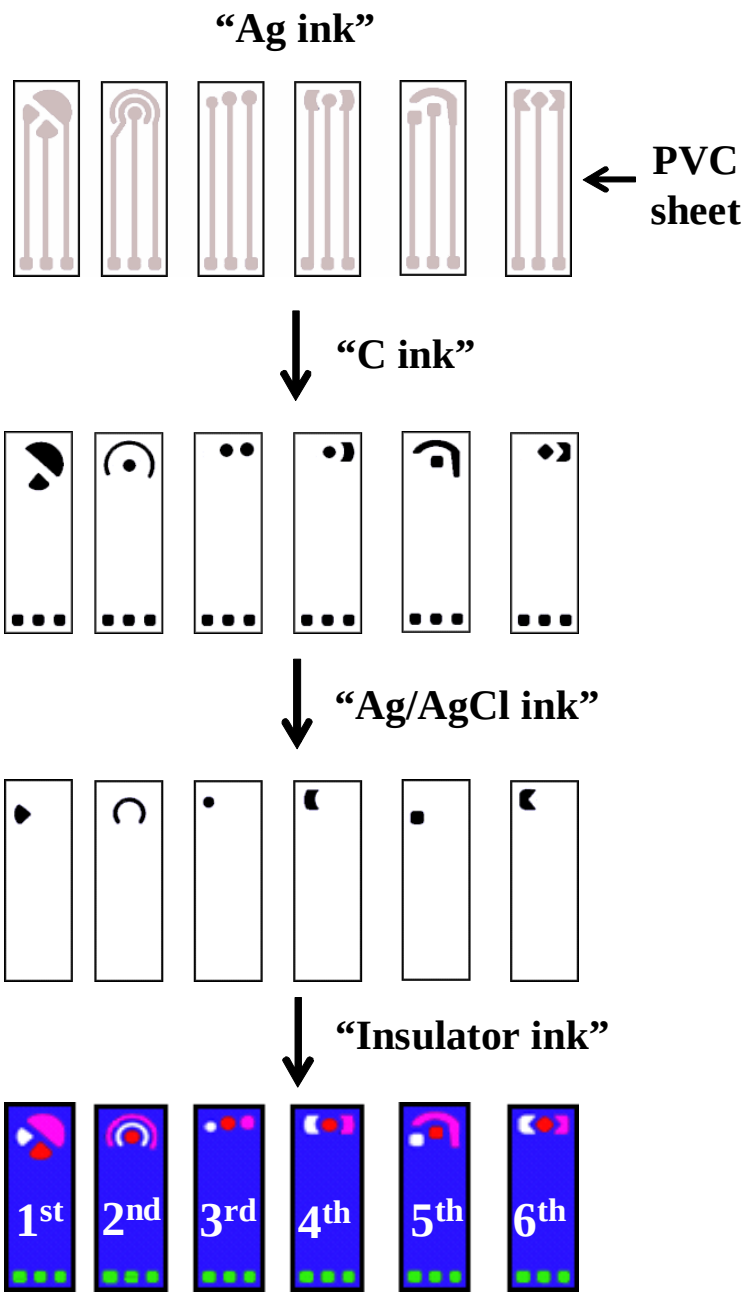


**Figure 4.3** Illustration of SPCE fabrication at six screen printed patterns through layer-by-layer screened start from Ag to insulator inks.

### 4.3.8 Electrode modifications

The selected SPCE was rinsed with DI water before use. A mixture solution of HRP (3 mg $mL^{-1}$), Au (0.43 nM) and CHIT (0.1 %) in DI water was prepared. The SPCE was dipped into the mixed solution while a fixed potential of –2.0 V was applied to the WE for the desired time. The CHIT was deposited with HRP and AuNP embedded on the electrode surface simultaneously as figure 4.4 with continuous $H_2$ gas bubbling. The electrode was then removed from the mixed solution and cleaned with DI water and kept at 4 °C when not in use. The detection process of $H_2O_2$ biosensor takes place on the HRP/AuNP/CHIT while $H_2O_2$ reach with these active materials, resulting in 2 electrons transfer from the SPCE.

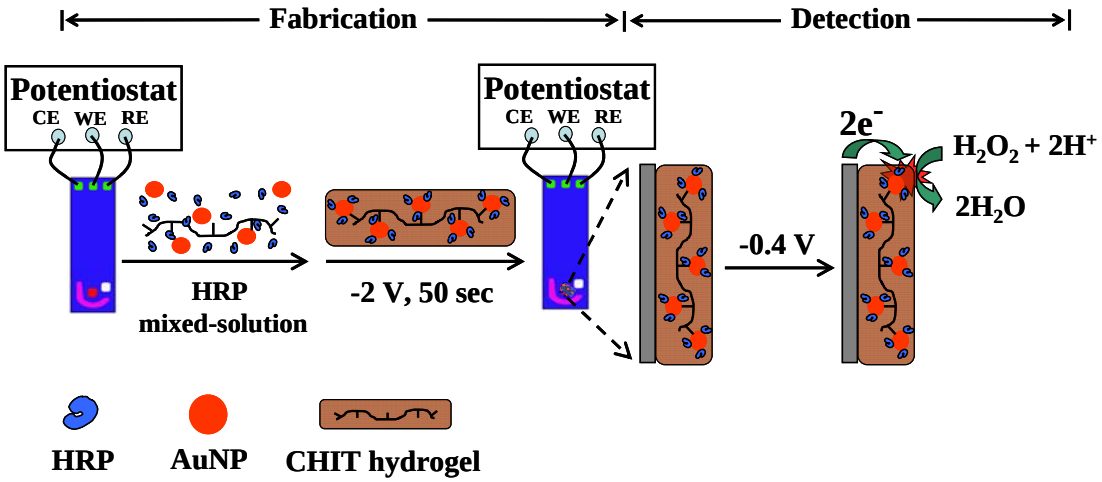


**Figure 4.4** Fabrication and detection processes scheme of $H_2O_2$ biosensors.

### 4.3.9 Electrochemical cell setup

The cell setup for $H_2O_2$ biosensor was showed in Appendix A.3.

### 4.3.10 Characterization of hydrogen peroxide biosensor

Four modifications of CHIT/SPCE, HRP/SPCE, HRP/CHIT/SPCE and HRP/AuNP/CHIT/SPCE were amperometric studied for optimization and evaluation

for the performance of $H_2O_2$ biosensors. The 10 µL of 250 mM $H_2O_2$ was spiked into a 5 mL stirred solution of citrate buffer to obtain 500 µM $H_2O_2$ in the final. The currents of each condition were compared. The optimizations were performed in working potential, pH and deposition times. For the performances were evaluated in detection limit, linearity range, reproducibility and life time storage.

## 4.4 Phosphate biosensor

### 4.4.1 Chemicals

Some chemicals were listed in section 4.3 and taken from the $H_2O_2$ part. The additional chemicals used in phosphate biosensor development were listed as table 4.7

**Table 4.7** of additional chemicals for fabrication of phosphate biosensor *

| Chemicals | Details |
|---|---|
| Ammonium molybdate tetrahydrate, 99.98% metal basis, $(NH_4)_6Mo_7O_{24} \cdot 4H_2O$ | Aldrich, USA |
| L-Ascorbic acid 99% | Sigma, USA |
| Calcium chloride dihydrate 99%, $CaCl_2 \cdot 2H_2O$ | Riedel-deHaën, Germany |
| Flavin adenine dinucleotide disodium salt hydrate 90%, FAD | Fluka, Switzerland |
| 4-(2-Hydroxyethyl)-1-piperazineethanesulfonic acid 99%, HEPES | Aldrich, USA |
| Magnesium chloride anhydrous ≥ 98%, $MgCl_2$ | Sigma, USA |

* Confer table 4.6

**Table 4.7** List of additional chemicals for fabrication of phosphate electrochemical sensor (CONTS.)

| Chemicals | Details |
|---|---|
| Phenolphthalein 98-120% | Sigma, USA |
| Potassium antimonyl tartrate trihydrate 99-103%, $C_8H_4K_2O_{12}Sb_2 \cdot 3H_2O$ | Fluka, Switzerland |
| Potassium chloride 99%, KCl, | Merck, Germany |
| Potassium dihydrogen phosphate 99%, $KH_2PO_4$ | Fluka, Switzerland |
| Potassium sulfate ≥99%, $K_2SO4$ | Merck, Germany |
| Pyruvate oxidase, PyOD, EC 1.2.3.3. from *Aerococcus* sp. | Sigma, USA |
| Sodium chloride 99.5%, NaCl | Merck, Germany |
| Sodium hydroxide ≥ 98%, NaOH | Sigma, USA |
| Sodium nitrate 99%, $NaNO_3$ | Merck, Germany |
| Sulfuric acid 98%, $H_2SO_4$ | Merck, Germany |
| Sodium pyruvate 99% | Sigma, USA. |
| Thiamine pyrophosphate chloride > 95%, TPP | Fluka, Switzerland |

### 4.4.2 Instrumentals

All of instruments in this section were listed in table 4.8.

**Table 4.8** List of instruments for fabrication of phosphate biosensor

| Instruments | Details |
|---|---|
| Analytical Balance | Denver instrument TC 254, Denver, CO, USA |
| DI water system, R ≥ 18.2 MΩ-cm | Barnstead/Thermolyne NANOPure UltraPure Water system Model D4742, Dubuque, IA, USA |
| Electrochemical instrument | Autolab-30, Eco Chemie B. V., The Netherlands |
| $H_2O_2$ biosensor | Homemade, IFEC laboratory, Mahidol University, Thailand (see details in section 4.3.8) |
| pH meter | ThermoOrion pH meter model 420 with a glass electrode model 15600, USA |
| UV-Visible spectrophotometer | PerkinElmer Lambda800, Waltham, MA, USA |

### 4.4.3 Preparation of reagent solution

**- 1 M NaOH/250 mL and 0.1 M NaOH/250 mL**

Weigh 10.10xx g NaOH and dissolve in 250 mL DI water, this step is for 1 M NaOH. For 0.1 M NaOH, pipette 25 mL 1 M NaOH and adjust to 250 mL by DI water.

**- 0.1 M Citrate buffer solution pH 6.5/100 mL**

Weigh 21.0 g citric acid monohydrate and dissolve in 200 mL 1 M NaOH. Mix 55 mL of 0.1 M citrate solution with 45 mL 0.1 M NaOH. Measure and adjust pH by 0.1 M NaOH or 0.1 M citrate solution to pH 6.5.

**- Mixed electrolyte solution for phosphate biosensor**

A mixed solution that use for phosphate biosensor development consists of cofactor, coenzyme, cosubstrate, and supporting electrolyte. It is needed to prepare of (i) $MgCl_2$, (ii) HEPES, (iii) TPP, (iv) FAD, and (v) sodium pyruvate with following procedure;

**(i) 3 M $MgCl_2$/10 mL stock solution**

Weigh 2.8751 g $MgCl_2$ and dissolve in 10 mL DI water.

**(ii) 1 M HEPES/10 mL stock solution**

Weigh 2.4070 g HEPES and dissolve in 10 mL DI water.

**(iii) 70 mM TPP/10 mL stock solution**

Weigh 0.3395 g HEPES and dissolve in 10 mL DI water.

**(iv) 1 M Sodium pyruvate/10 mL stock solution**

Weigh 1.1115 g sodium pyruvate and dissolve in 10 mL DI water.

**(v) 1 mM FAD/10 mL stock solution**

Weigh 9 mg FAD and dissolve in 10 mL DI water.

A mixed solution was prepared by taking of (i) 5 μL of 3 M $MgCl_2$ (ii) 50 μL of 1 M HEPES, (iii) 5 μL of 70 mM TPP, (iv) 5 μL of 1 M sodium pyruvate, and (v) 50 μL of 1 mM FAD. All of them is dissolved in 5 mL citrate buffer solution to obtain 3 mM $MgCl_2$, 10 mM HEPES 70 μM TPP, 1 mM pyruvate, and 10 μM FAD for use in electrolyte.

**- Solutions for interfering and cofactor studies**

Solutions for interfering and cofactor studies of phosphate biosensor have been prepared by the following;

**(i) 1 M Sodium chloride/100 mL**

Weigh 5.8733 g sodium chloride and dissolve in 100 mL DI water.

**(ii) 1 M Potassium chloride/100 mL**

Weigh 7.5303 g sodium chloride and dissolve in 100 mL DI water.

**(iii) 1 M Calcium chloride/100 mL**

Weigh 14.8505 g calcium chloride dihydrate and dissolve in 100 mL DI water.

**(iv) 1 M $MgCl_2$/10 mL**

Weigh 0.9584 g $MgCl_2$ and dissolve in 10 mL DI water.

**(v) 0.5 M Potassium sulfate/100 mL**

Weigh 8.8010 g potassium sulphate and dissolve in 100 mL DI water.

**(vi) 1 M Sodium nitrate/100 mL**

Weigh 8.5848 g sodium nitrate and dissolve in 100 mL DI water.

For studying interfering ($K_2SO_4$ and $NaNO_3$) and cofactor effects (NaCl, KCl, $CaCl_2$, and $MgCl_2$) spike each of NaCl, KCl, $CaCl_2$, $MgCl_2$ and $NaNO_3$ for 5 µL, while $K_2SO_4$ for 10 µL into a stirred 5 mL of mixed electrolyte solution (without $MgCl_2$). Each of them was 1 mM in final.

**- Phenolphthalein indicator**

Weigh 0.25 g Pheolphthalein and dissolve in 500 mL of 80% ethanol.

**- Combined reagent**

The solution of (i) sulfuric acid, (ii) ammonium molybdate, (iii) potassium antimonyl tartrate, and (iv) ascorbic acid need to prepare for the combined reagent.

**(i) 2.5 M Sulfuric acid solution/500 mL**

Pipette 70.00 mL of conc. sulfuric acid and dilute to 500 mL with DI water. The solution was stored in plastic bottle.

**(ii) 0.008 M Potassium antimonyl tartrate/500 mL**

Weigh 2.6984 g of potassium antimonyl tartrate trihydrate and dissolve in 500 mL DI water. Polyethylene bottle was selected as a solution container.

**(iii) 0.034 M Ammonium molybdate solution/500 mL**

Weigh 21.0390 g of ammonium molybdate tetrahydrate to dissolve and make up to 500 mL with DI water. This solution was stored in a polyethylene bottle.

**(iv) 0.1 M Ascorbic acid solution/100 mL**

Weigh ascorbic acid diary for 1.7789 g and dissolve in 100 mL DI water. This solution was stored in a polyethylene bottle in refrigerator prior to use.

A combined reagent was prepared in a 100 mL container. Briefly, the 50.0 mL of (i) 2.5 M $H_2SO_4$, 5 mL of (ii) 0.008 M potassium antimonyl tartrate, 15.0 mL of (iii) 0.034 M ammonium molybdate solution and 30.0 mL of (iv) 0.1 M ascorbic acid by transferring and mixing in container. The combined solution must be cleared solution. This solution must be used within 4 hours.

### 4.4.4 Biosensor modification

Use $H_2O_2$ biosensor from section 4.3 as the based biosensors, then drop aliquot of 10 Unit $mL^{-1}$ PyOD on the WE of $H_2O_2$ biosensor. Let it dried and rinsed with DI water prior to use. Figure 4.5 showed the procedure for phosphate biosensor preparation.

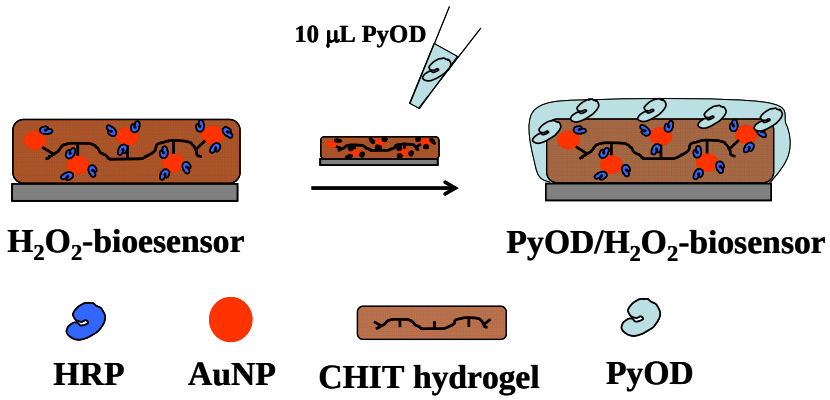


**Figure 4.5** Fabrication step of $PO_4^{3-}$ biosensor starting with dropping of pyruvate oxidase (PyOD) solution on $H_2O_2$ biosensor and let it dried to get PyOD/HRP/AuNP/CHIT or PyOD/$H_2O_2$ biosensor.

### 4.4.5 Electrochemical cell setup

The cell used in phosphate biosensor is as same as $H_2O_2$ biosensors as section 4.3.9 (see photo at Appendix A.3). Amperometric signal was recorded for PyOD/$H_2O_2$/AuNP/CHIT in an HEPES buffer solution. The experiments were carried out at the applying potential of –0.4 V vs. Ag/AgCl to carry out the reduction of enzymatic generated $H_2O_2$. A citrate buffer solution was placed into the cell and the steady-state current upon the first phosphate addition was monitored. The determination of phosphate ions in natural water, samples were obtained from Klong Rangsit, K1-K7. The samples were clear and colorless. Those samples have been measured for phosphate as received.

### 4.4.6 Phosphate biosensor validation

The phosphate biosensor has been validated with spectrophotometric molybdenum blue method [180]. Amperometric mearesurment for phosphate content in real samples at PyOD/HRP/AuNP/CHIT/SPCE ($E_{applied}$ = –0.4 V) were gradually added 2.5 mL of real samples into a 2.5 mL stirred solution of 0.1 M citrate buffer pH 6.5 containing 2 mM pyruvate, 15 μM FAD, 70 μM TPP, 3 mM $MgCl_2$, and 10 mM HEPES. The external standard calibration was prepared at 0, 10, 20 and 50 mM $PO_4^{3-}$ for calibration curve.

Briefly of molybdenum blue method; an aliquot of 10.0 mL natural water sample was transferred into a 25.0 mL volumetric flask. Phosphate have been prepared in a final concentration of 0, 0.1, 10, 20 and 50 μM $PO_4^{3-}$ for the standard calibration curve. Few drops of phenolphthalein indicator were added to these aliquots. 1 M NaOH solution was drop wisely added to the solution, after the color of solution was turned to a pink color, a drop of 2.5 M $H_2SO_4$ was added to change pink color to colorless. Bring 5 mL of combined reagent to those solution and follow by adjust to 25 mL with DI water. Those solutions must be carried out within 10-30 minutes with UV-Vis spectrophotometer at 680 nm.

# CHAPTER V
# RESULTS AND DISCUSSION

The design and development of four electrochemical sensors will be discussed thoroughly based on different electrode materials and the analytes. The determination of electroactive species as (5.1) insulin, electroinactive species as (5.2) glycosidases enzymes, electroactive enzymatic generated species as (5.3) hydrogen peroxide, and electroinactive species as (5.4) phosphate will be described in specific reaction.

## 5.1 Insulin sensor

### 5.1.1 Electrochemical study of insulin

Insulin is peptides that influence on metabolism of human body. The electrochemical approach to detect insulin with/without the separation process is amperometry by oxidation of the amino acids comprising peptides [181]. The unique electrochemical behavior of the amino acids had been studied at different modified electrode materials. The metal oxide modified nanotubes on carbon or metal electrodes have been attemped for the peptides detection. Electrocatalytic oxidation of insulin on ruthenium oxide/carbon nanotube ($RuO_x$/CNT) modified glassy carbon electrode (GCE) is a key reaction for characterizing the novel design insulin sensor by cyclic voltammetry (CV). The cyclic voltammograms at the $RuO_x$ (a), CNT (b) and $RuO_x$/CNT (c) modified GCE in the absence and presence of 72 μM insulin (dotted and solid lines, respectively) are shown in figure 5.1 (omit over scale of current at 0.8 - 1.0 V on figure 5.1c). The three modified electrodes display a defined insulin oxidation peak. However, the onset of the insulin oxidation at the $RuO_x$/CNT coated GCE occurs at a substantially lower potentials (0.29 V), compared to its $RuO_x$ (0.67 V) and CNT (0.48 V) counterparts. The $RuO_x$/CNT modified electrode yields

also a substantially higher sensitivity over the entire potential range (notice the different current scales; a versus b, c). Oxidation peak potentials of 0.83, 0.67 and 0.65 V were observed at the $RuO_x$, CNT and $RuO_x$/CNT modified electrodes, respectively.

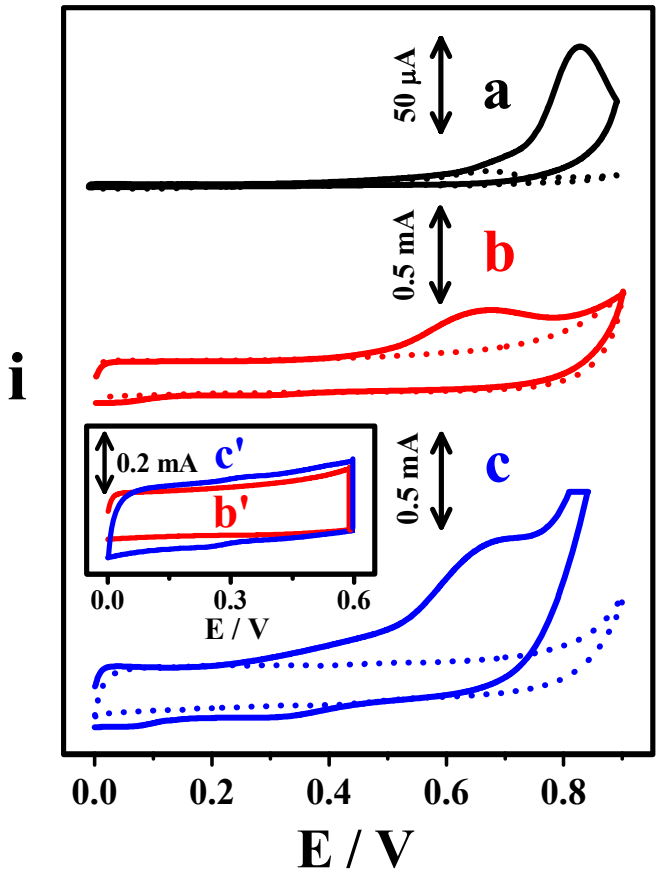


**Figure 5.1** Cyclic voltammograms in blank (dotted lines) and 72 µM insulin (solid lines) solutions at the (a) $RuO_x$, (b) CNT and (c) $RuO_x$/CNT modified GCE. Inset shows background current signals at the (b′) CNT and (c′) $RuO_x$/CNT modified GCE. Conditions: supporting electrolyte, 0.05 M phosphate buffer (pH 7.40) containing 0.10 M NaCl; scan rate 0.05 V $s^{-1}$.

No significant reduction peak in figure 5.1 was observed in the reversed scan (around 0.35 V), indicating that the electrochemically generated product cannot be readily reduced in the potential range studied. While the anodic signal of the $RuO_x$ modified surface reflects the mediated phenoxide oxidation by the

ruthenium in the film. The insulin response at CNT electrodes has been attributed to the accelerated oxidation of the tyrosine residues [10, 182] as in circle of figure 5.2. However, some work reported that the insulin oxidation occured via the disulfide bond in cystine residue by Ruthenium(II) terpyridine dendrimer/GCE [183].

The electrocatalytic oxidation of tyrosine is an important mechanism in insulin determination. The free tyrosine can be oxidized at gold, platinum, or carbon electrode [184, 185]. The electrochemical behavior is complicated and showed different reaction pathways, each pathway including several steps. At pH 7, a three-step oxidation reaction (R5.1-5.3) has been suggested with one electron transferred in both the first (R5.1) and third (R5.3) step [185]. However, the tyrosine oxidation produces hexacyclodienone and polyphenylene oxide alanyl in other reaction path way is suggested [186]. The anodic reaction of tyrosine is reversible involving one electron and one proton. At graphite electrode, 3,4-dihydroxyphenylalanine is proposed as a product from an irreversible two electron process by Brabec and Mornstein [187]. Under some conditions a polymeric product, suggested to be a polyphenylene oxide alanyl, has been formed that was proposed by Malfoy and Reynaud [188]. However, the exact nature of the insulin catalytic process at the $RuO_x$/CNT modified electrode is not fully understood at this stage. Such accelerated response is attributed to a synergistic enhancement, rather than a combination of the individual coatings or surface area effects.

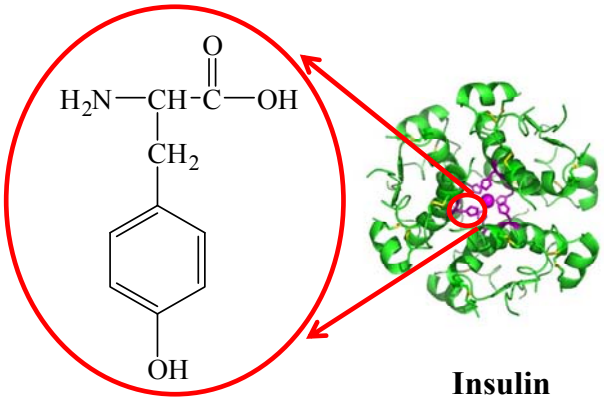


**Figure 5.2** Structure of tyrosine residue in insulin molecule [10].

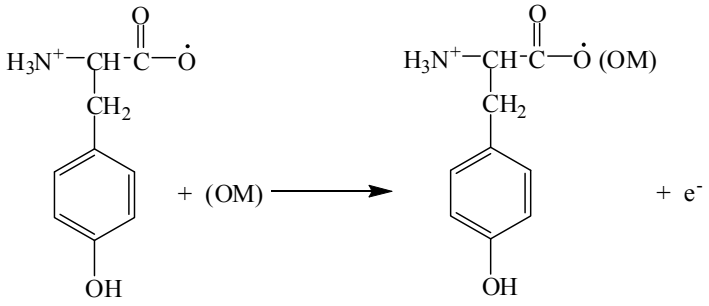


(R5.1)

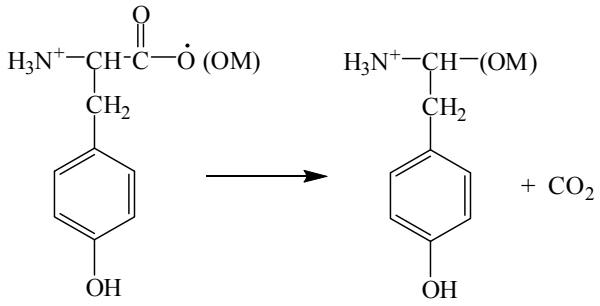


(R5.2)

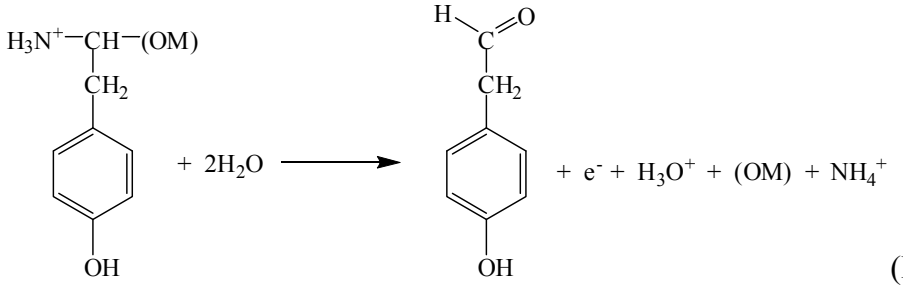


(R5.3)

The synergistic phenomena, the extra current obtains more than combining of the current from their own work, of $RuO_x$/CNT modifed electrode to insulin oxidizing is supported by the background cyclic voltammetric running in the blank solution (shown in the inset of figure 5.1) that indicates a negligible change in the background current envelop. The SEM data (figure 5.4) also indicated minimal change in the surface topology. It was shown in earlier works of Hrapovic *et. al.* [182] and Wang and Musameh [76] that the slow redox systems can be improved by coupling the CNT with catalytic metal centers.

At the CNT modified electrode involving a potential scanning (similar to that employed for plating the $RuO_x$) but without the $RuCl_3$, no apparent

change in the insulin oxidation peak was observed, indicating that such potential cyclization has no effect upon the electrocatalytic behavior.

### 5.1.2 Hydrodynamic voltammetric studies of insulin

Hydrodynamic voltammetric studies of insulin oxidation were conducted in a flow system. The hydrodynamic voltammograms in figure 5.3 developed point wise (in steps of 0.1 V) over the 0.3-0.9 V range during a flow injection operation display the same trend as CV in figure 5.1. The synergy in the $RuO_x$/CNT system is demonstrated that depicts typical hydrodynamic voltammograms (HDV) for the oxidation of 800 nM insulin at the $RuO_x$ modified (A, a), CNT-modified (A, b) and $RuO_x$/CNT modified (A, c) electrodes. The three modified electrodes thus exhibit defined anodic signals with oxidation starting at 0.60 V (A, c), 0.50 V (A, b) and 0.40 V (A, c). These HDV indicate that the $RuO_x$/CNT-coated electrode offers a greatly improved performance, with a substantially higher sensitivity over the entire potential range. Its current rises rapidly in potential range of +0.40 V up to +0.70 V and decreases slightly above +0.80 V. The marked electrocatalytic activity towards insulin permits the effectively low potential amperometric detection. This potential provides the highest current that is similar to work of Cox and Gray [68] that they reported HDV-evidence for the oxidation of 95 nM insulin at pH 2.0 on $RuO_x$ modified GCE. They found a well defined signal above the baseline and at 0.96 V versus Ag/AgCl.

The greatly improved low potential detection of insulin offered by the $RuO_x$/CNT surface depicts amperometric flow injection response (at +0.50 V) of the $RuO_x$ modified (figure 5.3B, a), CNT modified (figure 5.3B, b), and $RuO_x$/CNT modified (figure 5.3B, c) electrodes to the 800 nM insulin solution. As expected from the HDV profile, the $RuO_x$-coated electrode displays a negligible response to insulin at this potential. A defined response is observed at the CNT modified electrode. An even (five-fold) larger peak is observed at the $RuO_x$/CNT detector. This result was as same as parallel experiments that were carried out by our colleages; T. Vazquez-Alvarez and S. Loyprasert [189]. As will be illustrated below, similar improvements

can be obtained at significantly lower insulin concentrations, facilitating ultra trace measurements of this hormone.

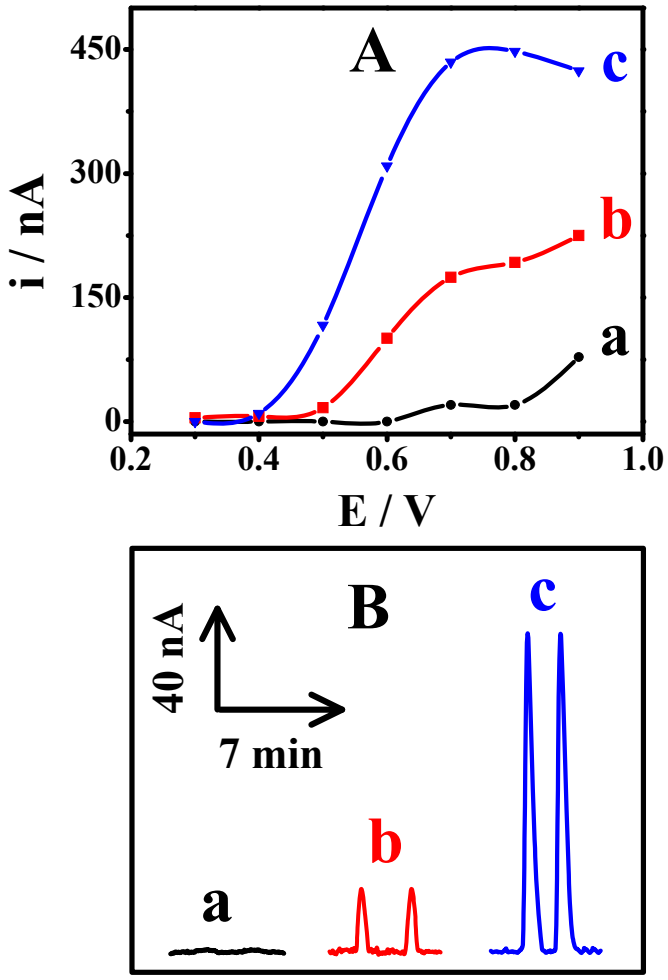


**Figure 5.3** (A) Hydrodynamic voltammograms of 800 nM insulin using the (a) $RuO_x$, (b) CNT and (c) $RuO_x$/CNT modified GCE. (B) The corresponding flow injection peaks recorded at +0.50 V. Conditions: carrier/supporting electrolyte, 0.05 M phosphate buffer (pH 7.40) containing 0.10 M NaCl; sample loop, 200 µL; flow rate, 1.0 mL $min^{-1}$.

### 5.1.3 Electrode modification order

The examinination of different routes for preparing $RuO_x$/CNT modified electrodes were conducted. These included the entrapment of CNT during the electrodeposition of the $RuO_x$ film, and bilayers involving casting of CNT onto the $RuO_x$ film or growing the $RuO_x$ film on a CNT layer. The latter approach offered the most favorable results and was used in all subsequent work.

The preparation of such $RuO_x$/CNT bilayer film was optimized by systematically varying the volume of the cast CNT between 10, 20, and 30 μL and the cyclic voltammetric electrodeposition times at 12.5, 25 and 37 min. The results were illustrated by linear sweep voltammograms as shown in figure A.3 in appendix A.1. The most favorable insulin response was obtained using 30 μL CNT in connection to a 12.5 min electrodeposition.

### 5.1.4 The modified electrode surface morphologies

The different modified electrodes were characterized by SEM. Figure 5.4 compares SEM images of the (A) bare, (B) $RuO_x$, (C) CNT and (D) $RuO_x$/CNT modified GCEs. The micrograph of the $RuO_x$ modified surface (figure 5.4B) shows spherical $RuO_x$ particles of ca. 50 nm diameter, covering quite uniformly the GC surface. As expected [190], casting the CNT on the carbon surface resulted in a highly porous layer comprising of interwoven tubes of ca. 40 nm diameter (figure 5.4C). The morphology of the $RuO_x$/CNT modified electrode was similar to that of the CNT electrode (figure 5.4D versus C), except of the presence of few non-uniformly dispersed ~80 nm $RuO_x$ particles.

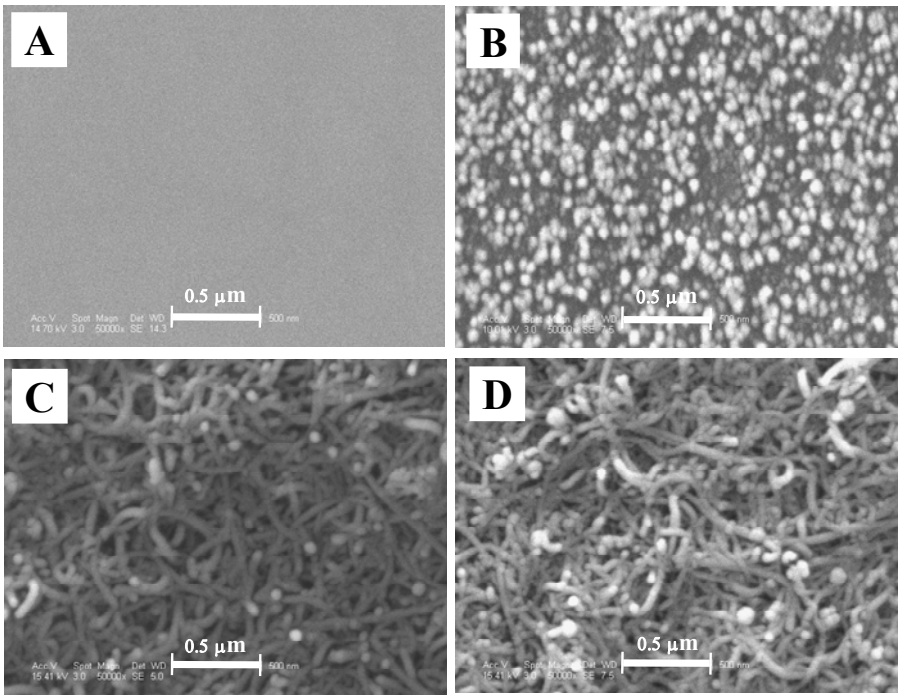


**Figure 5.4** SEM images of the surface of the (A) bare, (B) $RuO_x$, (C) CNT, and (D) $RuO_x$/CNT modified GCE. Scale, 0.5 µm; magnification, 50,000; accelerating voltage, (A) 14.7 kV, (B) 10.01 kV and (C and D) 15.41 kV.

### 5.1.5 Amperometric studies and flow injection analysis

Owing to the limited lifetime of the existing electrocatalytic insulin sensors (particularly those based on inorganic films), such devices cannot be used for routine in vivo monitoring of the insulin secretion. Such limited stability reflects the progressive fouling associated with the adsorption of the phenyl radicals products of the further phenolic oxidation process associated with the anodic detection of insulin, and a reduced stability of inorganic mediators. Recent studies illustrated that CNT surface coatings imparted higher stability onto amperometric insulin sensors [76]. A clearly detailed investigation of the oxidation process at CNT modified electrodes indicated a different reaction mechanism, proceeding through the tyrosine moieties [10]. As indicated in figure 5.5, the new $RuO_x$/CNT modified carbon electrode further enhances the operational stability compared to the CNT coated surface. This figure compares the amperometric response for 2 µM insulin recorded over different time periods at the (a) $RuO_x$, (b) CNT and (c) $RuO_x$/CNT modified GCEs (notice the

different time scales). The $RuO_x$ modified electrode displays a sharp and rapid loss of the signal (of 55 and 100% current depressions after 50 and 100 s, respectively), indicating a complete passivation of the oxidation process.

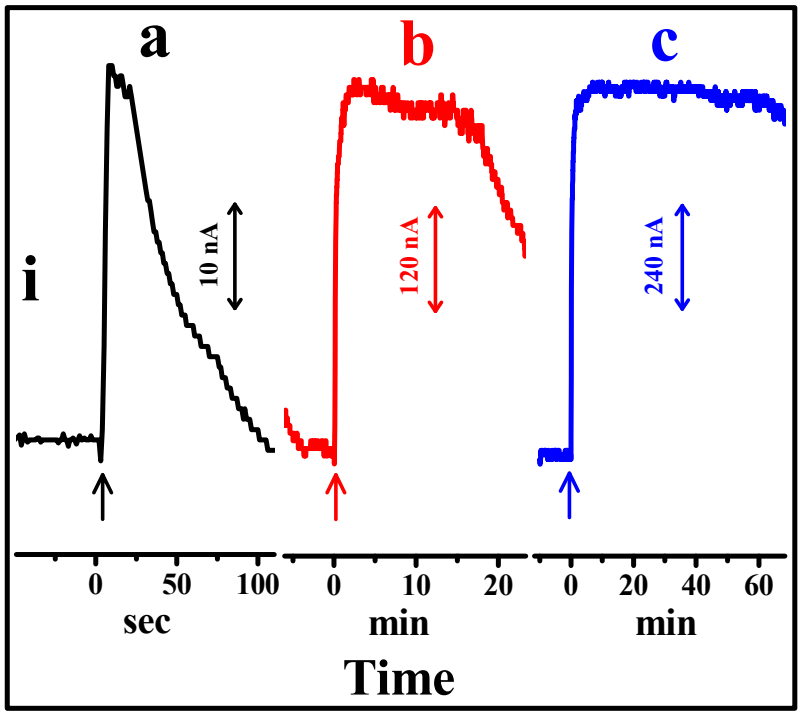


**Figure 5.5** Stability of amperometric response to 2 µM insulin at an applied potential of +0.70 V at (a) $RuO_x$, (b) CNT and (c) $RuO_x$/CNT modified GCE in a stirred solution of 0.05 M phosphate buffer (pH 7.40) containing 0.10 M NaCl.

The CNT coated electrodes retained more than 90% of the initial activity over the first 18 min of operation, but displayed a fast decay of the signal thereafter (to 55% of the initial response at 24 min). In contrast, the response of the $RuO_x$/CNT modified electrode remains highly stable throughout a significantly longer (1 h) operation, with only 1 and 3% current diminutions at 30 and 60 min, respectively. The high stability is illustrated in the figure 5.6 which depicts the reproducibility of the flow injection amperometric response to 20 successive injections of a 200 nM insulin solution over 60 min. This series yielded a stable response with a mean peak current of 110.5 nA, along with a relative standard deviation of 2.9%. CNT coatings have recently been shown useful for alleviating surface fouling associated with the

electrogeneration of phenoxy radicals [57], such as those generated during the oxidation of the insulin tyrosine residues. The resistance to fouling accrued from the coupling of $RuO_x$ with the CNT layer may due to ruthenium inherent stability at physiological pH (pH 7.4) and a combination of electron transfer mediation with oxygen transfer which was related to the acid/base chemistry of the film that this result is agreed with $IrO_x$ modified electrode of Pikulski and Gorski [72].

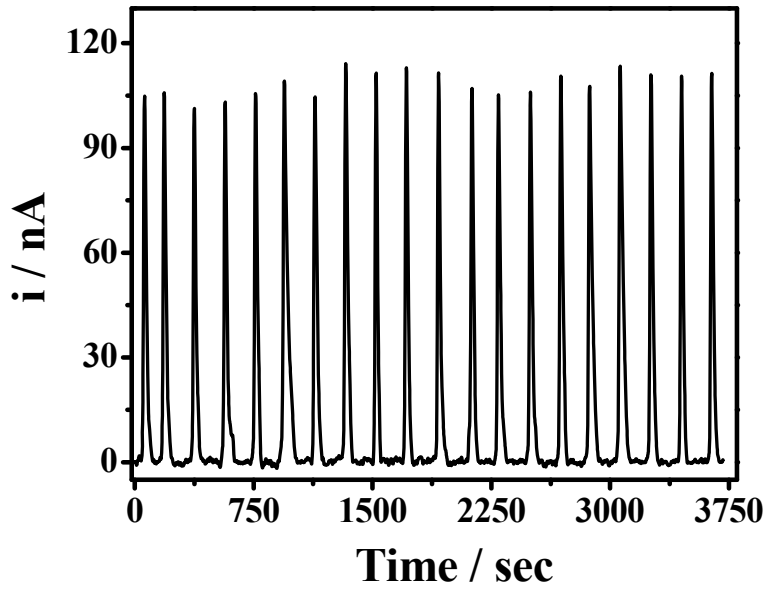


**Figure 5.6** The flow injection amperometric response of the $RuO_x$/CNT modified GCE to 20 repetitive injections of a 200 nM insulin solution.

The attractive analytical performance of the $RuO_x$/CNT electrode is demonstrated from the flow amperometric calibration data of figure. 5.7. This figure displays flow injection response peaks for increasing levels of insulin (10 - 800 nM, a - g). Well-defined current signals are observed for these nano molar changes in the concentration of insulin. The response increases linearly with the concentration, with sensitivity of 541 nA $\mu M^{-1}$ and $R^2$ of 0.999. Peaks of figure 5.7 indicate convenient measurements of extremely low insulin concentrations. A low detection limit of around 1 nM can be estimated from the signal-to-noise characteristics (S/N = 3). Detection limits of 30 [10] and 14 nM [76] insulin were reported for CNT modified electrodes and others were list in table 5.1.

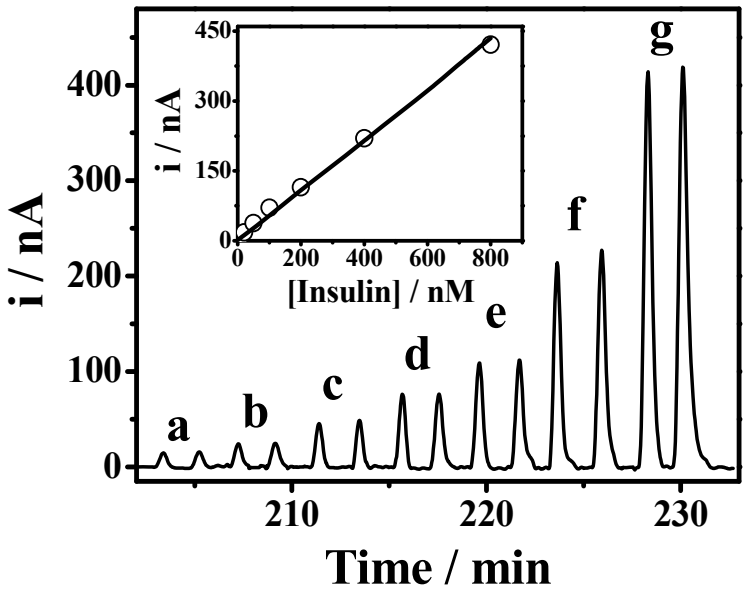


**Figure 5.7** Flow injection amperometric response obtained at the $RuO_x$/CNT modified GCE held at +0.70 V, for increasing levels of insulin: (a) 10, (b) 20, (c) 50, (d) 100, (e) 200, (f) 400 and (g) 800 nM. Inset shows the corresponding calibration plot. Conditions were as in figure 5.3.

**Table 5.1** Comparison of insulin sensor performance

| Electrode[1] | System[2] | Detection limit / nM | Sesitivity / nA $nM^{-1}$ | Linearity / nM | Shelf life / Day | References |
|---|---|---|---|---|---|---|
| $RuO_x$/CFE | FIA | 23 | $72 \times 10^{-6}$ | 100 - 1000 | 3 | Gorski *et. al.* [73] |
| $Ru^{II}$Den/GCE | FIA | 2 | 0.23 | 6 - 400 | 7 | Cheng *et. al.* [69] |
| $K_4Mo(CN)_8$/CCE | FIA | 0.04 | 8.10 | 0.1 - 0.5 | 14 | Salimi *et. al.* [191] |
| $K_4Mo(CN)_8$/CCE | Batch | 0.45 | 6.14 | 0.5 - 500 | 14 | Salimi *et. al.* [191] |
| [(Ru(bpy)(tpy)Cl]$PF_6$/ CCE | Chrono | 0.40 | 7.60 | 0.5 - 850 | 180 | Salimi *et. al.* [192] |
| $RuO_x$/NDE | FIA | 50 | 0.87 $\times 10^{-3}$ | 100 - 1000 | 10 | Wang and Zhang [193] |

**Table 5.1** Comparison of insulin sensor performance (CONTS.)

| Electrode[(1)] | System[(2)] | Detection limit / nM | Sesitivity / nA $nM^{-1}$ | Linearity / nM | Shelf life / Day | References |
|---|---|---|---|---|---|---|
| CHIT-CNT/GCE | Batch | 30 | 0.14 | 100 - 3000 | 60 | Zhang *et. al.* [10] |
| $CoFe(CN)_6$/CNT/CHIT /GCE | Batch | 40 | - | 100 - 3000 | - | Qu *et. al.* [194] |
| $IrO_x$/GCE | Batch | 20 | $35.20 \times 10^{-3}$ | 50 - 500 | 20* | Pikulski and Gorski [72] |
| $RuO_x$/CN-Ru/CFE | Batch | 0.04 | $0.44 \times 10^{-3}$ | - | 1* | Kennedy *et. al.* [74] |
| CNT/GCE | FIA | 14 | $48 \times 10^{-3}$ | 14 - 1000 | 2* | Wang and Musameh [76] |
| $RuO_x$/CNT/GCE | FIA | 1 | $541 \times 10^{-3}$ | 10 - 800 | 1* | This thesis |

(1) CCE = Carbon ceramic electrode, CFE = Carbon fiber electrode, CNT = Carbon nanotube, CPE = Carbon paste electrode, CHIT = Chitosan, GCE = Glassy carbon electrode, $K_4[Mo(CN)_8]$ = Potassium octacyanomolybdate(IV), NDE = Needle electrode, $[(Ru(bpy)(tpy)Cl]PF_6$ = Ruthenium bipyridyl terpyridine hexafluoro chlorate, $RuO_x$ = Ruthenium oxide, $RuO_x$/CN-Ru = Ruthenium oxide/cyanoruthenate, $Ru^{II}$Den = Ruthenium(II) terpyridine dendrimer

(2) Batch or FIA = Batch or Flow injection analysis - amperometric detector, Chrono = Chronoamperometry

* Continuous test (in hour)

Figure 5.8 indicates that the response time is not compromised by the bilayer coating. The $RuO_x$/CNT (figure 5.8c) electrode displays similar peak shape of the response to the 10 nM insulin solution as the CNT modified (figure 5.9b) electrodes, while the $RuO_x$ modified (figure 5.9a) electrode is not responding to this insulin concentration. Note an even larger and sharper peak is observed at the RuOx/CNT modified electrode.

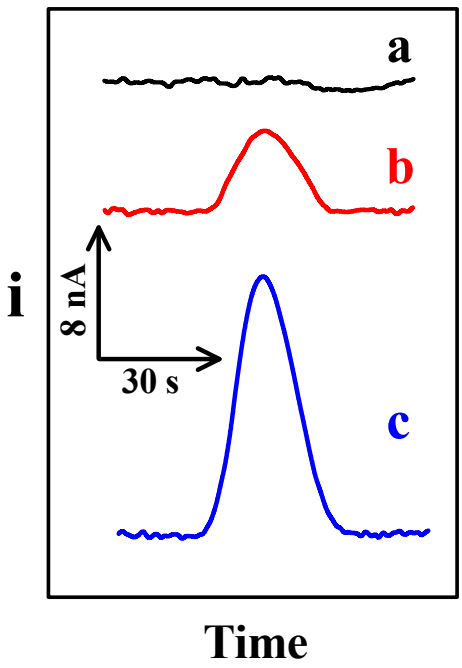


**Figure 5.8** Flow injection amperometric response to 10 nM insulin at an applied potential of +0.70 V using the (a) $RuO_x$, (b) CNT, and (c) $RuO_x$/CNT modified GCE. Other conditions were as in figure 5.3.

## 5.2 Glycosidases sensor

### 5.2.1 *p*-Nitrophenol study at SPCE and GCE

*p*-Nitrophenol (PNP) is an electroactive form of phenolic compounds that can be detected by voltammetric and amperometric electrochemical sensor. The oxidation of PNP can be electrochemically examined at the SPCE and GCE electrodes by square wave voltammetry. The electrooxidation product of PNP (R5.4) can be occurred as surface fouling of passive film covering the electrode surface, which is one of major problems for sensor development [84].

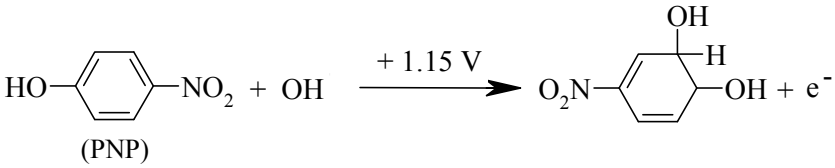


(R5.4)

The loaded Pt nanoparticles in the carbon ink for promoting PNP oxidation were examined on SPCE electrode. The greater sensitivity can be obtained because of catalytic properties of Pt nanoparticles. The electrochemical studies of Pt loaded SPCE were examined by square wave voltammograms in 1 mM PNP/0.05 M citrate buffer solution pH 4.4 as shown in figure 5.9. These square wave voltammograms were recorded at different Pt loaded SPCEs for figure 5.9 (a) 0, (b) 1, (c) 3, and (d) 5% and inset were corresponding to the current height at respective E = 1.12, 1.11, 1.03, and 1.04 for a, b, c, and d. The unloaded Pt SPCE displays the lowest signal, with 1.27 µA. The peak current increases to 1.70 µA at the 1% Pt loaded SPCE. The enhanced signal is likely to reflect by the existing of the Pt amount. The current reach maximum at the 3% Pt loaded (5.79 µA) and then decrease at the 5% Pt loaded (4.95 µA). The decreased current at the 5% Pt loaded is due to the PNP rapidly lead to the formation of a passivation film on Pt nanoparticles as reported by Boudenne *et. al.* [195].

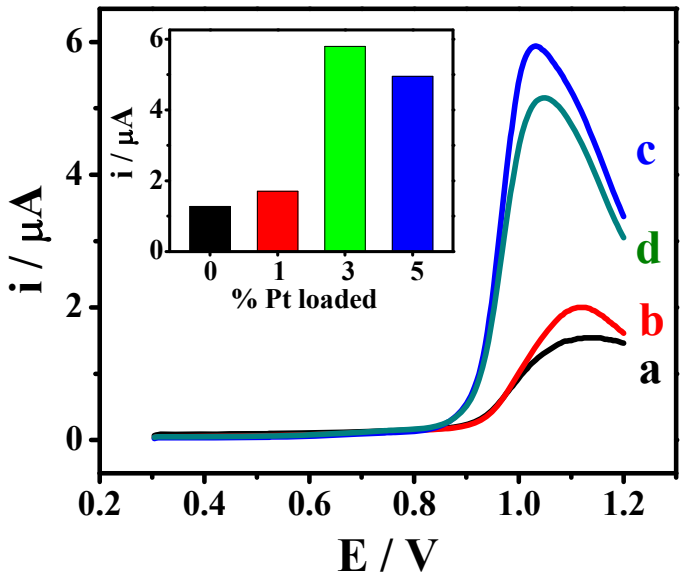


**Figure 5.9** Square wave voltammograms showing the 1st scan of 1 mM *p*-nitrophenol for many % Pt loaded SPCEs at (a) 0, (b) 1, (c) 3, and (d) 5%. Inset shows peak high from each % Pt. Conditions, 0.05 M citrate buffer solution pH 4.4, step potential = 4 mV, amplitude = 25 mV, and frequency = 25 Hz.

The catalytic property of the Pt loaded carbon ink on SPCE for PNP oxidation is quite impressive. Nevertheless, the stability of Pt activities on SPCE is poor as shown in figure 5.10, it losses activities after few cycles of cyclic voltammetric experiments in 1 mM PNP. This electrode shows irreversible reaction with the peak potential at 1.03 V that is similar to prior report of Wang *et. al.* [196]. They showed the passivation film of PNP occurring on electrode surface after cyclic voltammetric repetitive scanning. Consequently, the current of the Pt loaded SPCE signal is diminished rapidly during the first to fifth cycle and completely disappears at the 5$^{th}$ scan.

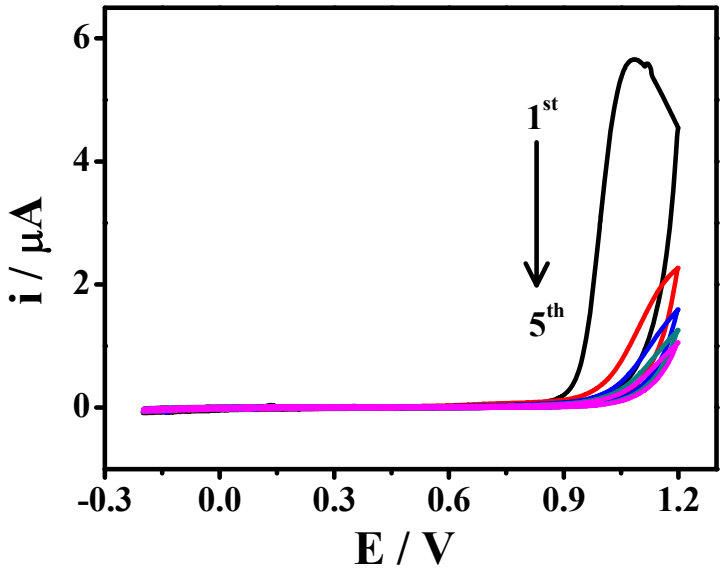


**Figure 5.10** Cyclic voltammograms showing of 5 repetitive scans of 1 mM *p*-nitrophenol obtained at the 3% Pt loaded SPCE in 0.05 M citrate buffer solution pH 4.4. Scan rate, 50 mV $s^{-1}$.

Since the Pt loaded SPCE was not stable enough for the PNP-based sensor, the GCE was replaced in further studies. The experiments were also conducted as described for SPCE. Figure 5.11 illustrates two square wave voltammograms of (A) Pt loaded SPCE (area = 9 $mm^2$), and (B) GCE (area = 7.06 $mm^2$). Both show well-defined peak potentials of 1.03 V and 1.00 V for SPCE and GCE, respectively. The GCE provides approximately three times higher current than the Pt loaded SPCE.

Note also, the current background of GCE is quite higher than that of the Pt loaded SPCE. Although the current of GCE is higher than the Pt loaded SPCE, but lack of stability is still a major problem as showed on continuously reduced the current on square wave voltammograms repetition 1-5 in appendix A.1.2, and this problem is also seen in the previous report of Wang *et. al.* [196].

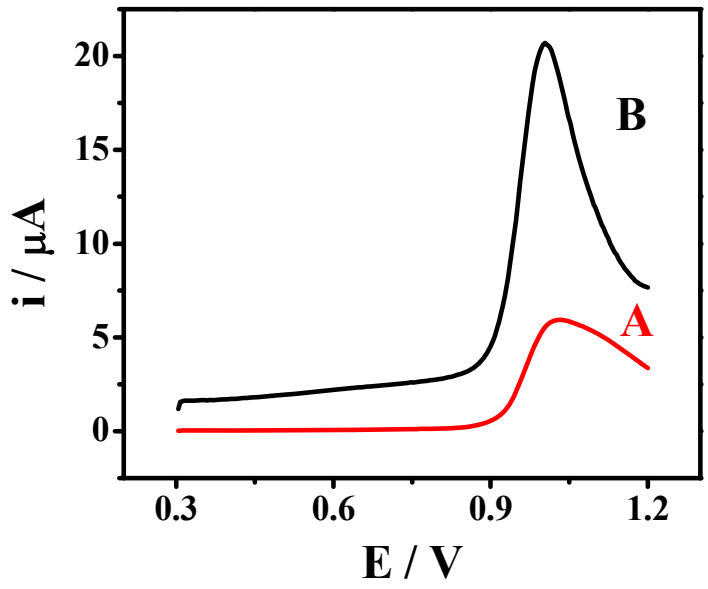


**Figure 5.11** Square wave voltammograms of 1 mM *p*-nitrophenol at the (A), 3% Pt loaded SPCE, and (B) GCE. Conditions, 0.05 M citrate buffer solution pH 4.4, step potential = 4 mV, amplitude = 25 mV, and frequency = 25 Hz.

### 5.2.2 The optimization of voltammetric and amperometric signals of *p*-nitrophenol on GCE

Figure 5.12 displays the influence of the applied potential at the GCE upon the amperometric response of PNP. No response is observed at potentials lower than 0.95 V, the current rises rapidly between 0.95 V and 1.15 V, and decreases slightly at the higher potentials. Subsequent electrochemical assays were thus carried out using a potential of 1.15 V.

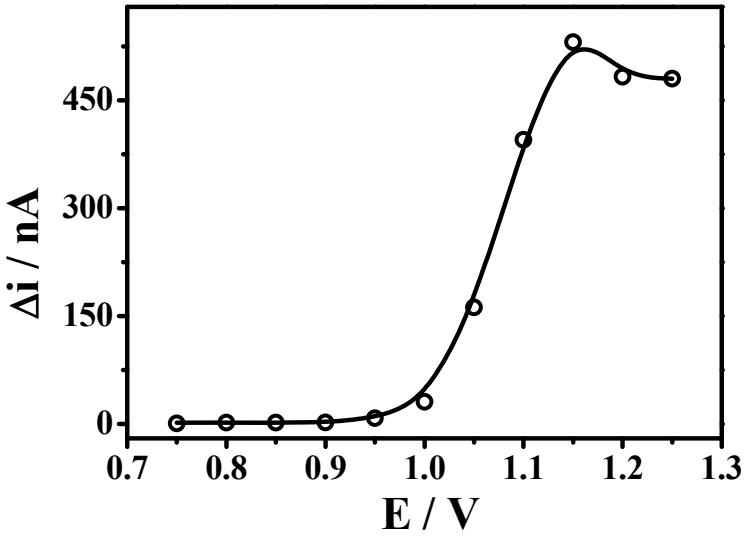


**Figure 5.12** Hydrodynamic voltammogram for the oxidation of 10 μM *p*-nitrophenol in stirred solution of 1.5 mL 0.05 M citrate buffer pH 4.4 at a glassy carbon electrode.

Figure 5.13 shows successive addition 10 μM PNP in 0.05 M citrate buffer solution pH 4.4. This small amount of PNP additions is not suffers from PNP passive film. However, the passivation film is occurred after few additions of 1 mM PNP. Other electrode materials, including CNT modified GCE was also examined, but results were not satisfaction displayed PNP response.

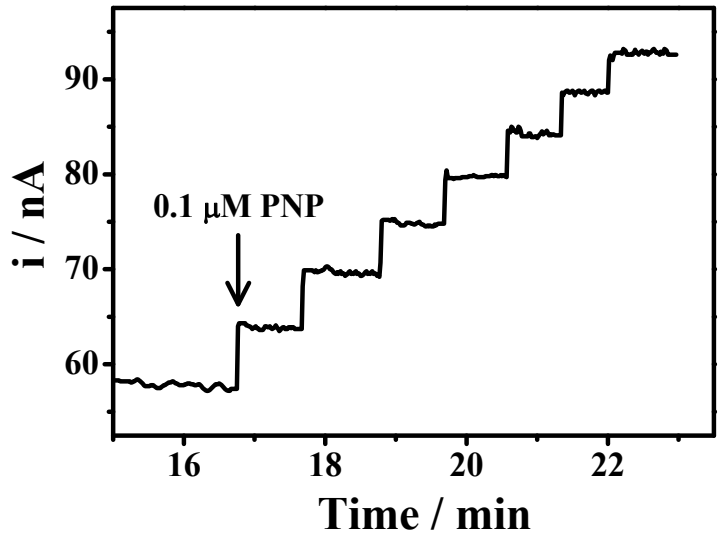


**Figure 5.13** Successive amperometric response (E = +1.15 V) to additions of 0.1 μM *p*-nitrophenol in a stirred 1.5 mL 0.05 M citrate buffer solution pH 4.4.

### 5.2.3 Amperometric and spectrophotometric studies of glycosidases enzyme

Amperometric assays have been used for measuring the activity of clinically important enzymes such as alkaline phosphatase [85] and alanine aminotransferase [86]. The new assay for glycosidases relies on the anodic detection of the enzymatically-generated PNP in the presence of a fixed concentration of the corresponding glycoside substrate. Generally, 10 μL of the enzyme solution was added to 1.5 mL of the stirred 200 mM substrate solution. The anodic signal arising from the oxidation of the PNP product described in figure 5.14, is proportional to the activity of the enzyme.

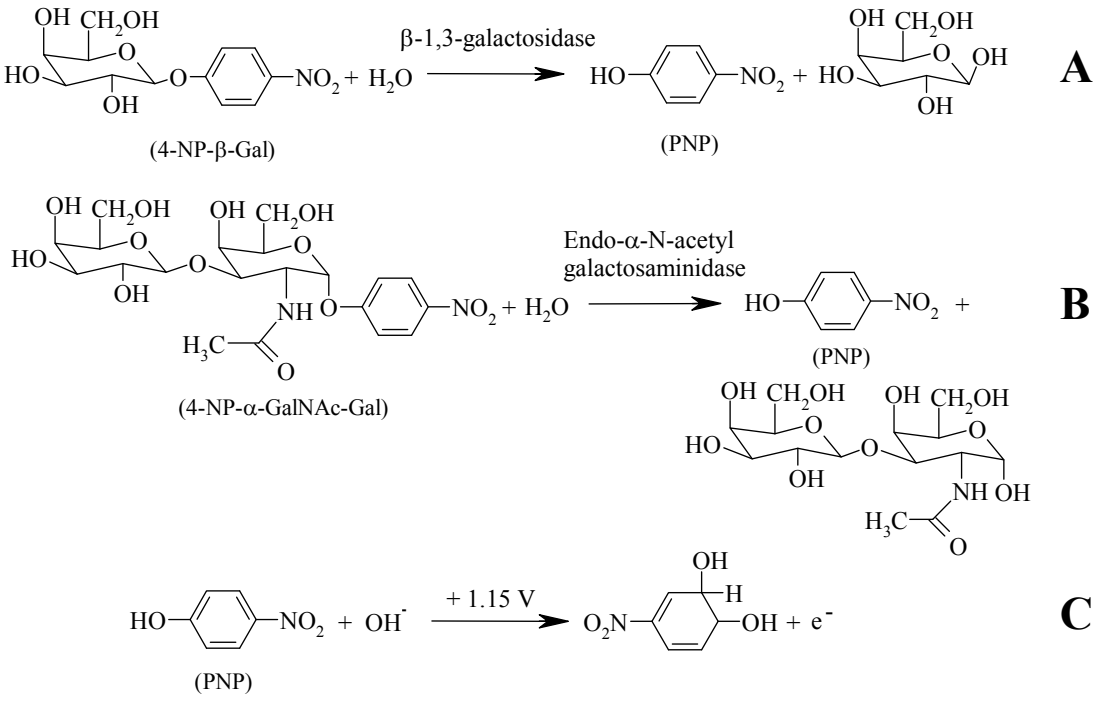


**Figure 5.14** Enzymatic reactions of (A) β-1,3-galactosidase, and (B) endo-α-N-acetylgalactosaminidase, followed by (C) the electrooxidation of the liberated *p*-nitrophenol on GCE at +1.15 V.

Figure 5.15 (A) shows the influence of the 4-nitrophenyl-β-galactopyranoside (4-NP-β-Gal) substrate concentration upon the response for 10 U β-1,3-galactosidase over the 5-200 μM 4-NP-β-Gal range (a-e). The response increases linearly with the time soon after addition and level. The current response at 60 s was found to be proportional to the substrate concentration. Figure 5.15 (B) show the corresponding linear plot. The optimized bioassay offers sensitive and rapid detection of glyco-active enzymes with the linearity of y = 0.324x + 9.2168, $R^2$=0.9864, where x and y are units in nA and μM, respectively.

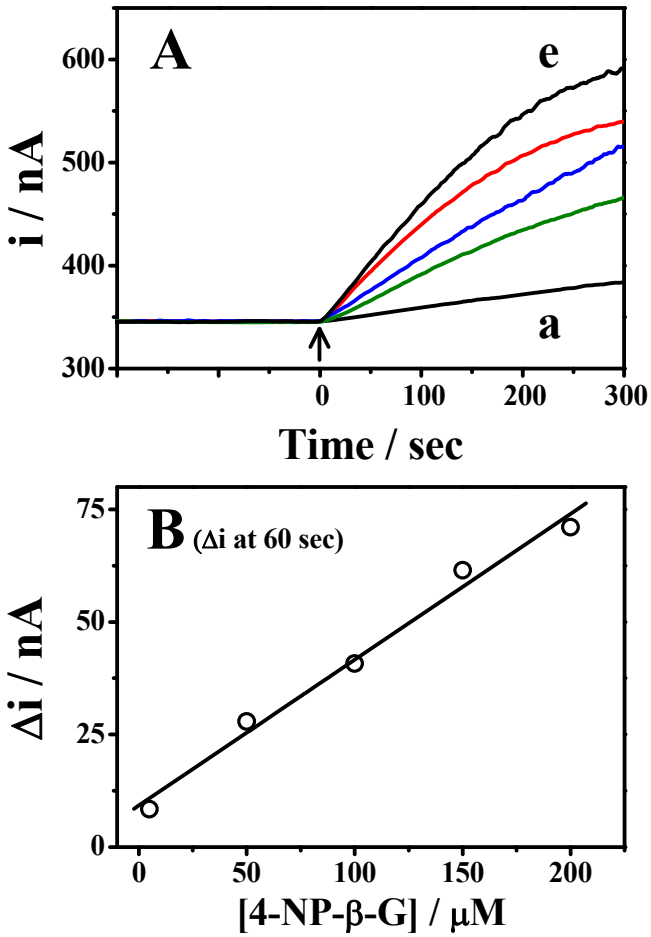


**Figure 5.15** (A) Amperometric responses at GCE of substrate additions of (a) 5, (b) 50, (c) 100, (d) 150 and (e) 200 μM of 4-NP-α-Gal into a 1.5 mL stirred 0.05 M citrate buffer solution (pH 4.4) containing 10 Unit of β-1,3-galactosidase. (B) The corresponding calibration plot based on measuring the current at 60 s after adding the 4-NP-β-Gal.

Figure 5.16 displays amperometric current-time tracings recorded upon adding different levels of (A) β-1,3-galactosidase and (B) endo-α-N-acetylgalactosaminidase. The amperometric current starts to increase upon adding the enzyme (see arrow), reflecting PNP production and oxidation. As expected [197], the shape of these amperograms depends on the enzyme activity [85]. As the concentration of the enzyme increases the observed curvature is shifted in the direction of shorter time periods. A sharp initial current rise (within the first 10 s) is also observed in the case of the endo-α-N-acetylgalactosaminidase. Such profiles allow convenient quantitation of the enzymatic activity. For example, measuring the response 60 sec after adding the enzymes results in linear current–activity dependence over the entire range (see insets for the corresponding calibration plots; (A) $y = 14.45x - 2.66$, $R^2 = 0.9784$ and (B) $y = 59.45 \times 10^3 x - 5.33 \times 10^3$, $R^2 = 0.9810$, where x and y are in activity unit and nanoampere, respectively). Note also the substantially higher sensitivity towards endo-α-N-acetylgalactosaminidase that facilitates convenient measurements of mUnit levels (vs. Unit ones for the β-1,3-galactosidase). A detection limit of 200 μUnit (1.5 $mL^{-1}$) can thus be estimated in connection to short reaction times of 20-40 sec (figure 5.16B, a). Such a detection limit corresponds to 49 fmol in the 1.5 mL solution. In contrast, in the standard optical assay [79] the detection of 200 μUnit (1.5 $mL^{-1}$) endo-α-N-acetylgalactosaminidase required significantly longer (600 sec) incubation time (figure 5.16C). Table 5.2 shows the figures of merit of enzymes electrochemical (for β-1,3-glycosidase and endo-α-N-acetylgalactosaminidase) and spectroscopic assays (for endo-α-N-acetylgalactosaminidase). Further, the assay measures only equilibrium reaction and does not provide real-time measurements.

The real samples, human serum, were tested with this system (please see results in appendix A.2). Three addition solutions of serum, serum + PNP, and serum + β-1,3-glycosidase enzyme + PNP illustrate similar in the current response. This effect may due to some species in the real serum is oxidized. To solve this problem in the future, the serum should be diluted and the working potential should be changed to lower.

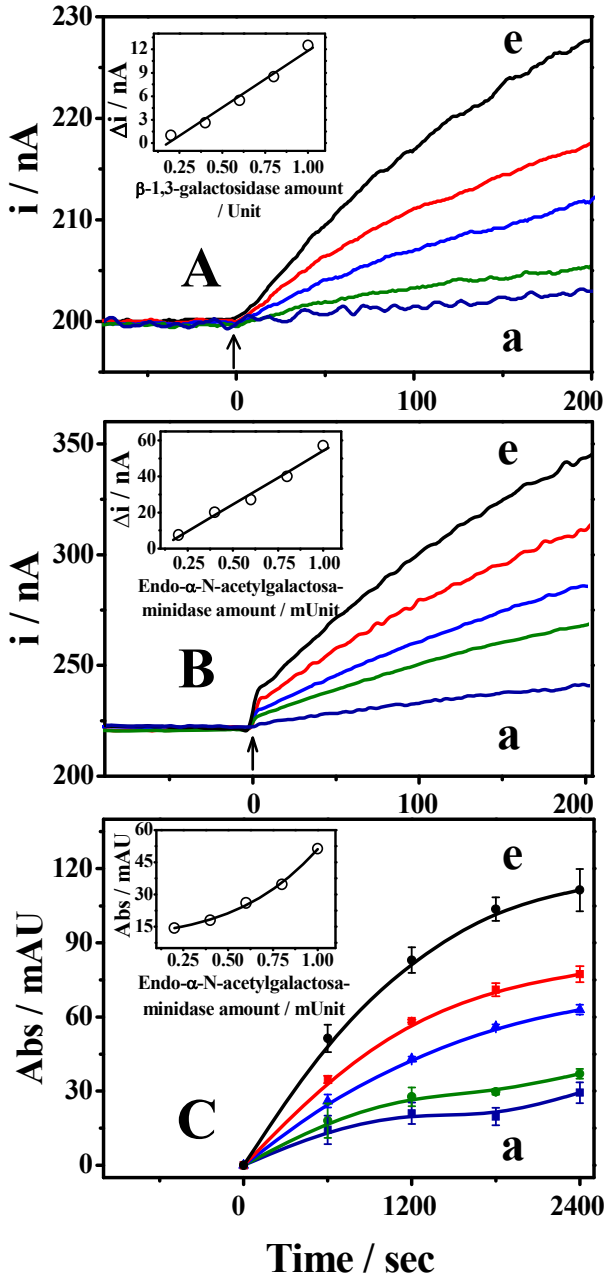


**Figure. 5.16** Comparision of glycosidases assays of (A, B) electrochemical sensor and (C) UV-Vis technique. Amperometric responses of additions of (A) 0.2 Unit β-1,3-galactosidase from (a) 0.2 to (e) 1.0 Unit in a stirred solution of 133 μM of 4-NP-β-Gal, and (B) 0.2 mUnit of endo-α-N-acetylgalactosaminidase from (a) 0.2 to (e) 1 mUnit in a stirred solution of 200 μM of 4-NP-α-GalNAc-Gal. UV-Vis absorbance at λ = 405 nm of (C) released PNP of (a) 0.2 to (e) 1.0 mUnit of endo-α-N-acetylgalactosaminidase.

**Table 5.2** Figures of merit of enzyme electrochemical and spectroscopic assays

| Analytes | Methods* | Detection limit / Unit $mL^{-1}$ | Sensing time / sec | Linearity / Unit $mL^{-1}$ | Sensitivity / nA $Unit^{-1}$ |
|---|---|---|---|---|---|
| β -1,3-galactosidase | EC | 0.10 | 60 | 0.13 - 16.70 ($R^2$ = 0.9784) | 14.45 |
| endo-α -N-acetylgalactosaminidase | i) EC | $130 \times 10^{-6}$ | 60 | $(0.13 - 0.67) \times 10^{-3}$ ($R^2$ = 0.9810) | $59.45 \times 10^{3}$ |
| | ii) SP | $133 \times 10^{-6}$ | 600 | - | $0.046 \times 10^{3}$ |

* EC = Electrochemical and SP = Spectroscopic assays

## 5.3 Hydrogen peroxide biosensor

### 5.3.1 The design of screen printed carbon electrode

The SPCE was designed in six configurations based on two theoretical concepts. Firstly, the reference electrode should be as close as possible to the working electrode to maintain the stability of the potential by minimizing the effect of resistance between the WE and RE. Secondly, the counter electrode should be of larger size than the others to allow unlimited current transfer in the circuit. The 6 designed SPCE configurations are shown in figure 5.17A and denoted as SPCEn (where n = 1, 3, 4, 5, and 6). The printed lay out of the SPCE1 are shown in figure 5.17B. Please see appendix A.2 for SPCE photographs. The first layer of SPCE is laid by Ag conducting ink that assist to provide the low background current. The resistances for silver based electrodes (CE, RE, and WE) of 6 SPCEs are measured by the multi-meter between the contact pad and electrode. The elecrotdes resistance meausurement was details in appendix A.3. No difference in resistance between 6 SPCEs from the carbon commercials, GCE and graphite electrodes (GPE). These resistance values are showed in table 5.3.

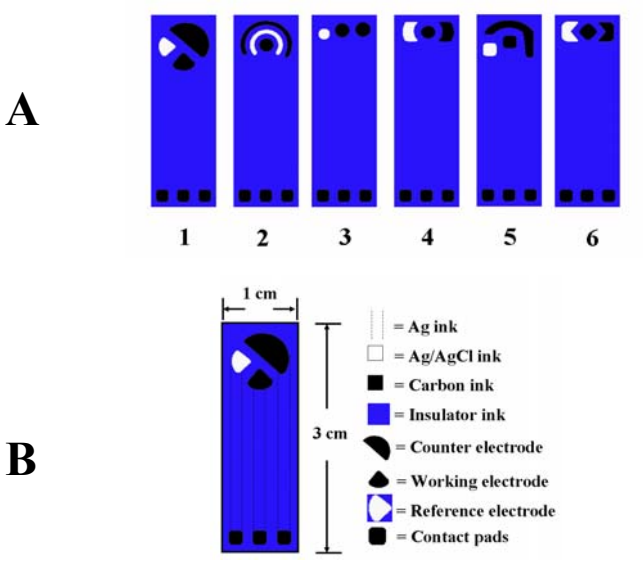


**Figure 5.17** (A) Six configurations of screen printed carbon electrodes (SPCEn, where n = 1 to 6) and (B) the details and dimension of SPCE1.

To investigate the performance and characteristic of the designed SPCE, cyclic voltammetric experiments were performed on the 6 SPCEn (n = 1 - 6) in aqueous solution of 10, 20 and 30 mM $K_3Fe(CN)_6$. Figure 5.18 and table 5.3 show cyclic voltammograms and corresponding peak high and potential of 6 SPCEs, respectively. These electrodes show a poor reversibility with large $\Delta E_p$ (from 1.1 to 1.4 V) and non-unity current ratio (oxidation slope is smaller than reduction slope). They also show small charge transfer with low sensitivity, 0.23 - 0.35 μA $mm^{-2}$ $mM^{-1}$ for oxidation and –0.69 - –0.85 μA $mm^{-2}$ $mM^{-1}$ for reduction reaction. Morrin *et. al.* [198] suggested that the material resistance affects the rate of electron transfer from the electrode surface to the conductive pads. The use of silver as conducting tracks might enhance the charge transfer. However, in this study the silver track does not improve the charge transfer.

**Table 5.3** The resistance and working area of SPCEn, glassy carbon, and graphite electrodes

| | SPCE1 | | | SPCE 2 | | | SPCE 3 | | | SPCE 4 | | | SPCE 5 | | | SPCE 6 | | | | |
|---|---|---|---|---|---|---|---|---|---|---|---|---|---|---|---|---|---|---|---|---|
| **SPCE** | **WE** | **RE** | **CE** | **WE** | **RE** | **CE** | **WE** | **RE** | **CE** | **WE** | **RE** | **CE** | **WE** | **RE** | **CE** | **WE** | **RE** | **CE** | **GPE** | **GCE** |
| **R / Ohm** | 5.8 | 5.7 | 6.2 | 6.0 | 5.5 | 6.2 | 6.3 | 5.9 | 6.5 | 6.4 | 5.7 | 6.6 | 6.1 | 5.3 | 6.3 | 6.3 | 5.8 | 6.6 | 1.3 | 4.3 |
| **A / mm$^2$** | 4.3 | 5.4 | 16.2 | 3.1 | 6.4 | 6.9 | 3.1 | 2.1 | 3.4 | 3.1 | 4.9 | 4.9 | 3.6 | 3.7 | 12.7 | 3.9 | 5.1 | 5.1 | 7.1 | 7.1 |

A = Area, CE = Counter electrode, GCE = Glassy carbon electrode, GPE = Graphite electrode, R = Resistance, RE = Reference electrode, SPCE = Screen printed carbon electrode, WE = Working electrode.

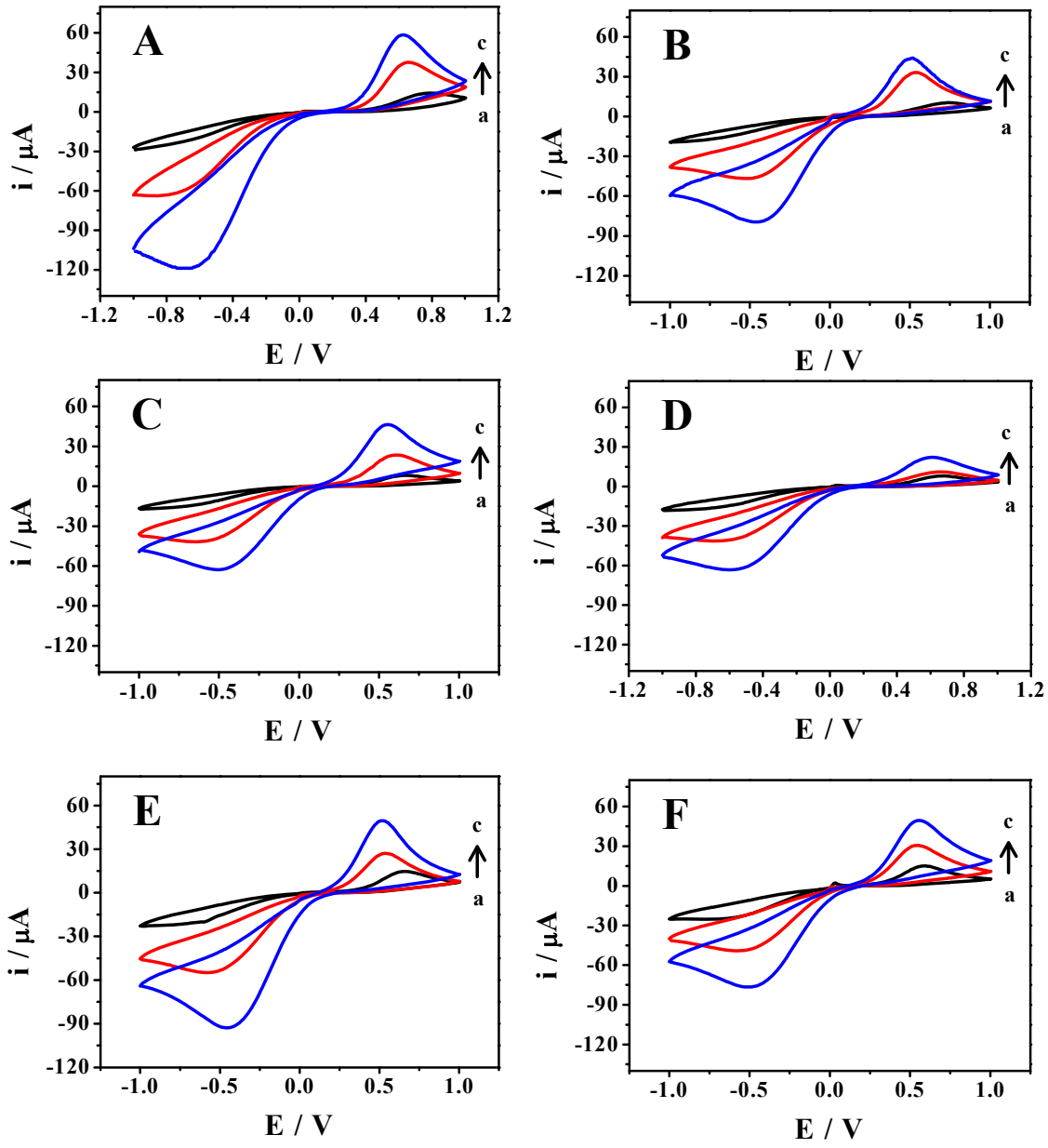


**Figure 5.18** Cyclic voltammograms of (a) 10 mM, (b) 20 mM, and (c) 30 mM $K_3Fe(CN)_6$ in DI water at SPCEn (n = 1(A) - 6(F)). Condition: scan rate 100 mV $s^{-1}$.

The peak potential is shifted slightly towards zero as the concentration of $K_3Fe(CN)_6$ is increased. The SPCE2 exhibits very inconsistency in the current measurements for electrode-to-electrode repetition. In this configuration the electron movement between the WE and CE is impeded by the RE due to its placement completely between the WE and CE. Other electrode configurations show a small value of deviation. The criteria for selection the best SPCE are high

sensitivity, high precision, unity redox current, and narrow different peak potential. Data in table 5.4 are slope of plot of current density vs. $K_3Fe(CN)_6$ concentration (for comparison the sensitivity), % RSD (precision), and different peak potential. The SPCEs were graded along with the selection criteria and they were A to D in the last column of table 5.4. The best one is for the SPCE5 as A, and others are as the SPCE1 = C, SPCE2 = D, SPCE3 = B, SPCE4 = B, and SPCE6 =$B^+$.

**Table 5.4** Performances and characteristics of 6 SPCEs

| SPCE | Peak potential* / V (±SD) | | | % RSD of peak current* | | Sensitivity** / µA $mm^{-2}$ $mM^{-1}$ | | SPCE graded |
|---|---|---|---|---|---|---|---|---|
| | Oxidation | Reduction | ΔE | Oxidation | Reduction | Oxidation slope ($R^2$) | Reduction slope ($R^2$) | |
| 1. | 0.63 (±0.03) | -0.77 (±0.04) | 1.40 | 6.13 | -5.21 | 0.23 (0.990) | -0.79 (0.999) | C |
| 2. | 0.58 (±0.08) | -0.65 (±0.07) | 1.23 | 12.45 | -14.09 | 0.35 (0.990) | -0.82 (0.999) | D |
| 3. | 0.58 (±0.05) | -0.67 (±0.04) | 1.25 | 3.93 | -3.61 | 0.30 (0.990) | -0.77 (0.990) | B |
| 4. | 0.60 (±0.03) | 0.67 (±0.03) | 1.27 | 5.93 | -7.25 | 0.28 (0.994) | -0.69 (0.994) | B |
| 5. | 0.54 (±0.03) | -0.56 (±0.02) | 1.10 | 4.72 | -3.85 | 0.35 (0.991) | -0.83 (0.998) | A |
| 6. | 0.55 (±0.04) | -0.58 (±0.03) | 1.13 | 5.18 | -3.84 | 0.32 (0.992) | -0.78 (0.998) | B+ |

* The data were estimated from 20 mM $K_3Fe(CN)_6$ with n = 3.

** The sensitivities (and regression parameter, $R^2$, in parenthesis) were accomplished with measurements in 10, 20 and 30 mM $K_3Fe(CN)_6$ (n = 3).

The SPCEn, (n = 3, 4 and 6) show similar response. The sensitivity of the corresponding calibration curves of current vs. concentration of $K_3Fe(CN)_6$ were compared in table 5.4. The most sensitive and reproducible SPCE was the SPCE5. The sensitivity of the SPCE5 is ascribed to the larger size of the counter electrode which does not hinder the large amount of ions passing through the electrodes. The SPCE5 was used in all of the following experiments. The linearity current response to the square root of the scan rate, in the range of 20 - 200 mV $s^{-1}$, imply a diffusion controlled process on the electrode in 20 mM $K_3Fe(CN)_6$ containing of 0.1 M KCl (please see appendix A.3 for cyclic voltammograms of current responses versus a plot of the square root of the scan rates) and is agreed with Muangkeaw, K. [199].

To compare SPCEn (SPCE5) with other carbon electrodes, the home-made carbon paste (CPE) [179], GCE, and also SPCE from KMUTT, Thailand, (K-SPCE) have been exploited. Figure 5.19 show the cyclic voltammetry of (A) SPCE5, (B) CPE, (C) GCE, and (D) K-SPCE. The shapes of CPE and GCE were similar to SPCE5. The different peak potentials (ΔE) of CPE and GCE are different from SPCE5 for 0.08 V and 0.21 V, respectively. The ΔE of CPE is closer to ΔE of SPCE5 than that of GCE. The GCE, a carbon that is cured by the high thermal until their show physical property quite differs from graphite based material, showed ΔE quite differ from CPE and SPCE5. For the K-SPCE, it was not clearly showed any peak. This problem may be due to their too long shelf storage of K-SPCE (3 years of storage life) and a loss of C-ink properties is occurred since the labeled from the manufacturer on C-ink bottom show not for used over ~10 months.

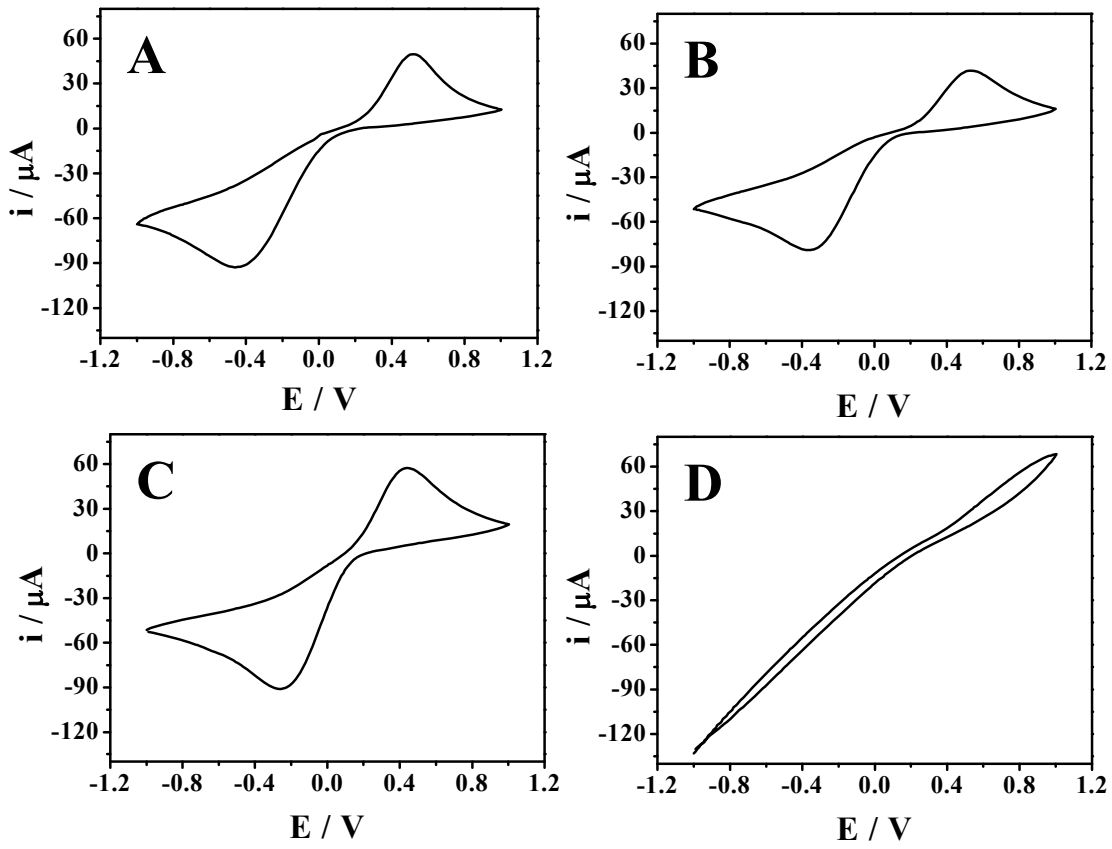


**Figure 5.19** Cyclic voltammograms of 30 mM $K_3Fe(CN)_6$ at (A) SPCE5, (B) CPE, (C) GCE, and (D) K-SPCE. Step potential 10 mV, scan rate, 100 mV $s^{-1}$.

### 5.3.2 AuNP synthesis

The AuNP were synthesized by reducing $HAuCl_4$ in trisodium citrate with modification according to Neiman *et. al.* [200]. The size and photometric adsorption properties of the AuNP were examined by TEM and UV-Vis spectrophotometry, respectively. The results are illustrated in figure 5.20. The AuNP were uniform with the size of the 16.8 nm (figure 5.20A). The concentration of AuNP solution was calculated at 0.85 nM by follow the literatures [136, 201] (see calculation method in Appendix A.3). The UV-Vis spectra of the synthesized AuNP shows a peak at 521 nm (figure 5.20B,a) with agreement with Na-citrate reduction methods [200] while the $HAuCl_4$ solution shows a shoulder absorption at 282 nm (figure 5.20B,b). These results demonstrate that the AuNP have good uniform particles in the nanometer size range and agree with Khanna *et. al.* [202].

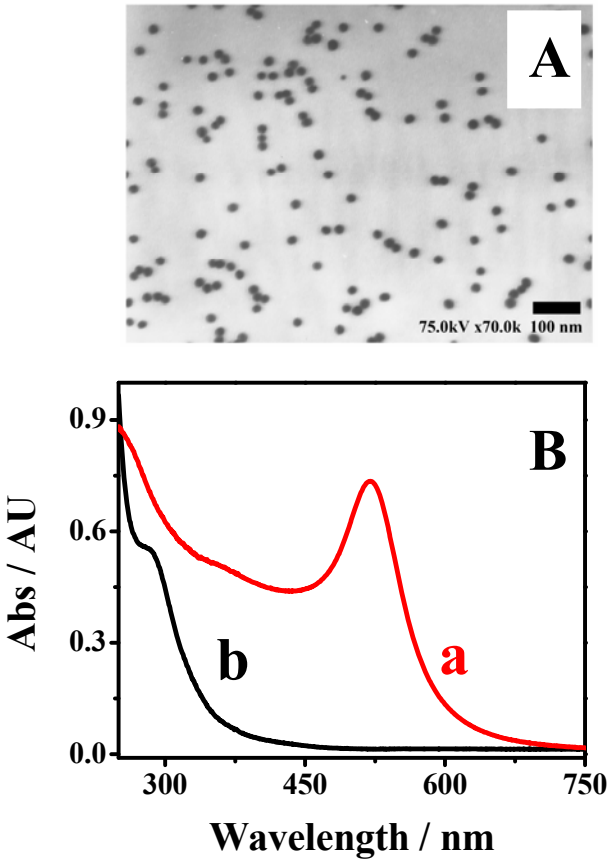


**Figure 5.20** (A) TEM micrograph of AuNP; (B) UV-Vis spectra of solutions of (a) 0.85 nM AuNP and (b) 0.01% $HAuCl_4$.

The size of the AuNP is very sensitive to the synthesized condition as temperature, and reducing agent amount. Figure 5.21A and B show TEM micrographs of AuNP obtained from room temperature (RT, ca. 30 °c) and 125 °C, respectively. Three Au:citrate ratios effect on AuNP is showed in figure 5.21a-c. At RT (figure 5.21A,a), the AuNP shape is not uniform, but at 125 °C is a clearly uniform shape (figure 5.21B,a) because Au(III) is completely reduced to $Au^0$.

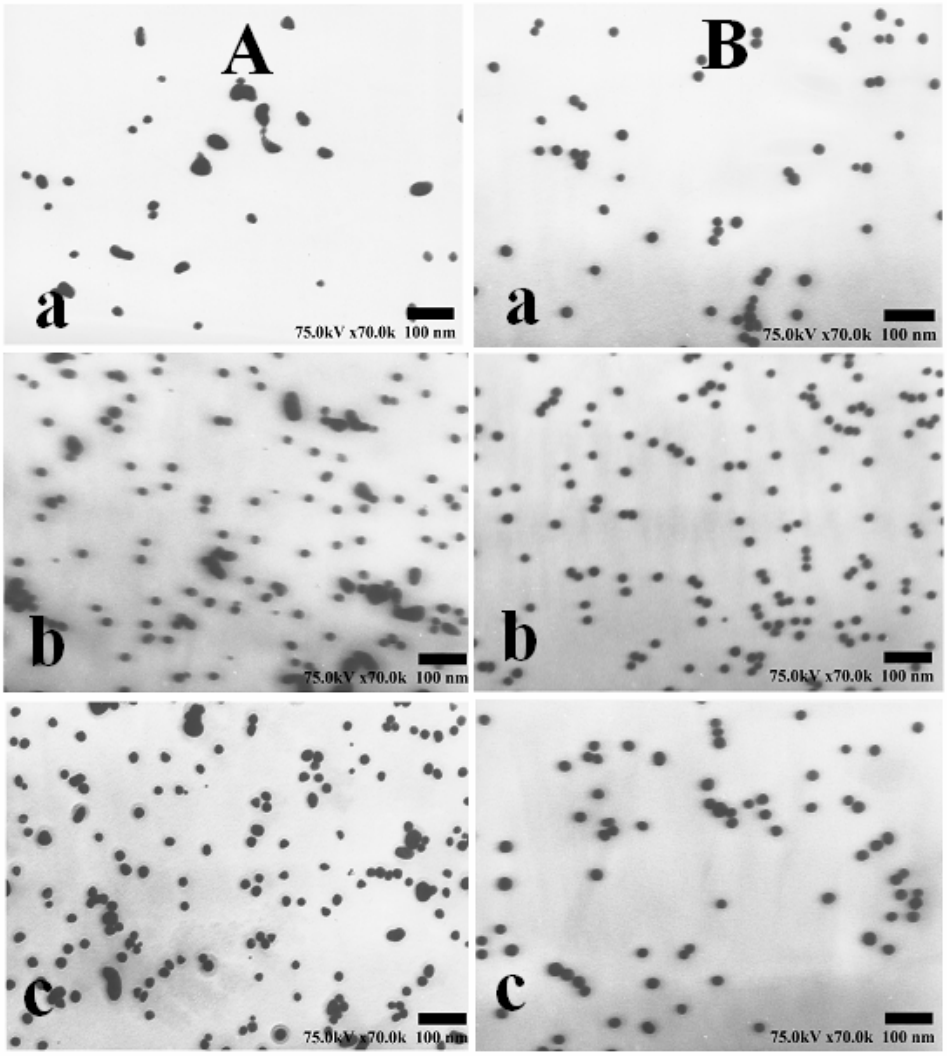


**Figure 5.21** TEM micrographs of gold nanoparticles at various conditions. Column showed TEM photographs of two synthesized temperatures of (A) RT and (B) 125 °C. Row showed TEM photographs of three different Au : Na-citrate mole ratios of (a) 1:32, (b) 1:47 and (c) 1:64. Period of conditions A and B were 12 and 0.5 hours, respectively.

To study the effect of Au:Nacit ratio, three different ratios of 1:32, 1:47, and 1:64 had been investigated. The Au:Nacit ratio on AuNP synthesis at RT (figure 5.21A (a-c)) showed the poor shape. Clearly homogeneous shape of all three Au:NaCit ratios is at 125 °C (figure 5.21 B (a-c)). The AuNP displayed smallest size at 1:47 of Au:Nacit ratio. This result is agreed with previously work of Neiman *et. al.* [200]. All sizes of synthesized AuNPs were list in table 5.5. The AuNP synthesis condition for 1:4.7 of Au:Nacit ratio and 125 °C for temperature is selected for using in $H_2O_2$ biosensor development.

**Table 5.5** Average size of AuNP and their standard deviation at various gold : sodium citrate mole ratio

| **Au : Sodium citrate / mole ratio** | **Temperature / °C** | **Size / nm** | **n**** |
|---|---|---|---|
| 1 : 3.2 | RT* | 23.33 (±8.93) | 33 |
| 1 : 3.2 | 125 | 20.14 (±0.90) | 59 |
| 1 : 4.7 | RT | 22.47 (±9.28) | 131 |
| 1 : 4.7 | 125 | 16.80 (±0.82) | 123 |
| 1 : 6.4 | RT | 24.73 (±5.49) | 98 |
| 1 : 6.4 | 125 | 22.40 (±1.08) | 68 |

* RT=Room temperature (ca. ~30 °C)

** n = number of particle

Figure 5.22 shows corresponding UV-Vis absorption spectra of figure 5.21. Figure 5.22A shows broad absorption pattern of UV-Vis spectra of the AuNP, synthesis at RT, compared to the characteristic spectra of AuNP, synthesis at 125 °C (figure 5.22B). The absorption peak of AuNP with RT synthesis (figure 5.22A(a-c)) is around 528 nm. The spectra of AuNP (125 °C) show narrow absorption peak around 520 nm. This result is agreed with Khanna *et. al.* [202]. They suggested that the AuNP stabilizing by various condition and showed wider sizes and broader UV-Vis spectrum at lower synthesis temperature. The peak width at half maxima (PWHM) increases with the increased size due to aggregation of gold nanoparticles

with red shift [203]. It is confirmed that the size distribution of the AuNP-125 is quite narrower than AuNP-RT. Moreover, the AuNP-RT is needed a minimum 12 hours to get a gold colloidal solution because the reduction process is slow.

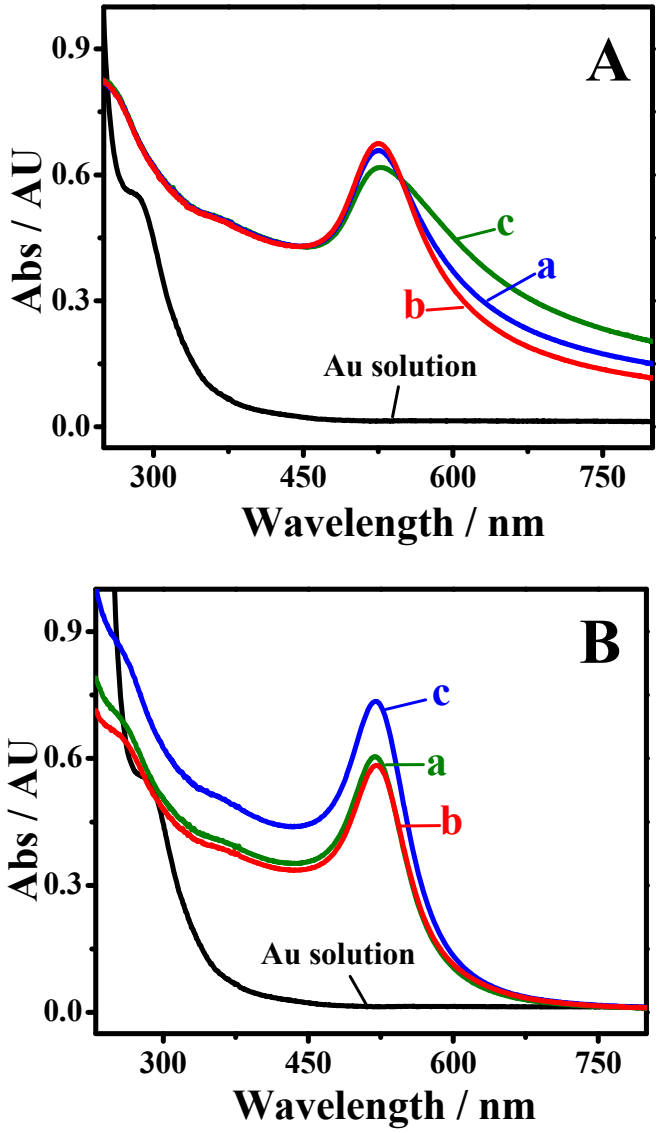


**Figure 5.22** UV-Vis absorption spectra of (A) AuNP-RT and (B) AuNP-125 at different Au : Na-citrate mole ratio of (a) 1:32, (b) 1:47 and (c) 1:64.

### 5.3.3 UV-Vis spectra of enzyme mixed solution studies

The UV-Vis spectrum of the chitosan (CHIT) solution (figure A.12A) exhibits a peak at 305 nm while the AuNP peak is at 521 nm (figure 5.23B). When mixed with the AuNP solution there is a slightly broad peak at 620 nm (figure 5.23C), which may be due to less aggregation of the AuNP with the biomolecule, a suppressed peak for the AuNP at 521 nm, but the CHIT still exhibits a distinct peak at 305 nm. The UV-Vis spectrum of HRP (figure 5.23D) shows absorption peaks at 278 and 403 nm, it is agreed with Lu *et. al.* [204]. The spectrum of the mixed solution of HRP/AuNP/CHIT (figure 5.23E) is distinct with the peaks of HRP and AuNP. The peak of the CHIT is covered by the HRP peak. One point should be highlighted that there is an increased absorption peak at about 643 nm (higher than figure 5.23B), which may be due to more aggregation of the AuNP with the CHIT and HRP molecules [205].

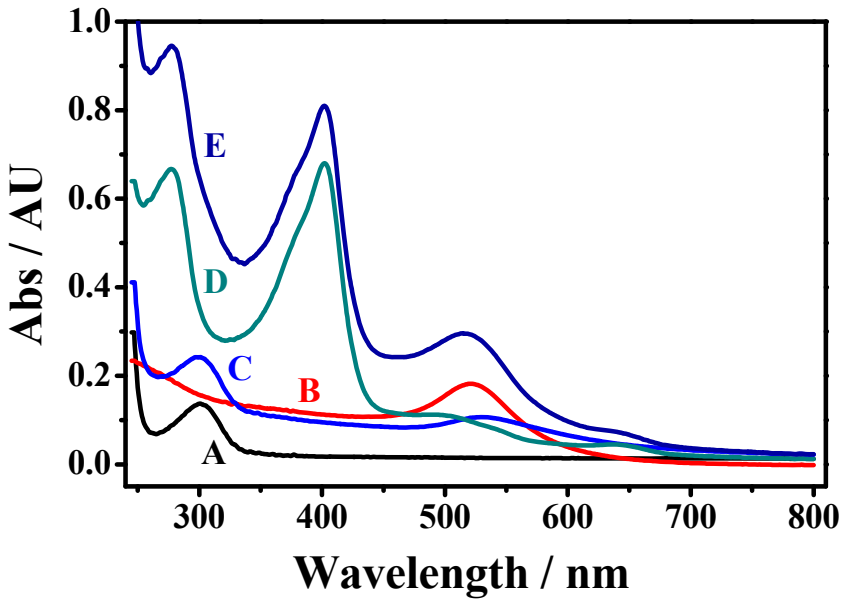


**Figure 5.23** UV-Vis absorption spectra of solutions of (A) 0.1% CHIT, (B) 0.43 nM AuNP, (C) mixed of AuNP-CHIT, (D) HRP, and (E) mixed of HRP-AuNP-CHIT.

### 5.3.4 Optimization of $H_2O_2$ biosensor

Horseradish peroxidase (HRP) is classified into plant peroxidase. It is a super family consisting of yeast peroxidase, plant ascorbate peroxidase, fungal peroxidases, and classic peroxidases. HRP is the most commonly used in practical analytical applications. The catalytic cycle of heme-containing horseradish peroxidase from the literatures [206-210] is concluded in reaction (R5.5) - (R5.7).

$$HRP(Fe^{3+}) + H_2O_2 \longrightarrow \text{Compound I} + H_2O \qquad \text{(R5.5)}$$

$$\text{Compound I} + H^+ + e^- \longrightarrow \text{Compound II} \qquad \text{(R5.6)}$$

$$\text{Compound II} + H^+ + e^- \longrightarrow HRP(Fe^{3+}) + H_2O \qquad \text{(R5.7)}$$

The reaction of (R5.5) is started with the native state $HRP(Fe^{3+})$ of the enzyme with hydrogen peroxide ($H_2O_2$), resulting in the oxidized form of the enzyme denoted as compound I and released of one water molecule. This initial reaction is then followed by two sequential one-electron reduction steps as reaction (R5.6) and (R5.7) with electron released from SPCE. In which an intermediate denoted as compound II is formed at (R5.6). Finally, the native state of $HRP(Fe^{3+})$ is recreated as a result of the second one electron released from SPCE to reduce the compound II and produced water (R5.7). Both reduction steps of (R5.6) and (R5.7) occur simultaneously. The overall reaction is summarized in equation R5.8.

$$H_2O_2 + 2H^+ + 2e^- \xrightarrow{\text{Horseradish peroxidase}} 2H_2O \qquad \text{(R5.8)}$$

In this section, the optimum conditions of $H_2O_2$ biosensor will be optimized in the following topics.

#### 5.3.4.1 Effect of HRP/AuNP/CHIT/SPCE to electrocatalytic reduction of $H_2O_2$

Four modified $H_2O_2$ biosensors were investigated, denoted as CHIT/SPCE, HRP/SPCE, HRP/CHIT/SPCE and HRP/AuNP/CHIT/SPCE. To avoid the blocking of $O_2$ from the electrocatalytic oxidation of $H_2O_2$, the electrocatalytic reduction of $H_2O_2$ to $H_2O$ was selected. The CHIT was immobilized on the SPCE by electrodeposition where the CHIT hydrogel film was visible on the electrode surface after immobilization.

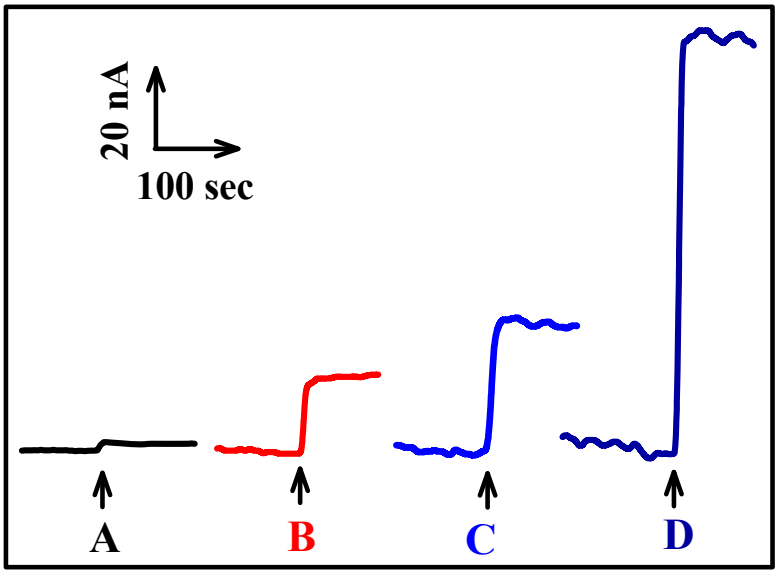


**Figure 5.24** Amperometric responses of single addition of 500 μM $H_2O_2$ into a stirred solution of 0.1 M citrate buffer pH 6.5.at (A) CHIT/SPCE, (B) HRP/SPCE, (C) HRP/CHIT/SPCE and (D) HRP/AuNP/CHIT/SPCE ($E_{applied}$ = –0.4 V).

The amperometric response at –0.4 V of the CHIT/SPCE (figure 5.24A) shows the lowest sensitivity. Since, HRP is easily modified on the electrode surface, so immobilized HRP on SPCE had been introduced by immersing the SPCE in a solution of 3 mg $mL^{-1}$ HRP for 1 hr. The amperometric response of $H_2O_2$ spiking the HRP/SPCE (figure 5.24B) was clearly observed. To stabilize HRP, and improve the amperometric response of $H_2O_2$, HRP was immobilized in the CHIT thin film.

The response of HRP/CHIT/SPCE to spiking with $H_2O_2$ was achieved 1.8 times higher than the HRP/SPCE (figure 5.24C). By a simple electrodeposition at an appropriated potential [211], CHIT become solid, due to slightly alkalinity at electrode surface. This technique is easily adaptable to incorporate AuNP and HRP in CHIT film. The amperometric response of $H_2O_2$ on HRP/AuNP/CHIT/SPCE (figure 5.24 D) is immediately (within 1-5 sec) with the highest current at 3.3 times and 5.7 times higher than the responses of HRP/CHIT/SPCE and HRP/SPCE, respectively. Due to the effective adsorption of enzyme on the large conductive surface area of AuNP, the more substrate ($H_2O_2$) is accumulated and reduced at electrode surface leading to the larger signal via the enhancement in the reduction current or rate of charge transfer for $H_2O_2$.

### 5.3.4.2 Hydrodynamic voltammogram

The electrocatalytic reduction of $H_2O_2$ by HRP to water at a fixed potential is used as the amperometric sensing principle. It has been shown that HRP can catalyze $H_2O_2$ by direct electron transfer (without a mediator). Within the low potential range, $H_2O_2$ has less interference from biological species, e.g. ascorbic acid and uric acid.

The hydrodynamic voltammogram has been examined for the HRP/AuNP/CHIT/SPCE in the range of –0.20 to –0.50 V with injection of 500 μM $H_2O_2$ (figure 5.25). The advantages of SPCEs are firstly, their single-use nature, no cleaning is necessary and secondly, the signal is reproducible (in each fabrication). At potential < –0.30 V, only the low current was seen. The current increases continuously with the more negative potential up to –0.5 V. As we known, at the high operating potential, interference from the reduction of unwanted species (e.g. $O_2$ reduction) is a problem. Therefore the operating potential of –0.40 V was selected for further study to give a good sensitivity and a short setting time.

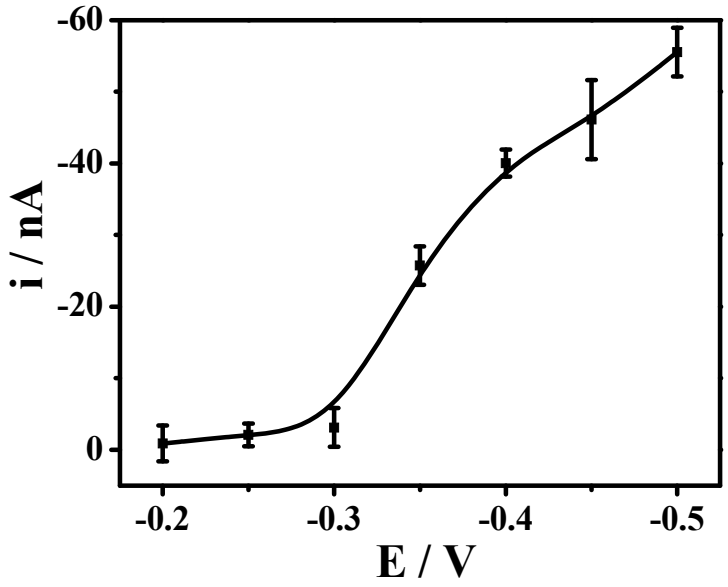


**Figure 5.25** Optimization of the potential on the HRP/AuNP/CHIT/SPCE while addition of 500 μM $H_2O_2$ into a stirred solution of 0.1 M citrate buffer pH 6.5, n = 3.

#### 5.3.4.3 Electrodeposition time

The effect of electrodeposition time on the performance of enzyme electrode was optimized. The current responses of the 500 μM $H_2O_2$ addition to the stirred solution of 0.1 M citrate buffer solution, pH 6.5, with an applied potential of –0.4 V to the HRP/AuNP/CHIT/SPCE were plotted w.r.t. the deposition time, as shown in figure 5.26. At 50 sec of deposition, the response current of $H_2O_2$ reached to the maximum. For longer electrodeposition time (t > 50 sec), in the range of 60-80 sec, the responses are more or less constant out the same level of 50 sec. The above effect was ascribed to the transferring of electrons in the conducting network of HRP/AuNP/CHIT affected by the amount of their molecules and distance on the SPCE surface. The lower currents are caused by the lower amount of HRP/AuNP/CHIT (10-30 sec), while the higher amount of HRP/AuNP/CHIT (60-80 sec) had reached the maximum kinetics for the enzyme-substrate reaction. On the other hand, the greater film thickness gave the larger background current, rendering the measurement difficult for low currents. The electrodeposition time of 50 sec was selected for the following experiments.

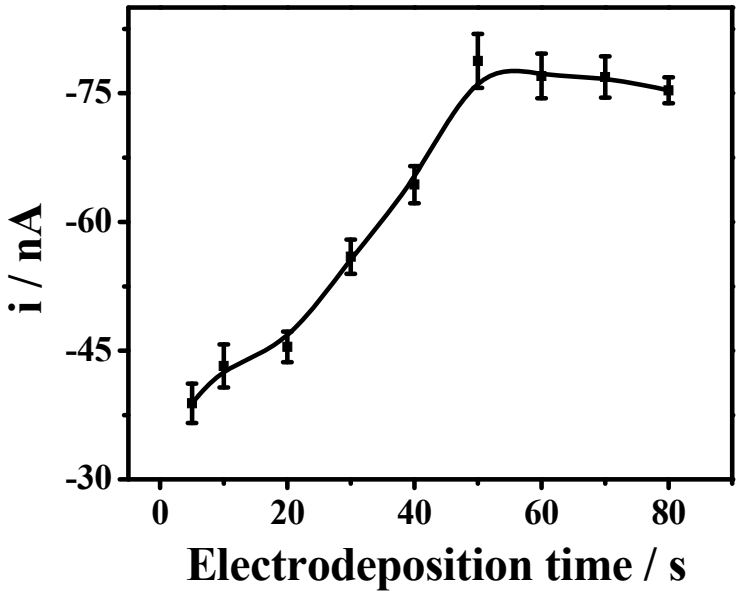


**Figure 5.26** The current response of addition of 500 μM $H_2O_2$ ($E_{applied}$ = –0.4 V) into a stirred solution of 0.1 M citrate buffer pH 6.5, n = 3 vs. the HRP/AuNP/CHIT/SPCE electrodeposition time.

#### 5.3.4.4 Effect of pH

The effect of pH (5.0 to 8.0) on the $H_2O_2$ biosensor is mainly due to the effect of pH on the activity of the enzyme. Figure 5.27 shows the current response at various. The maximum response is obtained at pH 6.5, as reported by Qian *et. al.* [212] and Lei *et. al.* [213]. The acidic solution enhances the reaction because $H^+$ is needed for HRP to reduce the $H_2O_2$ and produce water. Lei *et. al.* demonstrated that the biocatalytic properties of HRP towards $H_2O_2$ are maintained in the AuNP/CHIT microenvironment. To obtain the maximum sensitivity and bioactivity, a citrate buffer of pH 6.5 is used throughout the research.

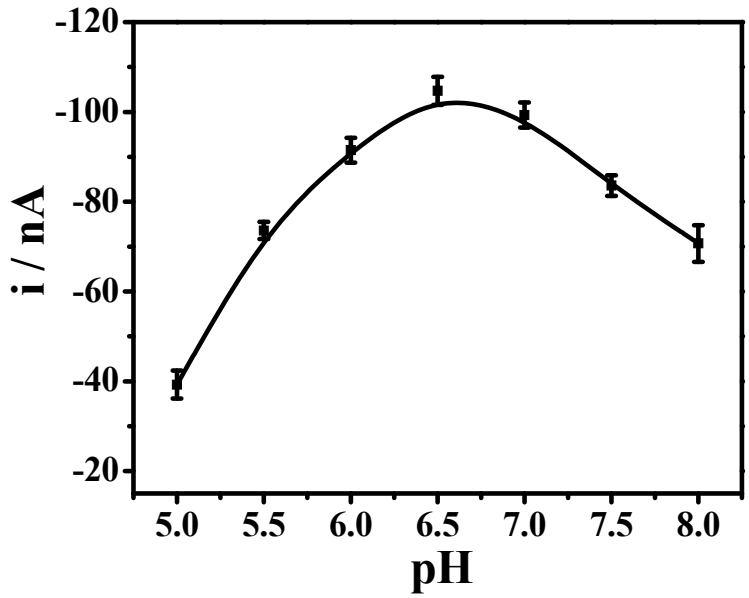


**Figure 5.27** The effect of pH on the current response of the HRP/AuNP/CHIT/SPCE while addition of 500 μM $H_2O_2$ ($E_{applied}$ = –0.4 V) into a stirred solution of 0.1 M citrate buffer pH 6.5, n = 3.

### 5.3.5 Amperometric measurements of HRP/AuNP/CHIT/SPCE toward $H_2O_2$ performance

To demonstrate the success of $H_2O_2$ determination at the HRP/AuNP/CHIT/SPCE, amperometric experiment had been performed for tracking the response of the successive additions of $H_2O_2$ (figure 5.28). With each additional aliquot of $H_2O_2$, the reduction current rises sharply and hits a stable plateau. The calibration plot of steady state current vs. $H_2O_2$ concentration is linear ($R^2$ = 0.995) in the wide range of 10 μM to 11.3 mM with a sensitivity of –176 nA $mM^{-1}$ (figure 5.28B).

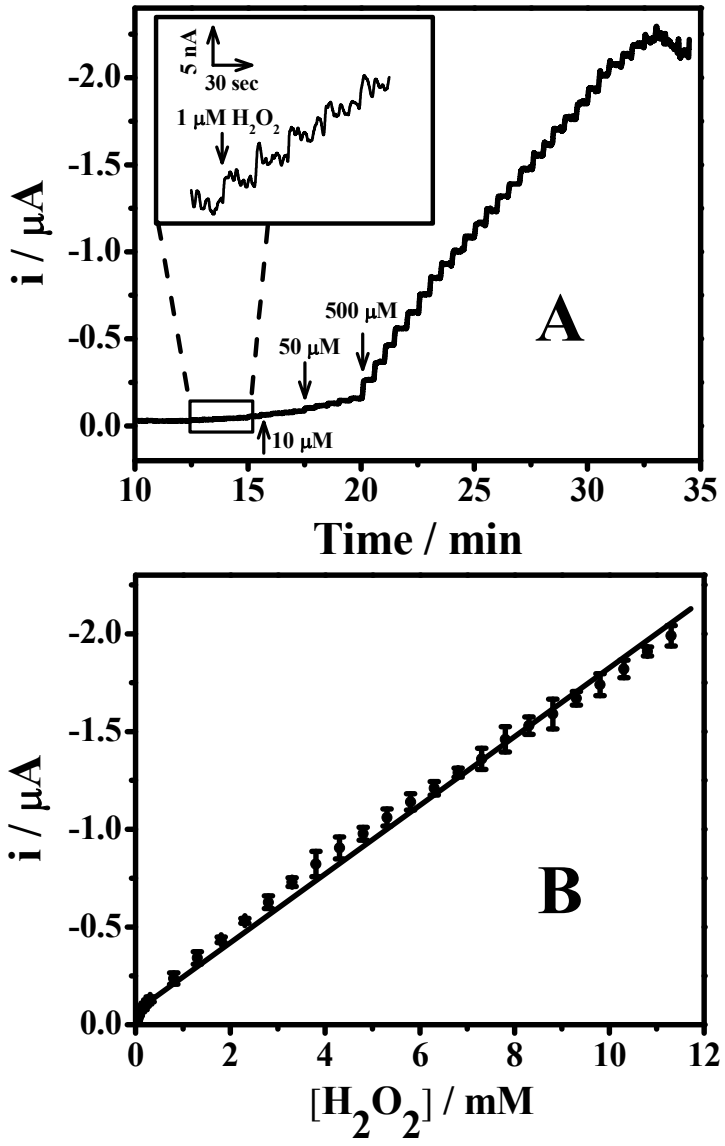


**Figure 5.28** (A) Amperometric of successive additions of various amounts of $H_2O_2$ at HRP/AuNP/CHIT/SPCE, and (B) shows a linear calibration plot of $H_2O_2$ concentration vs. the corresponding current. Inset (A) shows successive addition of 1 µM $H_2O_2$. Conditions; $E_{applied}$ = –0.4 V; stirred solution of 0.1 M citrate buffer pH 6.5.

The smallest spiked concentration of $H_2O_2$ was observed at 1 µM (figure 5.27A (inset)). The detection limit is obtained at 0.65 µM with a signal-to-noise ratio of 3. When the concentration of $H_2O_2$ is added over 11.3 mM (at around 33 min), the current response is unreliable. The linearity of this sensor has a range

with a magnitude order of 3. The high linear range can be attributed to first-order chemical kinetics, and is preferred for the development of sensors. The linear range of this sensor was higher in scale when compared to HRP/Au/SPCE [214] and PB modified GC particles/SPCE [102], with ranges of 0.8 μM to 2.2 mM and 0.3 μM to 1 mM $H_2O_2$, respectively, however all of them have the same magnitude of linearity.

The kinetic parameter, the apparent Michaelis-Menten constant ($K_m^{app}$), is an indication of the enzyme-substrate kinetics. According to Lineweaver-Burk equation [215] :

$$\frac{1}{I_{ss}} = \frac{1}{I_{max}} + \frac{K_m^{app}}{I_{max}} \times \frac{1}{C} \quad (5.1)$$

After successive additions of a certain concentration ($C$) of the substrate ($H_2O_2$) into the stirred solution, the current will reach a steady-state ($I_{ss}$). The maximum current when the substrate is saturated, ($I_{max}$), is used to determine the $K_m^{app}$ value by analysis of the slope and the intercept for the relation of the increased current versus $H_2O_2$ concentrations. The $K_m^{app}$ was found to be 4.51 mM and close to the $K_m^{app}$ of 1.3 mM from the system of HRP/AuNP/SPCE [214]. This value is smaller than $K_m^{app}$ value of 41 mM for immobilized hemoglobin in carbon nanotubes for direct electron transfer of $H_2O_2$ to the electrode surface [216]. Thus, these results indicate that the new environment of the AuNP/CHIT creates a good affinity of the immobilized enzyme for $H_2O_2$ electrocatalytic reduction. The comparison of perfomance of HRP/AuNP/CHIT/SPCE with others is showed in table 5.6.

**Table 5.6** Comparison of hydrogen peroxide biosensor performance

| Electrode* | System ** | Detection limit / µM | $K_m^{app}$ / mM | Sensitivity / µA mM$^{-1}$ | Linearity / µM | References |
|---|---|---|---|---|---|---|
| HRP/GA/MPE/AuNT/PC | Batch | 4 | 7.60 | 9.50 | 10 - 6000 | Delvaux *et. al.* [105] |
| HRP/AuNP/CPE | Chrono | 0.21 | 3.69 | - | 0.48 - 50 | Liu *et. al.* [217] |
| HRP/AuNP-Cys/AuE | Chrono | 0.58 | 2.30 | - | 1.40 - 2800 | Yi *et. al.* [218] |
| HRP/CMCS/AuNP/GCE | Batch | 0.41 | 0.57 | 0.62 | 5.00 - 1400 | Xu *et. al.* [219] |
| HRP/AuNP-cys/Naf/PtE | Chrono | 0.11 | - | - | 0.35 - 58700 | Liu *et. al.* [220] |
| Hb/Nafion/CNT/GCE | CV | - | 41 | - | 0 - 20000 | Cai *et. al.* [216] |
| HRP/AuNP/SPCE | Batch | 0.40 | 1.30 | 306.70 | 0.80 - 1000 | Xu *et. al.* [214] |
| HRP/sol-gel/CHIT/SPCE | Batch | 3 | - | 14.86 | 250 - 3400 | Miao and Tan [221] |
| HRP/DVB-*co*-AA/AuE | Batch | 0.50 | - | - | 1 - 8000 | Xu *et. al.* [222] |
| HRP/titania sol-gel/GCE | Batch | 1.50 | 1.89 | 61.50 | 80 - 560 | Yu and Ju [223] |
| HRP/$ZrO_2$-g-col/GCE | Batch | 0.25 | 0.28 | 73.72 | 1 - 73 | Zong *et. al.* [224] |
| HRP/THEOS/CHIT/SPCE | Batch | 0.40 | 2.20 | 2.23 | 1 - 250 | Wang and Zhang [225] |
| HRP/AuNP/CHIT/SPCE | Batch | 0.65 | 4.51 | –0.18 | 10 – 11300 | This thesis |

* AuE = Gold electrode, AuNP = Gold nanoparticles, AuNP-Cys = Gold nanoparticle-cystemine, AuNT = Gold nanotube, CHIT = Chitosan, CMCS = Carboxymethyl chitosan, CNT = Carbon nanotube, CPE = Carbon paste electrode, DVB-*co*-AA = Poly(divinylbenzene-*co*-acrylic acid), GA = Glutaraldehyde, GCE = Glassy carbon electrode, HRP = Horseradish peroxidase, MPE = 2-mercaptoethylamine acid, Naf = Nafion, NDE = Needle electrode, PC = Track-etched polycarbonate, THEOS = tetrakis(2-hydroxyethyl) orthosilicates, $ZrO_2$-g-col = $ZrO_2$-grafted collagen

** Batch = Batch amperometry, Chrono = Chronoamperometry, CV = Cyclic voltammetry

### 5.3.6 Reproducibility and stability of the HRP/AuNP/CHIT/SPCE

The reproducibility of this sensor was evaluated with successive additions of 500 μM $H_2O_2$ in a stirred solution. The mean steady-state current of HRP/Au/CHIT/SPCE is 107.3 nA with the relative standard deviation (RSD) of 4.9 % for 30 replications, hence, these electrodes are very reproducible. In stability studies, three types of $H_2O_2$ sensors were examined (figure 5.29).

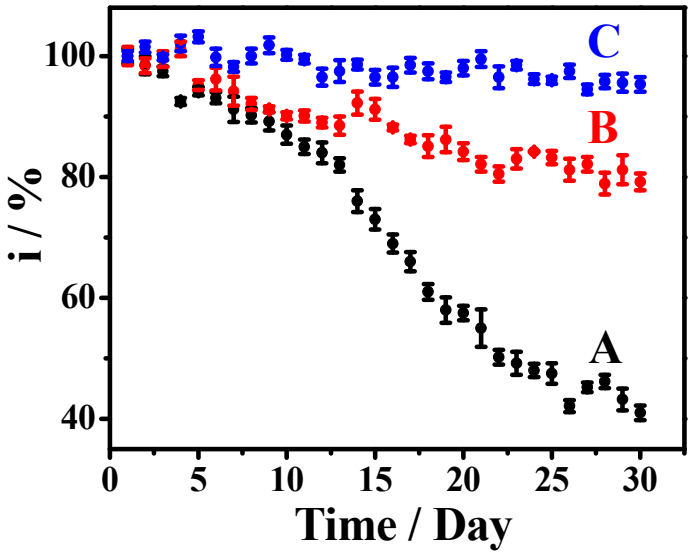


**Figure 5.29** Shelf life stability usage of (A) HRP/SPCE, (B) HRP/CHIT/SPCE, and (C) HRP/AuNP/CHIT/SPCE that was kept in 0.1 M citrate buffer pH 6.5 (at 4 °C) when not in use. The data was normalized with respect to the data on the day 1.

The current response was normalized with respect to the response on day 1. The HRP/SPCE electrode (figure 5.29A) shows the lowest stability: on the 3$^{rd}$ day the response was decreased to 90% of the initial signal with continued attenuation until day 20 when the signal decreased more than 50%. This degradation is due to the inactivation of the enzyme during storage. For the HRP/CHIT/SPCE (figure 5.29B), the electrode stability is better than HRP/SPCE, maintaining over 90 % of its initial signal on day 10 of use and over 80% on day 30. Overall the HRP/AuNP/CHIT/SPCE (figure 5.29C) exhibited the best storage life stability. It maintained its response over 95% up to day 30. This result shows an improvement in

the long-term stability when compared to the previous report on the stability of HRP/Silica sol-gel/CHIT for $H_2O_2$ biosensors, for 85% for 1 month storage [226]. In conclusion, the strong binding of AuNP and HRP prevents the loss of enzyme from the surface and the CHIT hydrogel serves as a biocompatible environment for stabilizing the enzyme activity.

## 5.4 Phosphate biosensor

### 5.4.1 Construction and optimization of the phosphate sensor system

The reduction of $H_2O_2$ generated by the pyruvate oxidase (PyOD) reaction is associated with phosphate ($PO_4^{3-}$) content in the system that contains thiamine pyrophosphate (TPP) and Flavin adenine dinucleotide (FAD) (as coenzymes), pyruvate (as cosubstrate), and magnesium ion ($Mg^{2+}$) (as cofactor). The PyOD catalyzes the oxidative phosphorylation of $PO_4^{3-}$ and pyruvate to acetylphosphate according to the reaction (R5.9) consuming oxygen and generating $H_2O_2$. Sensing response is consequently obtained via the reduction current of generated $H_2O_2$ (recalled R5.8).

$$\text{Pyruvate} + \text{Orthophosphate} + O_2 \xrightarrow[\text{TPP, FAD, } Mg^{2+}]{\text{Pyruvate oxidase}} \text{Acetyl phosphate} + H_2O_2 + CO_2 \quad \text{(R5.9)}$$

$$H_2O_2 + 2H^+ + 2e^- \xrightarrow{\text{Horseradish peroxidase}} 2H_2O \quad \text{(R5.8)}$$

The advantage of the combination activities of two enzymes, the novel $PO_4^{3-}$ biosensor had been attempted with the high sensitivity. The mechanism of PyOD/HRP is adapted from the previous study of Bergmann *et. al.* [227] toward the phosphorylation reaction as shown in figure 5.30.

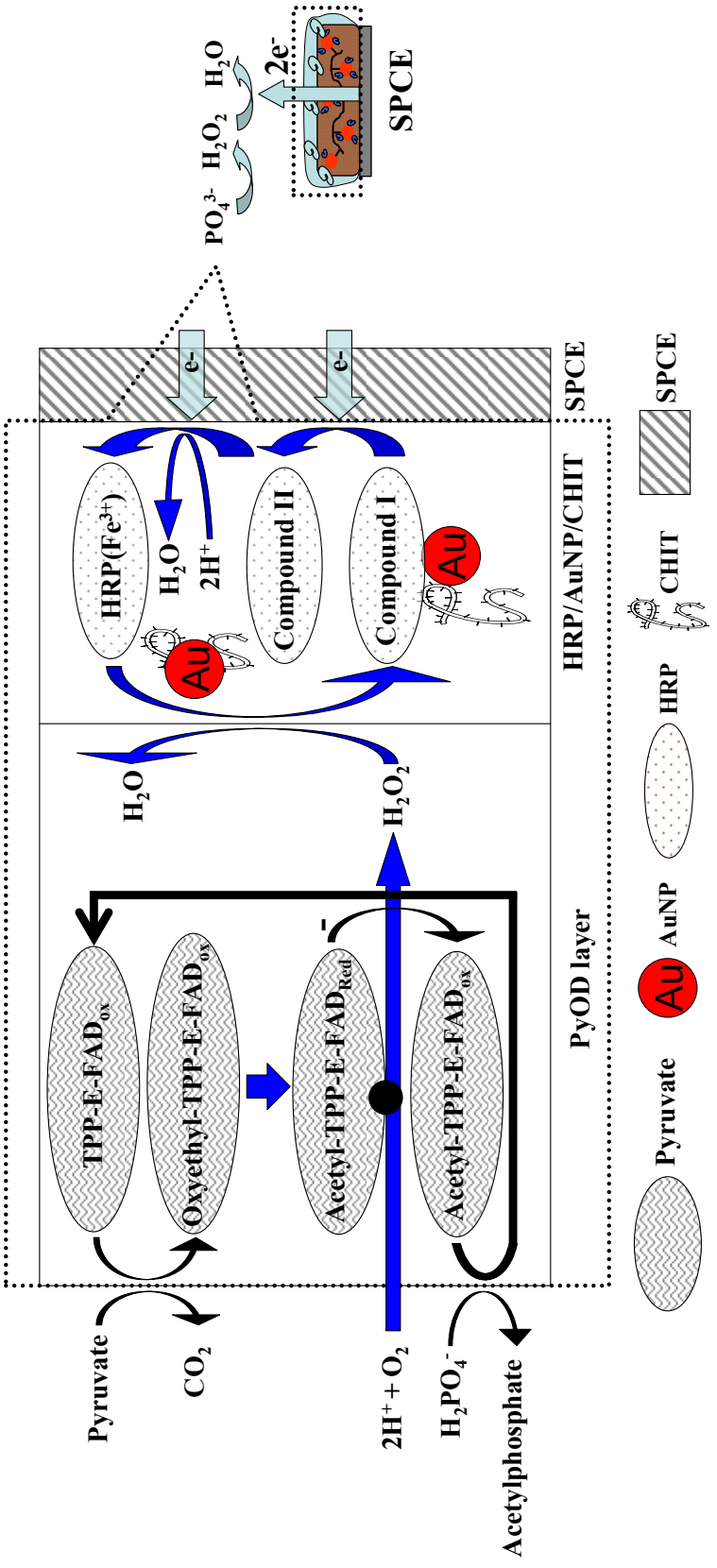


**Figure 5.30** Reaction sequence for an amperometric phosphate biosensor on co-immobilized pyruvate oxidase and horseradish peroxidase in gold nanoparticle-chitosan matrix on screen printed carbon electrode.

The cofactor TPP and FAD binding complex in oxidized form (TPP-E-$FAD_{ox}$) binds with pyruvate and then converted to oxyethyl-TPP-E-$FAD_{ox}$ with a concomitant release of carbon dioxide. An internal transfer of two electrons and two protons converts oxyethyl-TPP-E-$FAD_{ox}$ to acetyl-TPP-E-$FAD_{red}$, which is oxidized by $O_2$ generating $H_2O_2$. The catalytic cycle is closed by the phosphorylation (using of $PO_4^{3-}$) of acetyl-TPP-E-$FAD_{ox}$ regenerating the TPPE-$FAD_{ox}$ and releasing acetylphosphate.

From previous results on $H_2O_2$ biosensor (section 5.3), the optimum conditions of $H_2O_2$ biosensor were applied to the new design biosensor. The starting condition for $PO_4^{3-}$ biosensor was adapted from Kwan *et. al.* [168] which was 3 mM $MgCl_2$, 70 µM TPP, 10 µM FAD, 10 mM HEPES, and 1 mM pyruvate.

#### 5.4.1.1 Optimal amount of pyruvate oxidase

Since the PyOD is crucial on $H_2O_2$ generation, therefore the amount of PyOD had been optimized for the best signal w.r.t. $H_2O_2$ with related to amount of $PO_4^{3-}$. An aliquot of $PO_4^{3-}$ solution was injected to a stirred solution. Figure 5.31 shows effect of amount of enzyme PyOD loaded on PyOD/HRP/AuNP/CHIT/SPCE. The current signal from $H_2O_2$ generated enzyme reaction is steeply increasing from 0.1 Unit until 0.5 Unit, and then reaches a maximum at 0.7 Unit (or around 0.6 Unit on curve). At 0.9 Unit PyOD loaded, the signal is decreased. This result is agreed with Kwan *et. al.* [168, 228] that the high enzyme loaded is a high diffusion barrier may reduce the signal response. The PyOD amount is selected at 0.7 Unit for optimum amount of PyOD.

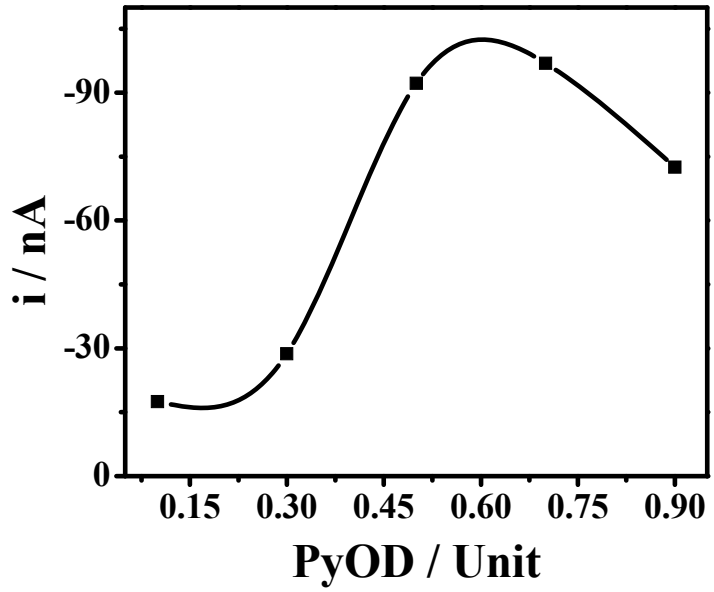


**Figure 5.31** Effect of pyruvate oxidase (PyOD) loaded on the $H_2O_2$ signal, for addition of 500 μM phosphate in a stirred solution to 0.1 M citrate buffer pH 6.5 containing 3 mM $MgCl_2$, 70 μM TPP, 10 μM FAD, 10 mM HEPES, and 1 mM pyruvate (cf. Kwan *et. al* [168]).

### 5.4.1.2 Optimal amount of cosubstrate pyruvate

The pyruvate is a cosubstrate in the PyOD enzymatic reaction. Figure 5.32 shows the pyruvate content effect on the generated current signal in the range of 0.5 - 2.5 mM, interval of 0.5 mM. The increase of pyruvate concentrations from 0.5 mM - 2.0 mM results in increase in signal. The pyruvate concentration at 2.5 mM shows the saturation of the response current. At this pyruvate concentration may be due to a limit concentration of oxygen as it is required for the reaction (R5.3). Gavalas *et. al.* [165] reported the amperometric response of the pyruvate sensor was also limited at 2.5 mM. The concentration of 2.0 mM pyruvate was therefore selected as the optimum concentration.

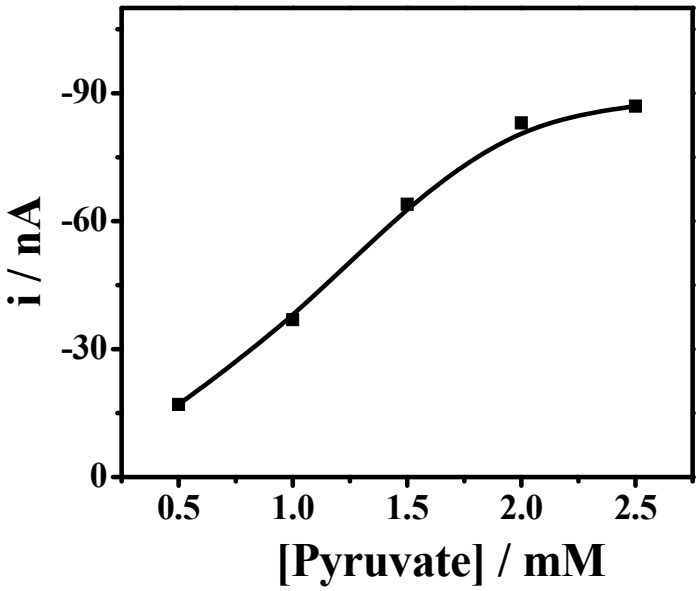


**Figure 5.32** Effect of pyruvate addition on the reductive current obtained for PyOD/HRP/AuNP/CHIT/SPCE in a stirred solution of 0.1 M citrate buffer pH 6.5 containing of 500 µM phosphate, 3 mM $MgCl_2$, 70 µM TPP, 10 µM FAD and 10 mM HEPES. 0.5 Unit Pyruvate oxidase is loaded on PyOD/HRP/AuNP/CHIT/SPCE.

#### 5.4.1.3 Optimal amount of coenzyme flavin adenine dinucleotide

Coenzyme flavin adenine dinucleotide (FAD) was optimized on the current generated for 500 µM $PO_4^{3-}$ addition. In figure 5.33, the response from $PO_4^{3-}$ biosensor increases with the FAD concentration from 1 to 10 µM, after then that reaches to saturation region at 15 µM. The decreased response of FAD at 15-20 µM may be related to the saturation of the active site of PyOD because it binds FAD as prosthetic groups [169]. The optimum FAD concentration was choosen at 10 µM.

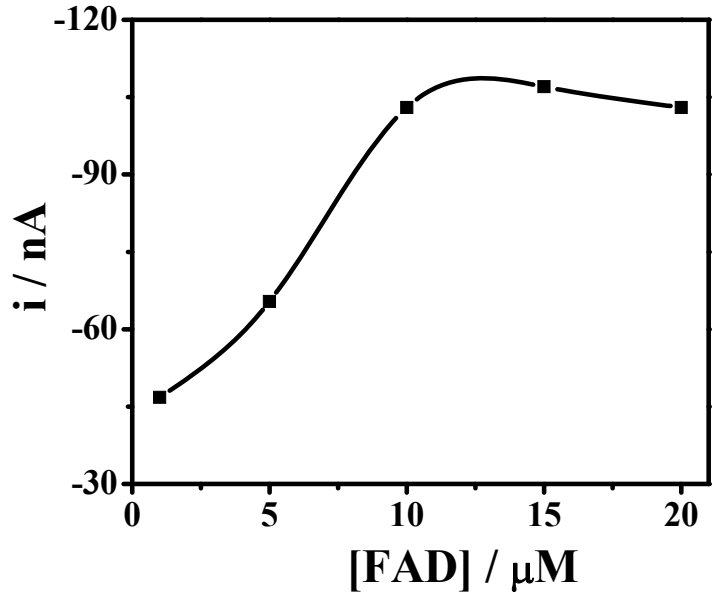


**Figure 5.33** Effect of coenzyme FAD addition on the reductive current obtained for PyOD/HRP/AuNP/CHIT/SPCE in a stirred solution of 0.1 M citrate buffer pH 6.5 containing of 500 μM phosphate, 3 mM $MgCl_2$, 70 μM TPP, 1 mM pyruvate and 10 mM HEPES. 0.5 Unit Pyruvate oxidase is loaded on PyOD/HRP/AuNP/CHIT/SPCE.

### 5.4.1.4 Optimal amount of coenzyme thiamine pyrophosphate

The coenzyme thiamine pyrophosphate (TPP) was optimized from 30 - 110 μM which current generated for 500 μM $PO_4^{3-}$ addition. Figure 5.34 shows the current vs. the coenzyme TPP concentration. The current increases form 30 μM TPP to the maximum at 70 μM, and then decreases at 90 - 110 μM TPP. This means that in this condition range (90 - 110 μM TPP), the $PO_4^{3-}$ biosensor could not show a linear response to increased TPP concentration. Like coenzyme FAD, the PyOD binds TPP at a prosthetic group. The TPP at 70 μM was selected as the optimal concentration.

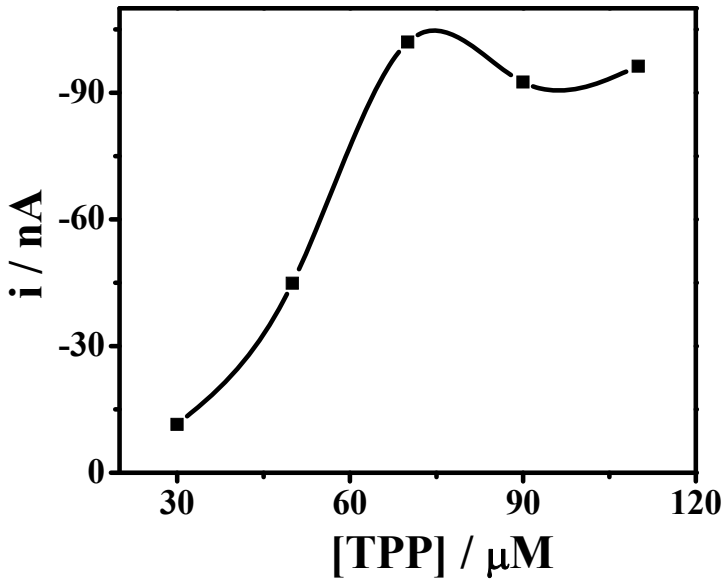


**Figure 5.34** Effect of coenzyme TPP addition on the reductive current obtained for PyOD/HRP/AuNP/CHIT/SPCE in a stirred solution of 0.1 M citrate buffer pH 6.5 containing of 500 μM phosphate, 3 mM $MgCl_2$, 10 μM FAD, 1 mM pyruvate and 10 mM HEPES. 0.5 Unit Pyruvate oxidase is loaded on PyOD/HRP/AuNP/CHIT/SPCE.

### 5.4.1.5 Effect of cofactor substances

Cofactors are an important parameter on the PyOD/HRP/AuNP/CHIT/SPCE biosensor. Ionic salts such as $CaCl_2$, KCl, NaCl, and $MgCl_2$ had tested with amperometrically. Table 5.7 show the current generated when addition of the selected cofactor into the citrate buffer solution containing of 500 μM $PO_4^{3-}$, 0.1 M citrate buffer pH 6.5 containing 2 mM pyruvate, 15 μM FAD, 70 μM TPP, and 10 mM HEPES.

All of salts ($CaCl_2$, KCl, and NaCl and $MgCl_2$) show effect on the amperometric response of the $PO_4^{3-}$ biosensor. These salts possibly act as cofactor for $PO_4^{3-}$ biosensor as equation (R5.9). However, the $MgCl_2$ is showed the highest response to the PyOD system for $PO_4^{3-}$ biosensor. It is selected for cofactor and spiked as 3 mM for saturated concentration.

**Table 5.7** Cofactors effect of some salts on the amperometric response of phosphate biosensor

| Cofactors* | Current without cofactor** ($i_{wo}$) / nA | Current with cofactor ($i_w$) / nA | Net currents ($i_w$ - $i_{wo}$) / nA | % effect of cofactor $(\frac{(i_w - i_{wo})}{i_{wo}} \times 100)$ |
|---|---|---|---|---|
| NaCl | –8.9 | –16.5 | –7.6 | 85.4 |
| KCl | –8.2 | –18.0 | –9.8 | 119.5 |
| $CaCl_2$ | –15.5 | –38.9 | –23.4 | 150.9 |
| $MgCl_2$ | –17.3 | –51.0 | –33.7 | 194.2 |
| mean | -12.5 (±4.6) | - | - | - |

* Spiking concentration was 1 mM.

** Electrolyte without cofactor was 0.1 M citrate buffer pH 6.5 containing 500 µM phosphate, 2 mM pyruvate, 15 µM FAD, 70 µM TPP, and 10 mM HEPES.

### 5.4.2 Phosphate biosensor performance

The $PO_4^{3-}$ biosensor was prepared by the optimal condition as; PyOD loaded, 0.7 Unit and operation in 2 mM pyruvate, 15 µM FAD, 70 µM TPP, 3 mM $MgCl_2$, 10 mM HEPES in a batch amperometric condition. Figure 5.35 shows successive addition of $PO_4^{3-}$ concentration. The shape of this amperometric response immediately increases at a point of $PO_4^{3-}$ addition and then decreases with a time. This phenomenon is likely the previous report by Rahman *et. al.* [169], but it was not clear why the current increased abruptly with every addition. This characteristic is less effective at higher $PO_4^{3-}$ concentration at 50 µM. This may be due to higher $PO_4^{3-}$ concentration produced more $H_2O_2$ and it's effectively converted to $H_2O$ by the HRP.

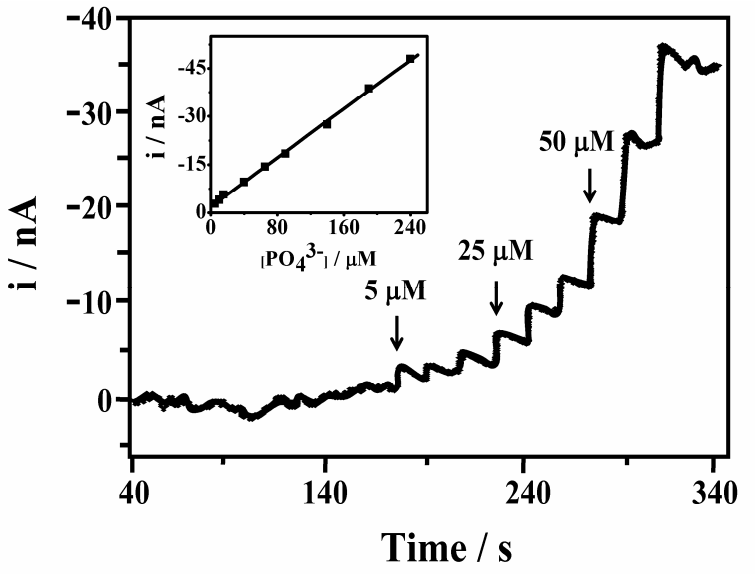


**Figure 5.35** Amperometric response at PyOD/HRP/AuNP/CHIT/SPCE ($E_{applied}$ = -0.4 V) for the successive addition of different concentrations of phosphate in a stirred solution of 0.1 M citrate buffer pH 6.5 containing 2 mM pyruvate, 15 μM FAD, 70 μM TPP, 3 mM $MgCl_2$, and 10 mM HEPES. Inset shows calibration plot for the corresponding phosphate addition.

Inset of figure 5.35 shows the corresponding plot of $PO_4^{3-}$ additions with a correlation of y = –190x – 1.965 and $R^2$ = 0.9984 (where x and y are in mM and nanoampere, respectively). The linearity of this sensor was 5 - 240 μM $PO_4^{3-}$, and the sensor reproducibility based on the response to 25 μM $PO_4^{3-}$ is 3.67% RSD. The detection limit of this sensor is 1.90 μM with signal to noise ratio of three. Comparison the detection limit and linearity to Kwan *et. al.* [168] (3.6 μM for detection limit and 7.6-625 μM for linearity), Rahman *et. al.* [169] (0.32 μM for detection limit and 1.0-100 μM for linearity), it is acceptable because there are the same order of the detection limit and linearity. Table 5.8 is comparison of this biosensor with the other $PO_4^{3-}$ biosensors development.

**Table 5.8** Comparison of the phosphate biosensors performance

| Electrode* | System** | Sesitivity / nA $mM^{-1}$ | Linearity / µM | Detection limit / µM | References |
|---|---|---|---|---|---|
| PCS/ PyOD-nafion/SPCE | SBR | -524 | 7.5 - 625 | 3.6 | Kwan *et. al.* [168] |
| PCS/ PyOD-PEI/SPCE | SBR | -213 | 20 - 500 | 5.0 | Mak *et. al.* [166] |
| PyOD/TTCA/GCE | Batch | -590 | 1.0 - 100 | 0.3 | Rahman *et. al.* [169] |
| PyOD/deae-dextran/PCE | FIA | $-10 \times 10^3$ | 50 - 1250 | 4.8 | Gavalas *et. al.* [165] |
| PyOD-gelatin/Teflon/$O_2$ electrode | Batch | - | 1 - 10 | - | Akvilmaz *et. al.* [229] |
| PyOD/HRP/AuNP/CHIT/SPCE | Batch | -190 | 5 - 240 | 1.9 | This thesis |

* AuNP = Gold nanoparticle, CHIT = Chitosan, deae-dextran = Diethylaminoethyl-dextran, GCE = Glassy carbon electrode, HRP = Horseradish peroxidase, PCE = Porous carbon electrode, PCS = Poly (carbamoyl) sulfonate, PEI = Polyethyleneimine, PyOD = Pyruvate oxidase, SPCE = Screen printed carbon electrode, and TTCA = Poly-5,2':5',2''-terthiophene-3'-carboxylic acid

** Batch or FIA or SBR = Batch or Flow injection analysis or Sequencing batch reactor - amperometric detector

### 5.4.3 Interference studies

The PyOD/HRP/AuNP/CHIT/SPCE biosensor had been tested amperometrically with some interference salts such as $K_2SO_4$, and $NaNO_3$. These salts present in real samples. Table 5.9 shows the current generated when addition of a selected interference in to the citrate buffer solution.

The results showed that $K_2SO_4$ and $NaNO_3$ were less of current generated. This means, they not interfere the $PO_4^{3-}$ biosensor. This result is agreed with Rahman *et. al.* [169] that anions such as $SO_4^{2-}$, $NO_3^-$, and $ClO_4^-$ did not interfere the PyOD system for $PO_4^{3-}$ biosensor.

**Table 5.9** Interference effect of some salts on the amperometric response of phosphate biosensor

| Interference* | Current without interference** ($i_{wo}$) / nA | Current with interference ($i_w$) / nA | Currents ($i_w$ - $i_{wo}$) / nA | % Interference $(\frac{(i_w - i_{wo})}{i_{wo}} \times 100)$ |
|---|---|---|---|---|
| $K_2SO_4$ | –10.6 | –10.6 | 0 | 0 |
| $NaNO_3$ | –9.3 | –9.4 | -1 | 1.1 |
| mean | -9.9 (±0.9) | - | - | - |

* Spiking concentration was 1 mM.

** Electrolyte without cofactor was 0.1 M citrate buffer pH 6.5 containing 500 µM $PO_4^{3-}$, 2 mM pyruvate, 15 µM FAD, 70 µM TPP, and 10 mM HEPES.

### 5.4.4 Phosphate biosensor validation

The $PO_4^{3-}$ biosensors, PyOD/HRP/AuNP/CHIT/SPCE, was validated with molybdenum blue technique. 25 µM $PO_4^{3-}$ was tested by this $PO_4^{3-}$ biosensor and UV-Vis standard methods for comparison their mean values obtained [230]. T-test is a statistical method uses for test two mean values while F-test is a statistical method for test for different of two variances. The equation for t-test and F-test is shown in Appendix B.3 and B.4, respectively. The statistical t-test and F-test of $PO_4^{3-}$ determination between the new $PO_4^{3-}$ biosensor (mean = 24.8 (±0.67) µM) and the conventional UV-Vis (mean = 25.0 (±0.36) µM) technique are in table 5.10.

**Table 5.10** Statistical t-test and F-test between phosphate biosensor and UV-Vis spectrophotometric technique

| Techniques/Statistical tests | Values |
|---|---|
| Biosensor* | 24.8 (±0.67) μM |
| UV-Vis* | 25.0 (±0.36) μM |
| **t-test (P = 0.05)** | $t_{cal}$ = 1.21 |
| | $t_{12}$ = 2.18 |
| **F-test (P = 0.05)** | $F_{cal}$ = 3.72 |
| | $F_{6,6}$ = 5.82 |

* n = 7, $t_{cal}$ = calculated t-test, $t_{12}$ = t-test value from table at degree of freedom 12. $F_{cal}$ = calculated F-test, $F_{6,6}$ = F-test value from table at degree of freedom 6 for both numerator and denominator.

The calculated t-test ($t_{cal}$ = 1.21) is smaller than table t-test ($t_{12}$ = 2.18) at P = 0.05. There is no significant difference between mean values of these two methods at the 95% confidence level. The new $PO_4^{3-}$ biosensor is accuracy as the UV-Vis spectrophotometry. For F-test, the calculated F-test ($F_{cal}$ = 3.72) is smaller than table F-test ($F_{6,6}$ = 5.82) at P = 0.05. Also, there is no significant different between these two variances at the 95% confidence level. The determination for $PO_4^{3-}$ is used by the new $PO_4^{3-}$ biosensor is precision as the UV-Vis spectrophotometry.

### 5.4.5 Phosphate examination with real samples

The PyOD/HRP/AuNP/CHIT/SPCE biosensor was tested the real samples for $PO_4^{3-}$ determination in the real samples from Klong Rangsit (K1-K7). This amperometric biosensor was applied by addition a real sample into the citrate buffer solution. The operation potential was done at –0.4 V in steady state current response mode. The external standard calibration method was used to determine the $PO_4^{3-}$ content in real samples. Figure 5.36 shows a correlation of $PO_4^{3-}$ content that

obtained from the UV-Vis spectrophotometry (molybdenum blue) method vs. the PyOD/HRP/AuNP/CHIT/SPCE biosensor (please see appendix A.4 for values). The regression equation of the correlation curve of these methods is y = 0.873x + 0.8407 with r = 0.9888. The PyOD/HRP/AuNP/CHIT/SPCE sensor described the accuracy for real sample.

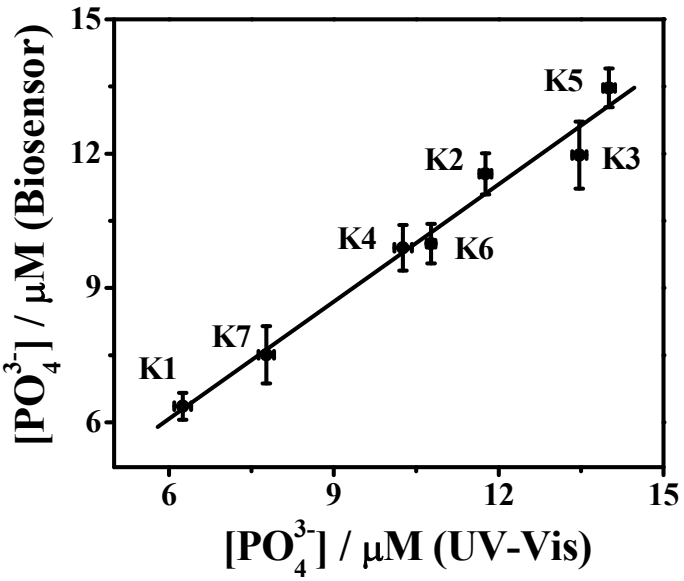


**Figure 5.36** Correlation plot for phosphate concentration in the real samples, obtained by biosensor and UV-Vis spectrophotometric technique from Klong Rangsit (K1-K7), n = 3.

# CHAPTER VI
# CONCLUSIONS

Four important design concepts of novel sensors for monitoring (i) electroactive species as insulin, (ii) electroinactive species as glycosidases by direct conversion to electroactive species as *p*-nitrophenol (PNP), (iii) electroactive spcecies as hydrogen peroxide ($H_2O_2$), and (iv) electroinactive species as phosphate ($PO_4^{3-}$) by assisting of the enzymatic reaction to generate a common electroactive species as $H_2O_2$ were demonstrated. The conclusions on the conceptual ideas of each sensor and future works are summarized in the following topics.

## 6.1 Insulin chemical sensor

An electroactive species as insulin was developed with the conceptual model of an electrochemical direct measurement on ruthenium oxide ($RuO_x$) onto a carbon nanotube (CNT), $RuO_x$/CNT, bilayer coated glassy carbon electrode (GCE) as shown in figure 6.1.

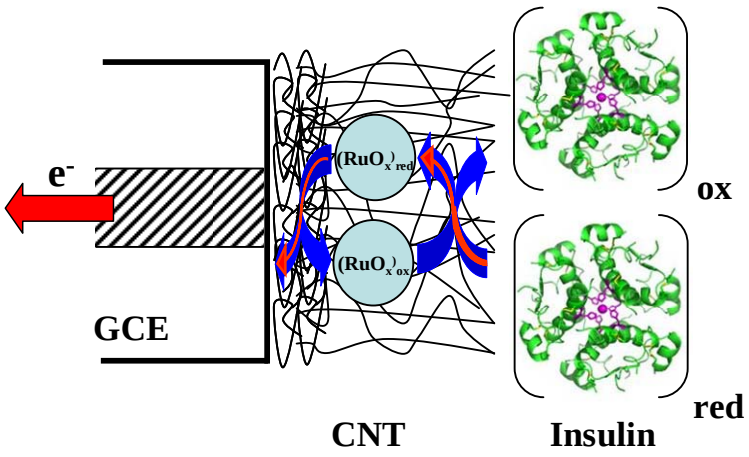


**Figure 6.1** A conceptual model for direct measurement of insulin on $RuO_x$/CNT bilayer coated GCE.

A bilayer surface coating, prepared by electrodepositing $RuO_x$ onto a CNT layer, offers dramatic improvements in the stability and sensitivity of voltammetric and amperometric measurements of insulin compared to the individual (CNT or $RuO_x$) coated electrodes. The enhanced electrocatalytic activity towards insulin is indicated from lowering the potential of the oxidation process (starting around 0.35 V versus Ag/AgCl) and the substantially higher sensitivity over the entire potential range. A wide linear dynamic range (10 - 800 nM) was achieved with a detection limit of 1 nM. The marked electrocatalytic activity of the $RuO_x$/CNT bilayer coating towards insulin is coupled with a greatly enhanced stability. For example, the insulin amperometric response of the $RuO_x$/CNT bilayer coated electrodes is highly stable, with 97% of the initial activity remaining after 60 min stirring of 2 μM solution (compared to significantly faster current diminutions at the $RuO_x$ or CNT coated surfaces). The results suggest great promise for miniaturized sensors and detectors for monitoring insulin.

In summary, the $RuO_x$/CNT bilayer modified electrodes exhibit greater electrochemical activity towards the oxidation of insulin compared to its $RuO_x$ and CNT counterparts. The observed improvements are attributed to synergistic enhancement rather than the combination of the two individual layers. The output of this topic was published in Analytica Chimica Acta [189]. The microscale-electrodes involve the modification of carbon-fiber ultramicroelectrodes with the $RuO_x$/CNT bilayer and understanding the unique behavior of $RuO_x$/CNT bilayer modified electrodes towards insulin are considered in the future work. The application of $RuO_x$/CNT bilayer modified microsensor for chromatographic detector for insulin is also interesting.

## 6.2 Glycosidases sensor

A conceptual model of the development of electroinactive species as glycosidases enzyme which associated with the oxidation current of converted *p*-nitrophenol (PNP) is shown in figure 6.2.

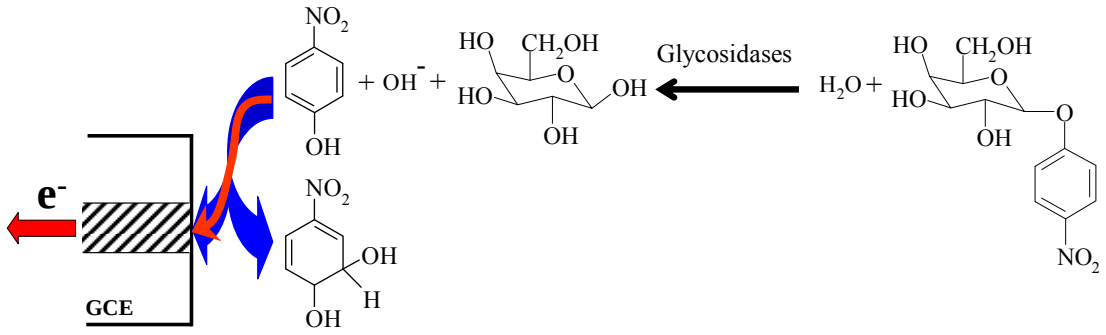


**Figure 6.2** A conceptual model for indirect measurement of glycosidases enzyme at bare GCE.

The oxidation of PNP was electrochemical examined on screen printed carbon electrode (SPCE) with loading the platinum nanoparticles (PtNP) in the SPCE ink. The PtNP loaded in SPCE provided the greater sensitivity of the PNP oxidation than unloaded PtNP SPCE. It was due to the catalytic properties of PtNP. However, the stability of PtNP loaded SPCE is poorer than bare GCE because of its occurred the PNP passivation film on electrode surface after 1-2 repetitive scanning. The GCE was selected thoroughly the experiments.

The fast and sensitive glycosidases sensor was successfully achieved at GCE at amperometry mode with $E_{applied}$ = +1.15 V in a stirred 1.5 mL 0.05 M citrate buffer solution (pH 4.4). Two species of enzymes were monitored; (i) β-1,3-galactosidase at GCE in a 1.5 mL of 133 µM of 4-NP-β-Gal, and (ii) endo-α-N-acetylgalactosaminidase in a 1.5 mL of 200 µM of 4-NP-α-GalNAc-Gal. The sensitivity of endo-α-N-acetylgalactosaminidase that facilitates convenient measurements of mUnit levels (vs. Unit ones for the β-1,3-galactosidase). A detection limit of 200 µUnit can thus be estimated in connection to short reaction

times of 20-60 sec. The detection limit was obtained at 49 fmol in 1.5 mL. In contrast, in the standard optical assay the detection of 400 μUnit endo-α-N-acetylgalactosaminidase required significantly longer of an incubation time at 600 sec than the electrochemical sensor which can be obtained at 60 sec. Further, the optical assay measures only endpoint results and does not provide real-time measurements. The output of this topic was published in The Analyst [231]. The developing reagentless glycosidases enzyme based on a surface confined substrate and different disposable electrode materials for routine point-of-care clinical applications is considered in the future work.

## 6.3 Hydrogen peroxide biosensor

A conceptual model of electroactive spcecies as the hydrogen peroxide ($H_2O_2$) biosensor on the screen printed carbon electrode (SPCE) is demonstrated as shown in figure 6.3. The signal is obtained via the reduction of $H_2O_2$ by registered horseradish peroxidase (HRP) in the matrix of gold nanoparticle (AuNP)/chitosan (CHIT).

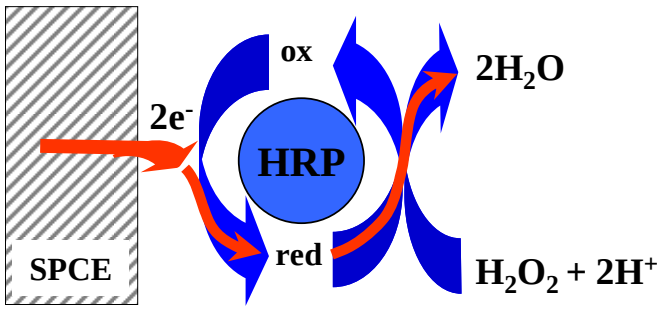


**Figure 6.3** A conceptual model for direct measurement of electroactive species as $H_2O_2$ at HRP/AuNP/CHIT/SPCE biosensor.

The SPCE fabrication method on a polyvinyl chloride substrate as a disposable sensor is described. Six configurations were designed on silk screen frames. The SPCEs were printed with four inks: silver ink as the conducting track, carbon ink as the working and counter electrodes, silver/silver chloride ink as the reference electrode and insulating ink as the insulator layer. The advantage of determining the best SPCE configuration makes it advanced in analytical

performance. Selection of the best configuration was done by comparing slopes from the calibration plots generated by the cyclic voltammograms at 10, 20 and 30 mM $K_3Fe(CN)_6$ for each configuration. The electrodes with similar configurations gave similar slopes. The 5$^{th}$ configuration was the best electrode that gave the highest slope.

Modifying the best SPCE configuration for use as a biosensor, horseradish peroxidase (HRP) was selected as a biomaterial bound with gold nanoparticles (AuNP) in the matrix of chitosan (HRP/AuNP/CHIT). Biosensors of HRP/SPCE, HRP/CHIT/SPCE and HRP/AuNP/CHIT/SPCE were used in the amperometric detection of $H_2O_2$ in a solution of 0.1 M citrate buffer, pH 6.5, by applying a potential of −0.4V at the working electrode. All the biosensors showed an immediate response to $H_2O_2$. The effect of HRP/AuNP incorporated with CHIT (HRP/AuNP/CHIT/SPCE) yielded the highest performance. The amperometric response of HRP/AuNP/CHIT/SPCE retained over 95% of the initial current of the 1$^{st}$ day up to 30 days of storage at 4 °C. The incorporation of the HRP with AuNP in the matrix of CHIT on the SPCE surface is for direct electron transfer of $H_2O_2$. The biosensor showed a linear range of 0.01-11.3 mM $H_2O_2$, with sensitivity and detection limit of −176 nA $mM^{-1}$ and 0.65 μM $H_2O_2$ (S/N = 3), respectively. The ease of the one-step immobilization creates a very reproducible and stable sensor for long term storage, which has proven difficult for other $H_2O_2$-based biosensors. It is inferred that this AuNP/CHIT material can provide a suitable microenvironment for HRP immobilization. The success of this work is published in Biosensors and Bioelectronics [232]. The low detection limit, long storage life and wide linear range of this biosensor are considerable applied for $H_2O_2$ sensor in the bioreactors and biosensors in future.

## 6.4 Phosphate biosensor

A novel conceptual model of electroinactive species as phosphate ($PO_4^{3-}$) is demonstrated by assisting of an enzymatic reaction to generate a common electroactive species as shown in figure 6.4. The pyruvate oxidase catalyzes the $PO_4^{3-}$ and pyruvate to acetylphosphate which consume oxygen and generate $H_2O_2$ and $CO_2$. The later step is followed by the reduction of $H_2O_2$ which the generated current associate with $PO_4^{3-}$ content in the sample.

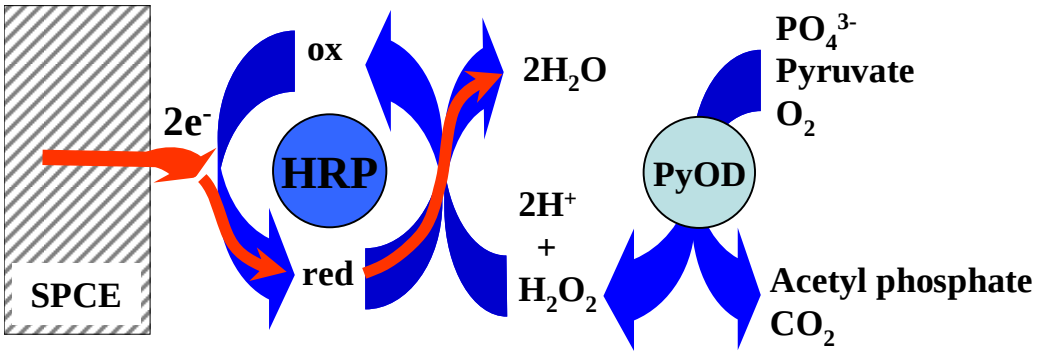


**Figure 6.4** A conceptual model for indirect measurement of electroinactive species as $PO_4^{3-}$ at PyOD/HRP/AuNP/CHIT/SPCE biosensor.

The deposition of pyruvate oxidase (PyOD) on HRP/AuNP/CHIT/SPCE was described for $PO_4^{3-}$ biosensor. The sensor was optimized the elements and amounts that effect on $H_2O_2$ generation. There were pyruvate oxidase, pyruvate, cofactor substances, coenzyme flavin adenine dinucleotide (FAD) and coenzyme thiamine pyrophosphate (TPP). It was found that the optimal condition for $PO_4^{3-}$ biosensor as; PyOD loaded, 0.7 Unit, 2 mM pyruvate, 15 µM FAD, 70 µM TPP and cofactor is $MgCl_2$. The current generated on an amperometric response is immediately increased at a point of $PO_4^{3-}$ addition and then decreased with a time. It was not clear why the current increased abruptly with every addition. This characteristic is less effective at higher $PO_4^{3-}$ concentration at 50 µM. This may be due to higher $PO_4^{3-}$ concentration produced more $H_2O_2$ and it's effectively converted to $H_2O$ by the HRP.

The $PO_4^{3-}$ biosensor had a sensitivity of −190 nA $mM^{-1}$. The linearity of this sensor was 5 - 240 µM $PO_4^{3-}$, and the sensor reproducibility based on the response to 25 µM $PO_4^{3-}$ was 3.67% RSD. The detection limit of this sensor was 1.90 µM with signal to noise ratio of three. The sensor was not interfered by $K_2SO_4$ and $NaNO_3$. The validation of this sensor is not significantly different from the standard method, the UV-Vis spectrophotometry, at the 95% confidence. Also, this PyOD/HRP/AuNP/CHIT/SPCE was determined for $PO_4^{3-}$ content in natural water samples from Klong Rangsit. It showed the accuracy for $PO_4^{3-}$ determination in real samples. The excellent potentials of this biosensor are considered the development in the future for long life, and on-field $PO_4^{3-}$ studies. A hand-held potentiostat is much required to develop for $PO_4^{3-}$ detection in the environmental field. In addition, the application of this sensor for medical application as pyruvate sensor is also considered in the future.

# REFERENCES

1. Clark LC, Jr., Lyons C. Electrode systems for continuous monitoring in cardiovascular surgery. Ann. N. Y. Acad. Sci. 1962; 102 (1): 29-45.
2. Scheller F, Schubert F. Biosensors. Amsterdam: Elsevier; 1992. p. 7-84.
3. Stradiotto NR, Yamanaka H, Zanoni MVB. Electrochemical sensors: A powerful tool in analytical chemistry. J. Braz. Chem. Soc. 2003; 14 (2): 159-73.
4. Bagotsky VS. Fundamentals of electrochemistry. Hoboken (NJ): John Wiley & Sons, Inc.; 2006. p. 573-593.
5. Willner I, Katz E. Bioelectronics. Strauss GmbH, Morlenbach: WILEY-VCH Verlag GmbH & Co. KGaA Weinheim; 2005. p. 99-126.
6. Velasco-Garcia MN, Mottram T. Biosensor technology addressing agricultural problems. Biosyst. Eng. 2003; 84 (1): 1-12.
7. Eggins BR. Chemical sensors and biosensors. West Sussex: John Wiley & Sons; 2002. p. 1-40.
8. Konrad D, Rudich A, Klip A. Insulin-mediated regulation of glucose metabolism. In: Kumar S, O'Rahilly S, editors. Insulin resistance: Insulin action and its disturbances in disease. Chichester: John Wiley & Sons Ltd.; 2005. p. 63-85.
9. Wikipedia. Insulin. [Access: 2007, Nov 2]; Available from: http://en.wikipedia.org/wiki/Insulin
10. Zhang M, Mullens C, Gorski W. Insulin oxidation and determination at carbon electrodes. Anal. Chem. 2005; 77 (19): 6396-401.
11. Attie AD. Lipoprotein/Cholesterol metabolism. In: Meyers RA, editors. Encyclopedia of physical science and technology : Biochemistry. 3rd ed. Tarzana (CA): Academic Press; 2001. p. 658-660.
12. Arneson W, Brickell J. Clinical chemistry : A laboratory perspective. Philadelphia (PA): F. A. Davis Company; 2007. p. 147-178.

13. Smith C, Marks AD, Lieberman M. Marks' basic medical chemistry : A clinical approach. 2nd ed. Philadelphia (PA): Lippincott Williams & Wilkins; 2004. p. 493-510.
14. Jones CW. Applications of hydrogen peroxide and derivatives. Cambridge: The Royal Society of Chemistry; 1999. p. 1-35.
15. Manahan SE. Environmental chemistry. 7th ed. Boca Raton: CRC Press LLC; 2000. p. Ch. 3.
16. Kulaev IS, Vagabov VM, Kulakovskaya TV. The biochemistry of inorganic polyphosphates. 2nd ed. West Sussex: John Wiley & Sons; 2004. p. 16-35.
17. Mueller DK, Helsel DR. Nutrients in the Nation's waters; too much of a good thing? Denver (CO): U.S. Geological Survey; 1996. Report No.: (200) Ci No.1136.
18. Sawyer DT. Electrochemistry. In: Meyers RA, editors. Encyclopedia of physical science and technology : Analytical chemistry. 3rd ed. Tarzana (CA): Academic Press; 2001. p. 161-197.
19. Sawyer DT, Sobkowiak A, Roberts JJL. Electrochemistry for chemists. New York (NY): John Wiley & Sons; 1995. p. 1-52.
20. IUPAC. Classification and nomenclature of electroanalytical techniques. Pure Appl. Chem. 1976; 45 (2): 81-97.
21. Fogg AG, Wang J. Terminology and convention for electrochemical stripping analysis. Pure Appl. Chem. 1999; 71 (5): 891-7.
22. Gosser D, K. Jr. Cyclic voltammetry : Simulation and analysis of reaction mechanisms. New York (NY): VCH Publishers; 1993. p. 28-69.
23. Osteryoung RA, Osteryoung J. Pulse voltammetric methods of analysis. Philos. Trans. R. Soc. London, A. 1981; 302 (1468): 315-26.
24. Kounaves SP, O'Dea JJ, Chandresekhar P, Osteryoung J. Square wave voltammetry at the mercury film electrode: Theoretical treatment. Anal. Chem. (Wash.). 1986; 58 (14): 3199-202.
25. Osteryoung J. Voltammetry for the future. Acc. Chem. Res. 1993; 26 (3): 77-83.
26. Kounaves SP, O'Dea JJ, Chandresekhar P, Osteryoung J. Square wave anodic stripping voltammetry at the mercury film electrode: theoretical treatment. Anal. Chem. 1987; 59 (3): 386-9.

27. Bard AJ, Faulkner LR. Electrochemical methods : Fundamentals and applications. 2nd ed. New York (NY): John Wiley & Sons; 2001. p. 293-299.
28. Wang J. Analytical electrochemistry. 3rd ed. Hoboken (NJ): John Wiley & Sons; 2006. p. 80-82.
29. Monk PMS. Fundamentals of electroanalytical chemistry. Chichester: John Wiley & Sons; 2001. p. 182-185.
30. Settle F. Handbook of instrumental techniques for analytical chemistry. Upper Saddle River (NJ): Prentice Hall PTR; 1997. p. 693-707.
31. Lacourse WR. Pulsed electrochemical detection in high-performance liquid chromatography. New York (NY): John Wiley & Sons, Inc.; 1997. p. 60-61.
32. Fifield FW, Kealey D. Principles and practice of analytical chemistry. 5th ed. London: Blackwell Science Ltd.; 2000. p. 228-266.
33. Harvey D. Modern analytical chemistry. Boston (BA): McGraw-Hill; 2000. p. 461-540.
34. Patnaik P. Dean's analytical chemistry handbook. 2nd ed. ed. Boston (BA): McGraw-Hill Inc.; 2004. p. 14.1-14.135.
35. Kissinger PT, Heineman WR. Laboratory techniques in electroanalytical chemistry. 2nd ed. New York (NY): Marcel Dekker, Inc.; 1996. p. 172-177.
36. Rieger PH. Electrochemistry. 2nd ed. New York (NY): Chapman & Hall; 1994. p. 165-168.
37. Cass AEG. Biosensors : A practical approach. Oxford: Oxford University Press; 1990. p. 55-58.
38. Skoog DA, Leary JJ. Principles of insturmental analysis. 4th ed. Fort Worth (TX): Saunders College Publishing; 1992. p. 535-567.
39. Barisci JN, Riley PJ, Wallace GG. Instrumentation. In: Smyth MR, Vos JG, editors. Analytical voltammetry. Vol.27. Amsterdam: Elsevier Science Publishers B.V.; 1992. p. 71-109.
40. Chen S. Practical electrochemical cells. In: Zoski CG, editors. Handbook of electrochemistry. Amsterdam: Elsevier B.V.; 2007. p. 31-55.
41. Skoog DA, West DM, Holler FJ, Crouch SR. Fundamentals of analytical chemistry. 8th ed. ed. Belmont (CA): Brooks/Cole-Thomson Learning; 2004. p. 187-191.

42. Nernst W. Principles. In: Ruzicka J, Hansen EH, editors. Flow injection analysis. 2nd ed. Vol.65. Chichester: John Wiley & Sons; 1988. p. 15-23.

43. Mikkelsen SR, Corto´n E. Bioanalytical chemistry. Hoboken (NJ): John Wiley & Sons; 2004. p. 16-38.

44. Cunningham AJ. Introduction to bioanalytical sensors. New York (NY): John Wiley & Sons, Inc.; 1998. p. 79-165.

45. Cao G. Nanostructures and nanomaterials : Synthesis, properties, and applications. London: Imperial College Press; 2004. p. 7-10.

46. Gogotsi Y. Nanotubes and nanofibers. Boca Raton (FL): Taylor and Francis Group, LLC.; 2006. p. 1-107.

47. Rao CNR, Govindaraj A, Gundiah G, Vivekchand SRC. Nanotubes and nanowires. Chem. Eng. Sci. 2004; 59 (22-23): 4665-71.

48. Meyyappan M. Carbon nanotubes : Science and applications. Boca Ratom (FL): CRC Press LLC; 2005. p. 137-278.

49. Rijn CJMV. Nano and micro engineered membrane technology. Amsterdam: Elsevier B.V.; 2004. p. 319-324.

50. Tsang SC, Guo Z, Chen YK, Green MLH, Hill HAO, Hambley TW, Sadler PJ. Immobilization of platinated and iodinated oligonucleotides on carbon nanotubes. Angew. Chem. Int. Ed. 1997; 36 (20): 2198-200.

51. Sun Y-P, Fu K, Lin Y, Huang W. Functionalized carbon nanotubes: properties and applications. Acc. Chem. Res. 2002; 35 (12): 1096-104.

52. Baughman RH, Zakhidov AA, de Heer WA. Carbon nanotubes-the route toward applications. Science. 2002; 297 (5582): 787-92.

53. Vu L, Pralong WF, Cerini F, Gjinovci A, Stocklin R, Rose K, Offord RE, Kippen AD. Short-term insulin-induced glycogen formation in primary hepatocytes as a screening bioassay for insulin action. Anal. Biochem. 1998; 262 (1): 17-22.

54. Trethewey J. Bio-assays for the analysis of insulin. J. Pharm. Biomed. Anal. 1989; 7 (2): 189-97.

55. Andersen L, Jorgensen PN, Jensen LB, Walsh D. A new insulin immunoassay specific for the rapid-acting insulin analog, insulin aspart, suitable for bioavailability, bioequivalence, and pharmacokinetic studies. Clin. Biochem. 2001; 33 (8): 627-33.

56. Marcovina S, Bowsher RR, Miller WG, Staten M, Myers G, Caudill SP, Campbell SE, Steffes MW. Standardization of insulin immunoassays: Report of the american diabetes association work-group. Clin. Chem. 2007; 53 (4): 711-6.

57. Wang J, Ibanez A, Prakash Chatrathi M. On-chip integration of enzyme and immunoassays: Simultaneous measurements of insulin and glucose. J. Am. Chem. Soc. 2003; 125 (28): 8444-5.

58. Birnbaum S, Bülow L, Hardy K, Danielsson B, Mosbach K. Automated thermometric enzyme immunoassay of human proinsulin produced by *Escherichia coli*. Anal. Biochem. 1986; 158 (1): 12-9.

59. Yang C, Huang H, Zhang H, Liu M. Analysis of insulin by high performance liquid chromatographic method with precolumn derivatization with 4-chloro-7-nitrobenzo-2-oxa-1,3-diazole. Anal. Lett. 2006; 39 (12): 2463 - 73.

60. Hancock WS, Knighton DR, Napier JR, Harding DR, Venable R. Determination of thermodynamic parameters for the interaction of a lipid-binding peptide and insulin with a reversed-phase column. J. Chromatogr. 1986; 367 (1): 1-8.

61. Toriumi C, Imai K. Determination of insulin in a single islet of Langerhans by high-performance liquid chromatography with fluorescence detection. Anal. Chem. 2002; 74 (10): 2321-7.

62. Steiner RF, McAlister A. Fluorescent insulin conjugates. J. Colloid Sci. 1957; 12 (1): 80-98.

63. Tao L, Kennedy RT. Online competitive immunoassay for insulin based on capillary electrophoresis with laser-induced fluorescence detection. Anal. Chem. 1996; 68 (22): 3899-906.

64. Nettleton EJ, Tito P, Sunde M, Bouchard M, Dobson CM, Robinson CV. Characterization of the oligomeric states of insulin in self-assembly and amyloid fibril formation by mass spectrometry. Biophys. J. 2000; 79 (2): 1053-65.

65. Hong J, Miao R, Zhao C, Jiang J, Tang H, Guo Z, Zhu L. Mass spectrometry assisted assignments of binding and cleavage sites of copper(II) and platinum(II) complexes towards oxidized insulin B chain. J. Mass Spectrom. 2006; 41 (8): 1061-72.

66. Kippen AD, Cerini F, Vadas L, Stocklin R, Vu L, Offord RE, Rose K. Development of an isotope dilution assay for precise determination of insulin, C-peptide, and proinsulin levels in non-diabetic and type II diabetic individuals with comparison to immunoassay. J. Biol. Chem. 1997; 272 (19): 12513-22.

67. Stocklin R, Vu L, Vadas L, Cerini F, Kippen AD, Offord RE, Rose K. A stable isotope dilution assay for the in vivo determination of insulin levels in humans by mass spectrometry. Diabetes. 1997; 46 (1): 44-50.

68. Cox JA, Gray TJ. Flow injection amperometric determination of insulin based upon its oxidation at a modified electrode. Anal. Chem. 1989; 61 (21): 2462-4.

69. Cheng L, Pacey GE, Cox JA. Carbon electrodes modified with ruthenium metallodendrimer multilayers for the mediated oxidation of methionine and insulin at physiological pH. Anal. Chem. 2001; 73 (22): 5607-10.

70. Kennedy RT, Huang L, Aspinwall CA. Extracellular pH is required for rapid release of insulin from Zn-insulin precipitates in β-cell secretory vesicles during exocytosis. J. Am. Chem. Soc. 1996; 118 (7): 1795-6.

71. Salimi A, Pourbeyram S, Haddadzadeh H. Sol-gel derived carbon ceramic composite electrode containing a ruthenium complex for amperometric detection of insulin at physiological pH. J. Electroanal. Chem. 2003; 542: 39-49.

72. Pikulski M, Gorski W. Iridium-based electrocatalytic systems for the determination of insulin. Anal. Chem. 2000; 72 (13): 2696-702.

73. Gorski W, Aspinwall CA, Lakey JRT, Kennedy RT. Ruthenium catalyst for amperometric determination of insulin at physiological pH. J. Electroanal. Chem. 1997; 425 (1-2): 191-9.

74. Kennedy RT, Huang L, Atkinson MA, Dush P. Amperometric monitoring of chemical secretions from individual pancreatic beta-cells. Anal. Chem. 1993; 65 (14): 1882-7.

75. Gorski W, Cox JA. Oxidation of N-nitrosamines at a ruthenium-based modified electrode in aqueous solution. J. Electroanal. Chem. 1995; 389 (1-2): 123-8.

76. Wang J, Musameh M. Electrochemical detection of trace insulin at carbon-nanotube-modified electrodes. Anal. Chim. Acta. 2004; 511 (1): 33-6.

77. Taeko M, Wada T, Yamaguchi K, Hata K. Sialidase and malignancy: A minireview. Glycoconj. J. 2004; 20 (3): 189-98.

78. Kodama K, Kobayashi H, Abe R, Ohkawara A, Yoshii N, Yotsumoto S, Fukushige T, Nagatsuka Y, Hirabayashi Y, Kanzaki T. A new case of α-N-acetylgalactosaminidase deficiency with angiokeratoma corporis diffusum, with Ménière's syndrome and without mental retardation. Br. J. Dermatol. 2001; 144 (2): 363-8.

79. Umemoto J, Matta KL, Barlow JJ, Bhavanandan VP. Action of endo-α-N-acetyl-D-galactosaminidase on synthetic glycosides including chromogenic substrates. Anal. Biochem. 1978; 91 (1): 186-93.

80. Thomas JH, Kim SK, Hesketh PJ, Halsall HB, Heinemana WR. Microbead-based electrochemical immunoassay with interdigitated array electrodes. Anal. Biochem. 2004; 328 (2): 113-22.

81. Lo J, Mukerji K, Awasthi YC, Hanada E, Suzuki K, Srivastava SK. Purification and properties of sphingolipid beta-galactosidases from human placenta. J. Biol. Chem. 1979; 254 (14): 6710-5.

82. Wang J, Krause R, Block K, Musameh M, Mulchandani A, Mulchandani P, Chen W, Schoning MJ. Dual amperometric-potentiometric biosensor detection system for monitoring organophosphorus neurotoxins. Anal. Chim. Acta. 2002; 469 (2): 197-203.

83. Lei Y, Mulchandani P, Wang J, Chen W, Mulchandani A. Highly sensitive and selective amperometric microbial biosensor for direct determination of *p*-nitrophenyl-substituted organophosphate nerve agents Environ. Sci. Technol. 2005; 39 (22): 8853-7.

84. Wang J, Krause R, Block K, Musameh M, Mulchandani A, Schoning Michael J. Flow injection amperometric detection of OP nerve agents based on an organophosphorus-hydrolase biosensor detector. Biosens. Bioelectron. 2003; 18 (2-3): 255-60.

85. Gyurcsányi RE, Bereczki A, Nagy G, Neumana MR, Lindner E. Amperometric microcells for alkaline phosphatase assay. Analyst. 2002; 127 (2): 235-40.

86. Cooper JM, McNeil CJ, Spoors JA. Amperometric enzyme electrode for the determination of aspartate aminotransferase and alanine aminotransferase in serum. Anal. Chim. Acta. 1991; 245 (1): 57-62.

87. Pemberton RM, Mottram TT, Hart JP. Development of a screen-printed carbon electrochemical immunosensor for picomolar concentrations of estradiol in human serum extracts. J. Biochem. Biophys. Methods. 2005; 63 (3): 201-12.

88. Wang J. Portable electrochemical systems. Trends Anal. Chem. 2002; 21 (4): 226-32.

89. Iniesta J, Michaud PA, Panizza M, Cerisola G, Aldaz A, Comninellis C. Electrochemical oxidation of phenol at boron-doped diamond electrode. Electrochim. Acta. 2001; 46 (23): 3573-8.

90. Wang J, Jiang M, Lu F. Electrochemical quartz crystal microbalance investigation of surface fouling due to phenol oxidation. J. Electroanal. Chem. 1998; 444 (1): 127-32.

91. Iotov PI, Kalcheva SV. Mechanistic approach to the oxidation of phenol at a platinum/gold electrode in an acid medium. J. Electroanal. Chem. 1998; 442 (1-2): 19-26.

92. Nagata R, Clark SA, Yokoyama K, Tamiya E, Karube I. Amperometric glucose biosensor manufactured by a printing technique. Anal. Chim. Acta. 1995; 304 (2): 157-64.

93. Miserere S, Ledru S, Ruille N, Griveau S, Boujtita M, Bedioui F. Biocompatible carbon-based screen-printed electrodes for the electrochemical detection of nitric oxide. Electrochem. Commun. 2006; 8 (2): 238-44.

94. Zhang C, Gao Q, Aizawa M. Flow injection analytical system for glucose with screen-printed enzyme biosensor incorporating Os-complex mediator. Anal. Chim. Acta. 2001; 426 (1): 33-41.

95. Ledru S, Ruille N, Boujtita M. One-step screen-printed electrode modified in its bulk with HRP based on direct electron transfer for hydrogen peroxide detection in flow injection mode. Biosens. Bioelectron. 2006; 21 (8): 1591-8.

96. Clark LC. The hydrogen peroxide sensing platinum anode as an analytical enzyme electrode. Methods Enzymol. 1979; 56 (1): 448-79.

97. Wang J, Naser N, Angnes L, Wu H, Chen L. Metal-dispersed carbon paste electrodes Anal. Chem. 1992; 64 (11): 1285-8.

98. Zhang Z, Liu H, Deng J. A glucose biosensor based on immobilization of glucose oxidase in electropolymerized *o*-aminophenol film on platinized glassy carbon electrode. Anal. Chem. 1996; 68 (9): 1632-8.

99. Vreeke M, Rocca P, Heller A. Direct electrical detection of dissolved biotinylated horseradish peroxidase, biotin, and avidin. Anal. Chem. 1995; 67 (2): 303-6.

100. Liu H, Ying T, Sun K, Qi D. A reagentless biosensor highly sensitive to hydrogen peroxide based on new methylene blue N dispersed in Nafion® gel as the electron shuttle. J. Electroanal. Chem. 1996; 417 (1-2): 59-64.

101. O'Halloran MP, Pravda M, Guilbault GG. Prussian blue bulk modified screen-printed electrodes for $H_2O_2$ detection and for biosensors. Talanta. 2001; 55 (3): 605-11.

102. Ricci F, Amine A, Tuta CS, Ciucu AA, Lucarelli F, Palleschi G, Moscone D. Prussian blue and enzyme bulk-modified screen-printed electrodes for hydrogen peroxide and glucose determination with improved storage and operational stability. Anal. Chim. Acta. 2003; 485 (1): 111-20.

103. Tseng K-S, Chen L-C, Ho K-C. Amperometric detection of hydrogen peroxide at a prussian blue-modified FTO electrode. Sens. Actuators, B. 2005; 108 (1-2): 738-45.

104. Yang M, Jiang J, Yang Y, Chen X, Shen G, Yu R. Carbon nanotube/cobalt hexacyanoferrate nanoparticle-biopolymer system for the fabrication of biosensors. Biosens. Bioelectron. 2006; 21 (9): 1791-7.

105. Delvaux M, Walcarius A, Demoustier-Champagne S. Electrocatalytic $H_2O_2$ amperometric detection using gold nanotube electrode ensembles. Anal. Chim. Acta. 2004; 525 (2): 221-30.

106. Lindgren A, Ruzgas T, Gorton L, Csöregi E, Ardila GB, I.Y.Sakharov, Gazaryan IG. Biosensors based on novel peroxidases with improved properties in direct and mediated electron transfer. Biosens. Bioelectron. 2000; 15 (9-10): 491-7.

107. Kong Y-T, Boopathi M, Shim Y-B. Direct electrochemistry of horseradish peroxidase bonded on a conducting polymer modified glassy carbon electrode. Biosens. Bioelectron. 2003; 19 (3): 227-32.

108. Jia N, Zhou Q, Liu L, Yan M, Jiang Z. Direct electrochemistry and electrocatalysis of horseradish peroxidase immobilized in sol-gel-derived tin oxide/gelatin composite films. J. Electroanal. Chem. 2005; 580 (2): 213-21.

109. Yaropolov AI, Tarasevich MR, Varfolomeev SD. Electrochemical properties of peroxidase. Bioelectrochem. Bioenerget. 1978; 5 (1): 18-24.

110. Razumas V, Jasaitis J, Kulys J. Electrocatalysis on enzyme-modified carbon materials. Bioelectrochem. Bioenerget. 1984; 12 (3-4): 297-322.

111. Kulys J, Samalius A. Dependence of the effiency of bioelectrocatalytic processes on the electrode surface state. Bioelectrochem. Bioenerget. 1984; 13: 163-9.

112. Bogdanovskaya VA, Tarasevich MR, Hintsche R, Scheller F. Electrochemical transformations of proteins adsorbed at carbon electrodes. Bioelectrochem. Bioenerget. 1988; 19 (3): 591-4.

113. Jonsson G, Gorton L. An electrochemical sensor for hydrogen peroxide based on peroixde adsorbed on a spectrographic graphite electrode. Electroanal. 1989; 1 (5): 465-8.

114. Csöregi E, Jonsson-Pettersson G, Gorton L. Mediatorless electrocatalytic reduction of hydrogen peroxide at graphite electrodes chemically modified with peroxidase. J. Biotechnol. 1993; 30 (3): 315-37.

115. Gorton L, Bremle G, Csöregi E, Jonsson-Pettersson G, Persson B. Amperometric glucose sensors based on immobilized glucose-oxidizing enzymes and chemically modified electrodes. Anal. Chim. Acta. 1991; 249 (1): 43-54.

116. Gorton L, Jonsson-Pettersson G, Csöregi E, Jonsson G, Dominguez E, Marko-Varga G. Amperometric biosensor based on an apparent direct electron transfer between electrodes and immobilized peroxidases. Analyst. 1992; 117 (8): 1235-41.

117. Csöregi E, Gorton L, Marko-Varga G. Carbon fibres as electrode materials for the construction of peroxidase-modified amperometric biosensors. Anal. Chim. Acta. 1993; 273 (1-2): 59-70.

118. Zhao J, Henkens RW, Stonehuerner J, O'Daly JP, Crumbliss AL. Direct electron transfer at horseradish peroxidase-colloidal gold modified electrode. J. Electroanal. Chem. 1992; 327 (1-2): 109-19.

119. Durliat H, Courteix A, Comtat M. Reactions of horseradish peroxidase on a platinum cathode. Bioelectrochem. Bioenerget. 1989; 22 (3): 197-209.

120. Comtat M, Durliat H. Some examples of the use of thin layer spectroelectrochemistry in the study of electron transfer between metals and enzymes. Biosens. Bioelectron. 1994; 9 (9-10): 663-8.

121. Ajayan PM, Schadler LS, Braun PV. Nanocomposite science and technology. Morlenbach: Wiley-VCH Verlag; 2003. p. 77-80.

122. Vo-Dinh T, Cullum BM, Stokes DL. Nanosensors and biochips : Frontiers in biomolecular diagnostics. Sens. Actuators, B. 2001; 74 (1-3): 2-11.

123. Gu H-Y, Yu A-M, Chen H-Y. Direct electron transfer and characterization of hemoglobin immobilized on a Au colloid-cysteamine-modified gold electrode. J. Electroanal. Chem. 2001; 516 (1-2): 119-26.

124. Liu S-Q, Ju H-X. Renewable reagentless hydrogen peroxide sensor based on direct electron transfer of horseradish peroxidase immobilized on colloidal gold-modified electrode. Anal. Biochem. 2002; 307 (1): 110-6.

125. Zhang J, Oyama M. A hydrogen peroxide sensor based on the peroxidase activity of hemoglobin immobilized on gold nanoparticles-modified ITO electrode. Electrochim. Acta. 2004; 50 (1): 85-90.

126. Gu H-Y, Chen Z, Sa R-X, Yuan S-S, Chen H-Y, Ding Y-T, Yu A-M. The immobilization of hepatocytes on 24 nm-sized gold colloid for enhanced hepatocytes proliferation. Biomaterials. 2004; 25 (17): 3445-51.

127. Zhang S, Wang N, Niu Y, Sun C. Immobilization of glucose oxidase on gold nanoparticles modified Au electrode for the construction of biosensor. Sens. Actuators, B. 2005; 109 (2): 367-74.

128. Yang W, Wang J, Zhao S, Sun Y, Sun C. Multilayered construction of glucose oxidase and gold nanoparticles on Au electrodes based on layer-by-layer covalent attachment. Electrochem. Commun. 2006; 8 (4): 665-72.

129. Abad JM, Mertens SFL, Pita M, Fernandez VM, Schiffrin DJ. Functionalization of thioctic acid-capped gold nanoparticles for specific immobilization of histidine-tagged proteins. J. Am. Chem. Soc. 2005; 127 (15): 5689-94.

130. Cai H, Xu C, He P, Fang Y. Colloid Au-enhanced DNA immobilization for the electrochemical detection of sequence-specific DNA. J. Electroanal. Chem. 2001; 510 (1-2): 78-85.

131. Wang M, Wang L, Wang G, Ji X, Bai Y, Li T, Gong S, Li J. Application of impedance spectroscopy for monitoring colloid Au-enhanced antibody immobilization and antibody-antigen reactions. Biosens. Bioelectron. 2004; 19 (6): 575-82.

132. Chu X, Xiang Z-F, Fu X, Wang S-P, Shen G-L, Yu R-Q. Silver-enhanced colloidal gold metalloimmunoassay for *Schistosoma japonicum* antibody detection. J. Immunol. Methods. 2005; 301 (1-2): 77-88.

133. Kumar MNVR. A review of chitin and chitosan applications. React. Funct. Polym. 2000; 46 (1): 1-27.

134. Sashiwa H, Aiba S. Chemically modified chitin and chitosan as biomaterials. Prog. Polym. Sci. 2004; 29 (9): 887-908.

135. Erbacher P, Zou S, Bettinger T, Steffan AM, Remy JS. Chitosan-based vector/DNA complexes for gene delivery: biophysical characteristics and transfection ability. Pharm. Res. 1998; 15 (9): 1332-9.

136. Luo X-L, Xu J-J, Zhang Q, Yang G-J, Chen H-Y. Electrochemically deposited chitosan hydrogel for horseradish peroxidase immobilization through gold nanoparticles self-assembly. Biosens. Bioelectron. 2005; 21 (1): 190-6.

137. Clescerl LS, Greenberg AE, Eaton AD. Standard methods for the examination of water and wastewater. 20th ed. New York (NY): American Public Health Association; 1998. p. 4-139.

138. Upchurch JB, Edzwald JK, O'Melia CR. Phosphates in sediments of Pamlico estuary. Environ. Sci. Technol. 1974; 8 (1): 56-8.

139. Yang L, Sturgeon RE, Lam JWH. On-line determination of dissolved phosphate in seawater by ion-exclusion chromatography inductively coupled plasma mass spectrometry. J. Anal. At. Spectrom. 2001; 16 (11): 1302-6.

140. Guo Z-X, Cai Q, Yang Z. Determination of glyphosate and phosphate in water by ion chromatography-inductively coupled plasma mass spectrometry detection. J. Chromatogr. A. 2005; 1100 (2): 160-7.

141. Dube G, Boulay G, Kimmerle FM. Determination of traces of phosphate by thin layer X-ray fluorescence. Anal. Chem. 1976; 48 (13): 1950-3.

142. Libby RA. Quantitative thin layer chromatography with X-ray emission spectrometry. Anal. Chem. 1968; 40 (10): 1507-12.

143. Shkinev VM, Spivakov BY, Vorob'eva GA, Zolotov YA. Dialkyltin salts as extractants in methods for the determination of arsenic and phosphorus. Anal. Chim. Acta. 1985; 167 (1): 145–60.

144. Chaniotakis NA, Jurkschat K, Ruhlemann A. Potentiometric phosphate selective electrode based on a multidentate–tin(IV) carrier. Anal. Chim. Acta. 1993; 282 (2): 345-52.

145. Carey CM, Riggan WB. Cyclic polyamine ionophore for use in a dibasic phosphate-selective electrode. Anal. Chem. 1994; 66 (21): 3587–91.

146. Liu J, Masuda Y, Sekido E. Response properties of an ionselective polymeric membrane phosphate electrode prepared with cobalt phthalocyanine and characterization of the electrode process. J. Electroanal. Chem. Interfacial. Electrochem. 1990; 291 (1-2): 67-79.

147. Lee D, Cheng KL. An anion-selective membrane electrode based on a mixture of insoluble lead salts. Talanta. 1990; 37 (9): 901–4.

148. Grabner EW, Vermes I, Konig KH. A phosphate-sensitive electrode based on $BiPO_4$-modified glassy carbon. J. Electroanal. Chem. Interfacial. Electrochem. 1986; 214 (1-2): 135-40.

149. Godiker W, Cammann K. Properties of a phosphate sensitive solid state electrode based on cerium-IV-hydrogenphosphate mixed with PVC. Anal. Lett. 1989; 22 (5): 1237-49.

150. Xiao D, Yuan H-Y, Li J, Yu R-Q. Surface-modified cobalt-based sensor as a phosphate-sensitive electrode. Anal. Chem. 1995; 67 (2): 299-1.

151. Chen Z, De Marco R, Alexander PW. Flow-injection potentiometric detection of phosphates using a metallic cobalt wire ionselective electrode. Anal. Commun. 1997; 34 (3): 93-5.

152. Guilbault GG, Nanjo M. Phosphate-selective electrode based on immobilized alkaline phosphatase and glucose oxidase. Anal. Chim. Acta. 1975; 78 (1): 69-80.

153. Guilbault GG, Sadar SH, Glazer R, Haynes J. Umbelliferone phosphate as a substrate for acid and alkaline phosphatase. Anal. Lett. 1968; 1 (5): 333-45.

154. Guilbault GG, Vaughan A, Hackney D. Fluorometric methods for analysis of acid and alkaline phosphatase. Anal. Chem. 1971; 43 (6): 721-4.

155. Dollard Marie A, Billard P. Whole-cell bacterial sensors for the monitoring of phosphate bioavailability. J. Microbiol. Methods. 2003; 55 (1): 221-9.

156. Fernandez JJ, Lopez JR, Correig X, Katakis I. Reagentless carbon paste phosphate biosensors: preliminary studies. Sens. Actuators, B. 1998; 47 (1-3): 13-20.

157. Haemmerli SD, Suleiman AA, Guilbault GG. Amperometric determination of phosphate by use of a nucleoside phosphorylase-xanthine oxidase enzyme sensor based on a Clark-type hydrogen peroxide or oxygen electrode. Anal. Biochem. 1990; 191 (1): 106-9.

158. Kulys J, Higgins IJ, Bannister JV. Amperometric dertermination of phosphate ions by biosensor. Biosens. Bioelectron. 1992; 7 (3): 187-91.

159. Durso EM, Coulet PR. Effect of enzyme ratio and enzyme loading on the performance of a bienzymatic electrochemical phosphate biosensor. Anal. Chim. Acta. 1993; 281 (3): 535-42.

160. Kubo I, Inagawa M, Sugawara T, Arikawa Y, Karube I. Phosphate sensor composed from immobilized pyruvate oxidase and an oxygen electrode. Anal. Lett. 1991; 24 (10): 1711-27.

161. Ikebukuro K, Wakamura H, Karube I, Kubo I, Inagawa M, Sugawara T, Arikawa Y, Suzuki M, Takeuchi T. Phosphate sensing system using pyruvate oxidase and chemiluminescence detection. Biosens. Bioelectron. 1996; 11 (10): 959-65.

162. Nakamura H, Ikebukuro K, McNiven S, Karube I, Yamamoto H, Hayashi K, Suzuki M, Kubo I. A chemiluminescent FIA biosensor for phosphate ion monitoring using pyruvate oxidase. Biosens. Bioelectron. 1997; 12 (9-10): 959-66.

163. Nakamura H, Tanaka H, Hasegawa M, Masuda Y, Arikawa Y, Nomura Y, Ikebukuro K, Karube I. An automatic flow-injection analysis system for determining phosphate ion in river water using pyruvate oxidase G (from Aerococcus viridans). Talanta. 1999; 50 (4): 799-807.

164. Mizutani F, Yabuki S, Sato Y, Sawaguchi T, Iijima S. Amperometric determination of pyruvate, phosphate and urea using enzyme electrodes based on pyruvate oxidase-containing poly(vinyl alcohol)/polyion complex-bilayer membrane. Electrochim. Acta. 2000; 45 (18): 2945-52.

165. Gavalas VG, Chaniotakis NA. Phosphate biosensor based on polyelectrolyte-stabilized pyruvate oxidase. Anal. Chim. Acta. 2001; 427 (2): 271-7.

166. Mak WC, Chan C, Barford J, Renneberg R. Biosensor for rapid phosphate monitoring in a sequencing batch reactor (SBR) system. Biosens. Bioelectron. 2003; 19 (3): 233-7.

167. Mak WC, Ng YM, Chan C, Kwong WK, Renneberg R. Novel biosensors for quantitative phytic acid and phytase measurement. Biosens. Bioelectron. 2004; 19 (9): 1029-35.

168. Kwan RCH, Leung HF, Hon PYT, Barford JP, Renneberg R. A screen-printed biosensor using pyruvate oxidase for rapid determination of phosphate in synthetic wastewater. Appl. Microbiol. Biotechnol. 2005; 66 (4): 377-83.

169. Rahman MA, Park D-S, Chang S-C, McNeil CJ, Shim Y-B. The biosensor based on the pyruvate oxidase modified conducting polymer for phosphate ions determinations. Biosens. Bioelectron. 2006; 21 (7): 1116-24.

170. Conrath N, Grundig B, Huwel S, Cammann K. A novel enzyme sensor for the determination of inorganic phosphate. Anal. Chim. Acta. 1995; 309 (1-3): 47-52.

171. Huwel S, Haalck L, Conrath N, Spener F. Maltose phosphorylase from *Lactobacillus brevis*: purification, characterization, and application in a biosensor for ortho-phosphate. Enzyme Microb. Technol. 1997; 21 (6): 413-20.

172. Nakamura H, Hasegawa M, Nomura Y, Arikawa Y, Matsukawa R, Ikebukuro K, Karube I. Development of a highly sensitive chemiluminescence flow-injection analysis sensor for phosphate-ion detection using maltose phosphorylase. J. Biotechnol. 1999; 75 (2-3): 127-33.

173. Mousty C, Cosnier S, Shan D, Mu S. Trienzymatic biosensor for the determination of inorganic phosphate. Anal. Chim. Acta. 2001; 443 (1): 1-8.

174. Guilbault GG, Cserfalvi T. Ion selective electrode for phosphate using enzyme systems. Anal. Lett. 1976; 9 (3): 277-89.

175. Wollenberger U, Scheller FW. Enzyme activation for activator and enzyme activity measurement. Biosens. Bioelectron. 1993; 8 (6): 291-7.

176. Watanabe E, Endo H, Toyama K. Determination of phosphate ions with an enzyme sensor system. Biosensors. 1987; 3 (5): 297-306.

177. d'Urso EM, Coulet PR. Phosphate-sensitive enzyme electrode: a potential sensor for environment control. Anal. Chim. Acta. 1990; 239 (1): 1-5.

178. Cosnier S, Lepellec A, Guidetti B, Isabelle Rico-Lattes. Enhancement of biosensor sensitivity in aqueous and organic solvents using a combination of poly(pyrrole-ammonium) and poly(pyrrole-lactobionamide) films as host matrices. J. Electroanal. Chem. 1998; 449 (1-2): 165-71.

179. Ponchio C. Hemin-polypyrrole film modified carbon paste electrode for phosphate determination in natural water [M.Sc. thesis in Applied Analytical and Inorganic Chemistry]. Bangkok: Faculty of Graduate Studies, Mahidol University, 2005. 117p.

180. JGOFS. Chapter 11: The determination of phosphorus in sea water [Access: 2007, Oct 25,]; Available from: http://store.pangaea.de/Projects/JGOFS/Methods/chap11.html

181. Brajter-Toth A, Chambers JQ. Electroanalytical methods for biological materials. New York (NY): Marcel Dekker, Inc.; 2002. p. 367-398.

182. Hrapovic S, Liu M, Male KB, Luong JHT. Electrochemical biosensing platforms using platinum nanoparticles and carbon nanotubes. Anal. Chem. 2004; 76 (4): 1083-8.

183. Holmstrom SD, Cox JA. Electrocatalysis at a conducting composite electrode doped with a ruthenium(II) metallodendrimer. Anal. Chem. 2000; 72 (14): 3191-5.

184. Reynolds NC, Kissela BM, Fleming LH. The voltammetry of neuropeptides containing L-tyrosine. Electroanal. 1995; 7 (12): 1177-81.

185. Macdonald SM, Roscoe SG. Electrochemical oxidation reactions of tyrosine, tryptophan and related dipeptides. Electrochim. Acta. 1997; 42 (8): 1189-200.

186. Nguyen NT, Wrona MZ, Dryhurst G. Electrochemical oxidation of tryptophan. J. Electroanal. Chem. Interfacial Electrochem. 1986; 199 (1): 101-26.

187. Brabec V, Mornstein V. Electrochemical behaviour of proteins at graphite electrodes II. Electrooxidation of amino acids. Biophys. Chem. 1980; 12 (2): 159-65.

188. Malfoy B, Reynaud JA. Electrochemical investigations of amino acids at solid electrodes. Part II: amino acids containing no sulfur atoms:tryptophan, tyrosine, histidine and derivatives. J. Electroanal. Chem. Interfacial Electrochem. 1980; 114 (2): 213-23.

189. Wang J, Tangkuaram T, Loyprasert S, Vazquez-Alvarez T, Veerasai W, Kanatharana P, Thavarungkul P. Electrocatalytic detection of insulin at RuOx/carbon nanotube-modified carbon electrodes. Anal. Chim. Acta. 2007; 581 (1): 1-6.

190. Lawrence NS, Deo RP, Wang J. Comparison of the electrochemical reactivity of electrodes modified with carbon nanotubes from different sources. Electroanal. 2005; 17 (1): 65-72.

191. Salimi A, Roushani M, Haghighi B, Soltanian S. Amperometric detection of insulin at renewable sol–gel derived carbon ceramic electrode modified with nickel powder and potassium octacyanomolybdate(IV). Biosens. Bioelectron. 2006; 22 (2): 220-6.

192. Salimi A, Pourbeyram S, Haddadzadeh H. Sol-gel derived carbon ceramic composite electrode containing a ruthenium complex for amperometric detection of insulin at physiological pH. J. Electroanal. Chem. 2003; 542 (1): 39-49.

193. Wang J, Zhang X. Needle-type dual microsensor for the simultaneous monitoring of glucose and insulin. Anal. Chem. 2001; 73 (4): 844-7.

194. Qu F, Yang M, Lu Y, Shen G, Yu R. Amperometric determination of bovine insulin based on synergic action of carbon nanotubes and cobalt hexacyanoferrate nanoparticles stabilized by EDTA. Anal. Bioanal. Chem. 2006; 386 (2): 228-34.

195. Boudenne JL, Cerclier O, Bianco P. Voltammetric studies of the behavior of carbon black during phenol oxidation on Ti/Pt electrodes. J. Electrochem. Soc. 1998; 145 (8): 2763-8.

196. Deo RP, Wang J, Block I, Mulchandani A, Joshi KA, Trojanowicz M, Scholz F, Chen W, Lin Y. Determination of organophosphate pesticides at a carbon nanotube/organophosphorus hydrolase electrochemical biosensor. Anal. Chim. Acta. 2005; 530 (2): 185-9.

197. Nagy G, Xu CX, Buck RP, Lindner E, Neuman MR. Amperometric microcell for enzyme activity measurements. Anal. Chem. 1998; 70 (10): 2156-62.

198. Morrin A, Killard AJ, Smyth MR. Electrochemical characterization of commercial and home-made screen-printed carbon electrodes. Anal. Lett. 2003; 36 (9): 2021-39.

199. Muangkeaw K. Pt-based nanoparticles synthesis and their electrocatalytic activies on modified FTO as model electrodes for PEMFC/DAFC [M.Sc. thesis in Applied Analytical and Inorganic Chemistry]. Bangkok: Faculty of Graduate Studies, Mahidol University, 2007. 175p.

200. Neiman B, Grushka E, Lev O. Use of gold nanoparticles to enhance capillary electrophoresis. Anal. Chem. 2001; 73 (21): 5220-7.

201. Liu X, Atwater M, Wang J, Huo Q. Extinction coefficient of gold nanoparticles with different sizes and different capping ligands. Colloids and Surfaces B: Biointerfaces. 2007; 58 (1): 3-7.

202. Khanna PK, Gokhale R, Subbarao VVVS, Vishwanath AK, Das BK, Satyanarayana CVV. PVA stabilized gold nanoparticles by use of unexplored albeit conventional reducing agent. Mater. Chem. Phys. 2005; 92 (1): 229-33.

203. Brown KR, Walter DG, Natan MJ. Seeding of colloidal Au nanoparticle solutions. 2. Improved control of particle size and shape. Chem. Mater. 2000; 12 (2): 306-13.

204. Lu X, Zhang Q, Zhang L, Li J. Direct electron transfer of horseradish peroxidase and its biosensor based on chitosan and room temperature ionic liquid. Electrochem. Commun. 2006; 8 (5): 874-8.

205. Luo X-L, Xu J-J, Du Y, Chen H-Y. A glucose biosensor based on chitosan–glucose oxidase–gold nanoparticles biocomposite formed by one-step electrodeposition. Anal. Biochem. 2004; 334 (2): 284-9.

206. Ferri T, Poscia A, Santucci R. Direct electrochemistry of membrane-entrapped horseradish peroxidase.: Part I. A voltammetric and spectroscopic study. Bioelectrochem. Bioenerget. 1998; 44 (2): 177-81.

207. Ferri T, Poscia A, Santucci R. Direct electrochemistry of membrane-entrapped horseradish peroxidase.: Part II: Amperometric detection of hydrogen peroxide. Bioelectrochem. Bioenerget. 1998; 45 (2): 221-6.

208. Li J, Dong S. The electrochemical study of oxidation-reduction properties of horseradish peroxidase. J. Electroanal. Chem. 1997; 431 (1): 19-22.

209. Mulchandani A, Rogers KR. Enzyme and microbial biosensors : Techniquues and protocols. Totowa (NJ): Humana Press Inc.; 1998. p. 93-120.

210. Ruzgas T, Gorton L, Emneus J, Marko-Varga G. Kinetic models of horseradish peroxidase action on a graphite electrode. J. Electroanal. Chem. 1995; 391 (1-2): 41-9.

211. Wu L-Q, Gadre AP, Yi H, Kastantin MJ, Rubloff GW, Bentley WE, Payne GF, Ghodssi R. Voltage-dependent assembly of the polysaccharide chitosan onto an electrode surface. Langmuir. 2002; 18 (22): 8620-5.

212. Qian J, Liu Y, Liu H, Yu T, Deng J. Characterization of regenerated silk fibroin membrane for immobilizing peroxidase and construction of an amperometric hydrogen peroxide sensor employing phenaine methosulphate as electron shuttle. J. Electroanal. Chem. 1995; 397 (1-2): 157-62.

213. Lei C-X, Hu S-Q, Shen G-L, Yu R-Q. Immobilization of horseradish peroxidase to a nano-Au monolayer modified chitosan-entrapped carbon paste electrode for the detection of hydrogen peroxide. Talanta. 2003; 59 (5): 981-8.

214. Xu X, Liu S, Ju H. A novel hydrogen peroxide sensor via the direct electrochemistry of horseradish peroxidase immobilized on colloidal gold modified screen-printed electrode. Sensors. 2003; 3 (9): 350-60.

215. Kamin RA, Wilson GS. Rotating ring-disk enzyme electrode for biocatalysis kinetic studies and characterization of the immobilized enzyme layer. Anal. Chem. 1980; 52 (8): 1198-205.

216. Cai C, Chen J. Direct electron transfer and bioelectrocatalysis of hemoglobin at a carbon nanotube electrode. Anal. Biochem. 2004; 325 (2): 285-92.

217. Liu S-Q, Ju H-X. Renewable reagentless hydrogen peroxide sensor based on direct electron transfer of horseradish peroxidase immobilized on colloidal gold-modified electrode. Anal. Biochem. 2002; 307 (1): 110-6.

218. Yi X, Huang-Xian J, Hong-Yuan C. Direct electrochemistry of horseradish peroxidase immobilized on a colloid/cysteamine-modified gold electrode. Anal. Biochem. 2000; 278 (1): 22-8.

219. Xu Q, Mao C, Liu N-N, Zhu J-J, Sheng J. Direct electrochemistry of horseradish peroxidase based on biocompatible carboxymethyl chitosan-gold nanoparticle nanocomposite. Biosens. Bioelectron. 2006; 22 (5): 768-73.

220. Liu Y, Yuan R, Chai Y, Tang D, Dai J, Zhong X. Direct electrochemistry of horseradish peroxidase immobilized on gold colloid/cysteine/nafion-modified platinum disk electrode. Sens. Actuat. B. 2006; 115 (1): 109-15.

221. Miao Y, Tan SN. Amperometric hydrogen peroxide biosensor with silica sol-gel/chitosan film as immobilization matrix. Anal. Chim. Acta. 2001; 437 (1): 87-93.

222. Xu S, Peng B, Han X. A third-generation $H_2O_2$ biosensor based on horseradish peroxidase-labeled Au nanoparticles self-assembled to hollow porous polymeric nanopheres. Biosens. Bioelectron. 2007; 22 (8): 1807-10.

223. Yu JH, Ju HX. Preparation of porous titania sol-gel matrix for immobilization of horseradish peroxidase by a vapor deposition method. Anal. Chem. 2002; 74 (14): 3579-83.

224. Zong S, Cao Y, Zhou Y, Ju H. Zirconia nanoparticles enhanced grafted collagen tri-helix scaffold for unmediated biosensing of hydrogen peroxide. Langmuir. 2006; 22 (21): 8915-9.

225. Wang GH, Zhang LM. Using novel polysaccharide-silica hybrid material to construct an amperometric biosensor for hydrogen peroxide. J. Phys. Chem. B. 2006; 110 (49): 24864-8.

226. Miao Y, Tan SN. Amperometric hydrogen peroxide biosensor with silica sol–gel/chitosan film as immobilization matrix. Anal. Chim. Acta. 2001; 437 (1): 87-93.

227. Bergmann W, Rudolph R, Spohn U. A bienzyme modified carbon paste electrode for amperometric detection of pyruvate. Anal. Chim. Acta. 1999; 394 (2-3): 233-41.

228. Kwan RCH, Chan C, Renneberg R. An amperometric biosensor for determining amino acids using a bienzymatic system containing amino acid oxidase and protease. Biotechnol. Lett. 2002; 24 (14): 1203-7.

229. Akyilmaz E, Yorganci E. Construction of an amperometric pyruvate oxidase enzyme electrode for determination of pyruvate and phosphate. Electrochim. Acta. 2007; 52 (28): 7972-7.

230. Miller JN, Miller JC. Statistics and chemometrics for analytical chemistry. 4th ed. Harlow: Pearson Education Limited; 2000. p. 44-48.

231. Tangkuaram T, Gerlach JQ, Xiang Y, Kawde A-N, Dai Z, Bhavanandan VP, La Belle JT, Veerasai W, Joshi L, Wang J. Sensitive and rapid electrochemical bioassay of glycosidase activity. Analyst. 2006; 131 (8): 889-91.

232. Tangkuaram T, Ponchio C, Kangkasomboon T, Katikawong P, Veerasai W. Design and development of a highly stable hydrogen peroxide biosensor on screen printed carbon electrode based on horseradish peroxidase bound with gold nanoparticles in the matrix of chitosan. Biosens. Bioelectron. 2007; 22 (9-10): 2071-8.

# APPENDIX

# APPENDIX A

## A.1 Insulin electrochemical sensor

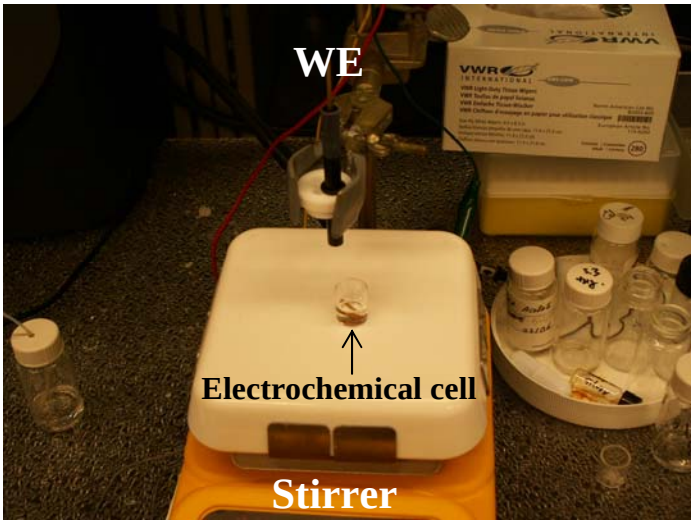


**Figure A.1** Electrochemical setup showing of cell and working electrode (WE).

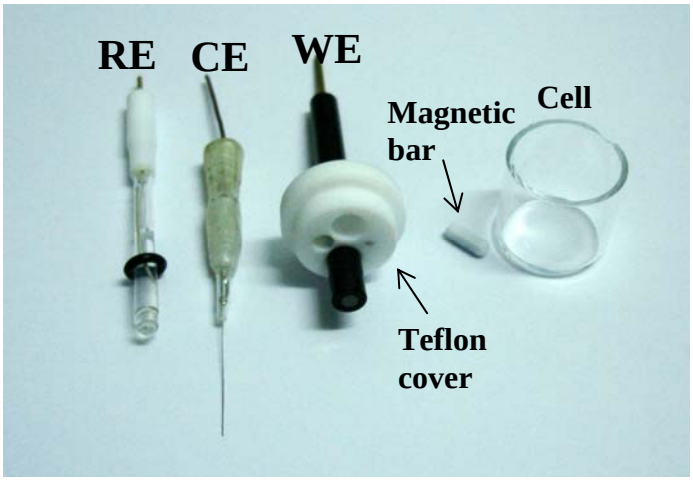


**Figure A.2** The compartment of electrochemical cell consisting of (from Left to Right) reference electrode (RE), counter electrode (CE), working electrode (WE) with Teflon cover cell, magnetic stirrer, and cell.

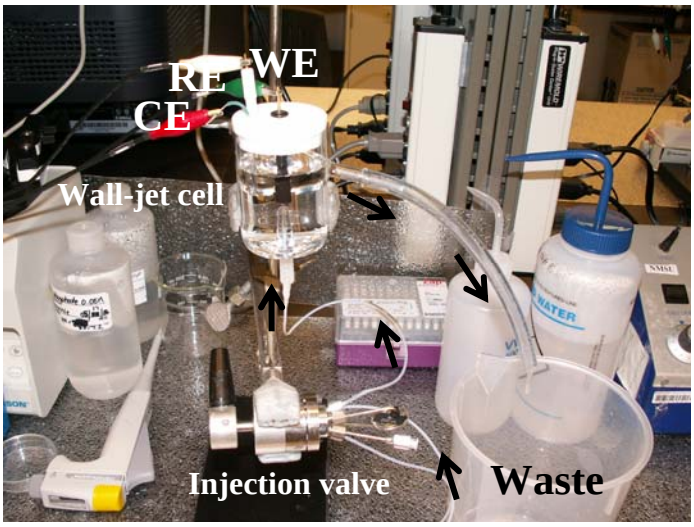


**Figure A.3** FIA setup showing injection valve, wall-jet cell, reference electrode (RE), counter electrode (CE), and working electrode (WE). Arrows indicate flow direction.

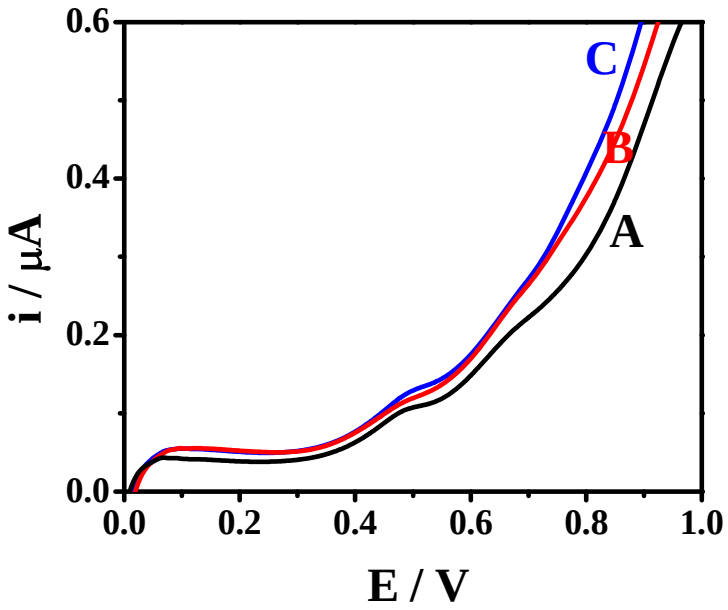


**Figure A.4** Linear sweep voltammogram (LSV) of 24 µM insulin using CNT at (A) 10, (B) 20, and (C) 30 µL of 2 mg $mL^{-1}$ casting on GCE. The CNT electrodes were $RuO_x$ covered for 25 minutes of cyclization. LSV conditions: supporting electrolyte, 0.05 M phosphate buffer (pH 7.40) containing 0.10 M NaCl, scan rate 20 mV $s^{-1}$.

## A.2 Glycosidases sensor

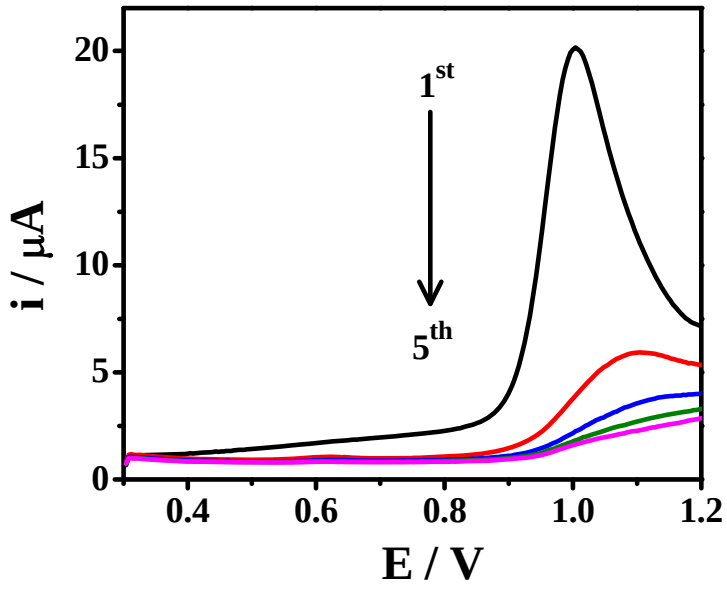


**Figure A.5** Square wave voltammograms showing 5 repetitive scans of 1 mM *p*-nitrophenol at GCE. Conditions, 0.05 M citrate buffer solution pH 4.4, step potential = 4 mV, amplitude = 25 mV, and frequency = 25 Hz.

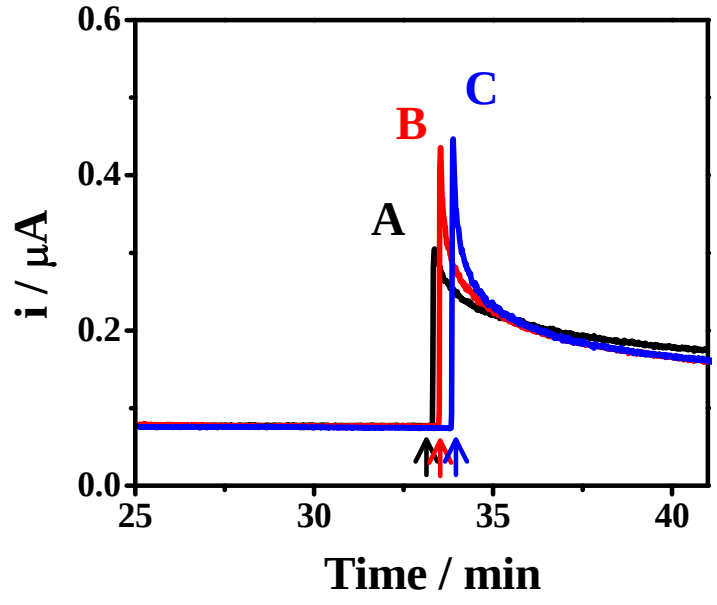


**Figure A.6** Amperometric response of glycosidases sensor for addition of (A) human serum, (B) serum + PNP, and (C) serum + glycosidases enzyme + PNP. Arrows indicate addition of solution A, B, and C.

# A.3 Hydrogen peroxide biosensor

## A.3.1 Fabrication of SPCE

**Fig A.7** SPCE screen frames.

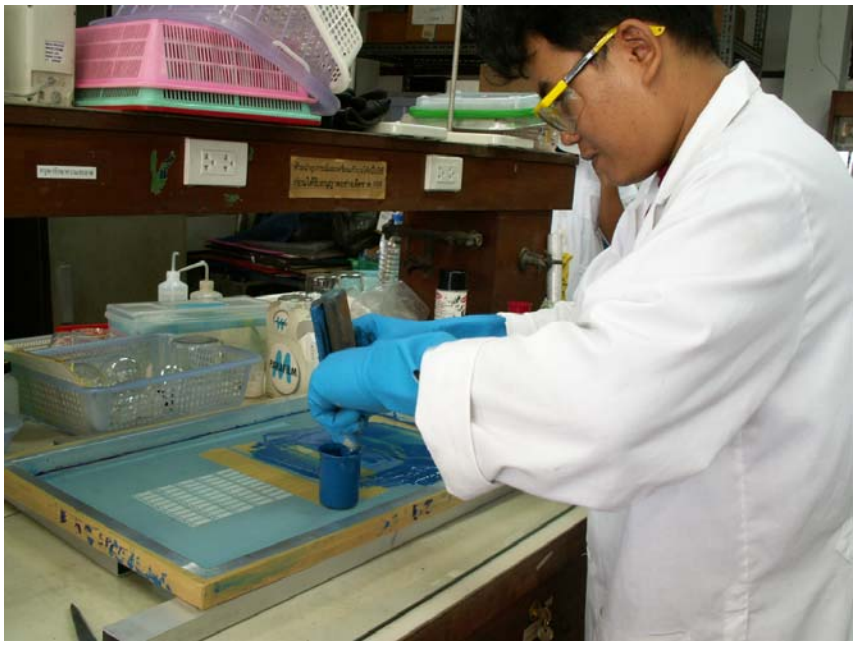

**Figure A.8** An insulator ink screen step in SPCE fabrication process.

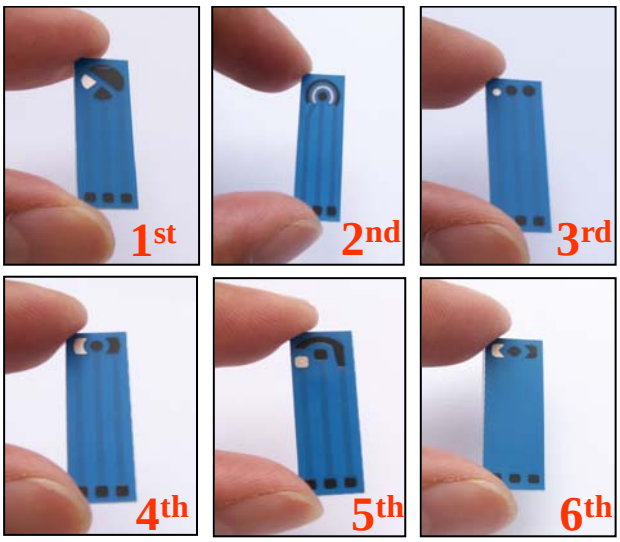


**Figure A.9** Photographs of six configurations SPCEn (n = 1 to 6).

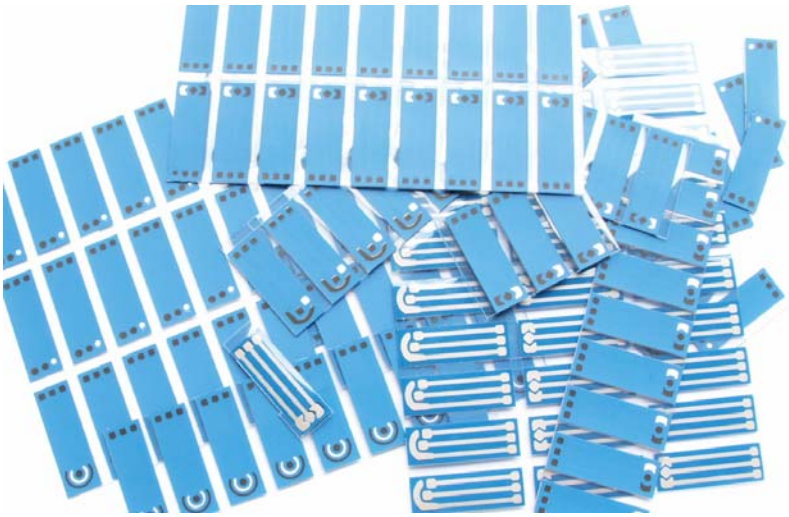

**Figure A.10** Production of SPCEs.

### A.3.2 SPCE resistance measurement

A multi-meter, MY68, was used to measure the resistance of the SPCE. A red wire (+) was touched at a reference electrode simultaneously with a black wire (–) touched to a contact pad. Switching the operation jog to Ω sign and read the value as figure A.11. For the working and counter electrodes, they were measured in similar manner of reference electrode resistance measurement.

**Figure A.11** SPCE resistance measurement.

### A.3.3 Electrochemical cell setup

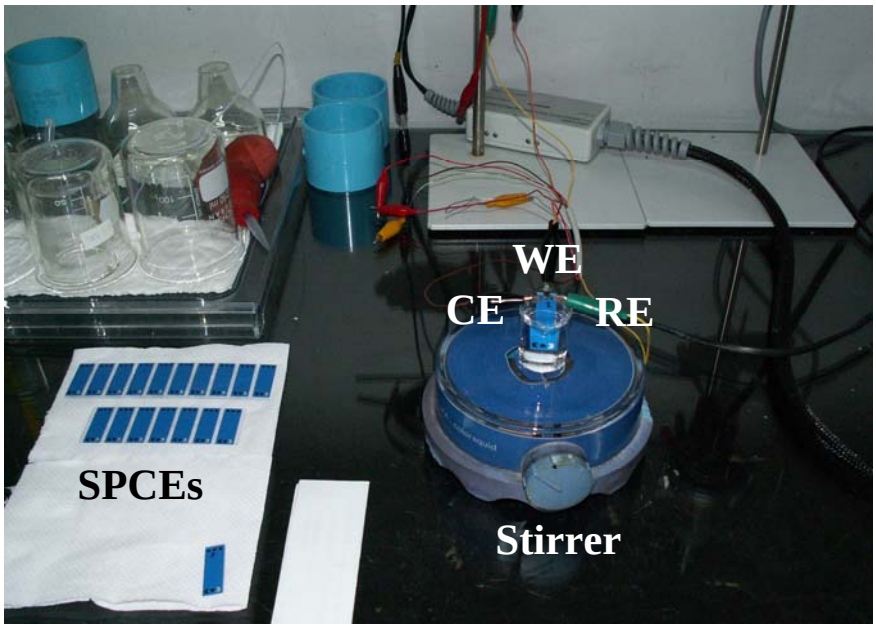


**Figure A.12** Electrochemical cell setup for hydrogen peroxide biosensor development. WE, CE and RE are working, counter, and reference electrodes, respectively.

### A.3.4 Variation of scan rate on cyclic voltammograms for SPCE5

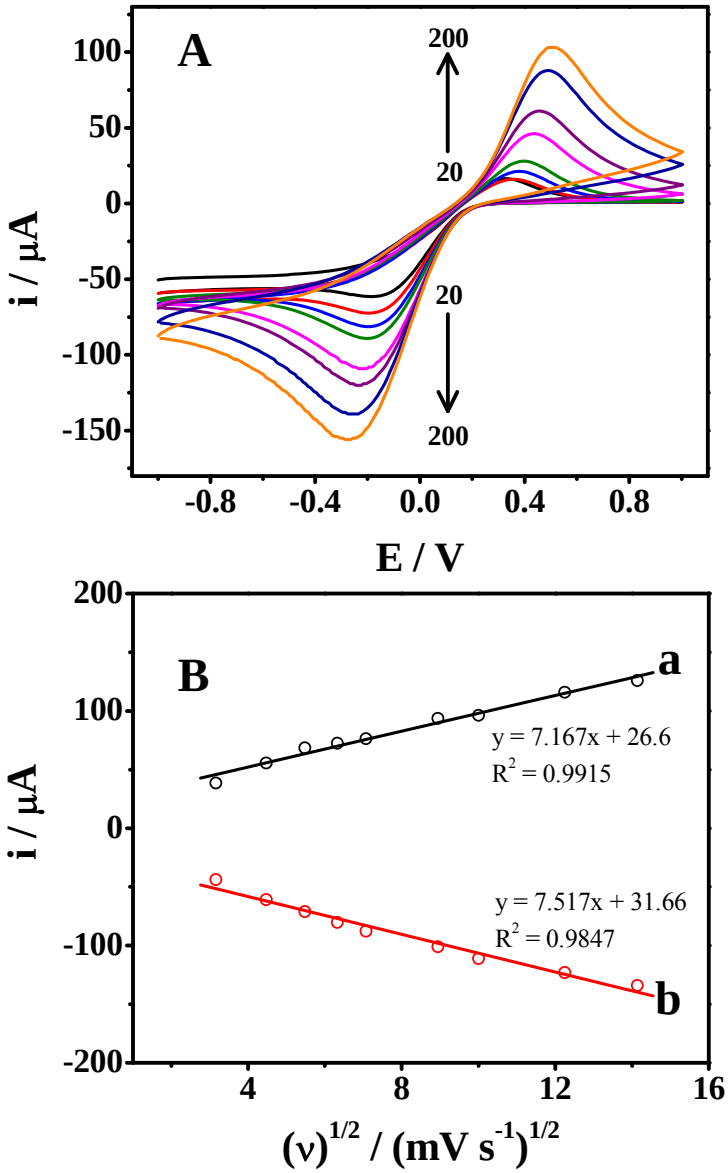


**Figure A.13** (A) Cyclic voltammograms for SPCE5 in 20 mM $K_3Fe(CN)_6$ containing 0.1 M KCl at different scan rates from inner to outer; 20, 30, 50, 80, 100, 150 and 200 mV $s^{-1}$. (B) Square roots of scan rates versus (a) anodic and (b) cathodic currents plots.

### A.3.5 Estimation of the gold nanoparticles concentration

It is of importance to estimate the concentration of the gold nanoparticles. From the size of the gold nanoparticles (16.8 nm), the estimate the average number of gold atoms ($N$) for a single gold nanoparticle was calculated by Eq. (A.1), where $\rho$ is the density for gold (19.3 g $cm^{-3}$), MW stands for atomic weight of gold (197 g $mol^{-1}$), and $N_A$ is the Avogadro's constant ($6.02 \times 10^{23}$).

$$N = \frac{4}{3} \times \pi \times r^3 \times \rho \times \frac{1}{\mathrm{MW}} \times N_A \qquad \text{(A.1)}$$

Knowing the initial mole of the gold solution ($1.24 \times 10^{-6}$ mole) and assuming that the reduction from gold (III) to gold atoms was 100% complete. The molar concentration ($C$) of the nanosphere solutions were calculated by dividing the total number of gold atoms ($N_{total}$), equivalent to the initial amount of gold salt added to the reaction solution, over the average number of gold atoms per nanosphere ($N$) according to equation (A.2), where $V$ is the volume of the reaction solution in liter ($V$ = 0.01 L). The molar concentration of gold nanoparticles is calculated to be 0.85 nM.

$$C = \frac{N_{\mathrm{total}}}{N \times V \times N_A} \qquad \text{(A.2)}$$

## A.4 Phosphate biosensor

**Table A.1** Comparison of phosphate content in Klong Rangsit, K1-K7, obtained from UV-Vis spectrophotometry and PyOD/HRP/AuNP/CHIT phosphate biosensor

| Sample | Phosphate content / μM | |
|---|---|---|
| | UV-Vis spectrophotometry | PyOD/HRP/AuNP/CHIT |
| K1 | 6.25 (±0.15) | 6.36 (±0.30) |
| K2 | 11.76 (±0.11) | 11.55 (±0.46) |
| K3 | 13.47 (±0.13) | 11.97 (±0.75) |
| K4 | 10.26 (±0.16) | 9.90 (±0.51) |
| K5 | 14.01 (±0.11) | 13.47 (±0.43) |
| K6 | 10.77 (±0.08) | 9.99 (±0.44) |
| K7 | 7.77 (±0.14) | 7.51 (±0.64) |

# APPENDIX B

## B.1 Mean ($\bar{x}$) and standard deviation (s), relative standard deviation (RSD)

### B.1.1 Mean ($\bar{x}$)

Sometime it is also called average, obtained by dividing the sum of replicate measurements by the number of measurements in the test,

$$\bar{x} = \frac{\sum_{i=1}^{N} x_i}{N} \qquad \text{(B1.1)}$$

where $N$ = number of replicate measurement, $x_i$ = represents the individual values of $x$.

### B.1.2 Standard deviation (s)

Sometime it is called SD. Which is a measure of the precision of a sample of data, the calculation is given by,

$$s = \sqrt{\frac{\sum (x_i - \bar{x})^2}{N-1}} \qquad \text{(B1.2)}$$

where $N$ = number of replicate measurement, $x_i$ = represents the individual values of $x$.

### B1.3 Relative standard deviation (RSD)

The RSD is calculated by dividing the standard deviation by the mean value of the data set. The RSD multiplied by 100% is call coefficient of variation (CV) or sometime call %RSD.

$$\%\text{RSD} = \frac{\text{s}}{x} \text{ x } 100\% \tag{B1.3}$$

## B.2 Statistical for comparison of two experimental means, t-test

T-test is statistical technique that used for comparison the two mean results of a new analytical method compared with the mean result obtained from second analytical method. This method assumes that the samples ($x_i$) are drawn from populations with equal standard deviations. In order to decide whether the different between two sample means, $\bar{x}_1$ and $\bar{x}_2$ is significant, that is to test the null hypothesis, $H_0 : \mu_1 = \mu_2$, the statistic $t$ is calculated by,

$$\text{t} = \frac{(\bar{x}_1 - \bar{x}_2)}{s\sqrt{\frac{1}{n_1} + \frac{1}{n_2}}} \tag{B1.4}$$

where $s$ is calculated from,

$$s^2 = \frac{(n_1 - 1)s_1^2 + (n_2 - 1)s_2^2}{(n_1 + n_2 - 2)} \tag{B1.5}$$

and t has $n_1 + n_2 - 2$ degree of freedom and n = number of samples.

## B.3 Statistical for comparison of two experimental variances; F-test

The difference between two sample variances is needed to test with F-test, this is to test $H_0 : \sigma^2 = \sigma^2$. The statistical is test by,

$$F = \frac{s_1^2}{s_2^2} \tag{B1.6}$$

where 1 and 2 are allowed in the equation so F is always $\geq 1$, and number of degree of freedom are $n_1 - 1$ and $n_2 - 1$ for numerator and denominator, respectively.

## B.4 Detection limit (DL)

The detection limit is a smallest concentration that can be reported with a certain level of confidence. The detection limit is employed from the calibration curve and is defined as the analyte concentration yielding a response of a confidence factor *k* higher than the standard deviation of the blank, $s_b$, as,

$$\mathrm{DL} = \frac{\mathrm{k}s_\mathrm{b}}{m} \tag{B1.7}$$

where m is the calibration sensitivity and k is usually to be 2 or 3. When the method is said a detection limit obtained at S/N = 3, it mean that method is defined detection limit at $s_b$=3.

# APPENDIX C

## C.1 Properties of chitosan

Chitin and chitosan are natural polyaminosaccharides, chitin being one of the world's most plentiful, renewable organic resources. A major constituent of the shells of crustaceans, the exoskeletons of insects and the cell walls of fungi where it provides strength and stability, chitin is estimated to be synthesized and degraded in the biosphere in the vast amount of at least 10 Giga ton each year. Chemically, chitin is composed of β(1→4) linked 2-acetamido-2-deoxy-β-D-glucose units (or N-acetyl-D-glucosamine), forming a long chain linear polymer as shown in figure 1.16. Chitosan, the principal derivative of chitin, is obtained by N-deacetylation to a varying extent that is characterized by the degree of deacetylation, and is consequently a copolymer of N-acetyl-D-glucosamine and D-glucosamine. Chitin and chitosan can be chemically considered as analogues of cellulose, in which the hydroxyl at carbon-2 has been replaced by acetamido and amino groups, respectively.

Chitosan is insoluble in water, but the presence of amino groups renders it soluble in acidic solutions below pH about 6.5. It is important to note that chitin and chitosan are not single chemical entities, but vary in composition depending on the origin and manufacture process. Chitosan can be defined as chitin sufficiently deacetylated to form soluble amine salts, the degree of deacetylation necessary to obtain a soluble product being 80-85% or higher.

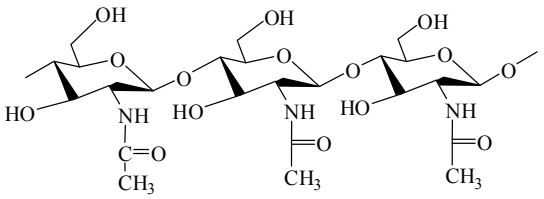

**Chitin**

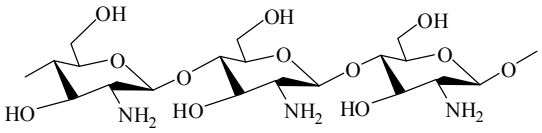

**Chitosan**

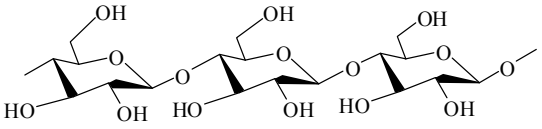

**Cellulose**

**Figure C.1** Structure of chitin, chitosan, and cellulose.

Chitosan possesses distinct chemical and biological properties. In its linear polyglucosamine chains of high molecular weight, chitosan has reactive amino and hydroxyl groups, amenable to chemical modifications. Additionally, amino groups make chitosan a cationic polyelectrolyte (p*K*a ≈ 6.5), one of the few found in nature. This basicity gives chitosan singular properties: chitosan is soluble in aqueous acidic media at pH < 6.5 and when dissolved possesses high positive charge on $-NH_3^+$ groups, it adheres to negatively charged surfaces, it aggregates with polyanionic compounds, and chelates heavy metal ions. Both the solubility in acidic solutions and aggregation with polyanions impart chitosan with excellent gel-forming properties. The chitosan application is briefly reviewed in chapter 3.3.

# BIOGRAPHY

| | |
|---|---|
| **NAME** | Mr. Tanin Tangkuaram |
| **DATE OF BIRTH** | April 9, 1976 |
| **PLACE OF BIRTH** | Roi-et, Thailand |
| **INSTITUTIONS ATTENDED** | Mahasarakham University, 1998 :<br>Bachelor of Science (Biology)<br><br>King Mongkut's Institute of Technology Ladkrabang, 2003 :<br>Master of Science (Chemistry)<br><br>Mahidol University, 2007 :<br>Doctor of Philosophy (Analytical Chemistry) |
| **RESEARCH GRANTS** | Staff Development Program, Commission on Higher Education through the Department of Chemistry, Faculty of Science, Maejo University, Chiang Mai, Thailand, 2003-2006.<br><br>The Center for Innovation in Chemistry: Postgraduate Education and Research Program in Chemistry (PERCH-CIC), 2003-2005.<br><br>Teaching Assistant Scholarship, Department of Chemistry, Faculty of Science, Mahidol University, Bangkok, 2005-2006. |
| **HOME ADDRESS** | 337 Moo 1, Tambol Wang,<br>Amphur Phonthong, Roi-et 45110, Thailand |